PREDICTION AND REAL-TIME COMPENSATION OF LINER WEAR IN CONE CRUSHERS

A Doctoral Thesis

by

Mojgan Moshgbar

Submitted in partial fulfilment of the requirements
for the award of

The Degree of Doctor of Philosophy of the Loughborough
University of Technology
1996

ABSTRACT

The Prediction and Real-Time Compensation of Liner Wear in Cone Crushers

M Moshgbar

In the comminution industry, cone crushers are widely used for secondary and subsequent stages of size reduction. For a given crusher, the achieved size reduction is governed by the closed-side setting. Hadfield Steel is commonly used to line the crushing members to minimize wear. Yet, liner wear caused by some rock types can still be excessive. Enlargement of discharge opening induced by wear of liners produces a drift in product size which, if unchecked, can lead to high volumes of re-circulating load. Alteration of closed-side setting is now commonly achieved via hydraulic means. However, compensation of liner wear still involves plant shut down and loss of production.

The continuous demand for better quality products and the high cost of re-processing or discarding unsaleable material, emphasizes the need for an improved wear compensation regime. The present research was initiated to address this requirement. The work involved a study of cone crusher tribology, experimental investigation of effective parameters using a laboratory size cone crusher, formulation of mathematical and Fuzzy models for prediction of wear, development of a new crusher model, and design of an adaptive control strategy for real-time regulation of discharge opening.

The liner wear caused by ten different rock types were compared for different crusher settings, feed size and moisture levels. It was found that for a given rock, the effect of crusher setting and rock moisture on wear is non-linear and best described by a second order model. To predict wear due to different rock types, a combination of several rock properties were found to be significant that include hardness, tensile strength, and Silica content. For moist rock, water absorption and pH value were also found to be significant. A strong interaction between rock properties, moisture content and closed-side setting was also observed. Multi-variable regression analysis was used to develop a number of rock-dependant and general models to predict liner wear at various crusher setting and rock moisture. Fuzzy modelling techniques were used to accommodate imprecise knowledge of moisture content.

Effect of moisture and wear-induced change in liner profile on product size were investigated and it was found that both factors contribute to producing a finer product than otherwise expected. A time-dependant crusher model, incorporating these effects, was formulated to allow prediction of product size in real-time. Based on this model, an adaptive control strategy for compensation of liner wear has been designed. The performance of the new control strategy was investigated using MATLAB simulation techniques. Compared to the currently available cone crusher control systems, the performance of the designed system was found to be considerably superior in terms of product quality and crusher efficiency.

ACKNOWLEDGEMENTS

The author would like to thank Professor R. Parkin of Loughborough University of Technology for his invaluable encouragement, supervision and support during the course of this work.

Dr M. Acar of Loughborough University of Technology also provided supervision and is acknowledged for his support.

Pegson Ltd provided both the testing equipment and essential data and information and are acknowledged for their support.

Dr R. Bearman, previously the research manager at Pegson Ltd, provided an insight into the quarrying industry as well as encouragement and support during the experimental tests and is gratefully acknowledged.

Grateful thanks are also due to my husband, Farshad Moshgbar, for his invaluable encouragement and support, and my children, Maziar and Artemis Moshgbar, for their incredible patience during the course of this work.

NOTATIONS AND ABBREVIATIONS

ν	Degrees of Freedom associated with a model
Ψ	Index of Plasticity
μ.	Coefficient Of Friction
τ_s	Mean Shear Strength
10%	The Ten Percent Fine Test Value
AAV	Aggregate Abrasive Value
ACV	Aggregate Crushing Value
A_e	Elastic Area of Contact
A_H	Hertzian Area Of Contact
AIV	Aggregate Impact Value
Al2O3	Alumina Content
ANOVA	Analysis of Variance
A_p	Plastic Area of Contact
B	Whiten's Breakage Function
BTS	Brazilian Tensile Strength
C	Whiten's Classification Function
CSS	Closed-Side Setting
CW/g	Wear of Concave in gramme
E	Young's Modulus
f	Size Distribution of Feed
Feed size	Average Feed Size
F_f	Macroscopic Friction Force
F_n	Normal Load
FT	Fracture Toughness
H	Hardness of Abrading Surface
H_a,	Hardness of Abrasive Particle
K_1	Particle Size below which no further breakage happens
K_2	Particle Size above which all particles undergo breakage
K_3	Probability Function For Breakage
L	Sliding Distance
Moist	Moisture Content added to rock in percentage of rock weight
MW/(g/T)	Wear of Mantle in gramme per tonne of crushed rock
MW/g	Wear of Mantle in gramme
N	Number of Experimental Runs

p	Size Distribution of Cone Crusher Product
PL	Point Load Strength
P_y	Yield Pressure
P_{yn}	Normal Component of Yield Pressure
r_H	Hertzian Radius of Contact
S	Standard Deviation
SI	Silica Content
SS_T	Square of Total of Output Variation in an experimental study
T	Sum of all Observed Outputs in an experimental study
T(h/T)	Crushing Time in hour per tonne
t_{max}	Maximum Shear Stress
TW/(g/T)	Total Wear in gramme per tonne of crushed rock
UCS	Uniaxial Compressive Strength
v	Statistical Variance
V	Volume of Material Removed
W	Rate of Wear
Wgt/kg	Weight of Rock in kg
x	Size Distribution of Material inside the crushing chamber
y_i	ith experimentally Observed Output

CONTENT

LIST OF FIGURES

LIST OF TABLES

LIST OF PLATES

Chapter 1 INTRODUCTION

1.1 Aggregate Industry - A Brief Overview

The minerals industry is a major industry world-wide. It can be broken down into four main sectors namely coal, metaliferous minerals, constructional raw materials and industrial minerals. In terms of the production volumes, constructional raw materials represent the largest sector of the minerals industry as shown in Figure 1.1. Figure 1.2 shows the tonnage per capita per year of sand, gravel and aggregates produced around the world. (Rock Products 1992a). The combined value of all the sand, gravel and aggregates produced in the world in 1990 totalled US $25 billion (Rock Products 1992a). The value of constructional aggregates produced in the UK in 1988 was £1.319 billion representing 21.6% of the total value of all minerals and a considerable 0.35% of the Gross Domestic Product (Bristow 1992). Despite the fall in sales volumes in recent years, as shown in Figure 1.3 (Rock Products 1993), the current UK aggregate output of around 230M tonnes per annum compares favourably with the troughs of 193M tonnes in 1977 and 182M tonnes in 1981.

Growing demands for constructional aggregates and increasing pressure from the environmental lobby has influenced several new trends in the industry. The first is a spreading consensus of opinion that large scale coastal superquarries will be required to meet the future demands in northern Europe. The essential characteristics (Gribble 1991) of a coastal superquarry in terms of geology (reserves of at least 250 Mtonnes of "uniform rock"), output (5 Mtonnes/year minimum for 50 years), coastal water depth (12m minimum and sheltered to allow easy shipping access), and location (not more than 2km from the sea and environmentally acceptable) is expected to minimize production costs, shipping costs and environmental impact. A second trend is an increased fervour for recycling of construction materials. The improved machinery designs provide the means to recycle asphalt, ordinary and even wire reinforced slabby material. Another front in the

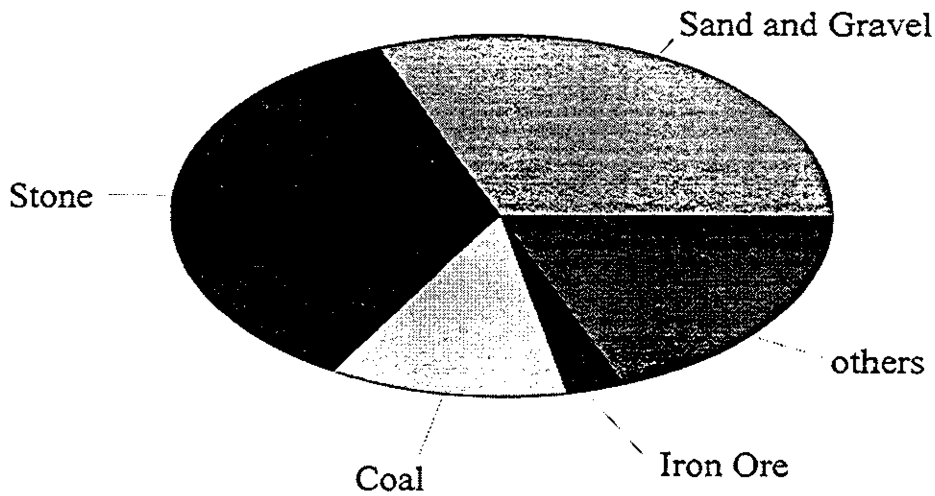

Figure 1.1World production of minerals (by weight)

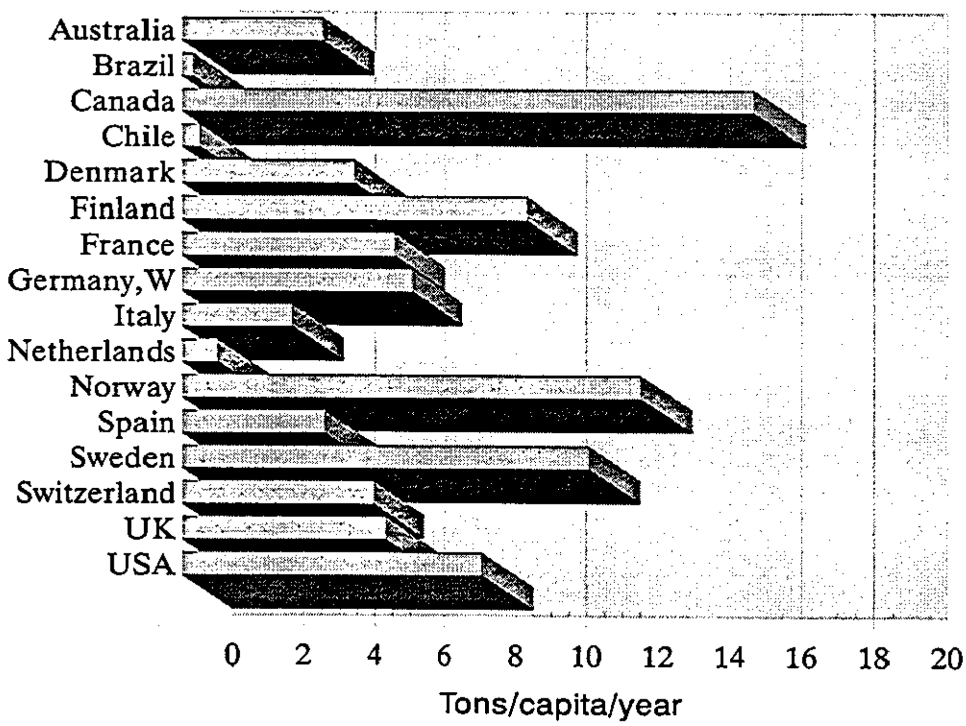

Figure 1.2 World per capita aggregate production in 1990

(Rock Products 1992a).

recycling trend is the increasing use of municipal slag (residue from burnt down domestic waste) and sewage to produce lightweight aggregates that reportedly have proven to be a suitable substitute for crushed stone for constructional purposes (Rock Products 1992a; Rock Products 1992b). However, despite the potential benefits offered by these technologies, they have still to make a major impact on the mainstream aggregate industry.

Table 1.1 shows the labour force engaged in extraction and processing of stone, clay, sand and gravel in UK during 1990 (Business Monitor 1991). Despite the economical advantage of relatively low labour intensity and a general rise in the price of aggregate products over the past three decades (Rock Products 1992b), the profit margins are not high. High rates of energy consumption, low added values, and the use of inefficient machinery and practices are among the factors responsible.

1.2 Cone Crushers in the Aggregate Industry

A wide range of rock crushers is used across the industry to reduce the size of excavated rock. These include jaw, gyratory, roll, cone, impact and pin type crushers. Of these the most widely used are jaw, impact and cone crushers. Cone crushers are commonly employed at secondary and subsequent stages of comminution to produce a progressive breakage of rock particles to a size suitable for either sale or further metallurgical treatment. In the aggregate industry, cone crushers are responsible for producing a large proportion of the final saleable products. Figure 1.4 shows a typical quarry flowchart.

The major proportion of the world's aggregate materials is used in road construction (50%) and production of concrete (40%) (Rock Products 1992a). The requirement of these industries is either single size or graded aggregate materials. Stringent specifications, laid down by the standard authorities, apply to the size and shape of suitable material for use in concrete and road construction. This imposes strict quality requirements on the saleability of aggregate products.

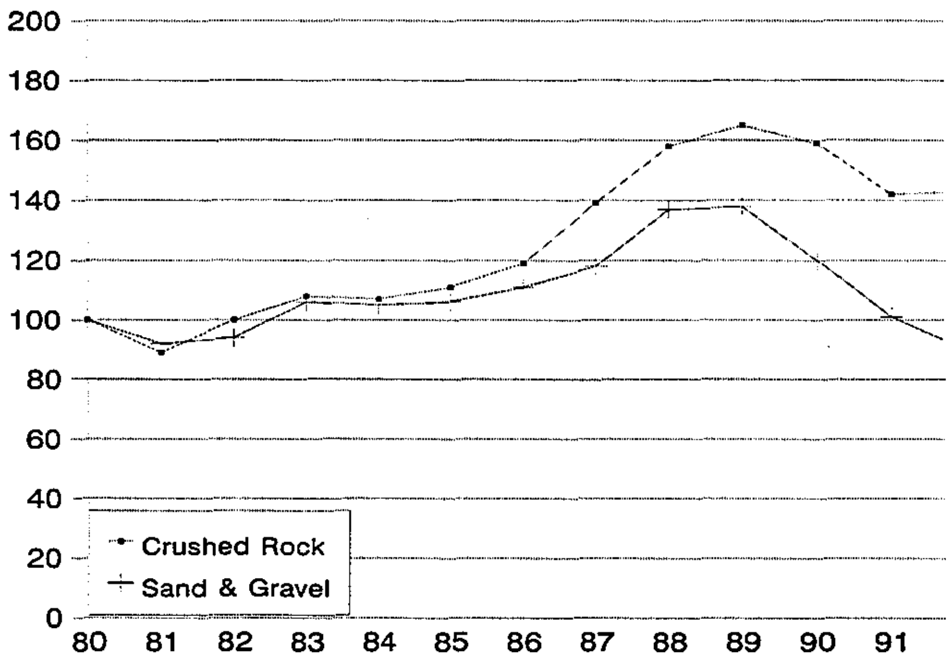

Figure 1.3 Aggregate demand trends 1980-1992
(Rock Products 1993)

Table 1.1The Employment Size Band Of Manufacturing Units In Extraction Of Stone, Clay, Sand And Gravel In 1992 (Business Monitor 1991)

Employment size	1-9	10-19	20-49	50-99	100-199	200-499	500 & over	TOTAL
No. of Units	242	122	40	3	2	1	0	410
Employment	1,025	1,590	1,171	188	233	287	-	4,494

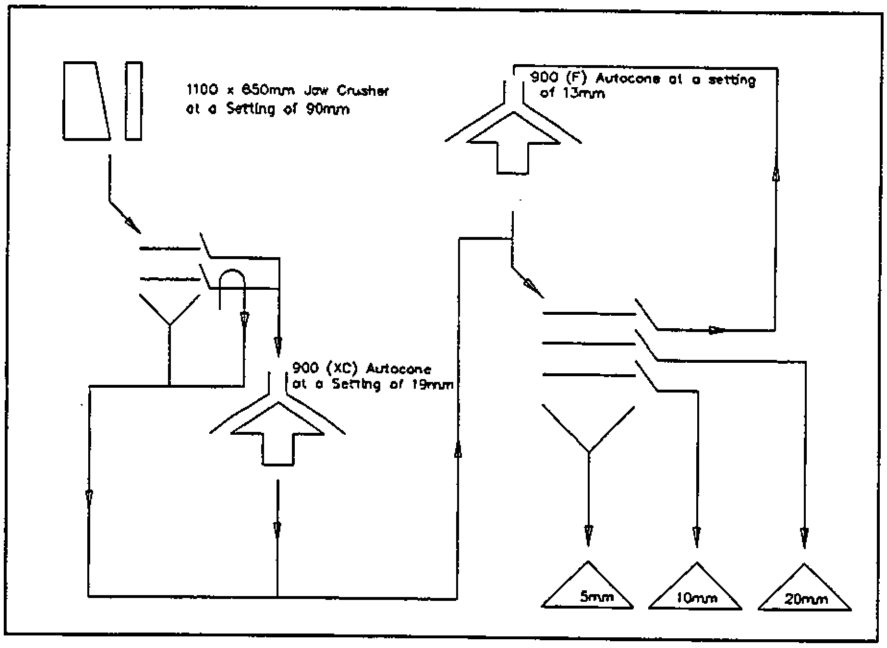

Figure 1.4 Atypical quarry flowchart

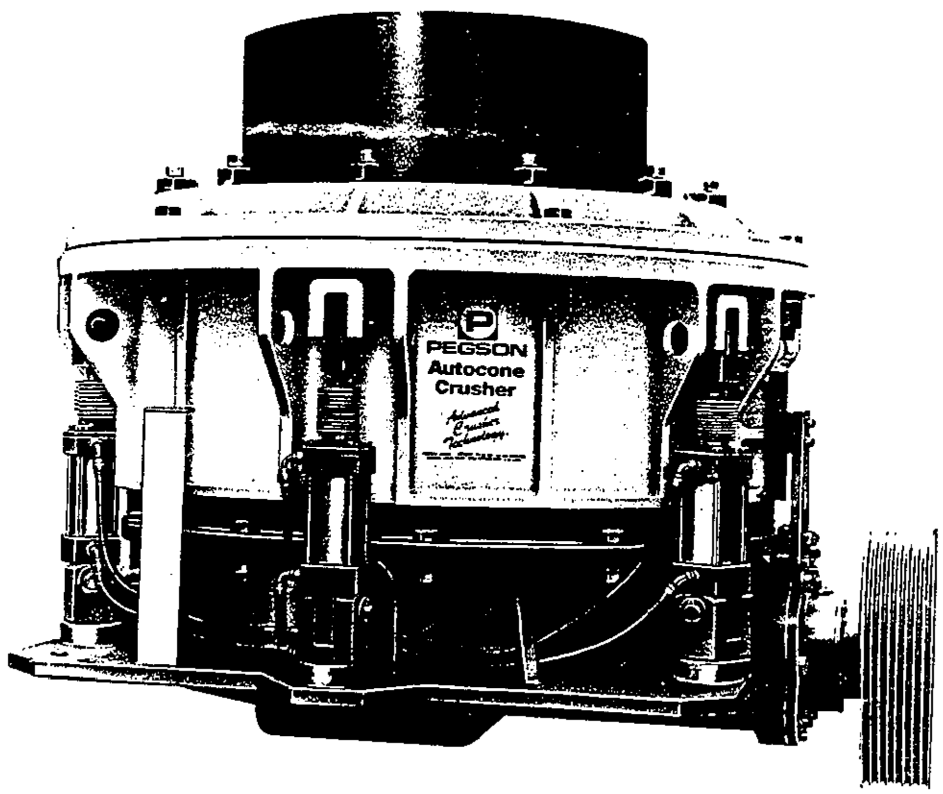

Figure 1.5 Pegson 900 Autocone

Due to the limitations of the current methods of cone crusher control, a considerable amount of oversize, low grade or unsaleable material is produced during the crushing process. The high cost of re-processing or discarding such materials emphasizes the urgency for the introduction of control strategies capable of ensuring product quality.

An examination of the energy consumption in the UK quarrying industry by Bearman (1991b) has shown that cone crushers consume up to 20% of the total electricity used in this industry. Therefore, any enhancement in the technology associated with cone crushers is sure to make a significant impact on the fortunes of the aggregate industry as a whole.

1.3 The Cone Crusher System

Different types and sizes of cone crushers are manufactured by all the leading mining and quarry plant manufacturers. Figure 1.5 shows the Autocone Cone crusher manufactured by Pegson Limited. Alternative concave and mantle designs are used to give various feed opening and differing degrees of product fineness. Cone crusher sizes are quoted as the diameter of the cone head, these vary from 0.45m to 3.05m with a concomitant variation in drive motors from 40kW to 750kW.

Within the limits set by the crusher design, the characteristics of cone crusher product is determined by the discharge opening (the gap between mantle and concave at the discharge end of crushing chamber) and the profile of the liners (nip angle). The combination of these two factors control the retention of feed in the crushing chamber and the length of the comminution cycle. The gap is regulated by the closed-side setting which involves the positioning of the upper frame of the crusher with respect to the inner cone. The movement of the upper frame is effected by different means depending on the design of cone crusher. Depending on their degree of sophistication, three types of cone crushers are distinguishable:-

1. closed-side setting adjusted via screw thread with spring loaded overload protection e.g., Pegson Gyrocone, Nordberg Gyradisc, Allis Symonds, Kue-Ken CT range,

2. closed-side setting adjusted via screw thread with hydraulic overload protection e.g., Nordberg Omnicone, Telsmith,

3. closed-side setting adjusted via hydraulic means with hydraulic overload protection e.g., Pegson Autocone, Automax and Autosand, Allis Hydrocone.

The majority of the modern cone crushers now fall within the third category. In contrast to screw thread cone crushers where the discharge opening is adjusted manually, in hydraulic cone crushers the setting is via electrical means offering the possibility of modern types of control.

1.4 Impact of Liner Wear on performance of Cone Crushers

The crushing elements of cone crushers are commonly lined with manganese steel (Hadfield steel). Despite the good work-hardening properties of Hadfield steel high rates of wear, in the range of 0.5-1.0 mm per hour, can be experienced. At these high rates of wear, the liners must be changed after approximately 80 hours of service. Apart from the usual implications of cost and downtime during relining, the wear has an important bearing on the quality of the product and crusher efficiency. Continuous wear degrades the nip angle and, if unchecked, due to the thickness loss of the liners increases the gap between the two crushing elements. This enlargement of the discharge opening causes a drift in the size distribution of the produced aggregates, where the volume of the oversize particles leaving the chamber increases. Hence to ensure the consistency and quality of the product, the crusher setting must be adjusted regularly to account for the liner wear.

At present crusher re-setting involves manual intervention and machine shutdown. The high cost of the downtime periods prohibits frequent re-settings. At the highest rates of wear, the crusher is usually re-set once per shift. However, in such cases the cumulative effect of wear between two successive re-settings is high enough to adversely affect the product quality. The wear induced under-crushing can overload the classifying screens reducing their efficiency and increasing the re-circulating load within the plant and thus inflating energy consumption and handling costs.

To avoid the problems associated with liner wear and to ensure optimum crusher efficiency and product quality, automatic methods of wear compensation must be sought and employed. In its most desirable form, such an automatic control system would measure or predict liner wear to estimate the gap size in real-time, and would effect any required adjustment in the crusher setting without any disruption. With such a capability, the discharge opening could be reset as frequently as required to maintain the crusher efficiency and the quality of its product.

1.5 Aims of the Present Research

The present work was carried out with the following main objectives:

1. to investigate the wear process of manganese steel liners used in cone crushers to determine the parameters affecting its rate,

2. to formulate suitable models capable of predicting rates of liner wear under various operational and environmental conditions,

3. to investigate the effect wear has on cone crusher performance and product characteristics,

4. to develop a new control strategy for real-time compensation of liner wear and optimization of product quality.

The work was carried out as part of a project, funded by DTI and SERC under the LINK initiative for High Speed Machinery, to develop the required technology for automation of cone crushers control. The cone crusher chosen for the study was Autocone 900 (shown in Figure 1.5) which is manufactured by the collaborating company Pegson Ltd.

Investigation of wear in complex industrial systems has received little attention from researchers in the field of tribology, and cone crushers are no exception. The undertaken study of liner wear and the formulation of predictive wear models has broken new grounds not only in the field of cone crushers, but also in the application of tribology in system control. Direct and in-process measurement of liner wear, although outside the boundaries of the current research, was considered as part of the LINK project. A number of prototype sensory devices were developed and successfully tested parallel to the course of the present work. The availability of this technology is a primary requirement for the application of the real-time control strategy suggested in this study. However, the extreme conditions of the crushing chamber and the unrecoverable nature of the prototype sensors extend the remits of the liner wear models, from merely predictive to an essential real-time diagnostic tool for validation of the sensory signals.

Chapter 2 REVIEW OF PREVIOUS WORK

Real-time compensation of wear in cone crushers is a multi-diciplinary task entailing predictive modelling of wear, instrumentation and measurement of variables, and system control. Accordingly, this chapter covers diverse fields of research which are nevertheless related to the current study.

2.1 Review of Mechanisms of Contact, Friction, and Wear

The understanding of wear and the ability to predict its rate in plant and machinery has obvious advantages for industry. The costs of wear in terms of metal wastage, plant maintenance and inefficiency due to non-optimized operation of machinery and equipment is very high, yet, tribological analysis of complex industrial systems remains a relatively neglected research area. The aggregates industry is no exception, and only a limited amount of research on wear in rock comminution has been conducted. No previous published work on wear in cone crushers can be cited despite exhaustive searches, and, as a result, fundamental questions about the tribology of the system remained to be resolved by the current study.

Tribology is a general concept embracing all aspects of the transmission and dissipation of energy and material which results from the motion of moving components in mechanical systems. It can be regarded as the frame-work linking the various processes connected with contact, friction and wear.

The theoretical treatment of the contact processes is concerned with the behaviour of the surfaces which come into contact under the influence of different loads. Analysis of friction involves the understanding of the resistive forces generated and dissipated during the relative motion of two contacting bodies, and wear is primarily concerned with progressive loss of material from the operating surface of a body due to friction.

2.1.1 Contact Processes

Contact processes include "contact mechanics" addressing the forces and displacements at the surfaces of the interacting bodies, and "contact physics and chemistry" which is concerned with interfacial interaction between the contacting bodies.

Contact Mechanics

Generally, contact of two bodies can lead to elastic (reversible) or/and plastic (irreversible) processes. In the analysis of contact mechanics, the geometry of the contacting bodies, their surface topography (rough or smooth), mechanical properties (hardness, toughness) and their relative motion (static, rolling, sliding, velocity, etc.) must be considered.

The classical Hertzian theory considers the "ideal" contact between two perfectly elastic bodies with the same modulus of elasticity and ideally smooth surfaces, where no tangential force acts at the contact. According to this theory, the radius of contact, $\mathbf{r_H}$, and area of contact, $\mathbf{A_H}$, are proportional to normal load $\mathbf{F_n}$. The fact that all real surfaces are covered by arrays of asperities and their contact occurs over discrete areas has long been recognised. For real surfaces, the real area of contact, $\mathbf{A_r}$ is defined as the sum of the separate microscopic areas at which the asperities are in contact. Two types of contact situation can be considered. The elastic contact mechanism is a reversible condition in which $\mathbf{A_r}$ is almost proportional to the applied force, i.e.

$$\mathbf{A_r = const.}\left|\frac{\mathbf{F_n}}{\mathbf{E}}\right|^c \qquad \mathbf{2.1}$$

where $4/5 < c < 44/45$ according to different models (Archard 1957; Greenwood & Tripp 1967), and **E** is the Young's modulus. While at low applied loads, the difference between the nominal and real areas of contact can be considerable, at higher loads an effective radius of contact can be defined which approaches the Hertzian radius and, like it, varies as the one third power of the applied load.

Plastic irreversible contact processes lead to dissipation of some mechanical energy. Greenwood and Williamson (1966) carried out a study of the subject and suggested the concept of a plasticity index Ψ, where

$$\Psi \propto \frac{E}{H} \qquad 2.2$$

where E is the Young's modulus, and H is the hardness of the material. When $\Psi < 0.6$ the contact remains elastic under all load conditions and for $\Psi > 1$, as is true for most surfaces, some part of the contact deformation processes will always be plastic and irreversible. Under plastic deformation, the real area of contact is given by (Bowden & Tabor 1964):-

$$A_r = \frac{F_n}{P_y} \qquad 2.3$$

where P_y is the yield pressure of the softer material.

Contact Physics and Chemistry

A surface represents an abrupt termination of solid structure giving rise to surface forces. The interaction with the environment leads to the formation of impurity and oxidation layers. For machined surfaces, other aspects, e.g. work hardened layers, surface texture and local stress fields are also important. As a result, the physical and chemical properties of the surface can differ from the bulk properties. The surface forces can lead to different interactions that can result in "interfacial bonding" and generation of "adhesive junctions" between the contacting surfaces.

2.1.2 Friction Processes

The static contact of two bodies under a pure normal force, F_n, on which a tangential force, F_t, is superimposed without causing macroscopic relative motion between the bodies, will modify the interfacial elastic and plastic contact deformation processes in several ways. Micro-displacement before sliding, increase in the contact area, which is usually referred to as "junction growth", and creation of elastic stresses and displacements are some of the examples. As the applied tangential force exceeds a certain value gross sliding between the contacting bodies occurs. Such sliding motion will result in sliding frictional forces. However, if an angular velocity is present between the two bodies, the frictional force generated is called rolling friction.

Sliding Friction

As the contact between two surfaces occurs only at discrete points, sliding friction can be considered as the interaction between the asperities of the two surfaces. The dissipation of energy occurs through creation and separation of micro-contact processes. These comprise elastic and plastic deformation of asperities, formation and destruction of adhesive junctions, and ploughing of softer surface by asperities of the harder surface.

Each of these partial processes involves a tangential force necessary to maintain the relative motion as well as a partial process of energy dissipation. Kragelski (1965) in a detailed study of the different causes of friction at a micro-contact suggested that the macroscopic friction force, $\mathbf{F_f}$, is given by:

$$F_f = \sum F_1 + \sum F_2 + \sum F_3 + \sum F_4 \qquad 2.4$$

where $\mathbf{F_1}$ is the resistance caused by an elastic displacement, $\mathbf{F_2}$ is the resistance caused by a plastic displacement, $\mathbf{F_3}$ is the resistance caused by ploughing of the material, and $\mathbf{F_4}$ is the resistance caused by shearing of the adhesive layers.

Ploughing Component of Sliding Friction

In the case of a very hard rough surface sliding over a soft one, the frictional resistance is mainly caused by the asperities of the harder surface ploughing through the softer one. Under such conditions, the coefficient of friction may be estimated from the force required for the plastic flow of the softer material. The normal load, $\mathbf{F_n}$, is balanced by the normal component of yield pressure, $\mathbf{P_{yn}}$, of the soft material acting via the real area of contact $\mathbf{A_r}$:-

$$\mathbf{F_n = A_r P_{yn}} \qquad 2.5$$

The resistance, $\mathbf{F_t}$, to the tangential motion is balanced by the yield pressure, $\mathbf{P_{yt}}$, of the soft material acting over the cross-sectional area of the groove, $\mathbf{A_g}$, (Figure 2.1):-

$$\mathbf{F_t = A_g P_{yt}} \qquad 2.6$$

Assuming that the plastically yielding material is isotropic, i.e. $\mathbf{P_{yn}=P_{yt}}$, the friction coefficient is given by:-

$$\mu = \frac{\mathbf{F_t}}{\mathbf{F_n}} = \frac{\mathbf{A_g}}{\mathbf{A_r}} \qquad 2.7$$

For the case of a conical indenter, as illustrated in Figure 2.1, it follows that

$$\mu = \frac{2}{\pi}\cot\phi \qquad 2.8$$

where ϕ is the semi-apex angle of the conical indenter for the plastic flow of the softer material.

Adhesion Component of Sliding Friction

Neglecting the effect of junction growth under a tangential force, the adhesive friction force is given by (Mitchell & Osgood 1976):-

$$\mathbf{F_f = A_r}\,\tau_s \qquad 2.9$$

and the coefficient of adhesive friction is given by

$$\mu = \frac{\mathbf{F_f}}{\mathbf{F_n}} = \frac{\tau_s}{\mathbf{P_y}} \qquad 2.10$$

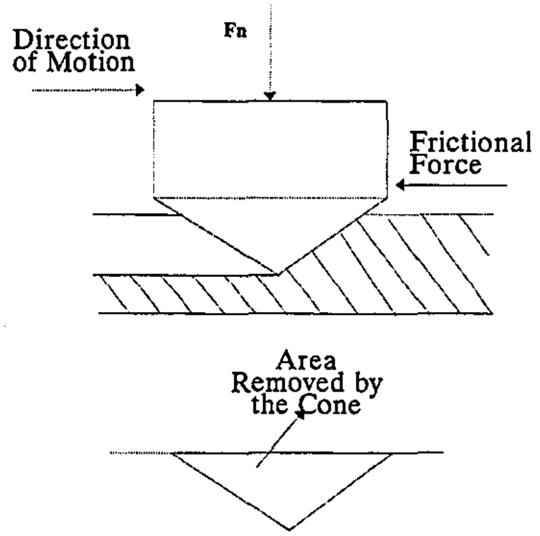

Figure 2.1 Linear wear model

where τ_s is the mean shear strength of the weakest adhesive plane. For metals that are not work-hardened, the mean shear strength, τ_s, of the interface is approximately equal to the critical shear stress of material **T**, and the yield pressure, P_y, has been shown to be approximately equal to 3**T** leading to a lower limit of 0.2 for μ.

Rolling Friction

Under rolling conditions, the forces acting at the interfacial plane are different from those present under sliding friction conditions. Due to these differences in kinematics, the contacting surfaces approach and separate in a direction normal to the interface rather than in a tangential direction. The main contributory processes are micro-slip, elastic hysteresis, plastic deformation, and adhesion effects. In the case of the rolling contact between two hard solids, the plastic deformation process is the dominant mechanism. It has been shown by Eldredge and Tabor (1955) that the rolling friction can be expressed empirically by

$$\mathbf{F_f} \propto \frac{\mathbf{F_n^{2/3}}}{\mathbf{r}} \qquad \mathbf{2.11}$$

where **r** is the radius of the rolling cylinder. In repeated rolling contact cycles, the above relationship does not hold. During subsequent rolling cycles the material is subjected to the combined action of residual and contact stresses. Further yielding is unlikely and a steady state may be reached in which the material is no longer stressed beyond its elastic limit. This process is known as "shake down". If rolling cylinders are subjected to loads in excess of the shake down limit a new type of plastic deformation occurs (Crook 1957; Hamilton 1963). For loads above the shake down limit continuous and accumulative plastic deformation is observed, whereas at loads below it, even though some yielding is caused initially, after a few cycles the system shakes down to an elastic cycle of stress deformations.

2.1.3 Dissipation of Energy

The dissipation of energy during a contact process can be divided into three main categories as follows:

1) Energy storage processes (generation of point defects and dislocation, strain energy storage),

2) Emission processes (phonons in the form of acoustic waves, photons in the form of tribo-luminescence),

3) Transformation to thermal energy (generation of heat and entropy).

The dissipation of energy by the first two processes is small in the majority of cases, and the bulk of the frictional energy is dissipated through thermal energy. An important feature of the generation of heat and the increase of the temperature of the contacting elements is its influence on the material properties of the friction partners which can, in turn, affect the tribological behaviour of the system. The temperature rise can take the form of a bulk temperature rise, temperature gradients and, more importantly, in often steep local temperature rises usually referred to as "flash temperatures". Theoretical treatment of the flash temperature problem can be found in Carlslaw & Jaege (1947), Holm (1948) and Blick (1937). These theories were combined by Archard (1958) to provide a simpler model. The distribution of heat into the two interacting bodies is also important and has been found to depend on the geometry, as well as physical properties of both bodies (Kounas et. al. 1972).

2.1.4 Wear Processes

Wear can be defined as the progressive loss of substance from the surface of a body, occurring as a result of friction. The wear process may involve the transfer of material from one partner to another, or to the environment. Two macroscopic rules of wear can be stated:-

1) the wear rate, **W**, i.e. the volume, **V**, of material removed per unit of sliding distance, **L**, is proportional to the normal load, $\mathbf{F_n}$:-

$$\mathbf{W} = \frac{\mathbf{V}}{\mathbf{L}} \propto \mathbf{F_n} \qquad \mathbf{2.12}$$

2) the wear rate, **W**, is independent of the apparent area of contact.

These macroscopic rules can be explained using a microscopic model of wear. The essential concept, as summarized by Archard (1958), is that the worn volume, **V**, produced in sliding a distance, **L**, can be related to the true area of contact, $\mathbf{A_r}$. Archard considered a unit wear event as the establishment of an area of contact considered to be a circle of radius **r** and area ΔA. He assumes that in sliding a distance **ΔL =2r**, a hemispherical particle of radius **r** and volume **ΔV** is generated. He suggested that not every unit event results in the formation of a wear particle. Introducing a probability factor, **k**, and summing over all micro-contacts, the total wear rate is:-

$$\frac{\mathbf{V}}{\mathbf{L}} = \frac{\mathbf{1}}{\mathbf{3}} \mathbf{k}\, \mathbf{A_r} \qquad \mathbf{2.13}$$

A_r is proportional to the normal load, $\mathbf{F_n}$, therefore it follows that

$$\mathbf{V \propto k F_n L} \qquad \mathbf{2.14}$$

as observed experimentally in many situations of dry wear of metals under steady state.

2.1.5 Classification of Wear Processes

Several classification schemes have been suggested. If the types of the relative motion between the interacting bodies are considered, sliding, rolling, fretting and impact wear modes can be distinguished. However, in real systems, the wear can be due to a combination of these modes, and traditionally wear is divided into 4 different mechanisms:- adhesive, abrasive, erosive or impact, and surface fatigue mechanisms (Burwell 1957). Table 2.1 summarizes these mechanisms and types of motion and surface appearance commonly associated with them.

Table 2.1 Classification of Wear

Wear Process	Relative Motion	Surface Appearance
Surface Fatigue	Sliding, Rolling, Impact, Fretting	Cracks, Pits
Abrasion	Sliding, Rolling, Impact	Scratches, Grooves
Adhesion	Sliding, Rolling	Cones, Flakes, Pits
Erosion	Flow	Cavitation, Grooves

<u>Surface Fatigue Wear Mechanism</u>

The effect of fatigue wear is normally associated with repeated stress cycling in rolling or sliding contacts. In fatigue wear, even moderate levels of alternating cycles of tension and compression stress can cause total material failure. Bayer et al (1962) carried out an extensive programme of research into the sliding wear and its contribution to surface fatigue. They identified two stages:- the "zero wear stage" during which the wear does not exceed half the original peak-to-valley height; and the " measurable wear stage" during which wear scar grows progressively. According to this theory, the cross section area of wear scar, **dA**, is given by:

$$\mathbf{dA} \propto (\tau_{max} \mathbf{L})^{9/2} \qquad \mathbf{2.15}$$

where τ_{max} is the maximum shear stress, and **L** is the pass length. The experimental observation of surface fatigue indicates that the mechanism is closely related to the stress concentration effects that govern crack initiation and propagation (Hornbogen 1975).

Adhesive Wear Mechanism

In adhesive wear, material interaction between the two surfaces is of primary importance. In contrast to the other wear mechanisms, adhesive wear can rapidly progress to severe forms of failure. "Scuffing" "galling" or "seizure" of moving parts due to "cold-welded" junctions are some of the features of adhesively worn surfaces.

To consider the physical mechanism of adhesive wear, the process of adhesion and fracture must be taken into account. The influence of the environment and surface contamination are also very considerable. Landheer and Zaat (1974) emphasized that sever forms of adhesion lead to the formation of an adhesive junction where, as a result of shear resistance in the boundary region, a field of iso-strain lines (plastic strain) moves through the metal in a direction opposite to the sliding friction, so that metal accumulates in the junction enlarging the surface boundary. This is followed by cracking of the metal at the rear side of the junction, by which material detaches. Stolarski (1990) proposed a model for adhesive wear based on the statistical properties of rough surfaces:-

$$\mathbf{V} = (1+3\mu)^{1/2} (\mathbf{k_e A_e} + \mathbf{k_p A_p})\mathbf{L} \qquad \mathbf{2.16}$$

where V is the wear volume, μ is the coefficient of friction, $\mathbf{k_e}$ is the wear factor characteristics of non-welded junctions, $\mathbf{A_e}$ is the elastic area of contact, $\mathbf{k_p}$ is the wear factor for welded junctions, $\mathbf{A_p}$ is the plastic area of contact and **L** is the sliding distance.

Impact Wear

Impact wear is mainly associated with erosive wear mechanism. Erosion can be defined as the wear due to stream of particles abrading a surface due to impact at shallow angles. It can be divided into two modes:- pure impact wear, and compound impact wear (Engel 1976). Compound impact wear is defined as the wear due to a normal particle blow combined with relative sliding on the worn surface. The severity of wear resulting from compound impact wear is found to be higher than that in pure impact, or pure sliding wear. Engel (1976) presented the results of a number of test series investigating the influence of sliding speed on the wear scar in several materials. In all cases, an increase in the wear process was observed with introduction of sliding and as the speed of sliding increased. The dependence of impact wear on hardness of the wearing surface is more complex during compound impact wear than that in the impactless abrasion or pure impact wear. Under this wear regime, the wear resistance of the surface rises initially in proportion with its hardness then remains constant, and finally drops as the hardness is further increased (Khruschov 1974).

Abrasive Wear

Abrasive wear processes is one of the main causes of material loss in industry and agriculture. It has been estimated that about 50% of all wear situations encountered in industry are due to abrasion (Eyre 1976). It occurs in contact situations in which one material is considerably harder than the other. The harder surface asperities press into the softer surface and cause plastic flow around the pressing asperities. When a tangential motion is imposed, the movement of the harder surface will cause ploughing and material removal from the softer material.

The linear wear model is the generally accepted quantitative model used for the analysis of abrasive wear (Rabinowicz 1965). In this model an abrasive asperity is approximated by a cone that ploughs out and removes material from the counter face. If the load, ΔF_n, on the indenter is only supported over the leading half of the contact and is balanced by the yield pressure, P_y, of the counter face acting via the contact area, A_r, it follows that:-

$$\Delta F_n = A_r P_y \tag{2.17}$$

$$\Delta F_n = \frac{d^2}{8} \pi P_y \tag{2.18}$$

The volume of material, ΔV, removed in sliding a distance, ΔL, is given by:-

$$\Delta V = \frac{d^2}{4} \Delta L . \cot \phi \tag{2.19}$$

substituting for **d** from above it follows that:

$$\frac{\Delta V}{\Delta L} = \frac{2 \cot \phi}{\pi P_y} \Delta F_n \tag{2.20}$$

and assuming that only a proportion, **k**, of all the contacts produce worn particles, it follows that

$$\frac{\Delta V}{\Delta L} = k \frac{2 \cot \Phi}{P_y} \Delta F_n \tag{2.21}$$

where $\cot\Phi$ is the average of all possible values of $\cot \Phi$. If the yield pressure is assumed to be equal to the indentation hardness, **H**, the last equation can be written as:

$$V = k \frac{F_n L \cot \Phi}{H} \tag{2.22}$$

This simple model, however, is unable to explain a great amount of the experimental observations. Over the years, a large number of models have been suggested to close the gap between theory and experimental data (Zum Gahr 1988; Torrence 1980).

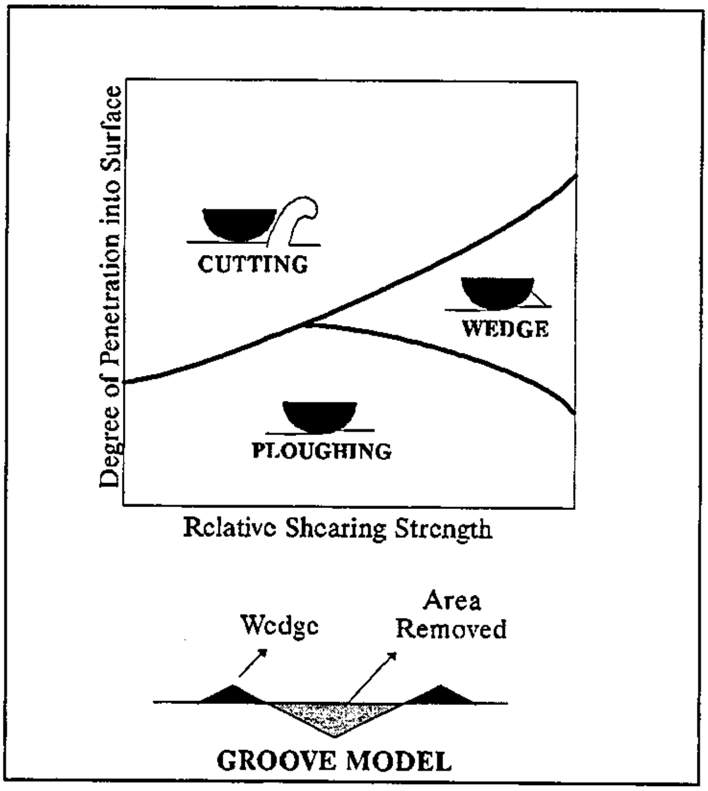

Figure 2.2 Transformation between different mechanisms of abrasive wear (Hokkirigawa & Kato 1989)

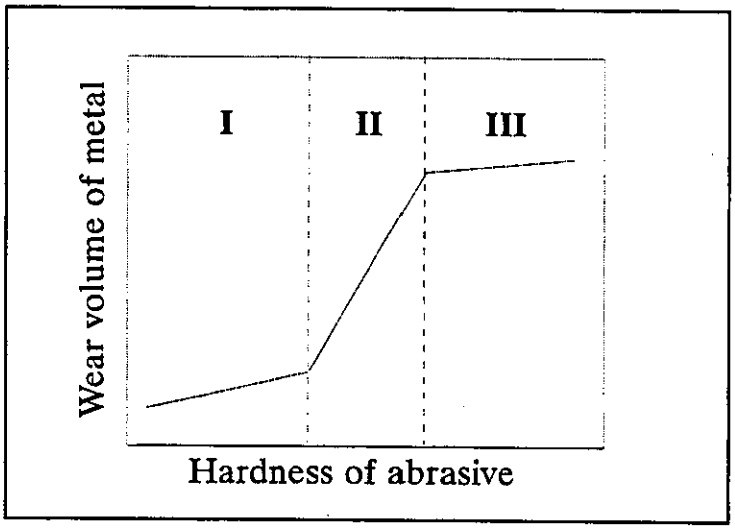

Figure 2.3 Influence of abrasive hardness on wear (Khruschov 1957)

Jacobson et al (1988) used a statistical method to analyze the multiple abrasive grooving of a surface with realistic topography. The model can predict the influence of grit size effect, load and hardness on wear. A number of alternative models are based on the analysis of repeated plastic deformation of the surface.

The model suggested by Hokkirigawa and Kato (1989) is based on the microscopically observed wear mechanisms of material removal in abrasion, namely ploughing, wedge forming, and cutting. The groove model used incorporates the effect of material built up in front and the sides of the grooves. The groove model and the transformation from one process to another are shown in Figure 2.2. To describe the wedge forming and cutting modes of abrasive wear, they introduced several factors and suggested the relationship:-

$$\mathbf{V} = \frac{\phi_{\mathbf{eff}}}{\mathbf{k}\psi}\left(\frac{\alpha_{\mathrm{w}}\beta_{\mathrm{w}}}{\mu_{\mathrm{w}}^{2}} + \frac{\alpha_{\mathrm{c}}\beta_{\mathrm{c}}}{\mu_{\mathrm{c}}^{2}}\right)\frac{\mathbf{F_n L}}{\mathbf{H}} \qquad \mathbf{2.23}$$

where **V** is wear volume, $\mathbf{F_n}$ is normal load, **H** is hardness, ϕ_{eff} is the proportion of effective asperities, **k** and ψ are shape factors of asperities, α_w, β_w, and μ_w are the factors describing wedge formation mode of abrasion, and α_c, β_c, μ_c are the factors describing cutting mode of abrasion. Wang and Wang (1988) suggested a model based on accumulated plastic flow to failure caused by repeated indentation of the worn surface by abrasive particles. They also introduced a number of coefficients to represent different variables affecting the wear volume, **V**:-

$$\mathbf{V} \propto \frac{\mathbf{F_n L}\left(1+\mathbf{H_m}\dfrac{\mathbf{K}}{\mathbf{2E}}\right)^{2}}{\mathbf{H_m}\,\pi\tan\theta} \qquad \mathbf{2.24}$$

where θ is the indentation angle, $\mathbf{H_m}$ is the material hardness, **E** is the Young's modulus and **K** is a coefficient moderating the influence of hardness.

Apart from the mechanical properties of the wearing surface, several other variables can affect wear that are not considered in the above models. In his classical study of abrasive wear, Khrushchov (1957) showed that volumetric wear depends on the hardness of abrasive particle, $\mathbf{H_a}$, as well as that of abraded material, $\mathbf{H}$, leading to three distinct wear regimes (Figure 2.3):-

1) a low-wear regime where $\mathbf{H_a} < \mathbf{H}$
2) a transitional regime where $\mathbf{H_a} \approx \mathbf{H}$
3) high- wear regime where $\mathbf{H_a} > \mathbf{H}$.

In a later study Khrushchov and Babichev (1960) concluded that the abrasive wear was independent of abrasive hardness when this was very much greater than the hardness of the wearing material. This conclusion was challenged by Nathan and Jones (1966) who found that even with very hard abrasives the volumetric wear still depends on abrasive hardness. This conclusion has been confirmed by other studies and is now generally accepted to be correct. Other important factors affecting the volume of wear are abrasive size and shape (Rabinowicz & Mutis 1965), tribo-induced temperatures (Moore 1971), and "surface physics and chemistry".

As discussed earlier, the interaction with the environment leads to the formation of impurity and oxide layers whose wear properties may vary from the bulk material. The presence of chemically active agents in the abrading material can result in accelerated wear due to synergistic action of abrasion and corrosion (Batchelor & Stachowiak 1988). The effect of the factors related to surface physics and chemistry is usually time-dependant. Lin and Cheng (1989) studied the time behaviour of wear and suggested a model which permits the wear rate to be dependent on time. Figure 2.4 shows two typical wear-time functions. It shows the running-in, the steady state and accelerated wear regimes. In materials with work hardening properties a curve similar to Figure 2.4b is commonly observed. Lin and Cheng suggested that the accelerated mode can be attributed to a number of factors including an increase in surface temperature or a transformation in the dominant mechanism of material removal. Abrasive wear is traditionally divided into two processes, two-body and three-body abrasive wear. Two-body abrasive wear refers to situations where only two contacting surfaces, one abrasive and one abrading. In Two-body abrasive wear, the abrasive particles are usually introduced intentionally to remove material from the wearing surface. Typical examples of two-body abrasion can be found in surface machining and finishing. Three-body abrasive wear involves two wearing surfaces with loose abrasive particles between them.

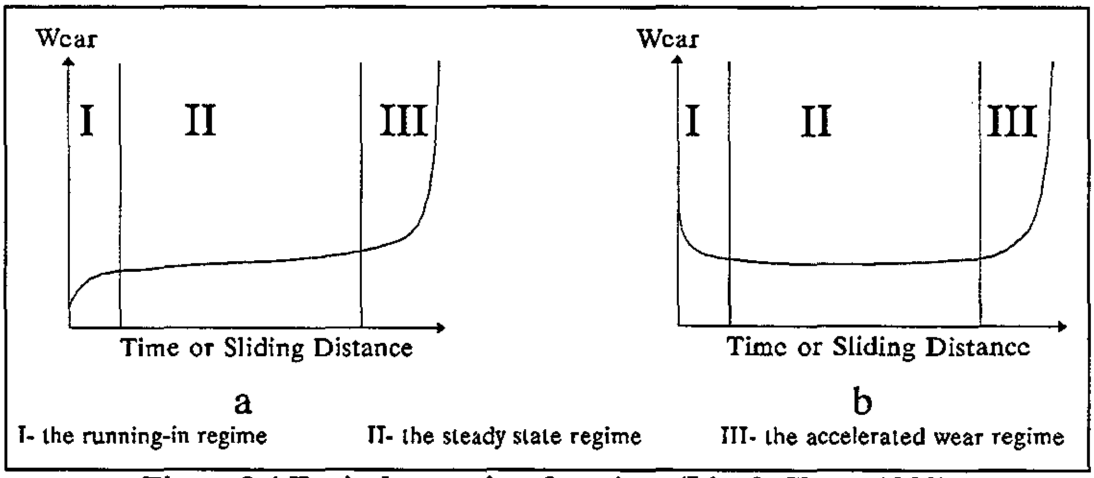

Figure 2.4 Typical wear-time functions (Lin & Cheng 1989)

Misra and Finnie (1980) considered the different types of abrasive wear and suggested a useful classification given in Figure 2.5. According to this classification, three-body abrasive wear can be divided into closed three-body abrasion and open three-body abrasion. Closed three-body abrasion is usually associated with the intrusion of abrasive particles between two very close surfaces, e.g. in bearings. This type of wear can usually be eliminated by using various preventive measures like seals or by flushing, etc. In contrast, open three-body abrasion is an inherent feature of the system and cannot be avoided completely. It is associated with wear of one or two surfaces of moderate separation by abrasive particles which can move relative to each other as well as rotating and sliding over the wearing surfaces. Depending on the nature of the forces involved, open three-body abrasion can be divided into three regimes:-

1) Gouging: usually associated with processes where high impact forces are present leading to impact abrasive wear (Sorokin et. al. 1991) which results in a rapid loss of material.

2) High-stress: here the contact forces involved are high enough to crush the abrasive particles and may include some impact component.

3) Low-stress: in this regime the contact forces are low and do not cause major crushing.

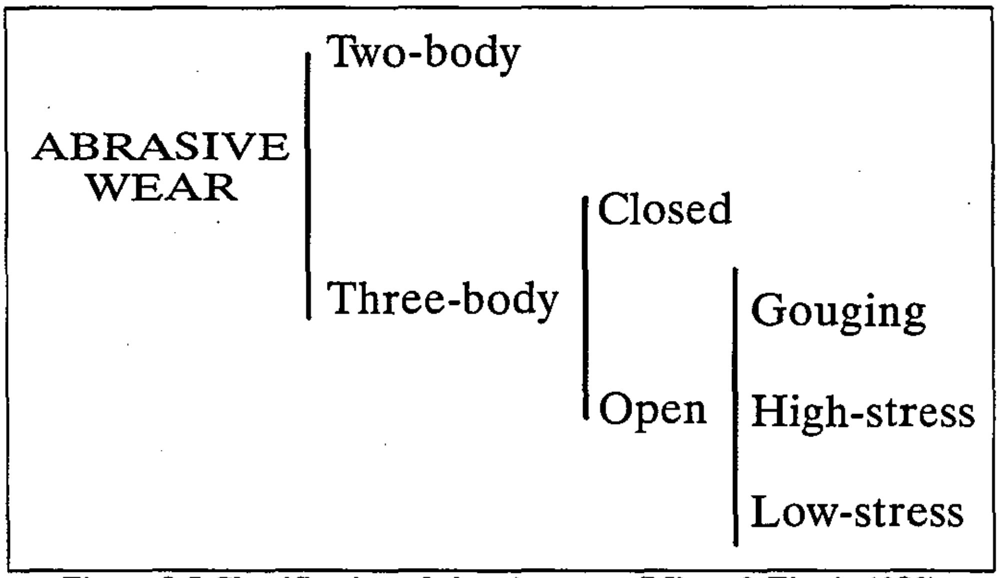

Figure 2.5 Classification of abrasive wear (Misra & Finnie 1980)

Rabinowicz et. al.(1961) carried out the first detailed study of three-body wear and showed that under identical loading conditions, about an order of magnitude less wear occurred in closed three-body abrasion compared with that in two-body abrasion. This was confirmed by the results obtained by Misra and Finnie (1980). In three-body abrasion, the relationship between material hardness and weight loss is more complicated than that in two-body abrasion (Fang et.al. 1991). In high-stress regime, where the abrasive particles are crushed, other mechanical properties of the abrasive material must be also taken into account (Bond 1964; Atkinson & Cassapi 1989).

2.1.6 Abrasive Wear in Rock and Minerals Processing

The majority of wear situations encountered in the minerals processing industry can be classified as open three-body abrasion. The main wear resistant material used in various crushing plants is steel. The wear caused by different rocks and minerals varies considerably. The evaluation of abrasivity of natural rocks and minerals is of major importance to the operators of plants and machinery, and over the years a number of tests have been designed for this purpose. However, the matter is far from being straightforward or conclusive. The result is very much dependant on the test conditions, in terms of the applied loads and the relative motion between abrasive and wearing surfaces. The International Society of Rock Mechanics (ISRM) Commission on Standardization of Laboratory and Field Tests (1978) in their report on "Suggested methods for Determining Hardness of Rocks" distinguishes between tests suitable for abrasive wear due to impact, attrition and pressure. Generally, the tests can be divided into two groups:- (a) tests for the measurement of hardness or relative abrasivity of rocks and minerals; and (b) tests for evaluation of wear in a specific plant or process.

2.1.7 Methods of Measuring Rock Hardness

The suggested tests are based on the unsound assumption that the relative abrasivity of a rock is a function of its hardness. The tests, summarized by Atkinson and Cassapi (1989), fall into two categories. In the first category a petrological approach is adopted. The percentage presence of each mineral group in the rock is found by a petrological analysis and the hardness of the whole rock is worked out by multiplying the Moh's hardness number, or the Rosiwal scale of hardness number, proportionally for each individual mineral.

In the second category, mechanical methods of measuring rock hardness are used. These include the use of penetrometer hardness tests (Vickers, Brinnell, Rockwell), the Cone Indenter hardness test, Shore Sclerescope rebound test and the Schmidt impact hammer test. Depending on the technique used, these tests provided information on either local (penetrometer and indenter tests) or bulk hardness of rock. However, the information provided by the above tests on the hardness of rock is of limited value. Apart from hardness, the relative abrasivity of rocks is affected by other petrological properties including the grain size, the angularity of the grains (Atkinson & Cassapi 1989) and other salient mechanical properties as will be discussed in future chapters.

Tests for Measurement of Rock Abrasiveness

A number of tests have been specifically designed to measure the abrasivity of rock. In such tests, the abrasion of a standard test surface after a specific action against the rock is measured. The tests include the Cerchar test (Atlas Copco 1981), the Hacksaw test and the steel cube test.

The Cerchar Abrasivity Index test has been widely used to measure the abrasivity of different types of coal and natural rocks. It is a straightforward test involving the abrasion of a metal pin after scratching over the freshly broken surface of rock. A number of researchers have investigated the relationship between the Cerchar Index and other rock properties. Suana and Peters (1982) examined the possibility of deducing the index from the petrology of rock and concluded that the technique over-rates the abrasivity index of hard rocks and under-rates that of the softer rocks. Most under-rated cases were found to be rocks consisting of abrasive mineral grains cemented in a soft matrix. They also found that for the Cerchar test to be reliable the grain size of the rock should be below one millimetre. Atkinson and Cassapi also examined the test and found that it gave consistent results with fine to medium grained competent rocks, but was unreliable with weak and unconsolidated materials (Atkinson & Cassapi 1989). West (1986) investigated the relationship between the Cerchar Abrasivity Index, Moh's hardness number, and the quartz content in a number of rocks. His results are shown in Figure 2.6. He concluded that for the rocks tested a good relation exists between the quartz content and the Cerchar Abrasivity Index.

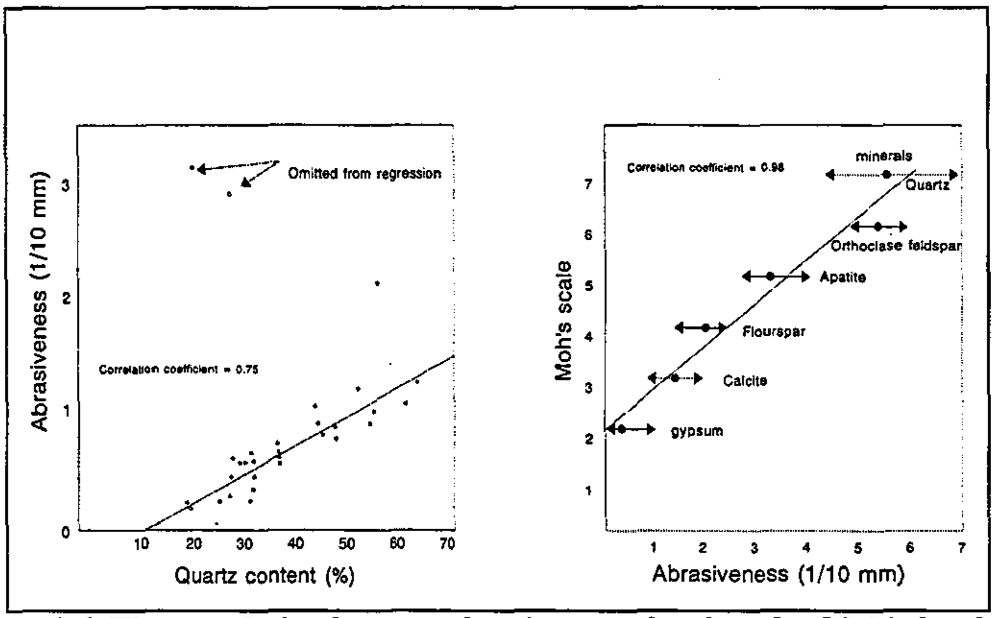

Figure 2.6 The correlation between abrasiveness of rock and a. Moh's hardness and b. quartz content (West 1986)

Table 2.2 Effect of Rock Properties on Wear

Rock	Compressive Strength MPa	Silica Content %
Bunter Sandstone	30-40	80
Little Whin Sill (Dolerite)	300	circa 1

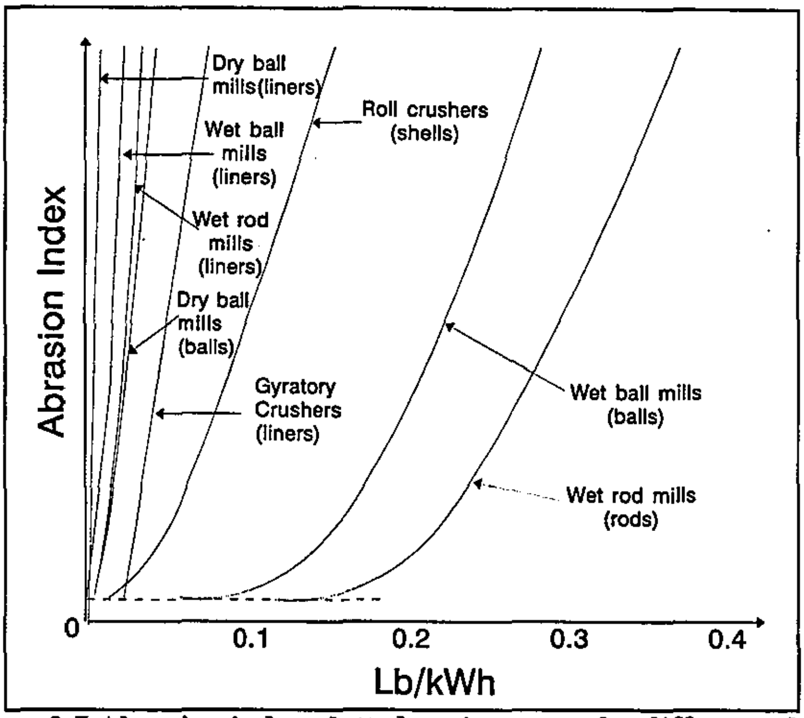

Figure 2.7 Abrasion index plotted against wear for different plants (Bond 1964)

Table 2.3 Average Abrasion Index Values For Different Rock Types (Bond 1964)

Material	Number of Tests	Specific Gravity	Abrasion Index A_i
Dolmite	5	2.70	0.0160
Shale	5	2.62	0.0209
L.S. for Cement	14	2.70	0.0238
Limestone	9	2.7	0.0320
Cement Clinker	8	3.15	0.0713
Magnesite	3	3.00	0.0783
Heavy Sulfides	10	3.56	0.1284
Copper Ore	24	2.95	0.1472
Hematite	7	4.17	0.1647
Magnetite	2	3.72	0.2217
Gravel	4	2.68	0.2879
Trap Rock	20	2.80	0.3640
Granite	11	2.72	0.3880
Taconite	7	3.37	0.6237
Quartzite	3	2.70	0.7751
Alumina	7	3.90	0.8911

Silica (quartz) content is often regarded as a measure of the abrasiveness of a rock, but this can lead to erroneous predictions. Table 2.2 shows two rock types of very different silica content, but of similar abrasiveness during excavation. In the rock with small silica content the high compressive strength causes high wear (Atkinson & Cassapi 1989).

Tests Simulating Open Three-Body Abrasive Wear Process

A number of test methods simulating the different types of open three-body abrasive wear in rock and mineral processing have been suggested. One of the earliest abrasion testers was designed by Bond (1964) which best reflects the conditions inside rod and ball mills. Bond used the tester to measure the abrasion index of a comprehensive number of rock types. Table 2.3 shows his results for average abrasion index values of different rock types. Figure 2.7 shows the abrasion index plotted against the normalized metal as observed in different crushers and mills. The results indicate the significance of plant's mechanical characteristics and kinematics on wear under otherwise similar conditions.

Spero et. al. (1991) presented a comprehensive review of test methods used in ore grinding. They used the concept of wear susceptibility, **B**, and wear coefficient, **k**, to compare the laboratory and field test results. The concept of wear susceptibility was suggested by Blickensderfer (1988) and is defined as the volume of material removed per unit of energy applied, **B=dV/dE,** which is dependant on the physio-mechanical properties of the abraded surface and abrasive particle as well as the environmental factors. Spero et. al. concluded that a reasonable correlation is observed between laboratory and production mills having similar values of the parameters **k** and **B**. They also suggested that a more fundamental understanding of the mechanistic processes involved in each case is required to establish more definitive correlations. The importance of such understanding of test conditions is an issue raised by a number of other authors (Macmillan 1989).

A number of other workers have studied the variables affecting wear in various mineral processing plants. These include an investigation of wear of digger teeth (Mashloosh et. al. 1984); the effect of abrasive sandstone present in coal on plant wear (Durning & Earle 1992), and an evaluation of material requirements for minimization of wear in mineral processing (Blickensderfer et.al. 1984).

In all the tests mentioned above, a close monitoring of the environmental parameters during the course of the test is lacking. The impact of tribo-induced temperatures and humidity on rate of abrasive wear is considerable. In the majority of cases, authors of published results fail to specify the test conditions with regards to these parameters. This failure renders any attempt to compare or correlate such experimental data susceptible to error. Furthermore, other than tests simulating a particular process, they only provide a rough guide on relative abrasive properties of various rock types. The use of specific testing rigs to simulate the tribo-mechanical conditions present in a particular plant is much more reliable. However, the results are only valid if attention is given to the effect of operational parameters, e.g. gap between wearing surfaces, speed of moving elements, applied loads, and abrasive size.

Borik and Sponseller (1971 a; 1971 b) used a laboratory size jaw crusher to investigate the wear resistance of different types of steel to gouging wear. They also investigated the effects of crusher setting, tribo-induced temperatures, hardness, and rock properties on the wear. Their results are highly relevant to the current study and will be further discussed in Chapter 3.

2.2 Modelling of Wear, Statistical and Fuzzy Techniques

The methods chosen for analysis of experimental data is an important and integral part of any study that involves empirical model building and model exploitation. It forms an integral part of the experimental design process that in turn must be appropriate to the phenomenon under study. Generally, three broad category of techniques are available. First, purely physical or mechanistic models are appropriate in situations where the prior knowledge of a system or phenomenon is sufficient to allow the deduction of a model. Second, statistical models appropriate in situations where no such knowledge is available but a reliable and well defined relationship between the output and system variables are expected. Third, Fuzzy modelling suitable in situations where due to uncontrollable conditions the output and system variables are either difficult to measure or subject to measurement errors.

Predictive analysis of wear in cone crushers require a combination of all three techniques. The parameters affecting the liner wear are varied and, as will be discussed in later chapters, fall in different groups. Operational parameters can be effectively determined and therefore their effect on wear could be formulated using a statistical approach. Environmental parameters on the other hand are not easily quantifiable and require a non-deterministic approach.

Statistical model building is an extended and well established branch of research (Box & Draper 1986; Weisberg 1985), the review of which is well beyond the scope of this chapter. However, the general background into the Response Surface methodology, the statistical technique chosen in the present study, is described.

2.2.1 Statistical Analysis and Modelling

Analysis of Variance

Analysis of Variance (ANOVA) is the main statistical technique used to study empirical results. The method provides a statistically based comparison tool for detecting the effect of different factors and their interaction by decomposing the observed output variation into accountable sources. Two factors, **A** and **B**, are said to interact (in their effect on the response) if the effect of **A** is different at different levels of **B**. For an experimental design involving three factors, a "three-way" ANOVA analysis is carried out that would reveal the variation due to: a) each of the three variables, b) the interaction between the variables and c) the experimental error. Using the Least Square Technique the total variation is given by:

$$SS_T = \sum_{i=1}^{N} y_i^2 - \frac{T^2}{N} \quad 2.25$$

where

SS_T	square of total output variation,
y_i	ith observed output,
T	sum of all observed outputs,
N	number of experimental runs.

An equation for total variance can be written in this case:

$$SS_T = SS_A + SS_B + SS_C + SS_{A\times B} + SS_{B\times C} + SS_{A\times C} + SS_{A\times B\times C} + SS_e \quad 2.26$$

where

$SS_{A,B,C}$	variation due to different variables,
$SS_{A\times B}$	variation due to interaction between A and B,
$SS_{B\times C}$	variation due to interaction between B and C,
$SS_{A\times C}$	variation due to interaction between A and C,
$SS_{A\times B\times C}$	variation due to interaction between A and B and C,
$SS_{e.}$	variation due to error.

The variation due to factor **A** is given by:

$$SS_A = \frac{(T_{A_1} - T_{A_2})^2}{N} \quad 2.27$$

where T_{A1} and T_{A2} are the total sums of observations with level 1 and level 2 of the factor A respectively. The variation due to factor **B** is given by:

$$SS_B = \frac{T_{B_1}^2}{n_{B_1}} + \frac{T_{B_2}^2}{n_{B_2}} + \frac{T_{B_3}^2}{n_{B_3}} - \frac{T^2}{N} \quad 2.28$$

where T_{B1},T_{B2} and T_{B3} are the total sums of observations with level 1 and level 2 and level 3 of the factor **B** respectively. The variation due to factor **C** can be calculated by:

$$SS_C = \frac{(T_{C_1} - T_{C_2})^2}{N} \qquad 2.29$$

where T_{C1} and T_{C2} are the total sums of observations with level 1 and level 2 of the factor **C** respectively. To calculate the interaction between A and B; B and C; and A and C the data must first be summed within possible combinations:

$$SS_{A\times B} = \sum_{i=1}^{k_A \times k_B} \frac{T^2_{(A\times B)_i}}{n_{A\times B_i}} - \frac{T^2}{N} - SS_A - SS_B \qquad 2.30$$

$$SS_{A\times C} = \frac{[(T_{A_1\times C_1} + T_{A_2\times C_2}) - (T_{A_1\times C_2} + T_{A_2\times C_1})]^2}{N} \qquad 2.31$$

$$SS_{B\times C} = \sum_{i=1}^{k_A \times k_C} \frac{T^2_{(A\times C)_i}}{n_{B\times C_i}} - \frac{T^2}{N} - SS_B - SS_C \qquad 2.32$$

$$SS_{A\times B\times C} = \sum_{i=1}^{k_A \times k_B \times k_C} \frac{T^2_{(A\times B\times C)_i}}{n_{(A\times B\times C)_i}} - \frac{T^2}{N} - SS_A - SS_B - SS_C \qquad 2.33$$

Error can be determined by finding the remainder of the total variation left from the known sources:

$$SS_e = SS_T - SS_A - SS_B - SS_C - SS_{A\times B} - SS_{A\times C} - SS_{B\times C} - SS_{A\times B\times C} \qquad 2.34$$

Another concept used in the study is degrees of freedom. One degree of freedom in a statistical sense is associated with each piece of information that is estimated from all the data. For the considered three-way ANOVA, the total degrees of freedom is given by:

$$\nu(T) = N - 1 \qquad 2.35$$

and the degrees of freedom associated with each factor is:

$$\nu(F) = k_F - 1 \qquad 2.36$$

where $\mathbf{v(F)}$ and $\mathbf{k_F}$ are the degrees of freedom and the number of levels associated with factor $\mathbf{F}$ respectively. For interacting factors, $\mathbf{F_1}$, $\mathbf{F_2}$,..$\mathbf{F_n}$, the degrees of freedom are given by

$$\nu(\mathbf{F_1} \times \mathbf{F_2} \times .. \mathbf{F_n}) = \nu(\mathbf{F_1}) \times \nu(\mathbf{F_2}) \times .. \nu(\mathbf{F_n}) \qquad 2.37$$

the degrees of freedom associated with the error is thus given by

$$\nu(\mathbf{e}) = \nu(\mathbf{T}) - \sum \nu(\mathbf{F}) - \sum \nu(\mathbf{int.}) \qquad 2.38$$

Finally the variance, **V**, and the standard deviation, **S**, are given by

$$\mathbf{V} = \frac{\mathbf{SS_e}}{\nu(\mathbf{e})} \qquad 2.39$$

$$\mathbf{S} = \sqrt{\mathbf{V}} \qquad 2.40$$

Response Surface Multiple Regression Theory

Response surface methodology comprises a group of statistical techniques used for empirical model building and model exploitation, adopted for the modelling of the wear experimental data. It uses the Least Square data analysis techniques to fit a polynomial to the observed data. In general the polynomial takes the form:

$$\mathbf{y(x,\beta)} = \beta_0 + (\beta_1 x_1 + \beta_2 x_2 + .. \beta_n x_n) + (\beta_{11} x_1^2 + \beta_{22} x_2^2 + \beta_{12} x_1 x_2 + ..) + (\beta_{111} x_1^3 + \beta_{222} x_2^3 + \beta_{112} x_1^2 x_2 + ..) + ... \qquad 2.41$$

where the bracketed terms are of the same order. The appropriateness of a fitted model is investigated using a number of tests that originates from the Analysis of Variance to divide variability as discussed in the previous section, and to compare models that include different sets of variables. In the overall analysis of variance, the simplest model, i.e. that with only one variable, can be compared sequentially with models of higher degrees. The appropriateness of including an additional variable in the model relies on the criteria

$$\mathbf{SS_T} > \mathbf{SS_e} \qquad 2.42$$

and for the difference between the two, denoted $\mathbf{Ss_{reg}}$,

$$\mathbf{SS_{reg}} > \mathbf{SS_e} \qquad 2.43$$

to be larger for the larger model. The difference between the two SS_{reg} values corresponds to the sum of squares of y explained by the larger model that is not explained by the smaller one. The reliability of statistical models can be tested by a variety of tests (Box & Draper 1986) according to the particularity of a given model. The statistical tests used in the present study will be described in Chapter 4.

2.2.2 Fuzzy Modelling Technique- Basic Theory

The Fuzzy Set Theory put forward by Zadeh (1965, 1975, 1988) was originally motivated by the observation that traditional mathematics and binary logic (true/false) with their emphasis on precision were ill-suited for modelling a large section of our everyday experiences that involve "soft, nonquantifiable" systems. In industry, it provides a robust technique for accommodating measurement uncertainty and error contaminated signals, and a proven technology for representation of heuristic knowledge and automation of subjective manual operations (Dutta 1993).The fundamentals of the Fuzzy mathematics are based on Fuzzy sets or variables (such as big, small, very tall) and Fuzzy operators (such as AND, OR, THEN) which manipulate the Fuzzy variables (Zadeh 1992).

Fuzzy Variables and Membership Functions

A Fuzzy set **F** of a universe of discourse **U**={**x**} is defined by a mapping or membership function $\mu_F(\mathbf{x})$:**U** (0,1) by which each **x** is assigned a number between 0 and 1 indicating the extent to which **x** has the attribute **F**. Figure 2.8a shows the membership function $\mu_{small}(\mathbf{x})$. The Fuzzy variables medium and large are also shown. Figure 2.9 shows a number of other possible shapes of Fuzzy sets.

Fuzzy Operations

Given the Fuzzy sets **A** and **B** the basic operations on **A** and **B** are

1. The complement (NOT) $\bar{\mathbf{A}}$ of **A**, defined by

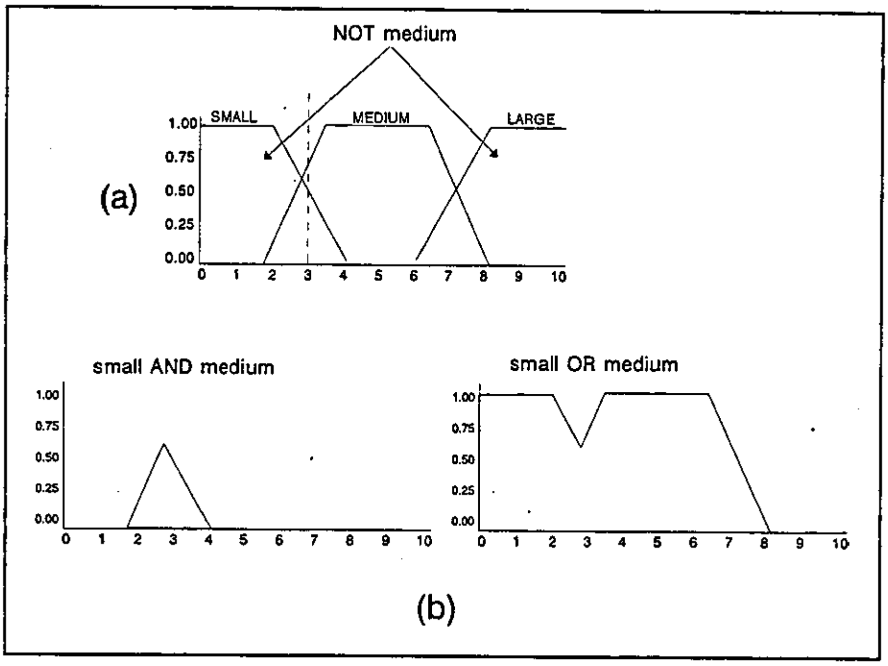

Figure 2.8 a. Three Fuzzy membership functions b. Fuzzy operations

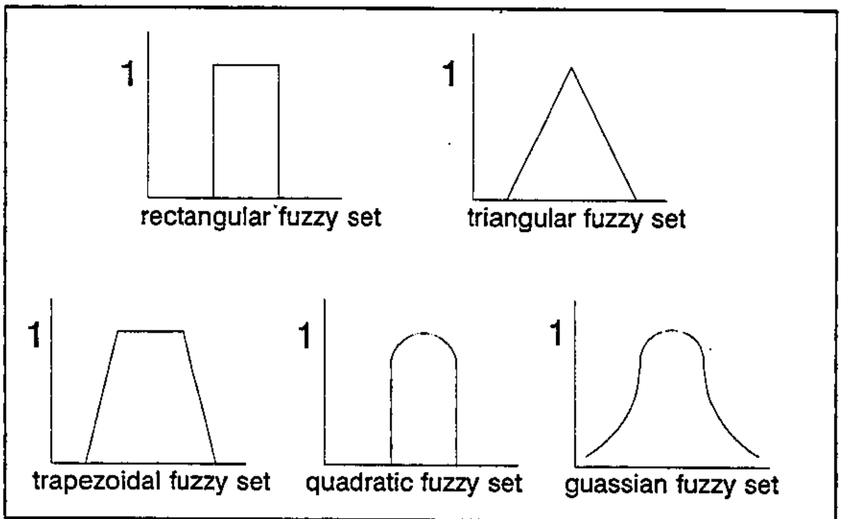

Figure 2.9 A number of possible Fuzzy sets

$$\mu_{\bar{A}}(x) = 1 - \mu_A(x) \qquad 2.44$$

2. The union (OR) **A** ∪ **B** of **A** and **B**, defined by

$$\mu_{A\cup B}(x) = \max[\mu_A(x), \mu_B(x)] \qquad 2.45$$

3. The intersection (AND) **A**∩ **B** of **A** and **B**, defined by

$$\mu_{A\cap B}(x) = \min[\mu_A(x), \mu_B(x)] \qquad 2.46$$

Fuzzy Relationships

A Fuzzy relationship between two or more Fuzzy variables may be used to define Fuzzy rules of the general format:-

IF **A** is $\mathbf{A_i}$ AND **B** is $\mathbf{B_j}$ THEN **C** is $\mathbf{C_k}$

The inference of such rules is defined by the Fuzzy phrase μ_P (A,B,C) given by:-

$$\mu_{A_i\times B_j\times C_k}(A,B,C) = \min[\min[\mu_{A_i}(A), \mu_{B_j}(B)], \mu_{C_k}(C)] \qquad 2.47$$

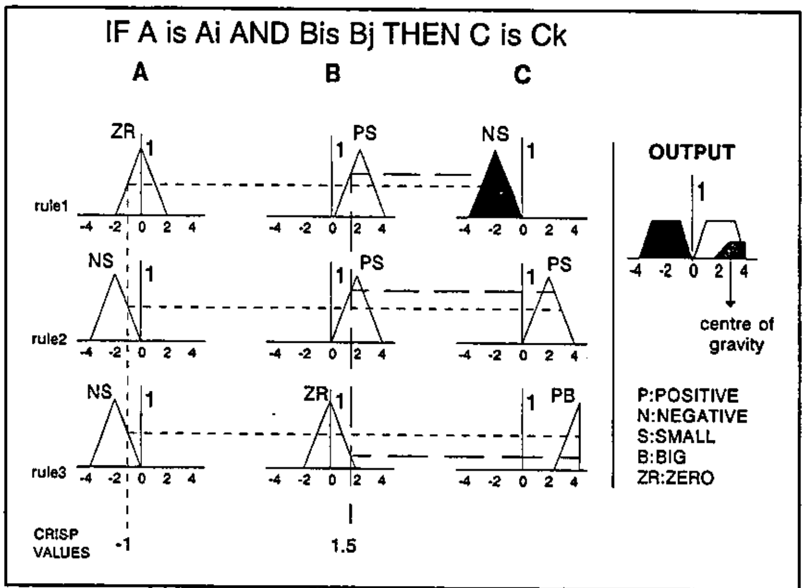

Figure 2.10 Inference of Fuzzy rules

The interaction between two or more rules, each represented by a Fuzzy phrase, connected by ELSE is given by a Fuzzy clause:-

$$\mu_Q(A,B,C) = \max[\mu_{P_1}, \mu_{P_2}, ..] \qquad 2.48$$

The Fuzzy modelling technique provides the capability to cater for the following situations:-

1. the system variables can only be estimated by Fuzzy linguistic variables (i.e. small, negative big etc.). In such cases the rules can be triggered directly.

2. some method of direct measurement is available providing crisp values (2, 60, 200 etc.) of each system variable. However, the measurements are subjected to inherent errors.

In the latter case, prior to the manipulation of the Fuzzy rules, the variables need to be "fuzzified". The fuzzification process may lead to a dual classification. This is due to the fact that a crisp value may be part of two Fuzzy sets with different (or even the same) grades of membership. In Figure 2.8, for example, the crisp value 3 is a member of Fuzzy set "small" with a membership grade of 0.45. It is also a member of the Fuzzy set "medium" but with a membership grade of 0.70.

Figure 2.10 is a graphic representation of the fuzzification process and the subsequent inference of the system output from different rules as discussed above. If the output needs to be expressed explicitly, a crisp value can be obtained by a "defuzzification" process. A popular defuzzification technique uses the centre of the gravity of the Fuzzy output as the required crisp value (Mamdani 1976). Other methods use the maxima or the average value of the output membership function (Zimmerman 1991)

The Inherent Advantages of Fuzzy Applications

The inherent properties of Fuzzy sets and operators, i.e. the ability to accommodate the uncertainty associated with linguistic variables provides a powerful method. In engineering, it has a proven record of success in dealing with several categories of problematic situations:

1. in the absence of adequate knowledge of a system Fuzzy techniques can be used to model and control the process (Shen & Leitch 1993)

2. in systems with inherent non-linearities or where the plant dynamics is time variable, self-organising (self-tuning) Fuzzy controllers provides a robust technique (Astrom et. al. 1986).

3. in situations where no reliable method of measuring significant system variables could be provided, Fuzzy techniques could be used to accommodate the error contaminated signals or use linguistic estimates of a parameter that can be provided by operators (Liu & Kelly 1989).

A reliable predictive wear model for cone crushers must be able to cope with unavoidable variations in rock moisture. Although, very difficult to correctly measure, the effect of such variations is too pronounced to ignore. It is therefore necessary and appropriate to incorporate some degree of Fuzzy manipulation in the wear model to cater for the uncertainty in the measurement of rock moisture.

2.3 Adaptive Control Strategy and Applications

Adaptive control methods can provide a systematic yet flexible approach to the regulation of processes that are not well understood, are slowly time varying, or have significant non-linearities (Chien et. al. 1985). For such processes, the adaptive strategy is expected to offer effective control and good system performance with respect to energy saving and product quality. In its most general format, the structure of an adaptive controller can be summarized as shown in Figure 2.11. The system performance is estimated by a comparison between plant output $\{y_k\}$, and the input (process demand set-point) $\{\mathbf{u}_k\}$. The estimated error in the output is used to select the pertinent control algorithm for minimizing the error. The technique is, therefore, well suited to the control of the complex processes where system dynamics is time-variant. In such systems the use of classic PID controllers is problematic as they would require frequent tuning.

Many different approaches to adaptive control have been proposed (Narendra & Monopoli 1980). Three schemes have received particular attention in the literature:- Self-Tuning Adaptive Regulators (Astrom & Wittenmark 1989), Model Reference (Model-based) Controllers (Martin-Sanchez 1975), and Adaptive Pattern Recognition Controllers (Bristol 1986).

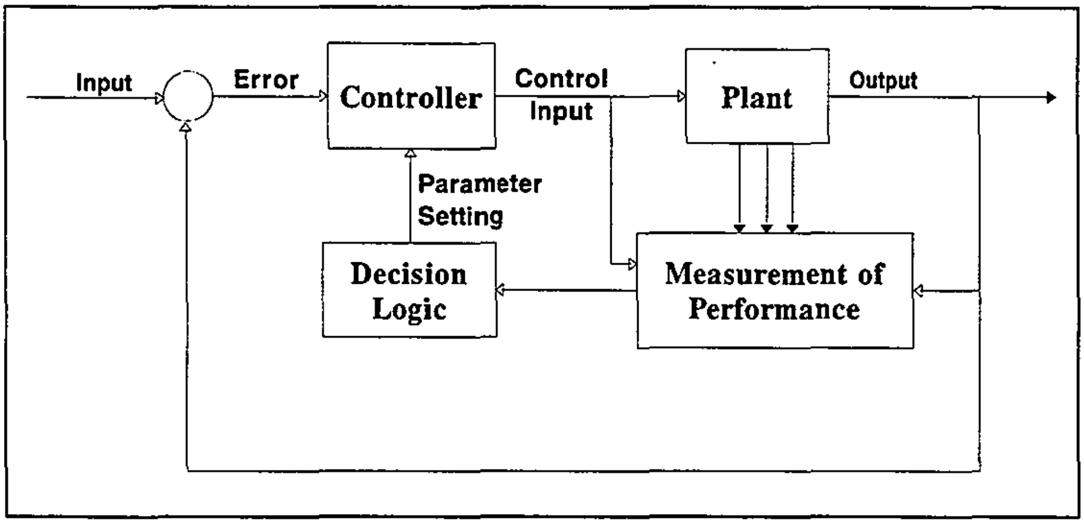

Figure 2.11 The general structure of adaptive controllers

2.3.1 Self-tuning Adaptive Control

Self-tuning adaptive controllers have been widely considered in the literature (Astrom et.al. 1977; Clark et.al. 1985; Goodwin & Sang Sin 1984). A block diagram of a self-tuning regulator is shown in Figure 2.12. The regulator can be thought of as composed of three parts, a recursive parameter estimator, a design calculator, and a regulator with adjustable parameters (Astrom 1980). the design method is chosen to give the desired result when the parameters characterizing the process are unknown but can be estimated.

In its simplest form, the action of the regulator can be demonstrated by considering a process described by (Astrom 1980):

$$y(t+1) = y(t) + bu(t) + e(t) \qquad 2.49$$

where **u** is process demand set point, **y** is the output, **e** white noise and **b** a constant parameter. Equation 2.49 is a sampled data model of a simple integrator. The control criterion is to minimize the function

$$\lim_{N\to\infty} E\frac{1}{N}\sum_{1}^{N} y^2(t) \qquad 2.50$$

If the parameter **b** is known, the control law which minimizes Equation 2. 50 is given by

$$u(t) = -\frac{1}{b}y(t) \qquad 2.51$$

If the parameter **b** is uncertain, **u(t)** is given by

$$u(t) = -\frac{1}{\hat{b}}y(t) \qquad 2.52$$

where $\hat{b}$ is the estimate of **b**.

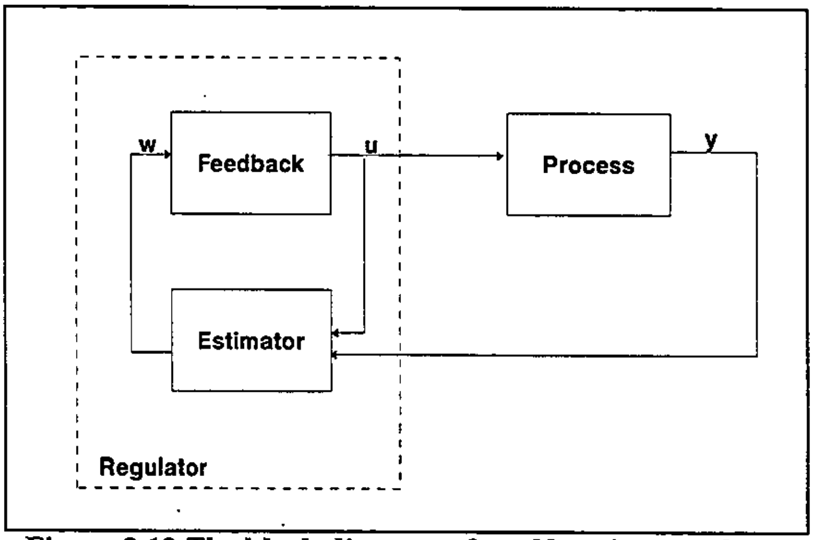

Figure 2.12 The block diagram of a self-tuning regulator

In the more general case, where the process has more than one system parameter, the plant input and output sequences are monitored to estimate its parameters. The estimated parameters are then used to choose (directly or indirectly) the parameters of the controller. Examples of this approach are the minimum-variance (MV) self-tuner designed by Clark et.al.(1985), and the pole-placement (PP) self-tuners of Lelic and Zarrop (1987). In the MV self-tuner a suitable cost function is used to develop the control law to properly predict $\{\mathbf{u}_k\}$. The PP self-tuner is designed to calculate the controller parameters so that the output $\{\mathbf{y}_k\}$ obeys the input $\{\mathbf{x}_k\}$ in some predefined manner.

2.3.2 Model-Based Adaptive Control

An alternative approach to the solution of adaptive control is the Model-based adaptive control system which is based on the assumption that the plant model is known and reversible. For systems of this nature, the inverse of the plant model can be used to convert the input signal $\{\mathbf{x}_k\}$ into the process demand signal $\{\mathbf{u}_k\}$ which when applied would drive the plant output $\{\mathbf{y}_k\}$ towards $\{\mathbf{x}_k\}$. A schematic diagram of a Model-based adaptive control system is shown in Figure 2.13. The system can be considered as comprising two loops. The inner loop is an ordinary control loop composed of the process and a controller. The parameters of the controller are adjusted in an outer loop in such a way that the error between the process output and the model output $\{\mathbf{y}_{Mk}\}$ is minimized. The key problem in this type of system is to determine the adjustment mechanism so that a stable system, where the error tends to zero, is obtained. The following parameter adjustment mechanism was used in the original Model-based adaptive control system (Butler 1992):

$$\frac{d\mathbf{v}_i}{dt} = -\mathbf{k}\frac{\partial \mathbf{e}}{\partial \mathbf{v}_i}\mathbf{e} \qquad \mathbf{i} = 1,..,\mathbf{n} \tag{2.53}$$

The variables $\mathbf{v}_1, .., \mathbf{v}_n$ are the adjustable controller parameters. The error $\mathbf{e}$ denotes the model error given by:-

$$\mathbf{e} = \{\mathbf{y}_k\} - \{\mathbf{y}_{M_k}\} \tag{2.54}$$

and $\partial e / \partial v_i$ are the sensitivity derivatives. The constant **k** is a parameter which determines the adjustment rate. This adjustment rule can be interpreted as an algorithm for minimizing $\mathbf{e}^2$. In the most general format, this type of algorithm can lead to instability (Astrom 1987). Over the years, many modifications, to solve the stability problem, have been suggested (Martin-Sanchez 1975; Sugiyama 1986). The most successful modifications use advanced filtering techniques to modify both the model error and the sensitivities derivative. Widrow & Stearns (1985) designed a system capable of coping with the reversibility of the plant model and instability caused. They introduced a delay between the input sequence $\{x_k\}$and its replica at the output of the plant They have used a finite impulse response (FIR) digital filter for the controller, and have proposed a least mean square algorithm for the controller adjustment.

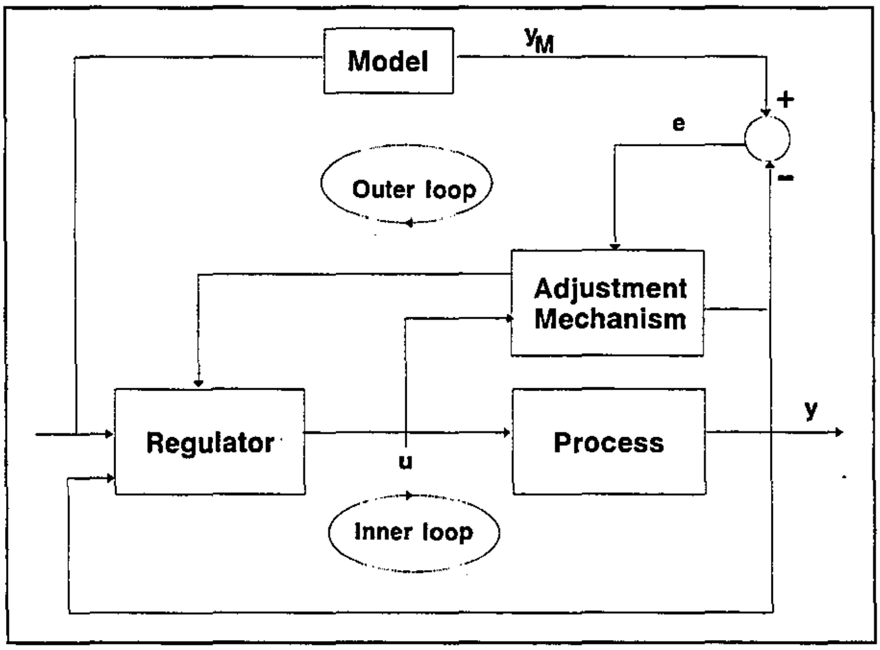

Figure 2.13 The block diagram of a model-based adaptive controller

2.3.3 Pattern Recognition Adaptive Control

Pattern recognition adaptive controllers perform the adaptation similar to a human operator in terms of evaluating the goodness of the control by observing the run of the process output variable, associate the run with performance characteristics and adjust the controller on the basis of empirical knowledge. It is a branch of intelligent control and uses output pattern recognition laws to classify the output as bad, good, stable, or unsatisfactory. The technique relies on availability of examples of such outputs to the system. Obviously, output can take so many different patterns. In order to minimize the number of examples necessary, Klein et.al.(1991) have suggested a technique for only storing elementary patterns which when combined could make up different output patterns. They claim a controller performance as successful as Model-based adaptive controllers for industrial applications. The strength of the techniques lies with the fact that virtually no prior knowledge of the system characteristics is necessary for the controller to behave adequately. The control algorithms are based on expert If / Then rules. However, as with all expert systems, at its best the control system performance is the same as an expert operator. A performance which is inadequate for a large number of complicated systems.

2.3.4 Applications of Adaptive Control

Many applications of adaptive control strategy have been reported (Johnson 1989; Butler 1992; Shah et. al. 1989). Two applications, one reported by Astrom (1980) on the control of a cone crusher, and the other reported by Centner & Idelsohn (1963) on the control of a metal cutting process, are of interest to the present work.

Adaptive Control of a Cone Crusher

The application reported by Astrom (1980) involves the design of a self-tuning regulator for a ore crushing plant in Kiruna in northern Sweden. The plant consists of an ore bin, a feeder, two screens, a cone crusher, and conveyor belts. Two screens, one for the feed and the second for crusher output, are used. At the second screens, particles with a diameter larger than 2.5 cm are recirculated to the crusher. The crusher, driven by an electric motor, uses a slip clutch for releasing the motor in an overload condition. The adaptive controller was designed to maximize the production rate, while avoiding overloading. The control variable was chosen to be the amount of ore fed into the line and the controlled variable was the power of the crusher motor.

The system disturbances, i.e. the causes of the change in plant's dynamics, were found to be due to variation in feed size, crushability of rock, and variation of crusher characteristics due to wear. The plant dynamics were characterized by a time delay of 70-80 seconds in the recycle loop and time constant of 10-20 seconds in the crusher itself. The control strategy adopted is a simple self-tuning regulator based on minimum variance (MV) algorithm to force the crusher power set-point closer to target and hence increase the average production. Figure 2.14 shows the controllers performance. It is described in terms of the sample covariance function, i.e. the variation in the output y plotted against time, and the cross-covariance function between the output and the control variable, i.e. the mis-match between the plant output y and process demand set point u. It shows that in both cases the function tends to zero, as expected for a good controller design.

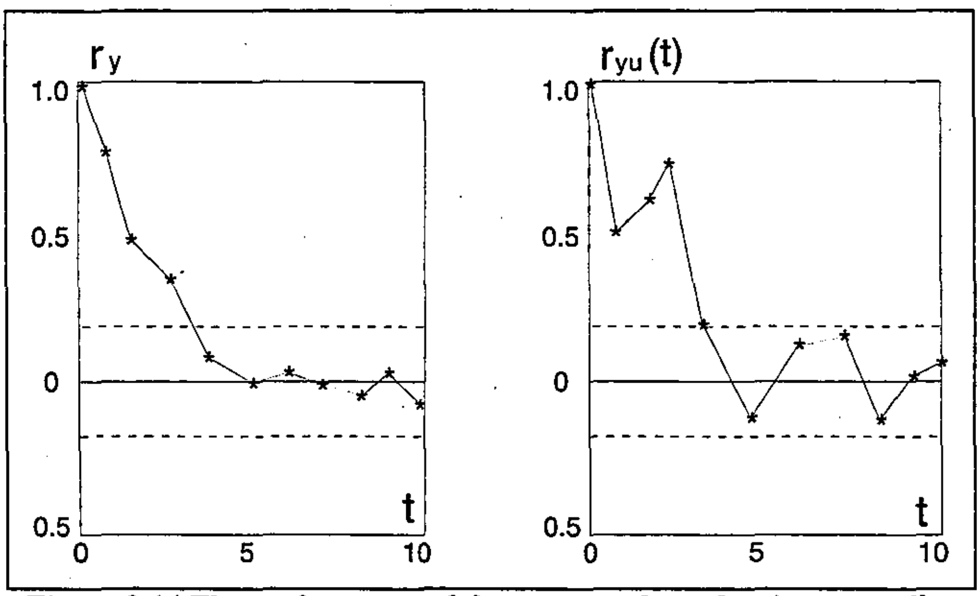

Figure 2.14 The performance of the cone crusher adaptive controller (Astrom 1980)

Adaptive Controller for a Metal Cutting Process

Although the metal cutting process is very different from that of cone crushing, a number of similarities between the two systems grants the work reported by Centner & Idelsohn (1963) has some bearing on the present work. In both systems the properties of the processed material (ore and metal) can vary and cause considerable disturbances in terms of system parameters. The effect of wear, in terms of variations in system characteristics, is also similar in both systems. Equally, the effect of environmental parameters on wear and system performance are very important in both systems.

The basis for the reported adaptive controller is to maximize the plant efficiency in terms of metal removal rate, tool wear or tool life, surface finish and dimensional accuracy. Although the exact process equations were not known, an on-line evaluation of the system performance in terms of the above factors was used to provide a feed-back to the adaptive controller. The control parameters used are the metal feed rate and the plant speed. A figure of merit, **H**, is used to quantify the system performance in terms of measurable variables and operator's input. The developed figure of merit is given by

$$\mathbf{H} = \frac{\mathbf{MRR}}{\mathbf{k_1} + \dfrac{(\mathbf{k_1 t} + \mathbf{k_2 B})\mathbf{TWR}}{\mathbf{W_0}}} \qquad 2.55$$

where

MRR	metal removal rate
TWR	tool wear rate
$\mathbf{W_0}$	maximum allowable tool wear
$\mathbf{k_1}$	direct labour cost + overhead rate
$\mathbf{k_2}$	cost per grind + initial tool cost / maximum number of re-grinds necessary
t	tool change downtime
B	a constant, $1 \geq \mathbf{B} \geq 0$, the value chosen depends on the criterion of maximizing the production rate, or minimizing cost or a combination of the two.

The controller is designed to optimize the control variables (feed and speed) so that the performance parameter **H** is always a maximum. Two optimizing strategies, Method

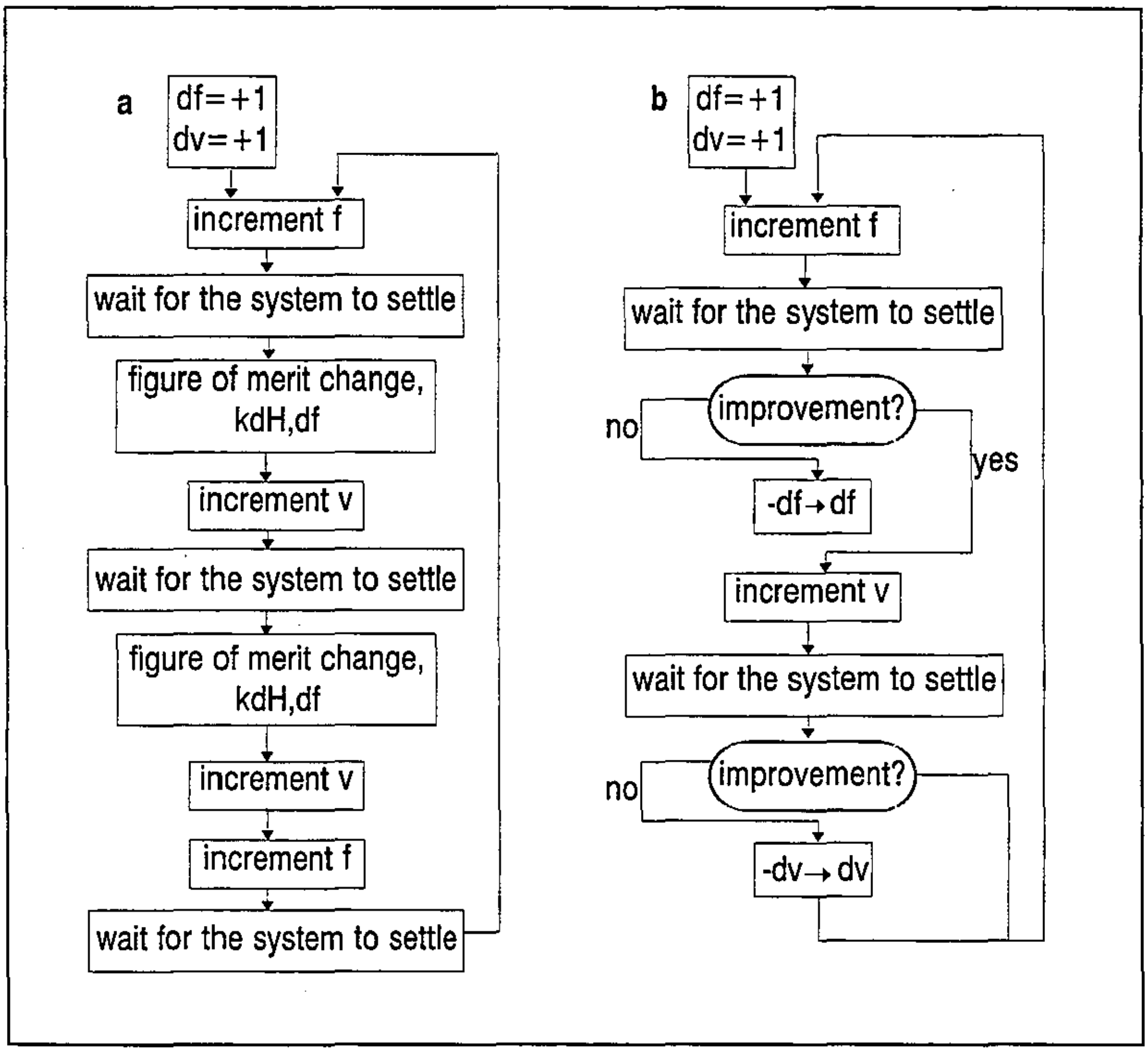

Figure 2.15 Two methods of performance optimization a. method of steepest ascent b. method of trial and error (Centner & Idelsohn 1963)

of Steepest Ascent and Method of Trial and Error have been considered by the authors. The flowcharts of the two techniques are shown in Figure 2.15. The inputs into the designed adaptive controller falls into three categories:-

I. Operator-entered parameters: remains constant during the course of a single cut
II. Machine-generated parameters: time-variant parameters, evaluated as part of the original system
III. Measured variables : time-variant parameters instrumented for control feedback purpose.

From their simulated results, the authors concluded that the method of steepest descent is more efficient than the trial and error. They also emphasized that to ensure stability, care must be taken in the design of the constraint-violation logic.

2.4 Model of Cone Crushing Process

Whiten's cone crusher model (Whiten 1972) has been widely accepted as a framework for describing the steady-state crushing process. The basis of the model is the simplification of cone crusher to a single breakage zone where particles can enter and re-enter before leaving the crushing chamber. Two internal mechanisms, each represented by a matrix, are used to describe the process. Figure 2.16 shows the two parts of the model. The vectors **f**, **p**, and **x** represent the size distribution of feed, product, and the material inside the crushing chamber respectively. The Classification function **C**, represented by a diagonal matrix describes the proportion of particles in each size interval entering the breakage zone and the Breakage function **B**, represented by a lower triangular matrix, gives the relative distribution of each size fraction after breakage. The consideration of mass balance at the two nodes in Figure 2.16, and the subsequent elimination of **x** gives the Whiten's crusher model equation:-

$$\mathbf{p} = (\mathbf{I} - \mathbf{C}) * (\mathbf{I} - \mathbf{B} * \mathbf{C})^{-1} * \mathbf{f} \qquad \mathbf{2.56}$$

which expresses the crusher product in terms of the feed provided matrices **B** and **C** are known.

2.4.1 The Breakage Function

The Breakage matrix is a material dependant function whose elements can be determined by a number of tests. One of the tests used is the twin pendulum breakage test carried out at a variety of input energies (Narayanan and Whiten 1988). The analysis of the pendulum test data is by using a family of curves with a single parameter t_{10}. The parameter t_{10} is defined as the cumulative percentage of broken particles smaller than one tenth of the geometric mean size of the test particle. This parameter can be used to fully describe the whole of the pendulum test product size distribution. This in turn is used to construct the **B** matrix (Anderson and Napier-Munn 1990) as follows:

$$\mathbf{B_{ij} = 0} \qquad \text{for } i<j$$
$$\mathbf{B_{ij} = 1.0 - P(x_i,x_{jm})} \qquad \text{for } i=j$$
$$\mathbf{B_{ij} = P(x_i,x_{jm}) - P(x_{i+1},x_{jm})} \qquad \text{for } i>j$$

where

$P(x_i,x_{jm})$ is the fraction of material less than size x_i derived from x_{jm}, x_i and x_{i+1} are the lower and upper limits of sieve fraction i,

x_{jm} is the geometric mean size of the j-1 to j size fraction, i and j are ith matrix row and jth matrix column respectively.

Bearman (1991a) showed that the Fracture Toughness of rock, measured by the standard chevron bend test, correlates well with parameter t_{10}. The relative simplicity of this test compared to twin pendulum test makes it an attractive option for obtaining the Breakage Function for different rock types.

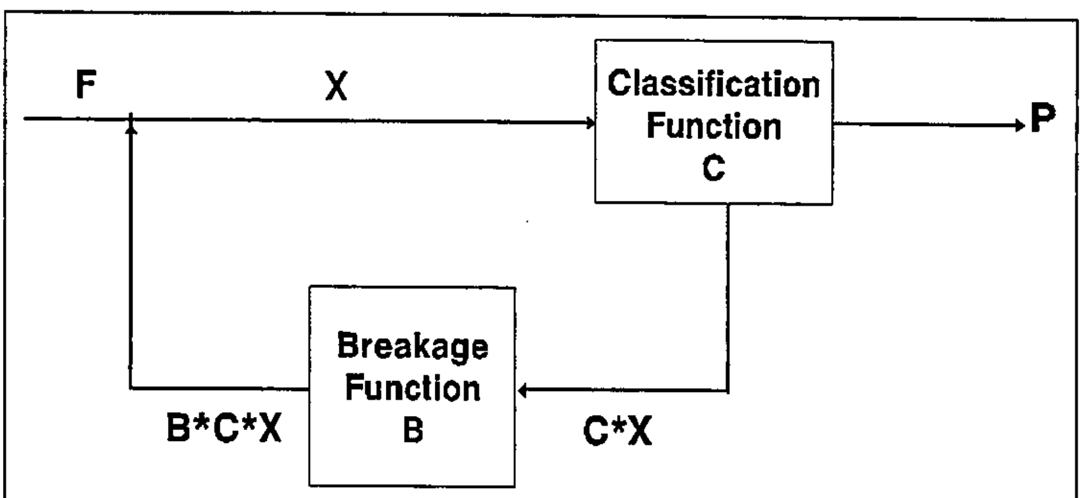

Figure 2.16 Crusher model (Whiten 1972)

2.4.2 The Classification Function

The Classification Function describes the probability of a given particle undergoing further breakage in the breakage zone. It is a material independent function whose parameters are related to the particle size and the operating conditions of crusher. Whiten (1972) described the selection probability using the following relationship, depicted in Figure 2.17.

$$\mathbf{C(x) = 0} \qquad x < K_1$$

$$\mathbf{C(x) = 1 - ((K_2\text{-}x)/(K_2\text{-}K_1))^{K_3}} \qquad K_1 < x < K_2$$

$$\mathbf{C(x) = 1} \qquad x > K_2$$

where $\mathbf{K_1}$, $\mathbf{K_2}$ and $\mathbf{K_3}$ are machine specific model parameters whose values are found to be related to a number of operational parameters. $\mathbf{K_1}$ is the particle size below which no further breakage happens. $\mathbf{K_2}$ is the size above which all particles undergo breakage and $\mathbf{K_3}$ describes the nature of the probability function between these two extreme cases. $\mathbf{K_3}$ is usually set to a constant value.

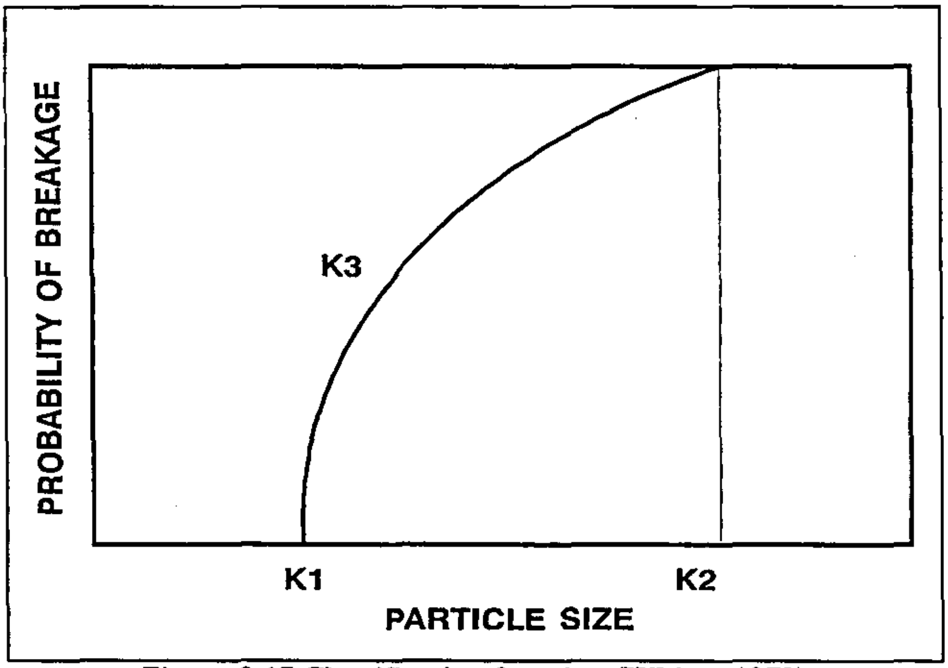

Figure 2.17 Classification function (Whiten 1972)

A number of workers have investigated the classification function for various cone crushers. Whiten (1972) found that for the 7-ft Symon short head crusher $\mathbf{K_1}$ and $\mathbf{K_2}$ were given by

$$\begin{aligned} K_1 &= 0.67g \\ K_2 &= 1.121g + 2.31q + T(t) \end{aligned} \qquad \textbf{2.57}$$

where $\mathbf{g}$ is the discharge setting size, $\mathbf{q}$ is the fraction plus one inch in the crusher feed and $\mathbf{t}$ is the feed tonnage, and the function $\mathbf{T(t)}$ is a natural spline function of degree 3. Anderson and Napier-Munn (1990) investigated the data from three different sites and found that

$$\begin{aligned} K_1 &= a_0 - a_1\, TPH + a_2\, F_{80} + a_3\, \text{Liner length} \\ K_2 &= a_0 + a_1\, g + a_2\, TPH \end{aligned} \qquad \textbf{2.58}$$

where **TPH** is the feed in tonnage /hour, $\mathbf{F_{80}}$ is feed 80% passing size (mm), and $\mathbf{a_0}$, $\mathbf{a_1}$, etc. are constants to be estimated from the operating data. For two of the sites investigated, the effect of the liner age could be recorded and it was found that $\mathbf{K_2}$ also depended on the liner age:-

$$\begin{aligned} K_1 &= a_0 - a_1\, TPH + a_2\, F_{80} \\ K_2 &= a_0 + a_1\, g + a_2\, TPH - a_3\, AGE \end{aligned} \qquad \textbf{2.59}$$

where AGE is a parameter defined as the fraction of expected liner service life expired at the time of the survey. The results obtained by Anderson and Napier-Munn (1990) are in general agreement with earlier works of White (1978) and Hatch et al. (1982) who also found a correlation between the liner profile and $\mathbf{K_1}$ and $\mathbf{K_2}$. In these studies the parameter $\mathbf{K_1}$ was found to increase with liner length resulting in an increase in the particle size below which particles leave the crusher without further breakage. $\mathbf{K_2}$ was found to decrease with an increase in the liner length, thus decreasing the particle size above which the probability of breakage is equal to 1. Liner wear in effect increases the length of the crushing zone (the parallel part of the crushing chamber) with similar increasing and decreasing effects on $\mathbf{K_1}$ and $\mathbf{K_2}$ respectively. The general effect of the liner wear over its life was found by Anderson and Napier-Munn (1990) to be significant and similar to a decrease of 3mm in the size of the discharge setting.

2.5 Instrumentation for Measurement of Wear and Product Size Distribution

An adaptive control strategy for real-time compensation of wear in cone crushers ideally requires direct measurement of liner wear and product size distribution. Thus, to some extent the credibility of the adaptive strategy proposed in the current research depends on the availability of sensory devices for these measurements. It is therefore useful to review some of methods and systems proposed in each category.

2.5.1 Measurement of Wear

Direct and on-line measurement of wear in industrial plants, is a demanding area of work as in most cases the access to the wearing surface is either limited or completely denied. Accordingly, the previous research is very limited. Acoustic sensing techniques have been used to obtain on-line information on the state of wear of parts in industrial plants and aircraft. Acoustic emission may be defined as transient elastic stress waves generated at a source by the rapid release of strain energy within a material. These radiating stress waves, that can take the form of either a pulse or pseudo-continuous emission, are detected at the surface of the body by a suitable sensor (Lingard & Ng 1989). The work carried out by Bonness & McBride (1991) and Bonness et.al.(1990) has shown that a relationship exists between the acoustic emission, in terms of the rms value of generated signal, and volume of wear that could be used as an indirect measurement of surface wear. The electrical nature of the signal generated provides the potential for exploitation of the technique in an on-line measurement system.

In some circumstances, it is possible to monitor the wearing surface using vision and image processing techniques. In abrasive waterjet cutting process, for example, wear causes an increase in the inside diameter of the nozzle. Here, the diameter of the water jet could be monitored using vision techniques to provide an on-line measurement of nozzle wear (Kovacevic & Evizi 1990). A second technique for measuring the nozzle wear (Kovacevic 1991) uses a sacrificial conductive sensor embedded in the nozzle. The sensor comprises a number of conductive loops spaced 0.05mm apart. The sensor is placed at the tip of the nozzle and subjected to the same abrasive and erosive modes of wear as the nozzle itself. Each conductive loop will be cut when the nozzle has worn to its position, resulting in an open circuit which is detected to give the advance of the wear.

The sacrificial wear sensors developed as part of the current LINK project are based on similar general principles as the sensor described above. The sensors have a diameter of between 0.5 -1.5 mm and are inserted into the liner. The design utilizes conductive, resistive, and capacitive principles for transducer elements design (provisional patent ref. No. 9494835.2). When inserted in the liners, the sensors are subjected to wear similar to that of the liner. The electrical signal generated by the sensor is in all cases proportional to the sensor length. As the liner and the inserted sensors wear, the sensor output changes providing a direct measure of the remaining liner thickness. A range of laboratory and industrial trials have been conducted validating the transducer designs and sensors robustness.

2.5.2 Measurement of Particle Size

The high volumes of production in a crushing circuit rules out the possibility of measuring the size of all particles produced. Instead, the measurement must be based on samples taken at appropriate sample times. For the size distribution of the sample to be characteristic of the product , its volume must not be less than a certain lower limit. In the manual case, the material on 1 metre of the conveyor belt is usually taken as the sample size. The size distribution of the sample is determined in laboratory using classifying sieves.

Automatic means of particle size measurement are based on different optical and laser techniques. Simple techniques use a laser beam and light detector that are placed perpendicular to the direction of falling particles. The sensor is based on generating light and shadow sequences as the particles pass through the sensors field of view. The time between light and shadow sequences gives a measure of particle size. More elaborate techniques use vision techniques to view the particles on the conveyor belt, or on the classifying screens (Prisector sampling Plc. 1993). The Visual Size Identification (VSI) system developed by Prisector sampling Plc., is a specialized system targeting the quarry industry. Image processing techniques are used to measure the size of rock particles while lying on a bed under the camera. The system uses the measurements to construct and display the size distribution curve and relevant statistics. The company claims that during in-house and site trials at a number of quarries the system has been validated.

A system designed by Yeo et.al. (1991) for determination of rock fragment sizes in a muckpile immediately after blasting uses automatic vision and image analysis techniques. The processing power is provided by a transputer array. Authors claim that the use of parallel processing techniques has reduced the computation time from 10 minutes (using a PC/AT) to less than 2 minutes.

In all these techniques, particle overlapping is a problem that reduces the reliability of the measurements made. In the case of the vision-based systems, the potentially high system costs are prohibitive. A new measurement system, designed as part of the current research has obtained research funding and is expected to provide a more reliable system at lower cost (Calkin & Parkin 1994).

Chapter 3_ TRIBOLOGY OF CONE CRUSHERS

In order to determine the process of wear in cone crushers, the kinematics of the system, mechanisms of material removal, the profile of wear and the primary parameters that influence it's rate must be understood.

3.1 System Kinematics

Figure 3.1 shows a schematic view of the crushing chamber of a cone crusher. The eccentric shaft mounted about the main stationary shaft imparts a rocking motion to the mantle that also gyrates at the same time. The concave is stationary except for occasional movement in the vertical direction to effect different crusher settings.

Cone crushers commonly use choke feeding that ensures a continuous feed. Depending on the size of the crushing chamber and that of the feed particles, several layers of rock particles may exist between mantle and concave. Therefore, only a fraction of the feed particles keep in contact with one or both of the liners while passing through the crushing chamber. The rest of the feed may only contact the liners temporarily or in the case of particles staying in the middle layers, not contact them at all. The movement of the particles relative to each other as well as the liners can be classed as a combination of rolling, sliding and impact. Except in unusual cases, the feed particles vary in size and shape, and may have sharp or rounded edges.

The comminution process on each particle continues until it is small enough to pass through the discharge opening. The time spent in the crushing chamber depends both on the available crushing force and feed's resistance to breakage. It may also be affected by factors external to the crushing process itself that could nevertheless cause clogging and delay the passage of the product through the discharge opening. These include excess fines, high moisture or a combination of both.

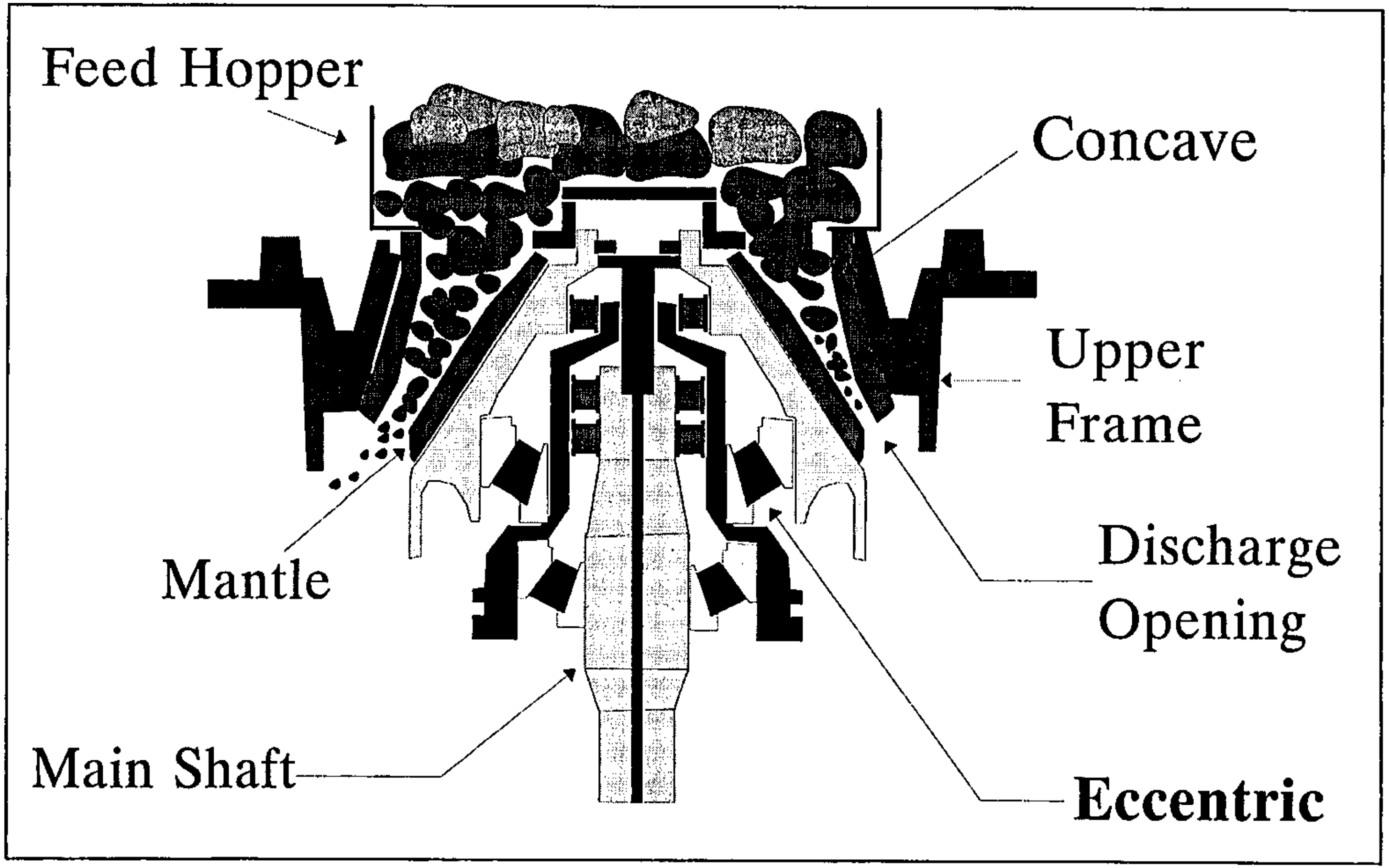

Figure 3.1 A schematic view of crushing chamber

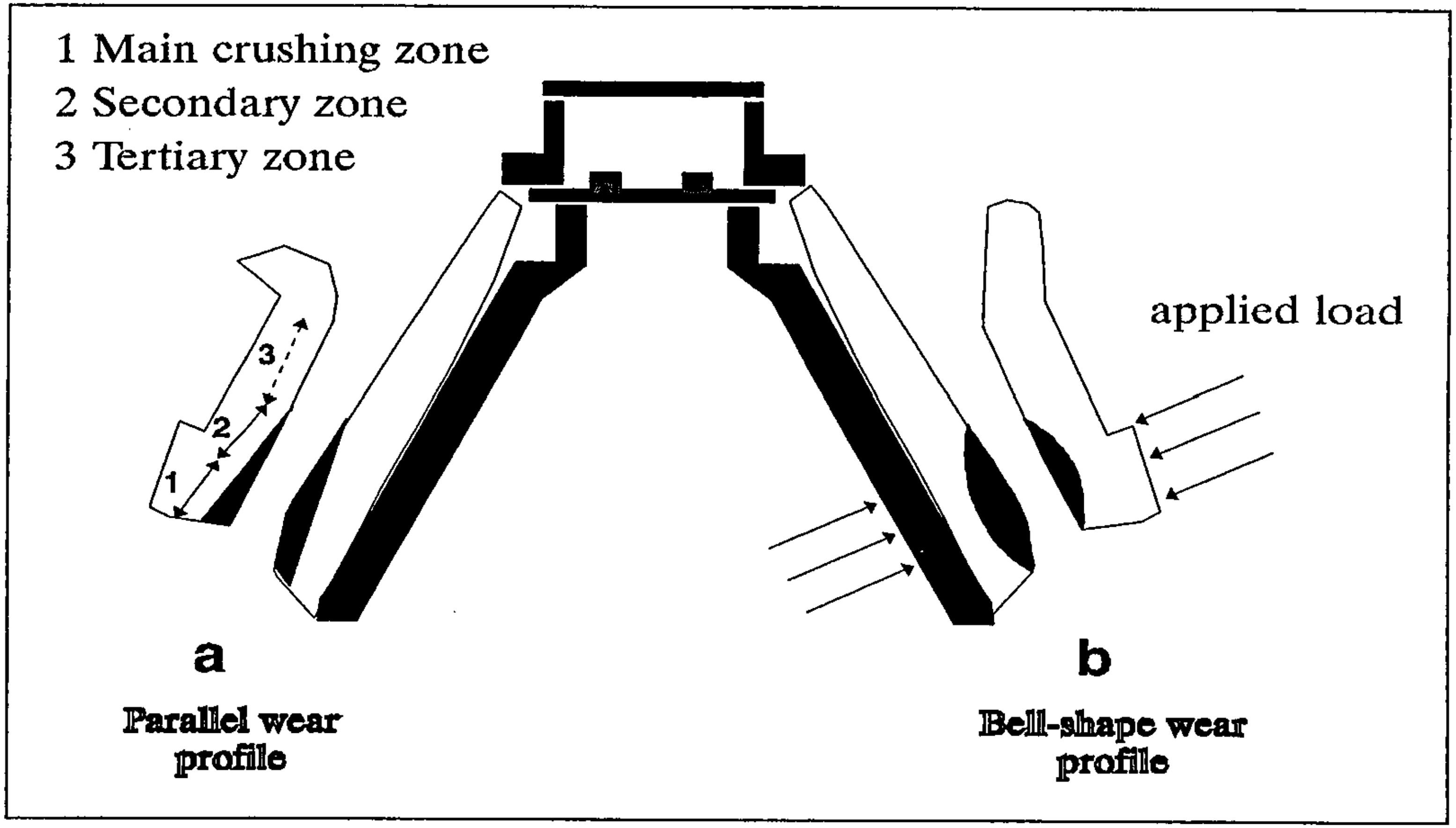

Figure 3.2 The industrially observed wear profiles

When the chamber is empty, the mantle gyrates at 200 revolutions per minute. However after contact with the feed particles, this reduces drastically to 6 revolutions per minute. The motion of the mantle subjects the feed to repeated compression cycles. The generated torque in the main shaft is superimposed with the impact force delivered by the eccentric to produce a high crushing force. The available crushing force depends on the crusher mechanical characteristics that is usually defined by Machine Design Variables (MDV). The main variables are:-

a. cone head angle
b. eccentric throw distance
c. cone head speed
d. liner profile.

The combination of MDV is usually fixed for a particular model of cone crusher, although some manufacturers offer limited variability for a set base design. For varying combinations of MDV wide variations in crushing force can be achieved. At present there is a trend towards very high impact forces which enable the crushing of multiple layers of material and thus increase crusher throughput. The higher impact forces are generally achieved by increasing the eccentric throw and the speed of cone head.

The size of the feed particles reduces progressively as they move down the crushing chamber. The product consists of particles of reduced but varying sizes. The size distribution of the product depends on the crusher type and the closed-side setting. For a given type of cone crusher, alternative concave and mantle designs are usually used to give various feed opening and different product grades.

3.2 Industrially Observed Wear Rates and Profiles

Figure 3.2 is a schematic representation of the general wear profiles observed in cone crushers. Figure 3.2a shows the most commonly observed wear profile in cone crushers. It represents a differential wear rate along the slope of the liners, with the highest wear coinciding the principal crushing zone. Figure 3.2b depicts a problematic bell shaped wear profile, usually termed "dishing", where the highest wear happens at the middle parts of the liner. It is usually associated with incompatibility between the feed size and crusher design and in the cases of single graded feeding which leads to a high degree of material breakage in the middle parts of the chamber.

To avoid costly repercussions of liner cracks, cone crusher operators tend to change the liners when the remaining liner thickness at the thinnest section is around 3cm. The rate of wear can be represented in two different ways:- a) metal wastage, in terms of liner's thickness or weight, per hour; and b) metal wastage per tonne of product. In traditional cone crushers no accurate means of determining the elapse of liners' service life is available. A combination of previous experience and the total movement of upper-frame during re-setting of the discharge opening, is used as a guide. The latter provides a rough measure of thickness loss at the discharge end of the liners. In the case of bell shaped wear profiles, this can lead to erroneous estimates, as the thinnest section of the liner is in the middle and not at its discharge end.

The rate of wear, in the most general terms, is found to depend on the crusher design and the material used to produce the liners. In agreement with Equation 2.12:-

$$\mathbf{W} \propto \mathbf{F_n} \qquad \mathbf{2.12}$$

the higher crushing forces generated in the high impact crushers result in faster rates of wear. However, in such cases the enhanced crushing power leads into an improved throughput, and therefore the service life of the liners, in terms of metal wastage per tonne of product, does not decrease as sharply.

Cone crusher liners are commonly sand cast from Hadfield steel. As discussed in the previous chapter, the rate of wear is very much dependent on the material properties of the wearing surface. In the Equation 2.12, under constant environmental conditions, the coefficient of proportionality is determined by the liner properties.

Considering the dependency of wear on machine and liner variables, the qualitative and quantitative investigations carried out in this project have aimed a particular make of cone crushers, the Pegson Autocone 900 series. In order to establish the effect of MDV, the wear of the Autocone 1200 and the Automax cone crushers have been also briefly investigated. However, the qualitative results of the study regarding the wear process and mechanisms of material removal, and the variables determining its rate, are general and should be applicable to other makes of cone crushers.

3.3 Autocone Cone Crushers Series

Pegson Autocone cone crushers, chosen as the subject of this study, are a family of high impact cone crushers. Two cone sizes, 900 and 1200, and 3 basic liner designs, fine, coarse and extra coarse, are available. In each case one standard mantle and protean concave designs are used to vary the product specification. Table 3.1 summarizes the basic characteristics of the crushers in the series.

Figure 3.3 and Table 3.2 show the profile and dimensions of the liners used in each type of Autocone 900 cone crushers. Figure 3.4 and Table 3.3 show the predicted "ideal" wear profile based on the assumptions of uniform wear and optimum metal utilization (above 60%). However, none of these assumptions are usually attainable and the observed wear profiles are highly differential leading to non-optimal metal utilization rates.

Crusher Size and Model	Speed	Power	Concave		Rec. Min. D.S.	Feed Opening	
	Min^{-1}	kW	Type of bowl	Type of ring	mm	Open Side	Closed Side
				XF	5	45	25
			F	F	6	55	30
				MF	8	90	60
900	737.5	75-90	C	MC	10	110	85
				C	13	135	105
			XC	XC	19	190	170
			F	F	8	70	50
				MF	10	95	70
1200	617	132-150	C	MC	13	135	115
				C	19	180	165
			XC	XC	25	240	225

Table 3.1 Design characteristics of Autocone Cone Crushers

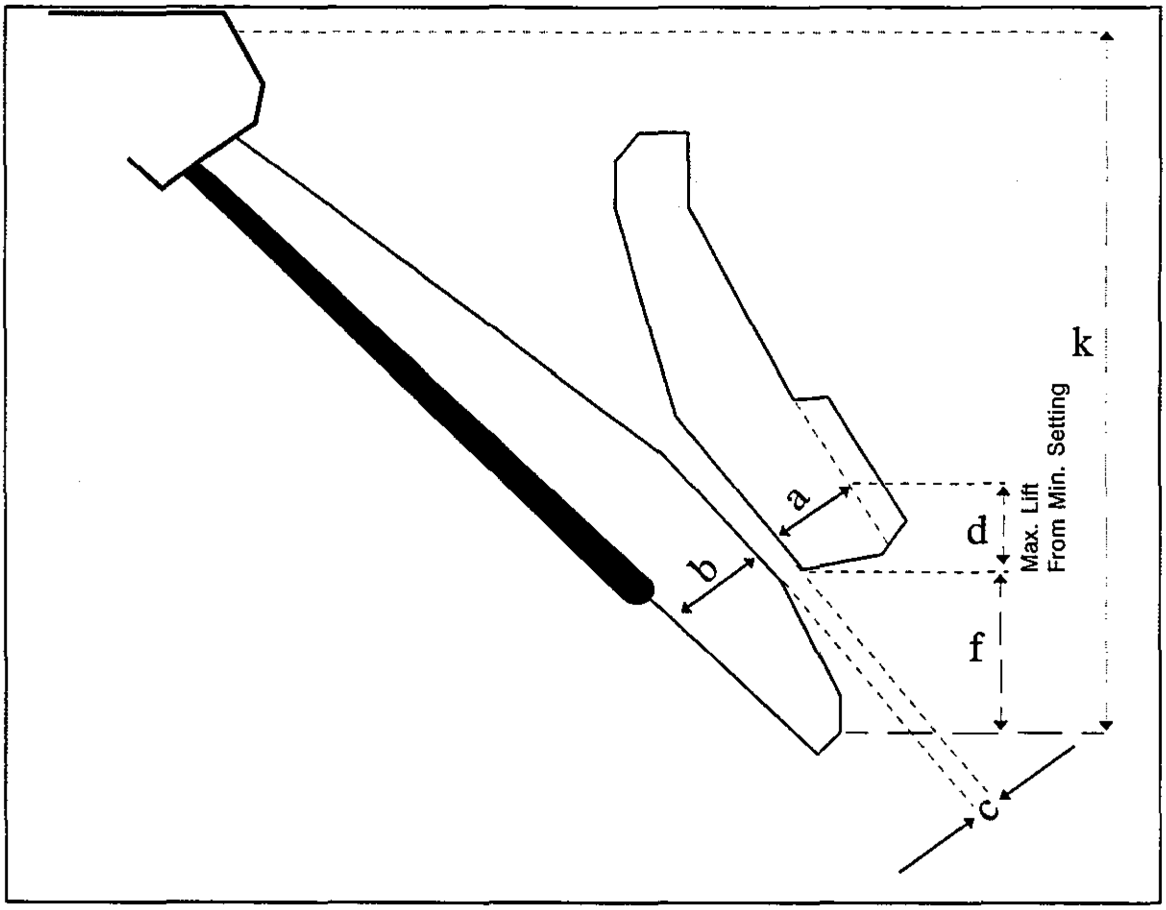

Figure 3.3 Autocone 900 liner profiles

Table 3.2Liner dimensions (cm) for different types of Autocone 900 cone crushers

	XF	F	MF	MC	XC
a	52	52	53	57	59
b	52	52	52	52	52
c	5	6	8	10	19
d	46	52	47	50	38
f	106	100	105	102	114
k	537	529	532	528	535

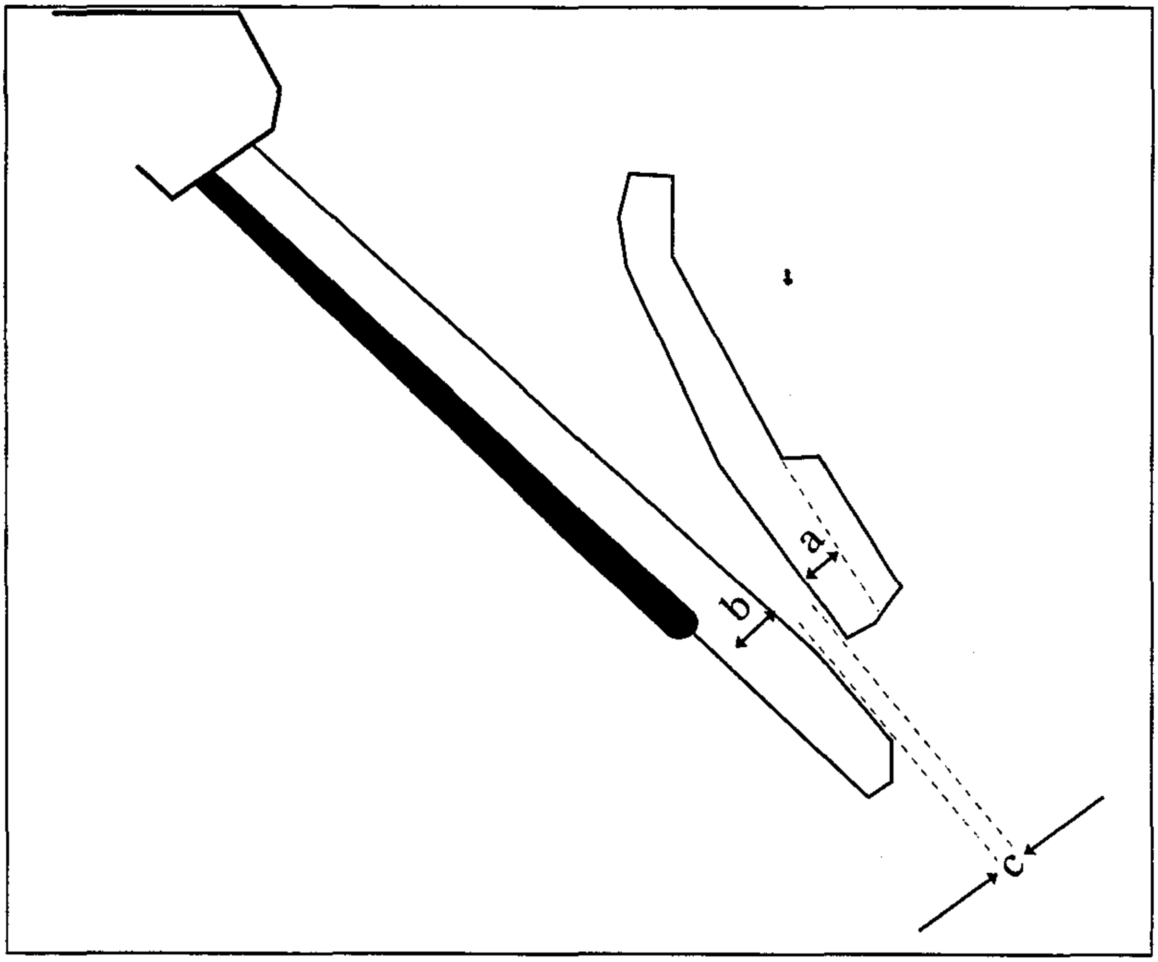

Figure 3.4 The ideal wear profile

Table 3.3 Ideal metal utilization rates

	XF	F	MF	MC	XC
utilization (%)	67	63	66	61	68
a	17	19.5	18	22	19
b	17	19.5	18	20	17
c	5	6	8	10	19

3.4 Properties of Hadfield Steel

Commercial Hadfield steel is an austenitic steel that characteristically contains about 11-13% Manganese (Mn) and about 1.0 to 1.2% Carbon (C). Austenitic steels have high tensile but low elastic strength. However, the material work hardens rapidly, so that the elastic strength of cold worked austenite may be brought up close to optimum (Bullens 1939). Chromium (Cr) is usually added to Hadfield steel used in the minerals industry. It improves the work hardening properties of the steel and provides essential hardness and improved yield during the early stages of the service when work hardening has not yet taken place. The amount of Cr added is usually between 0.75 and 2%. Table 3.4 summarizes the material properties of these steels.

Table 3.4 Material Properties of Hadfield Steel

Ref.	C%	Mn%	Cr%	Tensile Strength MNm^{-2}	Unworked Brinnell Hardness
(1)	1.20	12.50	0.0	849	200
(2)	1.28	12.90	1.5	933	220
(3)	1.38	13.05	2.0	982	286

(1): Higgins 1983; (2):Bullens 1939; (3): Clark& Coutts 1932.

The structure of Hadfield steel is marked by large crystals, as shown in Figure 3.5. After casting, an appropriate heat treatment cycle material is essential to produce the austenite structure. The heat treatment cycle must then be followed by quenching to retain the homogeneous austenite structure and its characteristically high toughness, ductility and resistance to wear. If it is too slowly cooled through the temperature range of 900-1400 degrees centigrade, carbide segregation occurs. These carbides tend to collect at grain boundaries. This segregation, especially when the grains are large and the total boundary surface small, tends to envelop the tough austenite with a honeycomb of brittle carbide and thus weaken the whole structure. The wear properties of these steels have been found to be highly dependent on the cohesion between the carbides and its matrix (Hurricks 1973).

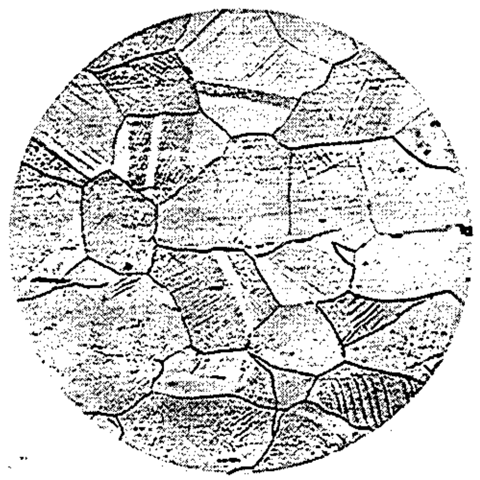

Figure 3.5 The grain structure of Hadfield Steel (Bullens 1939)

3.5 Industrial Investigations

In order to obtain a qualitative understanding of liner wear and determine which variables to include in the quantitative experimental work, a series of investigations were carried out as follows:

I. examination of surface attributes and observation of wear scars. As described in section of the previous chapter, the surface appearance is one of the key considerations in the understanding of the mechanisms of wear and material removal that in turn reveals the mode of wear.

II. exploration of wear rates and profiles experienced at quarries that employ Pegson cone crushers, and thus determine the possible parameters responsible for varying liner performance in industry.

III. investigation of possible variation in material properties of Hadfield steel. This is the primary factor affecting liner wear when other conditions have remained constant.

These studies have provided the information required for classification of the wear process in cone crushers and for identification of the variables affecting its rate and profile.

3.5.1 Surface Topography

Slices through a worn mantle and concave, supplied by Pegson Ltd, were used to study the surface characteristics of cone crusher liners. The liners came from Pegson Automax cone crusher (Autocone 900 cone crusher with System 4 control system offering constant setting / constant power facility) employed at Shap Blue Quarry in Leicestershire. Table 3.5 shows the properties of the rock crushed at Shap Blue quarry.

Figure 3.6 shows the way each of the two original slices were further cut into 4 pieces to investigate the variation in the surface attributes along the length of the liners. The investigation was carried out using three techniques:- Optical Microscopy, Surface Metrology, and Scanning Electron Microscopy.

Optical Examination of the Surface

The optical examination of the surfaces was carried out using a Vickers M55 optical microscope. Under a magnification of 100 (the maximum available on the microscope) the surface of all eight pieces, were found to be very similar in appearance, showing a large amount of grooves and scratches. The majority of the scratches were found to be spiral in shape, although straight scratches were also observed. This observation suggests that the rock lumps rotate while sliding across the crushing elements and hence the contact between the rock and the liners are not primarily a sliding one.

Surface Metrology

To study the texture of the surface a TALYSURF machine was used. The TALYSURF uses a stylus to pick up any texture variation in the surface and converts it into an electrical signal which is then processed and plotted. The average of the measured signal amplitudes, $\mathbf{R_a}$, is calculated that represents the average roughness of the surface. The plot of the signal provides a visual representation of the surface texture.

The surface of each piece was examined at several previously marked parallel positions along the length of the liners. The results are shown in Figure 3.7 . Considering the average values of the $\mathbf{R_a}$, the surface roughness decreases from top to bottom. This can be explained by considering the size effect of rock particles. At the top of the crushing chamber the rock size is much larger with sharp edges that produce considerable surface roughness. As the rock is crushed and reduced in size, it produces a finer wear scar. The effect is similar to the difference in the texture obtained when a coarse and fine sand paper are used on a surface.

Scanning Electron Microscopy

Two samples from each of the four strips, shown in Figure 3.6, were prepared by using a fine flame Plasma Cutter. The use of the plasma cutter minimized the surface damage during sample preparation and hence the bulk of surface features were preserved. A Scanning Electron Microscopic technique was used to study the wear scars on all the sixteen samples (eight samples from both concave and mantle) and hence determine the mechanisms of material removal.

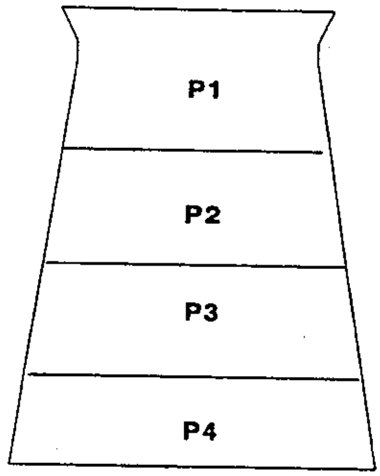

Figure 3.6 Sections cut form the liners

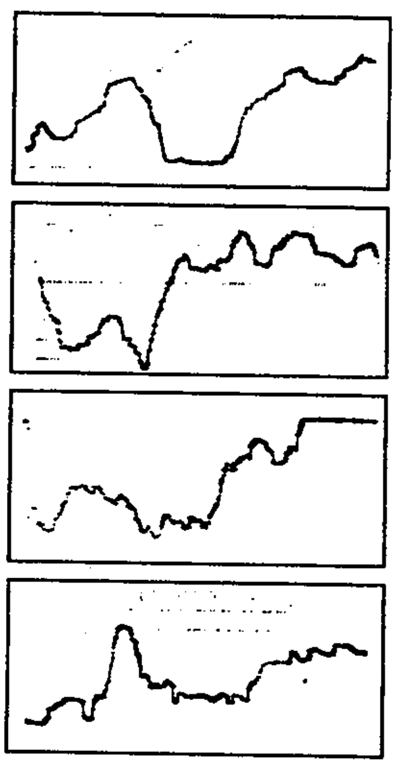

Ref. Smooth Steel **R** = 0.19

P1

R = 13.4
R = 12.9
R = 14.0 Average **R** = 13.9

P2

R = 9.1
R = 9.9
R = 9.8 Average **R** = 9.6

P3

R = 7.6
R = 7.9
R = 7.2 Average **R** = 7.6

P4

R = 6.1
R = 6.3
R = 5.8 Average **R** = 6.0

Figure 3.7 The results of surface roughness tests

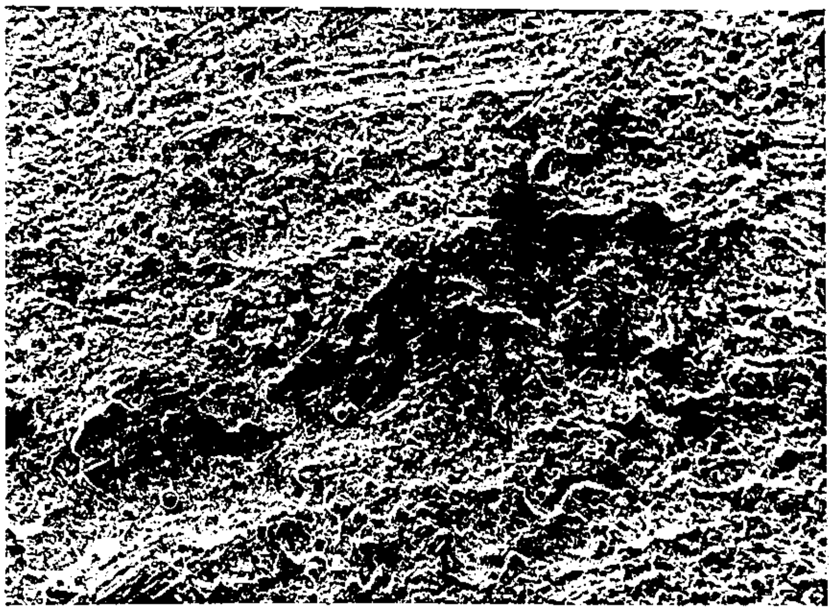

Plate 3.1 Micrograph of P1 sample showing plastic deformation of the surface and micro-cuts, × 100.

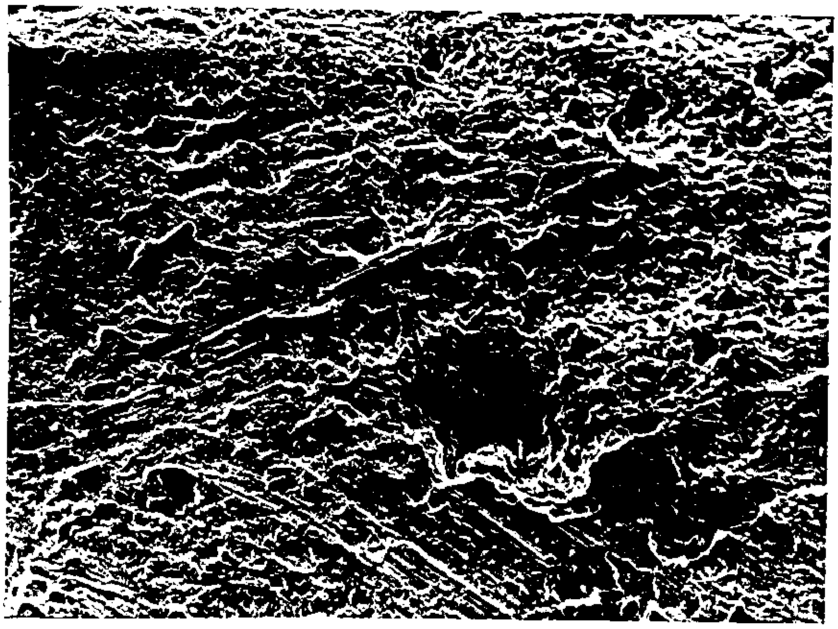

Plate 3.2 Micrograph of P1 showing cavitation and grooves at perpendicular directions, × 356.

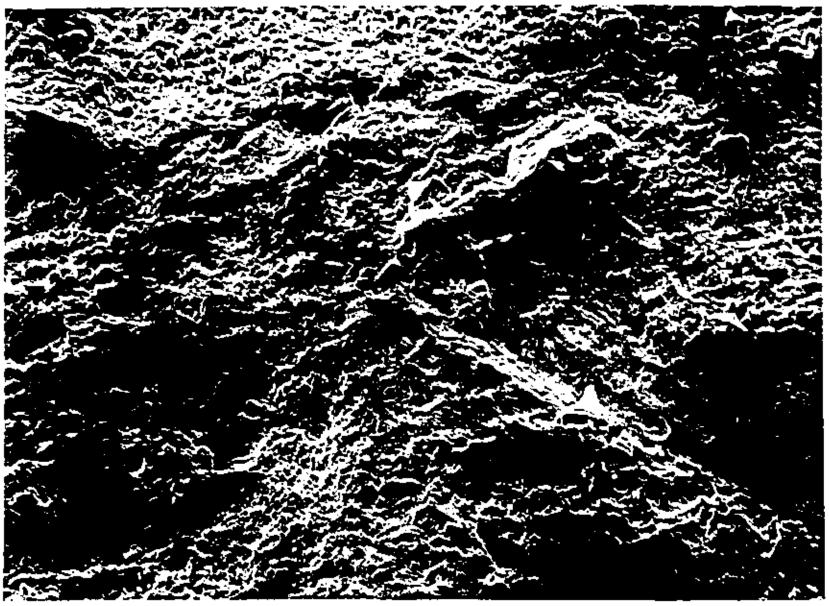

Plate 3.3 Micrograph of P2 showing material pile up in front of a large groove, × 160.

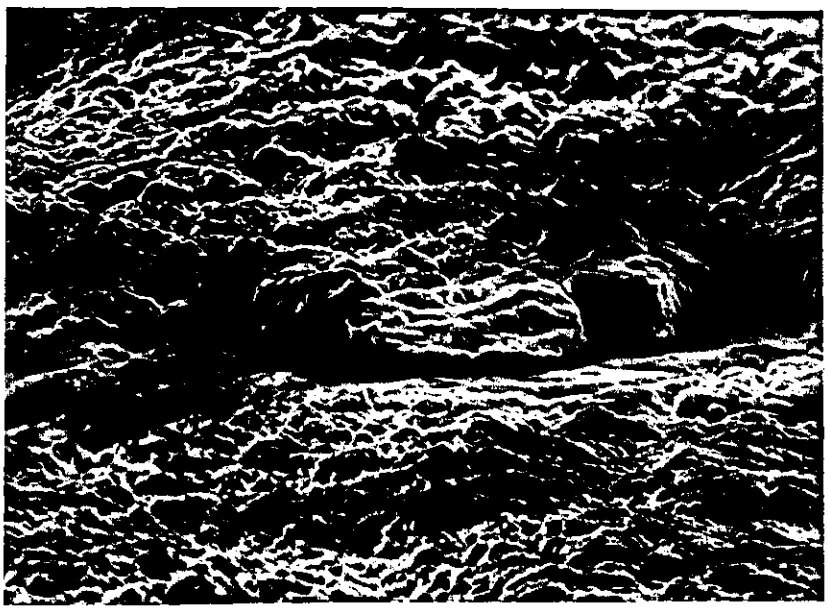

Plate 3.4 Micrograph of P2 showing extensive plastic deformation and a micro-cut, ×1000.

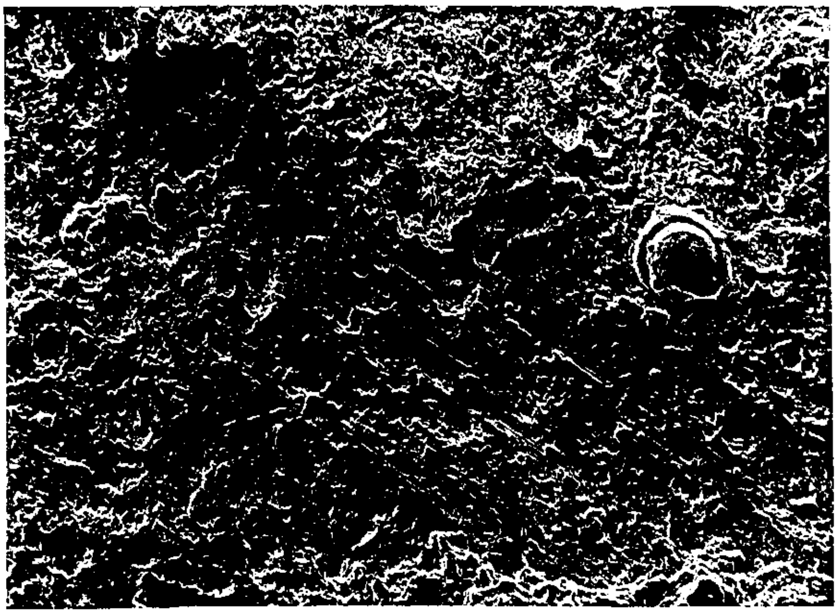

Plate 3.5 Micrograph of P3 showing plastic deformation of the surface ×100.

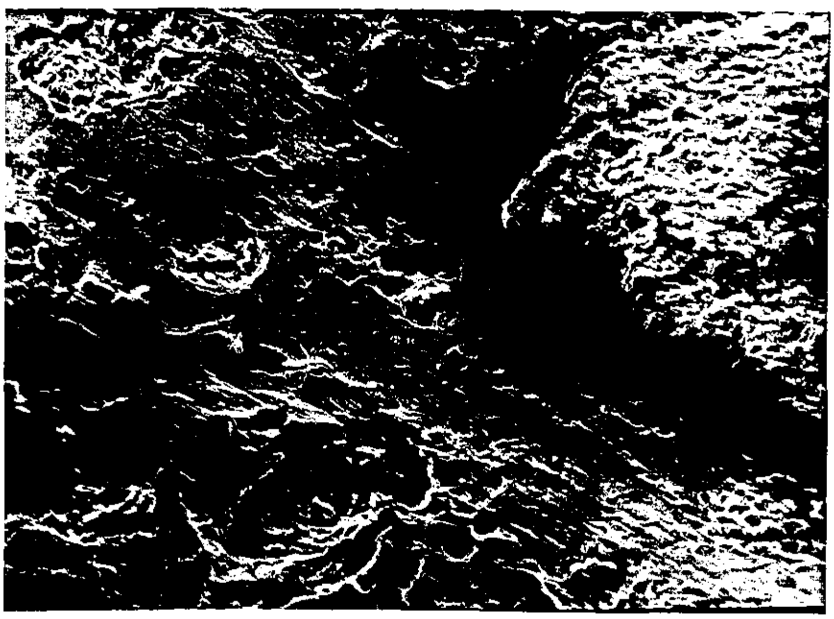

Plate 3.6 Micrograph of P3 showing a number of impact cavities at the bottom of a groove, ×600

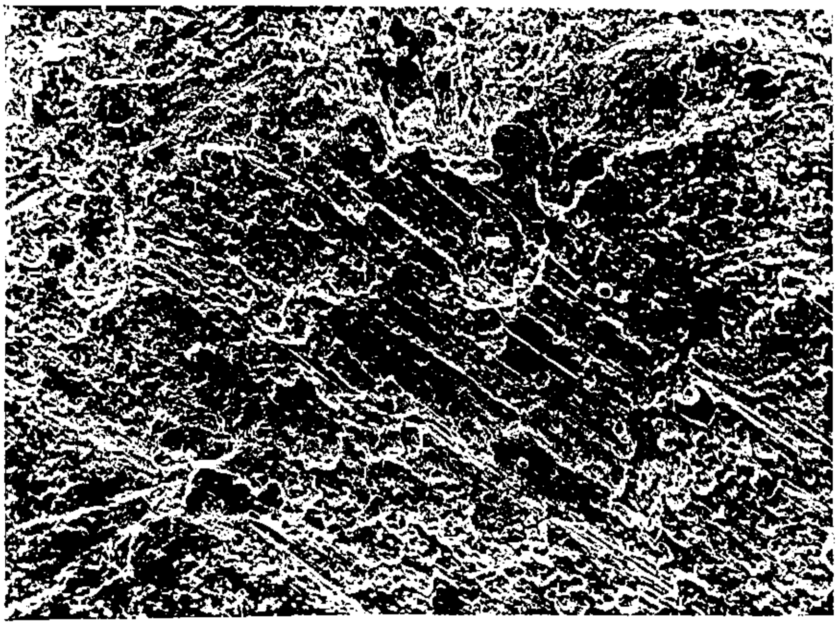

Plate 3.7 Micrograph of P4 showing plastic deformation, grooves and a number of cavities, ×250.

Plate 3.8 Micrograph of P4 showing a multi- groove cut ×550.

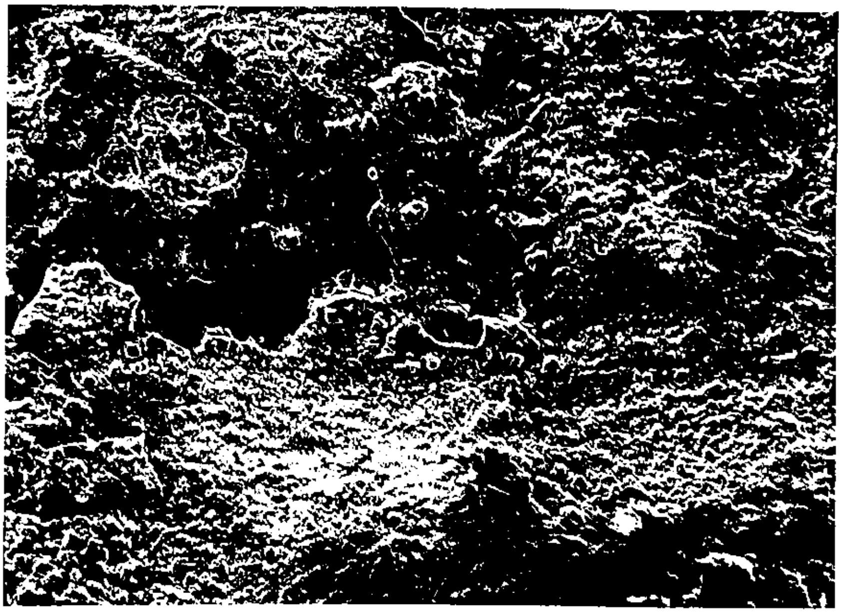

Plate 3.9 Micrograph of P2 showing a cross shaped crack and surface fatigue × 225.

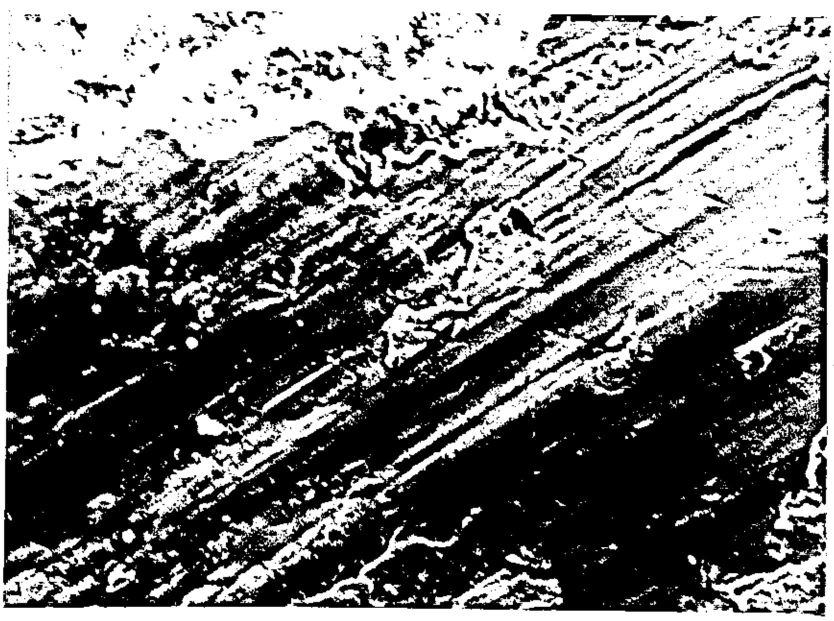

Plate 3.10 Micrograph of P4 showing several micro-cracks at the bottom of a groove ×1140.

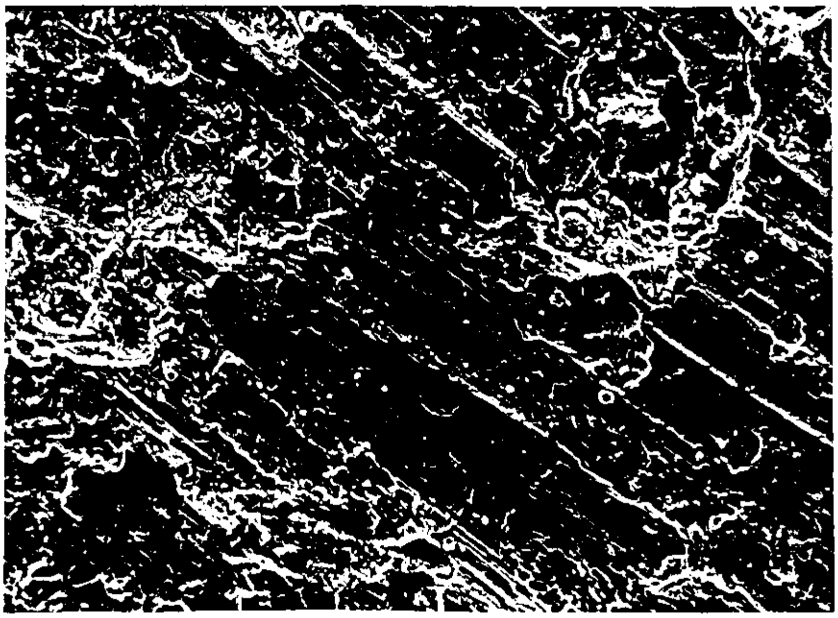

Plate 3.11 Micrograph of P1 showing a large cavity embeded with rock ×550.

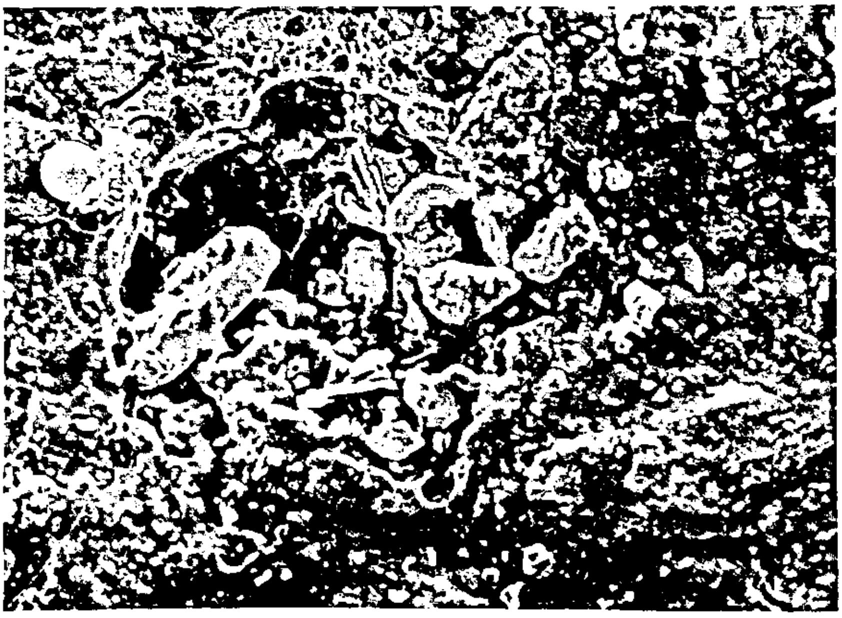

Plate 3.12 The rock particles embeded in the cavity shown in Plate 3.11 ×1400.

Plates 3.1 to 3.12 show a typical selection of micrographs taken from each sample. From a detail examination of the micrographs, the following observations were made:

a) the surface of the samples taken from mantle and concave exhibited similar wear scars,

b) the surfaces had suffered a great deal of plastic deformation in the form of wedges and ploughing grooves, as well as abundant scratches and deeper micro-cuts,

c) some degree of cavitation and micro-cracking was also present.

From these observations it has been concluded that the mechanisms of wear in all parts of the two liners are largely identical and the material removal is primarily due to abrasion with a secondary contribution from the surface fatigue and the impact modes of wear.

3.5.2 Wear Profiles

Figure 3.8 to 3.10 are the thickness markings of three sets of worn liners, exhibiting the two basic wear profiles discussed previously. The marking is produced from pieces cut from the liners at the end of their service life. The Vickers hardness of the surface is measured and marked at three points along the strip for two of the liners.

The higher impact energies delivered by the eccentric to the discharge end of the crushing chamber leads to slightly higher worked skin hardness values. Allowing for this variation and for the experimental errors, it can be seen that the hardness of the liners is typical of that expected for work hardened Hadfield steel of optimum properties.

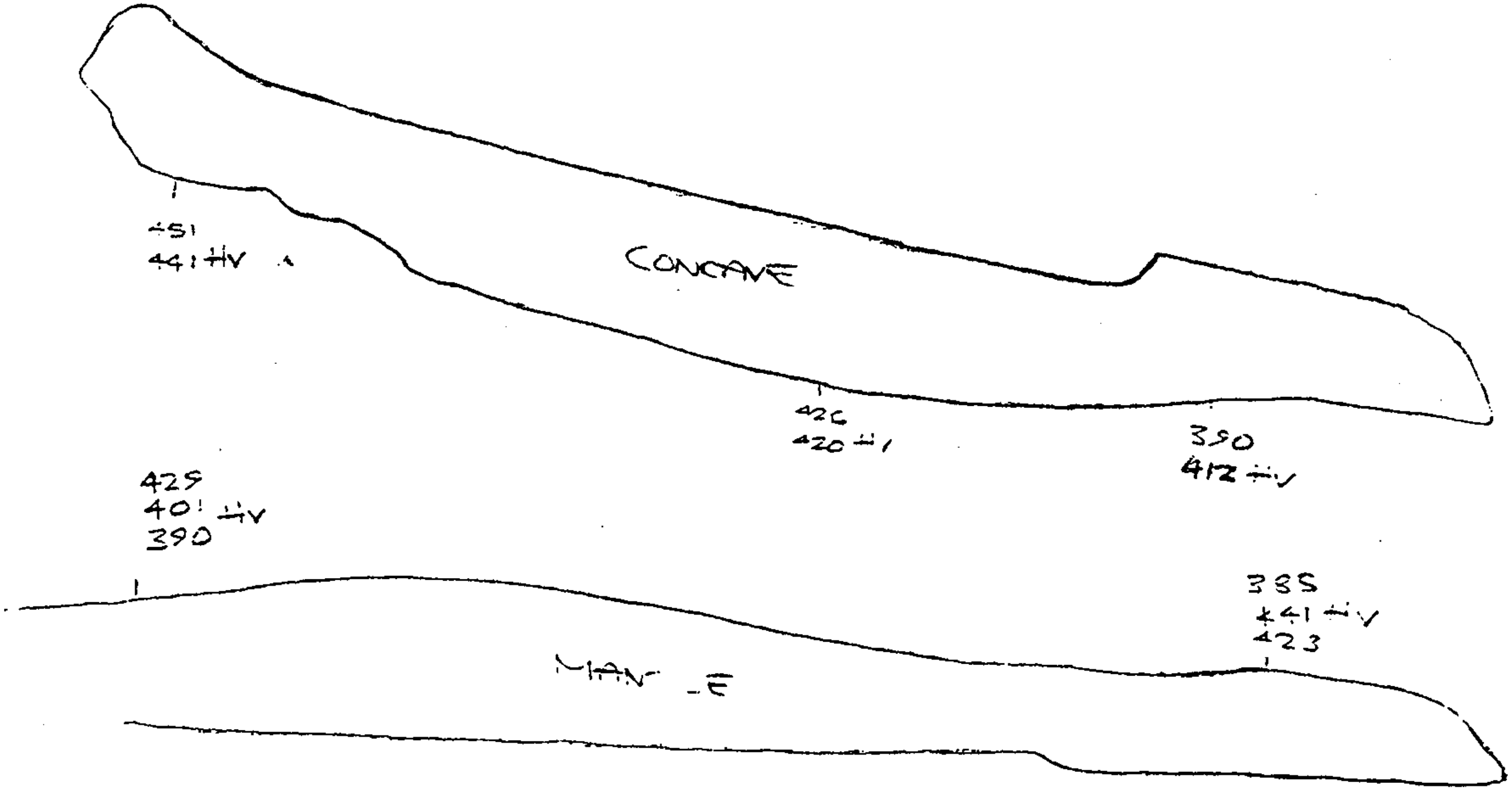

Figure 3.8 Bell-shape liner profile with slight "dishing", Auto one 900 XC, ARC Shardlow.

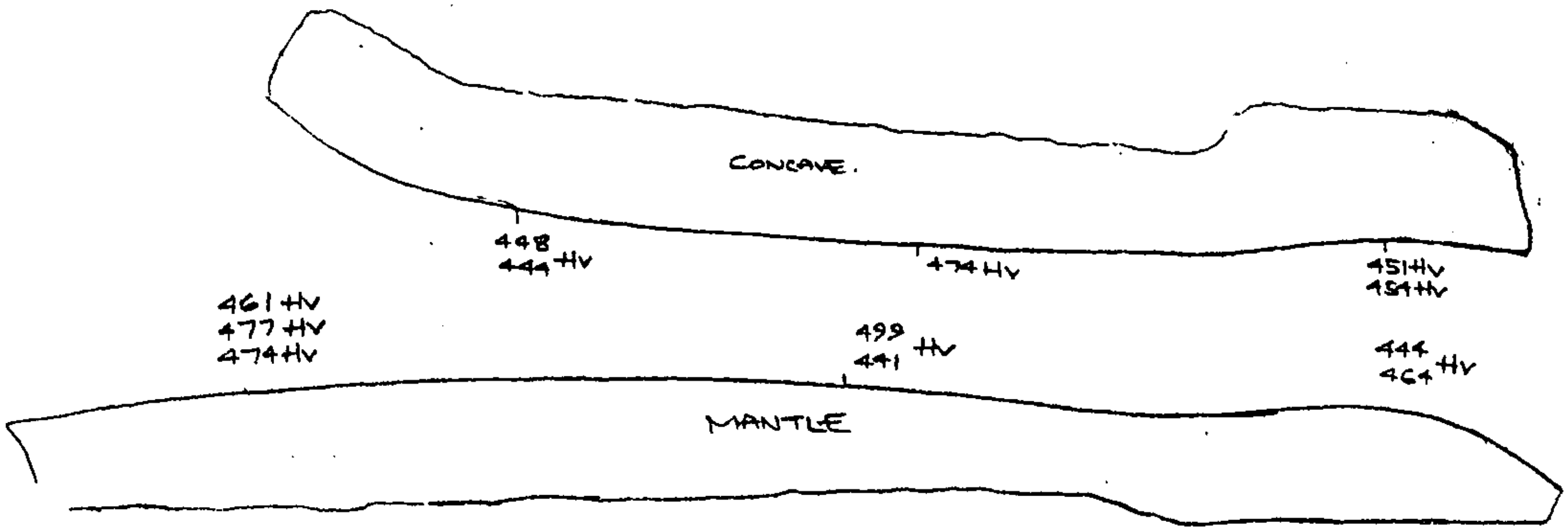

Figure 3.9 Parallel wear profile, Automax, Shap Blue Quarry.

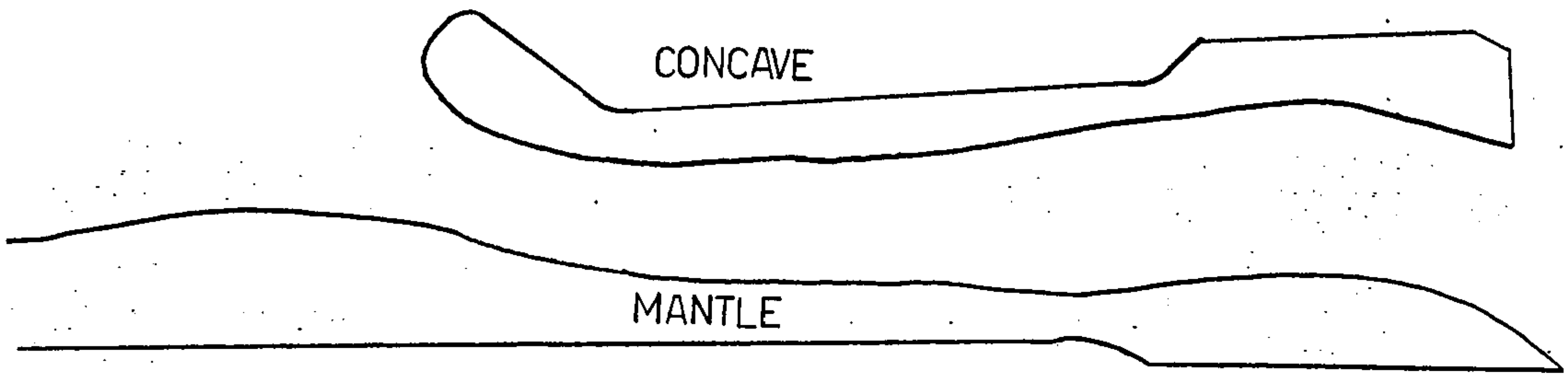

Figure 3.10 Bell-shape wear profile with extensive "dishing", Tarmac Hoverington.

Hence, the variation in the wear profiles and different metal utilization rates are not primarily due to any inconsistency in the liner properties. Therefore, it must be concluded that liner wear profile is highly dependant on a combination of MDV, operational parameters, and feed properties. A wider investigation of the observed liner profiles in the industry was carried out as part of a quarry survey, the result of which is discussed in the next section and shown in Table 3.6.

353 Survey of Liner Wear in Industry

A number of UK quarries, at which place different types of Pegson cone crushers are installed, were approached to provide information on the performance of the steel liners utilized in their cone crushers. Apart from information on wear, they were asked to provide information on the type and properties of their rock, shown in Table 3.5 , and the normal operational conditions of the cone crushers utilized.

Table 3.6 summarizes the findings of the survey. Figure 3.11 shows a bar chart of liner's service life of different types of cone crushers plotted against the Silica content of the rock. It can be seen that although there is a tendency for the liner service life to increase when the silica content decreases, the variation can not be entirely explained by this simple relationship. In the case of Autocone 900 MF, liner wear for one rock type (Gore quarry) is uncharacteristically low if the Silica content was the only rock property affecting the wear. The liner wear seems to be dependant on a combination of variables that includes rock properties (but not only the Silica content), MDV and operational parameters.

The occurrence of the problematic bell-shape wear profile can not be explained from the information available, but it seems that MF and XF liner types are more prone to this problem.

Table 3.5 Aggregate Abrasion Value and Chemical Composition (in % of weight) of Rock Types Included in the Industrial Survey

	Gwyndy	Gore	Pottal Pool	Shardlow	Shap	Pant	Whitwick
AAV	3.70	4.90	0.60	2.70	1.43	-	3.40
SiO_2	35.00	65.80	91.30	93.90	52.12	0.52	60.13
Al_2O_3	-	15.10	5.05	1.76	18.21	0.12	14.99
Fe_2O_3/FeO	1.00	5.22	0.38	0.10	5.57	0.15	7.52
MnO/MnO_2	-	0.10	-	0.18	0.79	0.02	0.21
$CaCO_3$	10.00	0.00	-	-	5.94	98.90	-
Mg_2CO_3	0.00	0.00	-	-	0.79	0.25	-
K_2O	45.00	1.59	1.81	0.03	2.66	0.02	-
Na_2O	-	2.50	0.09	0.69	2.65	0.01	-
CaO	-	3.01	0.40	0.16	5.94	-	3.92
MgO	-	3.12	0.38	0.10	3.48	-	2.45
TiO_2	-	0.56	-	2.23	-	-	-
SO_3	-	0.18	-	-	-	-	-
P_2O_5	-	0.23	-	0.09	-	-	-

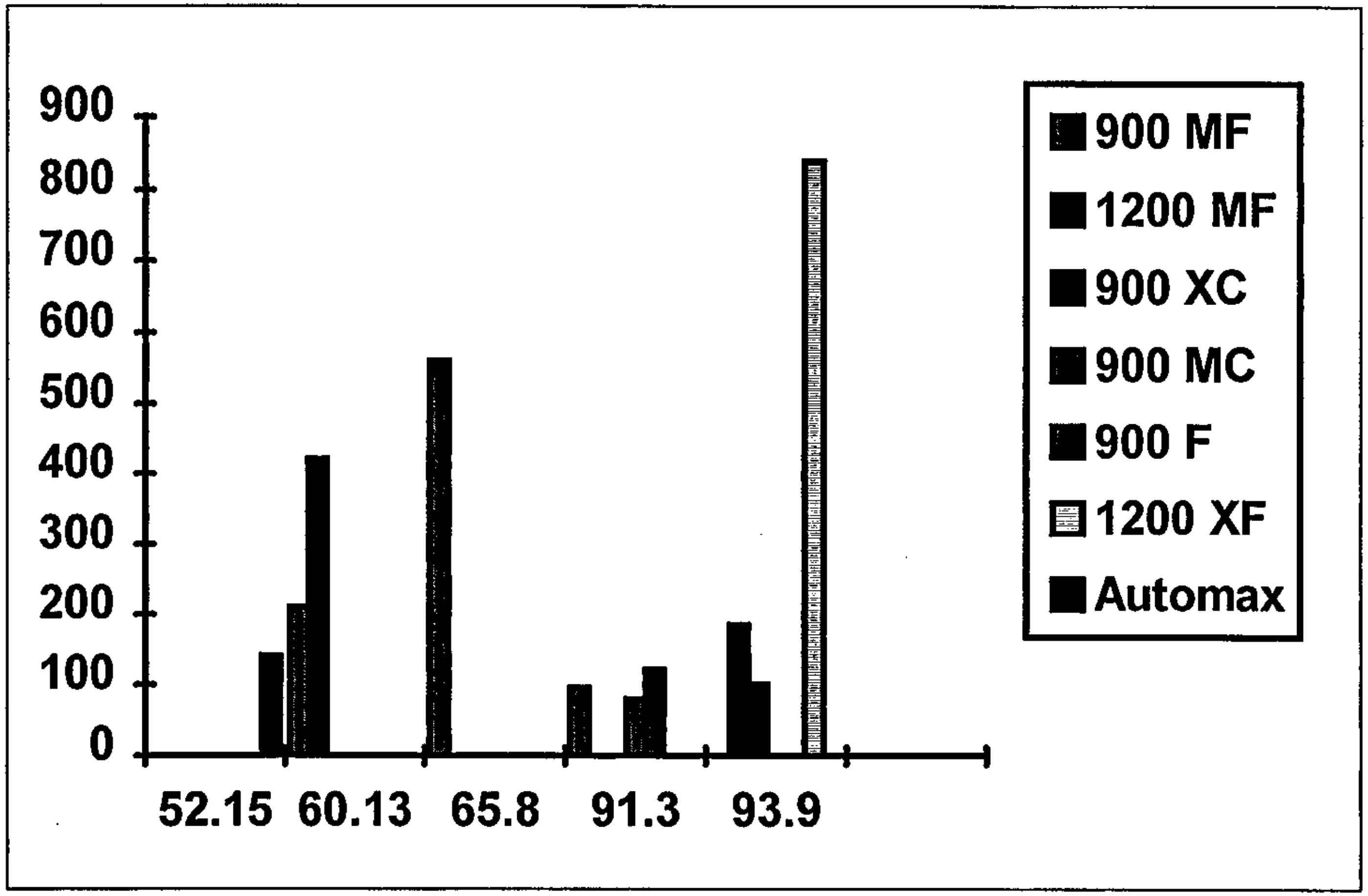

Figure 3.11 Bar representation of liners service life (hours) against rock silica content

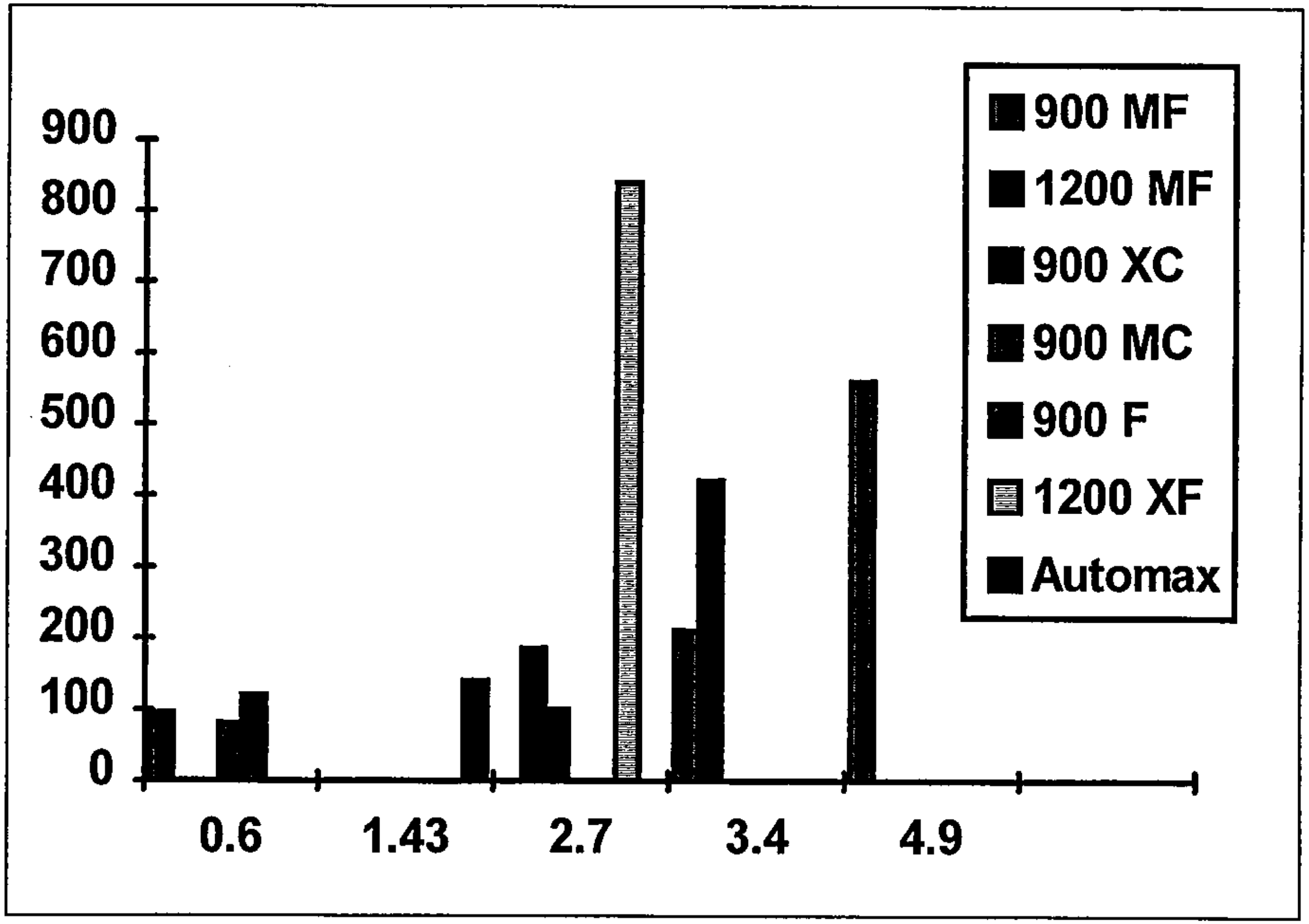

Figure 3.12 Bar representation of liners service life (hour) against the Aggregate Abrasion Value (AAV)

Table 3.6 The Results of the Survey of Liner Wear in Industry

Quarry	Rock Type	Autocone 900				Autocone 1200		Others	Operational Parameters			Wear	
		XC	MC	MF	F	XF	MF		D.S. mm	f.size mm	moist.	profile	life / hours or (tonnes)
Pottal Pool	Quartzite Gravel		✓						27	+40-75	wet	parallel	80 (10500)
Pottal Pool	Quartzite Gravel			✓					22	+20-40	wet	parallel	95
Pottal Pool	Quartzite Gravel				✓				10	+14-20	wet	parallel	120
Gwyndy	Altered Granite							700	20	+20-40	dry	parallel	288 (7776)
Shardlow	Quartzite Gravel	✓							25	+40-150	dry	parallel	100
Shardlow	Quartzite Gravel						✓		20	+20-40	wet	parallel	185 (32400)
Shardlow	Quartzite Gravel					✓			10	+14-20	wet	b.shape	840*
Whitwick	Prophyritic Dacite			✓					22	+28-50	wet	b.shape	210*(21600)
Whitwick	Prophyritic Dacite						✓		20	+20-40	wet	b.shape	420*
Gore	Greywacke gritstone							700	10	14	dry	parallel	1330[4]
Gore	Greywacke gritstone			✓					20	50-28	dry	parallel	560* (63400)
Shap	Biotite Hornfels							Automax	Var.	Var.	wet	parallel	140*(18000)
Pant	Limestone							Automax	Var.	Var.	dry	parallel	5040 (580000)

* Figures based on service life in weeks, 1 week taken as 35 hours var. : Variable

3.5.4 Effect of Liner Properties

Autocone liners are manufactured to Pegson Standard PS 1181, i.e. Austenitic manganese steel castings to ASTM A128-c. This is basically an austenitic manganese steel with up to 2% Cr added to raise the yield, as described before, in the Unworked condition. If manufactured to the right standards, the properly heat treated steel should exhibit conforming hardness and wear resistance. However, at present no quality control measures are in force to ensure the steel is manufactured to consistent and optimum standards. This results in variations in the performance of liners that are not easily accounted for.

Two sets of liners were supplied by Pegson Ltd., taken from one of their Autocone 900 cone crushers at one of the Leicestershire's quarries, for investigation into their differing performance. Both liners were manufactured from material to Pegson Standard PS 1181. One set of liners (No. 2) had suffered excessive wear resulting in a crack in the middle part of the mantle. It was reported that this set was used to crush rock from a new quarry face. However, the new rock type seemed to be less consolidated and easier to crush than that previously quarried. Therefore, the excessive wear could not be primarily explained by the change in the rock properties. Samples of the two rock types were also provided for examination.

The two sets of liner were cut and two samples were made from each of them for metallurgical studies. The rocks were supplied in rod shape blocks and were cut into small discs for examination.

Table 3.7 shows the results of the tests carried out on the rock samples, that included Rockwell Hardness test, Shore Sclerescope hardness test and spectrum analysis to obtain spot and average compositions. In the absence of necessary equipment for petrological analysis, the latter test was adopted to provide some information on the relative presence of different constituents in the rocks.

Table 3.7 Properties Of the Two Rock Samples

Rock Type	Colour	Rockwell C Hardness	Scleroscope Hardness	Si (counts)	Al (counts)
1	black	47.0	75	168288	25210
2	brown	34.5	55	151461	15720

It can be seen that the rock involved in the accelerated wear rate (No.2), is a softer material with less abrasive constituents, Silicon and Aluminium. It was therefore concluded that the new rock type could not be responsible for the observed excessive wear.

Table 3.8 The Results of Hardness Measurement on the Liner Samples

	Concave No 1	Mantle No 1	Concave No 2	Mantle No 2
Worked Vickers Hardness	423	412	313	299
Unworked Vickers Hardness	271	274	252	249

Table 3.8 shows the Vicars hardness measured on the worked surface of the liners as received. Also shown are the average unworked bulk hardness measured on the surface of the samples taken from each liner. It can be seen that the worked and unworked hardness of the liners with excessive wear are considerably lower than that of the other set. In order to find the cause of lower hardness, metallography techniques were used to examine the liner samples both in un-etched condition and after etching in 2% nital.

In the unetched condition, all samples showed some evidence of inter-dendritic micro-porosity. The etched samples were examined at two magnification levels. The structure of each sample is shown as observed in Plates 3.13 to 3.20. The results of the metallographic examinations of the samples can be summarized as follows.

Concave No. 1(423 HV)

The sample was observed to contain relatively equiaxed grains of austenite. Mainly fine and well distributed carbides were present in the structure, some of which occurred at the grain boundaries.

Concave No.-2(313 HV)

The sample contained large grains of austenite. Although the carbides observed at high magnification were found to be fine and well distributed, a considerable amount of larger and segregated carbides present mainly at grain boundaries was also evident.

Mantle No.-1 (412 HV)

The structure was observed to contain large grains of austenite. A fine and well distributed network of carbides were present, some of which occurred at the grain boundaries.

Mantle No.-2 (299 HV)

Examination of the sample at low magnification revealed some of the original dendritic as-cast structure of the material. At higher magnification it was evident that quite large aggregation of carbides had been precipitated at the inter-dendritic locations.

In general it can be stated that the structure of samples taken from the first set of liners indicated correctly heat-treated cycles resulting in typical equiaxed grains of austenite with some well distributed fine carbides. However, samples taken from the second set of liners demonstrated, to a varying degree, a structure which can result when the heat-treatment cycle is not entirely satisfactory (Bullens 1939).

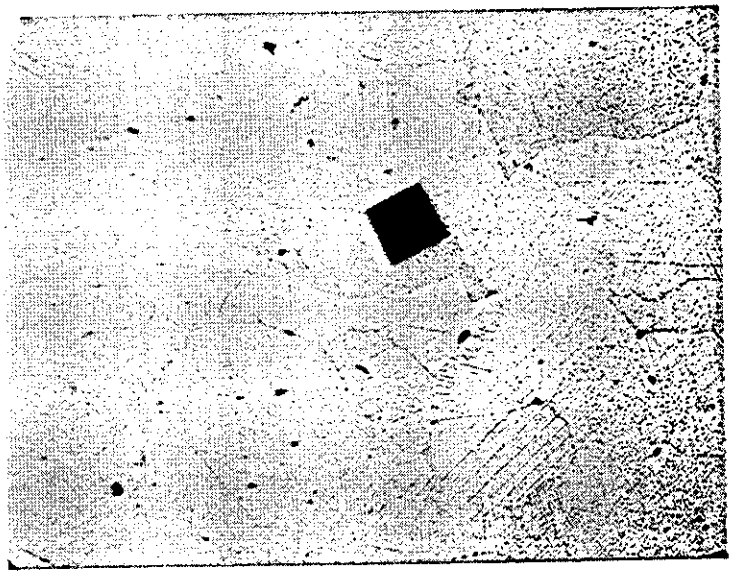

Plate 3.13 Micrograph of concave No. 1 ×25 showing the grains and some fine carbides at grain boundaries

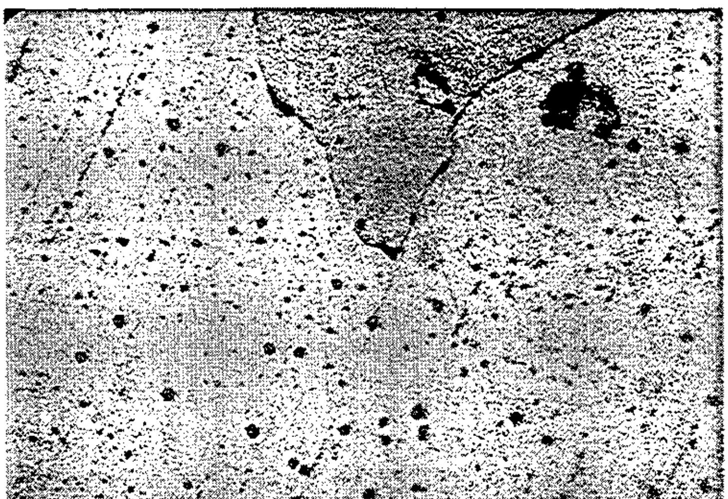

Plate 3.14 Micrograph of concave No. 1 ×250 showing a well distributed mainly fine carbides

Plate 3.15 Micrograph of concave No. 1 ×25 showing the grains and some fine carbides at grain boundaries

Plate 3.16 Micrograph of Mantle No. 1 ×250 showing a well distributed mainly fine carbides

Plate 3.17 Micrograph of concave No. 2 ×25 showing the grains and segregated carbides at grain boundaries

Plate 3.18 Micrograph of concave No. 2 ×250 showing some well ditributed fine carbides and some larger ones at grain boundaries

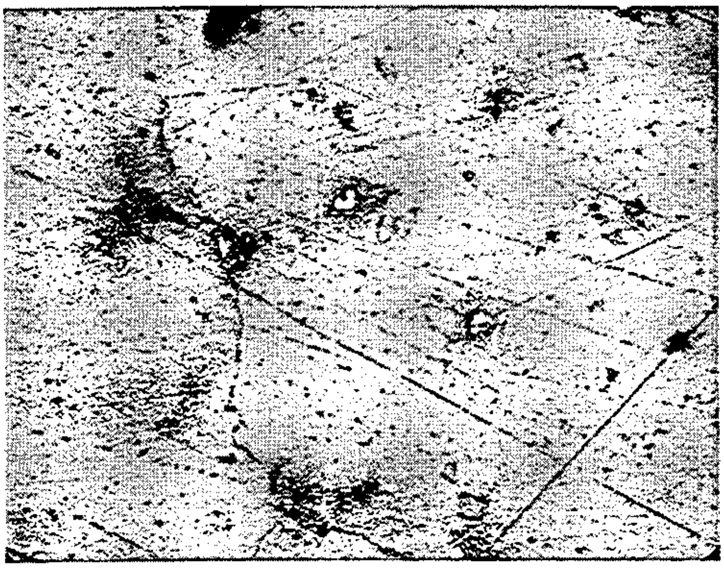

Plate 3.19 Micrograph of mantle No. 2 ×25 showing the grains and highly segregated carbides

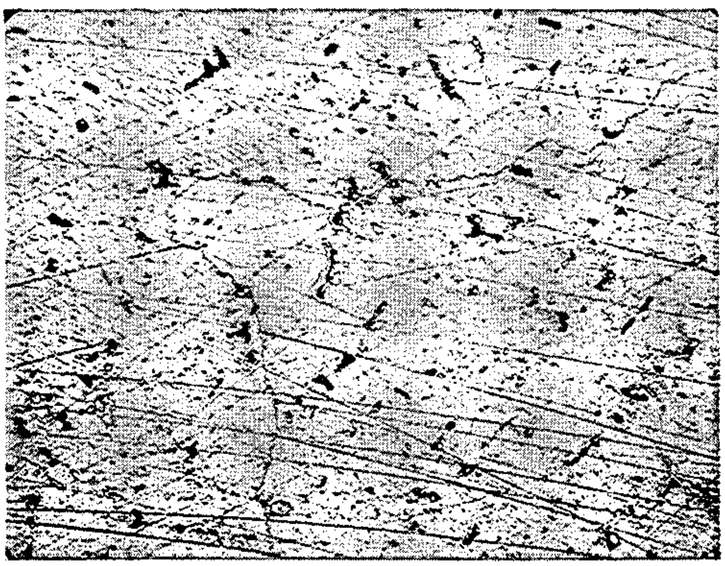

Plate 3.20 Micrograph of mantle No. 2 ×250 showing the harge segregated carbides

This investigation highlights the significance of the material properties of liners in determining their industrial performance. The destructive nature of metallurgical tests necessary to verify the structure of the steel, emphesizes that the wear properties of liners can not be entirely established prior to installation. In the absence of an effective quality control procedure, the variation in the metallurgical properties of liners introduces an unpredictable factor in the estimation of wear based on other measurable parameters.

3.6 Classification Of The Wear Process And Effective Parameters

Classification of the wear process in cone crushers relies on the understanding of the system kinematics, the nature and variation of the crushing force, the common wear profiles and the mechanisms of material removal as evident from the appearance of the worn surfaces. The results of the investigations described in this chapter have provided ample information on all these subjects enabling the classification of the wear process to be carried out confidently.

The main findings relevant to the classification of the wear are as follows:

1. the normal component of the impact force generated by the torque in the main shaft and the eccentric are the force inducing the wear,

2. the profile of the liners are such that the separation between them decreases from top to bottom,

3. the rock particles are usually tightly packed between the liners, however they can rotate and slide relative to each other as well as against the liners,

4. in most cone crushers a multi-layer of rock particles are present in the crushing chamber, therefore, only a proportion of rock particles come into contact with the surface of the liners,

5. the surface roughness decreases along the length of the liners. Wear scars observed are mainly spiral,

6. the most common industrial wear profile observed is differential and the material loss intensifies along the length of liners,

7. from wear scars observed, the main wear mechanisms are ploughing, wedge forming and micro-cutting. Evidence of surface fatigue and impact wear as well as macro-cutting can also be found.

On the strength of these observations and based on the discussions presented in the previous chapter, it can be concluded that the main wear process in cone crushers is open three-body abrasion. The wear regime changes from low-stress (associated with low crushing force and little or no breakage) to high-stress (associated with high crushing force) open three-body abrasion along the length of liners, as the distance between the two liners decreases and the crushing force intensifies. The change in the wear regime is manifested in the observed differential wear and the intensification of material loss along the liners length.

Open three-body abrasive wear is a complex wear process and its rate, as is evident from the results reported here, is primarily dependant on three factors:

a) the properties of wearing surfaces,

b) the properties of abrasive particles,

c) the relative geometry of involved surfaces and the value of the acting force.

In the case of metal surfaces, environmental factors i.e. moisture and temperatures are also very significant. In the specific case of cone crusher system, the effective parameters are identified as follows:

1. the crusher characteristics in terms of Machine Design Variables,

2. the material properties of Hadfield steel, used to manufacture the liners, in terms of composition, micro-structure, hardness and tensile strength,

3. the material characteristics of rock, in terms of composition, physical and mechanical properties,

4. the operational parameters in terms of crusher setting, feed size and throughput,

5. the environmental parameters in terms of rock moisture and tribo-induced temperatures.

The liner wear in cone crushers is a multi-variable phenomenon, the modelling of which would require appropriate experimental design and data analysis techniques. In the quantitative study of liner wear, the effect of all the above parameters, except the Machine Design Variables, were investigated. The exclusion of the MDV was due to the lack of essential industrial test rigs and therefore unavoidable.

Chapter 4 EXPERIMENTAL INVESTIGATION OF WEAR

The aim of the experimental work was to determine the quantitative effect of the primary variables, discussed in the previous Chapter, on the wear of liners and hence provide data for formulation of a predictive wear model. In this chapter the test equipment, procedure and methods of measurements, experimental design and the data analysis techniques used in the study are discussed.

4.1 Experimental Procedure and Methods of Variable Monitoring

4.1.1 Laboratory Size Cone Crusher

The primary variables affecting liner wear, as discussed in the previous Chapter, are:

1. Liner properties: hardness, micro-structure.
2. Rock Properties: physical, chemical and mechanical,
3. Operating Parameters: crusher setting, feed size,
4. Environmental Parameters: moisture content, tribo-induced temperature.

The wear experiments were carried out using a laboratory size Massco GY-Roll cone crusher, shown in Figure 4.1. The relevant specifications for the crusher are summarized in Table 4.1. A feed hopper and a trolley for collection of product were made and added to the crusher.

Table 4.1 Basic Specifications of The Laboratory Size Cone Crusher

Power Consumption Crusher Idling (Kilowatts)	0.17
Head Diameter (cm)	15.24
Dimensions(cm)	58 ×38 ×38

Figure 4.1 The Laboratory Size Cone Crusher

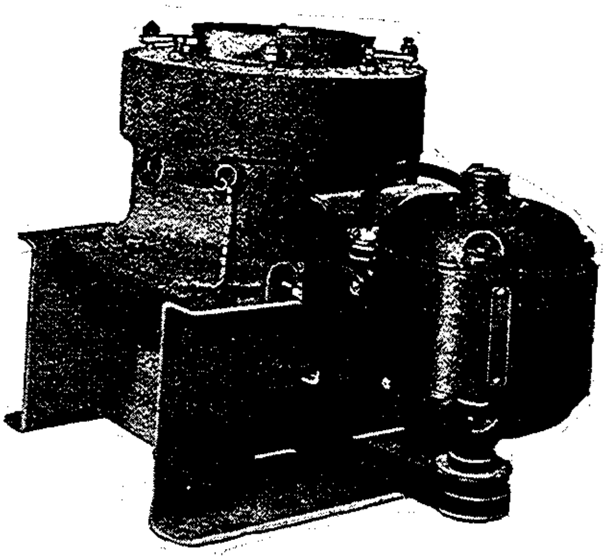

The basic operation and kinematics of the Massco GY-Roll laboratory size cone crusher is comparable to that of industrial cone crushers and can be summarized as:

a) the eccentric and gyratory movement of the head subjected the rock particles to a compressive crushing force,

b) the crusher was choke fed, and the size of the crushing chamber, at all the settings chosen for the experiments, was large enough to accommodate a multi-layer of feed particles.

4.1.2 The Crusher Liners

Five pairs of concave and mantles were manufactured by a foundry that regularly produces liners for Pegson's Autocone cone crushers. In order to minimize the variation in liners' properties, the foundry was requested to cast all the liners using one batch of Hadfield steel, produced to the Pegson PS 1181 standard. The cast liners were subsequently machined to specification. Despite the machining process, the weight of the liners displayed a variation, as shown in Table 4.2 .

The machining process is expected to result in a certain degree of work hardening. however, to ensure a uniform work hardening condition, and to allow a meaningful comparison between the performance of the liners, they were all subjected to an identical crushing run prior to the main experiments. The procedure followed was to crush 25 Kg of Pottal Pool rock, the hardest rock tested, at a 4mm setting to allow maximum work hardening of the liners. The liners were then removed, cleaned and weighed again. The final weights are shown in table 4.2. No conclusion should be made from this initial weight loss, as this depends on the original work hardened state of each liner. The comparison between the liners performance was planned by two further runs of crushing test, using 25 Kg of

Pottal Pool and Whitwick rocks, at a setting of 4mm, as presented in the next chapter.

Table 4.2 Weight of the Liners

Liner Set No.	Original Weight (gramme)		Weight After Work Hardening (gramme)	
	Concave	**Mantle**	**Concave**	**Mantle**
1	1970.2	1322.4	1969.5	1321.5
2	1896.7	1351.0	1895.9	1349.8
3	2071.0	1553.6	2070.1	1552.4
4	1795.7	1647.4	1794.7	1646.3
5	1780.9	1651.1	1779.3	1649.8

Each concave and mantle was used in the crushing of two rock types. Alternating concave and mantle arrangements, as shown in Table 4.3, were chosen to allow the capture of wear scars produced by each rock type for later examination.

Table 4.3 The Liner Sets Used

Rock Type	Liner Used	Liner Used to Capture Wear Scars
Cliffe Hill	1C 5M	5M
Shap	1C 1M	1C
Water Swallows	2C 1M	1M
Shardlow	2C 2M	2C
Pottal Pool	3C 2M	2M
Whitwick	3C 3M	3C
Pant	4C 3M	3M
Ingleton Grey	4C 4M	4C
Judkin	5C 4M	4M
Breedon	5C 5M	5C

Due to the destructive nature of the required tests, the hardness and structure of the liners were determined after the completion of the main wear experiments.

4.1.3 Rock Types Chosen for the Study

The rock types used in the experimentation were chosen to cover a wide range of chemical, physical and mechanical properties and to be representative of the rocks normally used in the construction industry in the UK. They were obtained in single grades of +10-14mm and, in the majority of the cases, from the operating quarries that employ Pegson cone crushers. The rock types and the corresponding operating quarries are shown in table 4.4.

Table 4.4 Rock Types Used in the Wear Experimentation

Operator	Quarry	Rock Type
Breedon Plc	Breedon	Limestone
Amey Roadstone Corporation	Judkins	Quartz/Diorite
Amey Roadstone Corporation	Pottal Pool	Quartzite
Amey Roadstone Corporation	Shardlow	Quartzite
Tarmac Roadstone Ltd	Waterswallows	Basalt
Amey Roadstone Corporation	Shap Blue	Hornfels
Amey Roadstone Corporation	Pant	Limestone
Amey Roadstone Corporation	Ingleton	Greywacke
Amey Roadstone Corporation	Whitwick	Andesite
Tarmac Roadstone Ltd	Cliffe Hill	Micro Diorite

The properties of the rocks were not determined as part of this study, but provided either by the corresponding quarries or Pegson Ltd. Due to unavailability of the required equipment, independent petrological study of the rocks was not possible. Although, the grain size is believed to influence the wear, its effect was not considered to be of primary significance and was therefore eliminated from the studies. The rock properties included in the study were:

Mechanical Properties:

The mechanical properties included in the study were:

1. Fracture Toughness
2. Uniaxial Compressive Strength (UCS)
3. Brazilian Tensile Strength (BTS)
4. Point Load strength Index:
5. Rebound Hardness.

Bearman (1991) investigated the relationship between rock characterisation tests and found that a strong correlation exist between the fracture toughness test and a number of other rock parameters, in particular, the strength parameters tested by Schmidt hammer, Young's Modulus and Seismic properties. Therefore, it was decided to limit the mechanical properties included in the present study to those listed above. The values for all mechanical properties were provided by Pegson Ltd and are shown in Table 4.5. The following describes the tests briefly.

Fracture Toughness

Two methods of testing are recommended by the ISRM, the chevron Bend and the Short Rod methods. The fracture toughness values included in this study were obtained by Pegson Ltd using the Chevron Bend method. The equation for determination of fracture toughness using this method is:

$$\mathbf{Kcb} = (\mathbf{A} \times \mathbf{F_{max}}) / \mathbf{D}^{1.5} \qquad \mathbf{4.1}$$

where **A** is a dimensionless factor that depends on the geometry of the core specimen, **D** is the diameter of the core and $\mathbf{F_{max}}$ is the maximum load applied to test piece.

Uniaxial Compressive Strength (UCS)

The test is according to ISRM recommendations of a 42mm core specimen with a length diameter ratio of 2.5:1. The application of the load is in a stiff testing machine.

Brazilian Tensile Strength (BTS)

For this test the ISRM recommendations are for a disk test specimen with a minimum diameter of 54mm. The specimen needs special holder to ensure a distributed load over a set arc of 15 degrees at the circumference of the disc. The application of the load is carried out in a stiff testing machine. The BTS is calculated by:

$$\sigma_t = 2P/\pi t D \qquad 4.2$$

where **P** is force at failure, **t** and **D** are thickness and diameter of the disk respectively.

Point Load Strength Index

The tests for Point Load Index is determined using 42mm diameter core specimens. The determination of the index is by:

$$I_S = P/D^2 \qquad 4.3$$

where **P** is force at failure and **D** the diameter of test piece. The value obtained by equation 4.2 must then be corrected either using the available correction charts or by the correction factor presented by Franklin and Dessault (1989):

$$I_{S50} = F(P/D^2) \qquad 4.4$$

where F is the dimensionless correction factor given by:

$$F = (D/50)^{0.45} \qquad 4.5$$

Schmidt Rebound Hardness Test

The rebound hardness test was considered a more appropriated test of hardness in this study, as it provides a macro-hardness value compared to the micro-hardness measured by penetrative techniques described in Chapter 2. The test procedure, as outlined by ISRM is carried out on a core of 54mm diameter, clamped securely perpendicular to the plane of hammer movement.

Chemical Properties

The chemical composition of the rocks, as supplied by the quarries and are shown in Table 4.6. Also included in the table is the pH value of the rock types.

Basic Physical Properties:-

These are the fundamental rock properties, relative density and water absorption. The tests are conducted according to BS 812, part 2. The basic properties were considered to be of importance in this study because they provide information on the micro-structure of the rock. Low density and high water absorption usually indicates high porosity and low mechanical strength. The values used were supplied by the quarries and shown in Table 4.7.

British Standard Aggregate Tests

The aggregate tests are commonly used in the quarrying industry to characterize feed to crushers. These are as follow:

1. Aggregate Crushing Value (ACV)
2. Aggregate Impact Value (AIV)
3. Aggregate Abrasion Value (AAV)
4. 10% Fines

The ACV test measures the resistance of an aggregate to a crushing load and is measured according to BS 812, part 110. AIV similarly expresses the resistance to impact forces and is measured to BS 812 part 112. AAV provides a measure for abrasive potential of the rock and is measured according to BS 812, part 113. !0% Fines test is a measure of the force needed to produce 10% of -2.36mm material from a given sample grading and measured according to BS 812, part 111. The test values used in the study were supplied by the quarries and are shown in Table 4.7.

4.1.4 Measurement of Test Variables

The experimental work involved the measurement or monitoring of the following Parameters:

a. Input Parameters

1. closed-side setting
2. weight of rock
3. moisture content

b. Output Parameters

1. liner wear
2. liner temperature
3. crushing time
4. power consumption
5. product size distribution.

A Grant Squirrel 12 bit data logger with a sample rate of 1 Hz was used to record all electrical signals. Figure 4.2 shows a schematic view of the experimental set up. The measurement method used for each parameter was as follows.

Closed-Side Setting

The crusher setting was adjusted via a threaded cap to the upper main frame. The setting was confirmed by passing a lump of aluminium foil through the crusher, and measuring its thickness, after emerging from the crusher, to two decimal

Table 4.5 Mechanical Properties of the Tested Rocks

Quarry	Rock Type	Schmidt Hardness	FT $MN/m^{1.5}$	UCS MPa	BTS MPa	PL MPa
Breedon	Limestone	37	2.100	175.63	12.97	10.61
Judkin	Quartz/Diorite	39	2.338	200.33	14.16	11.87
Pottal Pool	Quartzite	55	2.880	260.02	18.06	14.44
Shardlow	Quartzite	51	2.734	254.23	17.66	13.88
Waterswallows	Basalt	38	2.600	212.78	16.55	12.85
Shap	Hornfels	41	2.959	320.19	24.60	14.78
Pant	Limestone	21	1.855	151.23	11.90	9.28
Ingleton	Greywacke	51	2.382	226.26	15.19	12.30
Whitwick	Andesite	40	2.174	139.20	14.49	11.68
Cliffe Hill	Diorite	43	2.770	274.82	18.42	13.50

Kcb: Uncorrelated Fracture Toughness,
BTS : Brazilian Tensile Strength,
UCS: Uniaxial Comprehensive Strength,
PL: Point Load Index.

Table 4.6 Chemical Properties, by % of weight, of the Tested Rocks

	Breedon	Judkin	Pottal Pool	Shardlow	Water swallows	Shap	Pant	Ingleton	Whitwick	Cliffe Hill
SiO_2	0.73	53.80	91.3	93.9	50.15	52.12	0.52	58.52	60.13	51.6
Al_2O_3	1.25	15.20	5.05	1.76	16.68	18.21	0.12	15.13	14.99	24.9
Fe_2O_3/FeO	0.06	11.54	0.38	0.10	12.39	5.57	0.15	5.13	7.52	19.3
MnO/MnO_2	0.00	0.00	0.00	0.18	0.00	0.79	0.02	0.07	0.21	0.21
$CaCO_3$	55.81	0.00	0.00	0.00	0.00	5.94	98.9	0.00	0.00	0.00
Mg_2CO_3	41.75	0.00	0.00	0.00	0.00	0.79	0.25	0.00	0.00	0.00
K_2O	0.00	2.30	1.81	0.03	0.00	2.66	0.02	3.20	0.00	0.00
Na_2O	0.00	2.92	0.09	0.69	9.83	2.65	0.01	1.59	0.00	0.00
CaO	*	4.77	0.40	0.16	6.47	*	0.00	5.17	3.92	0.00
MgO	*	3.36	0.38	0.10	0.00	*	0.00	3.33	2.45	3.40
TiO_2	0.00	0.00	0.00	2.23	0.00	0.00	0.00	0.70	0.00	0.48
SO_3	0.00	0.00	0.00	0.00	0.00	0.00	0.00	0.00	0.00	0.13
P_2O_5	0.00	0.00	0.00	0.09	0.00	0.00	0.00	0.15	0.00	0.00
PH	-	6.6	7.1	7.2	6.5	6.7	9.1	8.6	7.8	7.9

* exists in compound form

Table 4.7 Basic and Aggregate Crushing Test Values for the Tested Rocks

Quarry	Rock Type	Relative Density APP.	Water Absorption (% by Weight)	AIV Dry (Soaked)	ACV	AAV	10% Fines /kN. Dry (Soaked)
Breedon	Limestone	2.78	0.60	21	-	-	19.3 T
Judkin	Quartz/Diorite	2.72	0.70	14	13	6.7	348 (269)
Pottal Pool	Quartzite	2.72	0.01	17	17	0.6	340
Shardlow	Quartzite	2.72	0.01	17	16	2.7	340
Waterswallows	Basalt	2.93	0.70	10 (11)	12	3.6	342 (279)
Shap	Hornfels	2.83	0.50	9	10	1.4	380
Pant	Limestone	2.39	0.78	20	19	-	190
Ingleton	Greywacke	2.74	0.70	11	10	3.1	390
Whitwick	Andesite	2.77	0.60	12	14	3.4	328 (290)
Cliffe Hill	Diorite	2.82	0.60	9 (11)	12	3.0	320 (290)

places. The crusher setting could not be fine adjusted and a spread of +/-0.2mm in the chosen setting values was found to be unavoidable.

Weight of Rock

Due to differing wear properties of the rocks, a variable amount of rock was used in each case to produce a measurable amount of wear. The weight chosen in the majority of the cases were 25Kg which in the case of less abrasive rocks was increased accordingly. The weight was measured using an electronic scale accurate to 10 grammes.

Moisture Content

Prior to the tests, a manageable amount of rock was brought in to the heated laboratory , spread to allow complete drying and then stored in open bunkers. To achieve a required moisture content, water was measured, by percentage of rock weight and added to the feed placed in a water tight bucket. The rock was then mixed thoroughly with the water to allow a uniform moisture distribution. The content of the bucket, including any unabsorbed water, was used to feed the crusher.

Liner Wear

Liner wear was characterized by weight loss during the crushing. To measure the weight accurately, the liners had to be washed and dried thoroughly to get rid of any rock particles or dust. The weight was first measured before the liners were installed in the crusher for each test. After the completion of the test, the liners were removed cleaned, dried and weighed again. The weight was measured using an electronic scale accurate to 0.1 of a gramme.

Liner Temperature

A very small self-adhesive thermocouple (RS 646-599 KType) was attached to unexposed surface of the concave to monitor the temperature. The output from the thermocouple was fed into the Squirrel data logger. The maximum temperature recorded was 26 degrees centigrade, against an ambient temperature of 22 degrees centigrade. The maximum temperature variation recorded was 4 degrees. Such small temperature variations would not have any impact on wear. Therefore, the effect of temperature was eliminated from the rest of the study.

Crushing Time

The crushing time of test batches was monitored both by a stop watch and as an integral part of the data logging devices used. The crusher throughput was then determined from batch weight and the crushing time.

Power Consumption

The power Consumption by the crusher was not considered to influence the wear. It was however monitored mainly for fault detection purposes. An EW 604 wattmeter was used to monitor the power supplied. Output pins from the wattmeter were used to feed the signal both to a X-Y plotter and the squirrel data logger for later analysis.

Product Size Distribution

A sample of crusher product, in the range of 3-4 Kg, was taken at the end of all test runs. These were then sent to ARC Central laboratory for sieve analysis. The sieve results were used to produce size distribution curves and determine the eighty percent passing size.

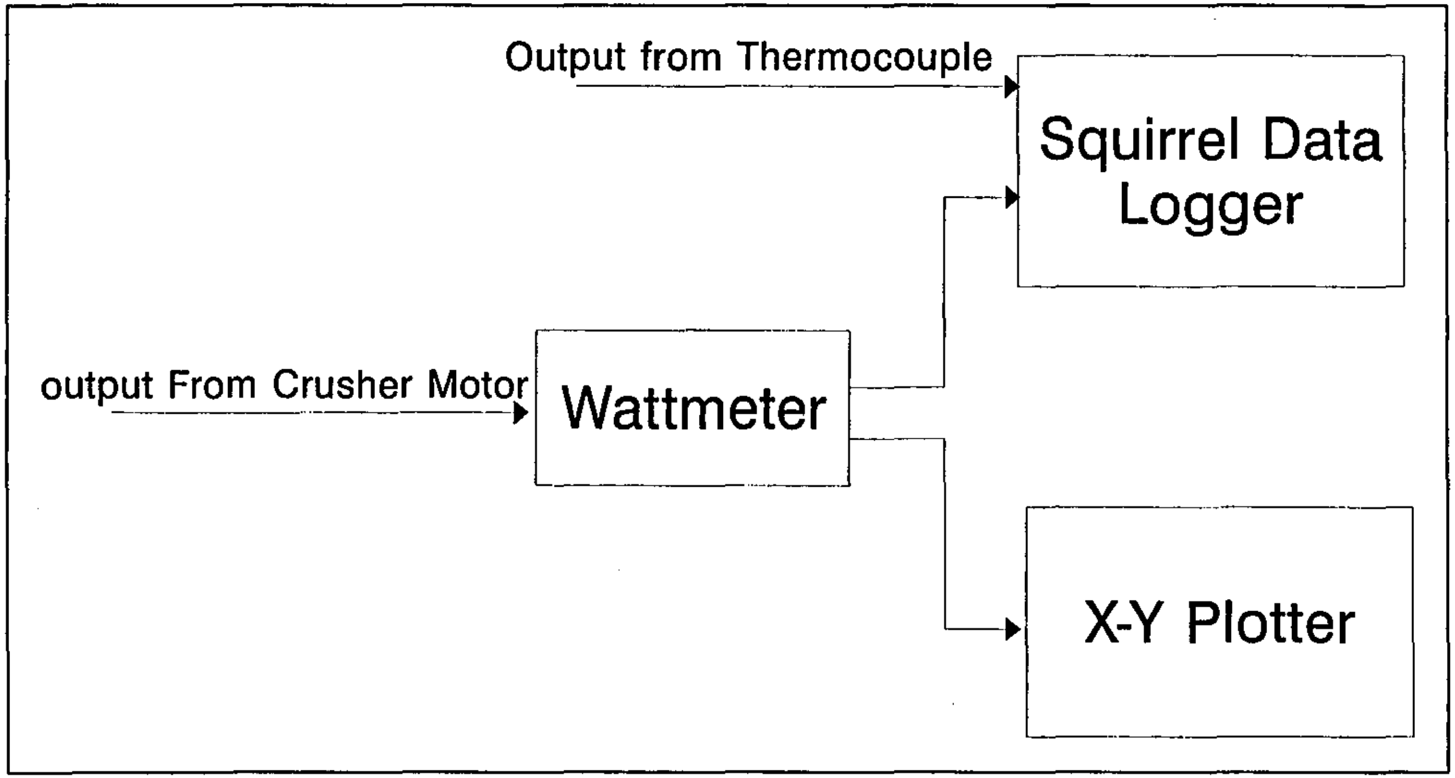

Figure 4.2 The experimental set up for measurement of power and temperature

4.2 Experimental Design

4.2.1 Full Factorial Design

The multi-variable nature of wear called for an appropriate experimental design, capable of producing easily interpreted results on the significance of each variable as well as revealing any interaction that may exist between them. The full factorial experimental design offers these desirable properties and was chosen for the experimentation.

A full factorial design in **k** factors or variables is obtained by choosing $\mathbf{n_1}$ levels of factor 1, $\mathbf{n_2}$ levels of factor 2, and $\mathbf{n_k}$ levels of factor k, and carrying out $\mathbf{n} = \mathbf{n_1} \times \mathbf{n_2} \times ... \times \mathbf{n_k}$ experimental runs obtained by taking all possible combinations of the levels selected. Table 4.8 shows the experimental plan for a 3 ×2 ×2 factorial design, where **A**, **B** and **C** are the variables; and **y** the investigated response or output. Such a design would require 12 experimental runs if no repetition is carried out.

Table 4.8 A 3 ×2 ×2 Factorial Design

	A_1	A_2	A_3	
$\mathbf{B_1}$	$y(A_1B_1C_1)$	$y(A_2B_1C_1)$	$y(A_3B_1C_1)$	$\mathbf{C_1}$
	$y(A_1B_1C_2)$	$y(A_2B_1C_2)$	$y(A_3B_1C_2)$	$\mathbf{C_2}$
$\mathbf{B_2}$	$y(A_1B_2C_1)$	$y(A_2B_2C_1)$	$y(A_3B_2C_1)$	$\mathbf{C_1}$
	$y(A_1B_2C_2)$	$y(A_2B_2C_2)$	$y(A_3B_2C_2)$	$\mathbf{C_2}$

4.2.2 Experimental Plan

The input variables were investigated at levels shown in Table 4.9.

Table 4.9 Experimental Plan

Variable	Rock Properties	Discharge Setting	Feed Size	Moisture
No. of Levels	10	5	2	5

The selection of the levels should ideally correspond to either a geometric or arithmetic progression. This was possible for discharge setting, feed size and moisture content, but not for the rock properties. The selected rocks were however, chosen to provide a reasonable range of rock properties.

The experiments were organised according to three separate factorial plans. These were designed to provide information on the interaction between all the parameters, while keeping the number of test runs at a manageable level.

1. <u>The effect of crusher setting and rock properties on wear</u>: the experimental plan is shown in Table 4.10. It represents a single variable (discharge setting) experimental design at 5 levels, that was repeated for each rock. The experiments were carried out with dry rock.

2. <u>The effect of crusher setting, moisture and rock properties on wear</u>: the experimental plan is shown in Table 4.11. It represents a two variable (discharge setting and moisture) experimental design at 3 and 5 levels respectively that was repeated for each rock.

<u>The effect of feed size, moisture and rock properties on wear</u>: the experimental plan is shown in table 4.12. It represents a two variable (feed size and moisture) experimental design at two levels that was repeated for each rock.

Table 4.10 Experimental Plan 1: Effect of discharge setting and rock properties on liner wear

Feed Fraction Size (mm)	+10-14	+10-14	+10-14	+10-14	+10-14
Moisture (% of rock weight)	0.0	0.0	0.0	0.0	0.0
Discharge Setting (mm)	4	5	6	7	8

Table 4.11 Experimental Plan 2: Effect of discharge setting, moisture and rock properties on liner wear

Feed Fraction Size(mm)	+10-14					+10-14					+10-14				
Discharge Setting (mm)	4					6					8				
Moisture (% of rock weight)	0.0	0.5	1.0	1.5	2.0	0.0	0.5	1.0	1.5	2.0	0.0	0.5	1.0	1.5	2.0

Table 4.12 Experimental Plan 3: Effect of Feed size, moisture and rock properties on wear

Discharge Setting (mm)	4		4	
Feed Grade (mm)	+6.3-10		+10-14	
Moisture (% of rock weight)	0.0	2.0	0.0	2.0

4.3 Data Analysis Techniques

The analysis of wear data was carried out using the MINITAB statistical analysis computer package. The techniques used in the analysis of data were based on Analysis of Variance (ANOVA), and the Response Surface modelling techniques, discussed in Chapter 2.

A number of statistical tests were conducted in the study, to examine the significance and reliability of the regression models presented. The following sections briefly describes each test.

The F-test for regression

For a larger model, i.e. a model based on a larger subset of variables, to be more significant than a smaller one, the sum of squares for regression $\mathbf{SS_{reg}}$, discussed in Chapter 2 Section 2.2.1, must be bigger for the larger model. This means that the output, **Y**, is related to the added parameter and therefore its inclusion in the regression model is appropriate. However, to be able to judge this criterion quantitatively, the F-test is used. the **F** value is given by

$$\mathbf{F} = \frac{\mathbf{SS_{reg}}/\nu_{reg}}{\mathbf{SS_e}/\nu_e} = \frac{\mathbf{MS}}{\mathbf{V}} \qquad \mathbf{4.6}$$

where **MS** is the mean square of the $\mathbf{SS_{reg}}$ and **V** is the variance. This can be written as $\mathbf{F} \approx \mathbf{F(p,\nu_{reg}, \nu_e)}$, where **p** is the significance level associated with the computed **F** value. Tables of **F** values at different combinations of $\mathbf{p},\nu_{reg}$ and ν_e are available that could be used for comparison with any computed F-test. The p-values are given in terms of the risk associated with the regression, hence a p-value of 0.01 corresponds to a confidence level of 99.99 given by

$$100 - 0.01 = 99.99.$$

The coefficient of determination, R^2

The coefficient of determination, R^2, is defined as

$$R^2 = \frac{SS_{reg}}{SS_T} = 1 - \frac{SS_e}{SS_T} \qquad 4.7$$

and provides a single figure summary of the strength of the relationship between the **Y** and the variables includes in the model. It represents the proportion of variability in **Y** explained by regression on the included variables **X**. It is given in percentage term and a R^2 value of 99% would mean that 99% of the observed variability in the output is explained by the parameters included in the regression model. R^2 is the same as the square of the sample correlation between **X** and **Y**. However, it is easily appreciable that R^2 gets automatically larger when the model is extended by one variable, even if the added parameter is of no real significance. To compensate for this, R^2 value could be adjusted for the degrees of freedom i.e.

$$R^2(adj) = 1 - \frac{SS_e/(n-p)}{SS_T/(n-1)} \qquad 4.8$$

where **n** is number of observations and **p** the number of variables included in the model.

The t-ratio test

Another test used in the regression analysis is the t-ratio test which provides a confidence level for the model coefficients, β_i, to be non-zero. The value of t-ratio computed from the relation

$$t = \frac{\beta_i}{se(\beta_i)} \qquad 4.9$$

where $se(\beta_i)$ is the standard error calculated for β_i, can be compared with the t-ratio $t(p,\nu)$, where ν is the degrees of freedom associated with β_i.

Chapter 5 WEAR RESULTS AND THE REGRESSION MODELS FOR DRY ROCK

5.1 Comparison of the Wear Performance of Used Liners

To investigate the performance of the liners in terms of wear resistance, two sets of experiments were conducted after the liners were work hardened as described in the previous chapter. The rocks used were Pottal Pool rock, a very abrasive rock, and Whitwick rock, with moderate abrasivity. The experiments were carried out at a Closed-side setting of 4mm. Table 5.1 presents the results that are shown graphically in Figure 5.1. It can be seen that the wear for both of the liners, concave and mantle, are practically constant for each rock type. The results indicates that the wear properties of the liners were very similar. This means that the wear resistance of the liners could be safely eliminated as a contributory factor to the observed variation in wear under various conditions. This permits a direct comparison between the wear data obtained for the five sets of the liners.

Another early observation was that the wear of concave and mantle, although very close in magnitude, was not identical and mantle generally showed a higher degree of wear than concave.

Table 5.1 Comparison Between Wear Performance of Different Liners

CSS/mm	Wgt/Kg	CW/g	MW/g	Concave	Mantle	Rock
4.0	25	1.1	1.3	1	1	PP
4.1	25	1.1	1.4	2	2	PP
4.0	25	1.0	1.2	3	3	PP
3.9	25	1.2	1.3	4	4	PP
4.1	25	1.1	1.3	5	5	PP
4.1	25	0.6	0.5	1	1	W
4.0	25	0.5	0.5	2	2	W
4.0	25	0.5	0.5	3	3	W
4.2	25	0.6	0.5	4	4	W
4.1	25	0.6	0.6	5	5	W

PP: Pottal Pool Rock; W: Whitwick Rock.

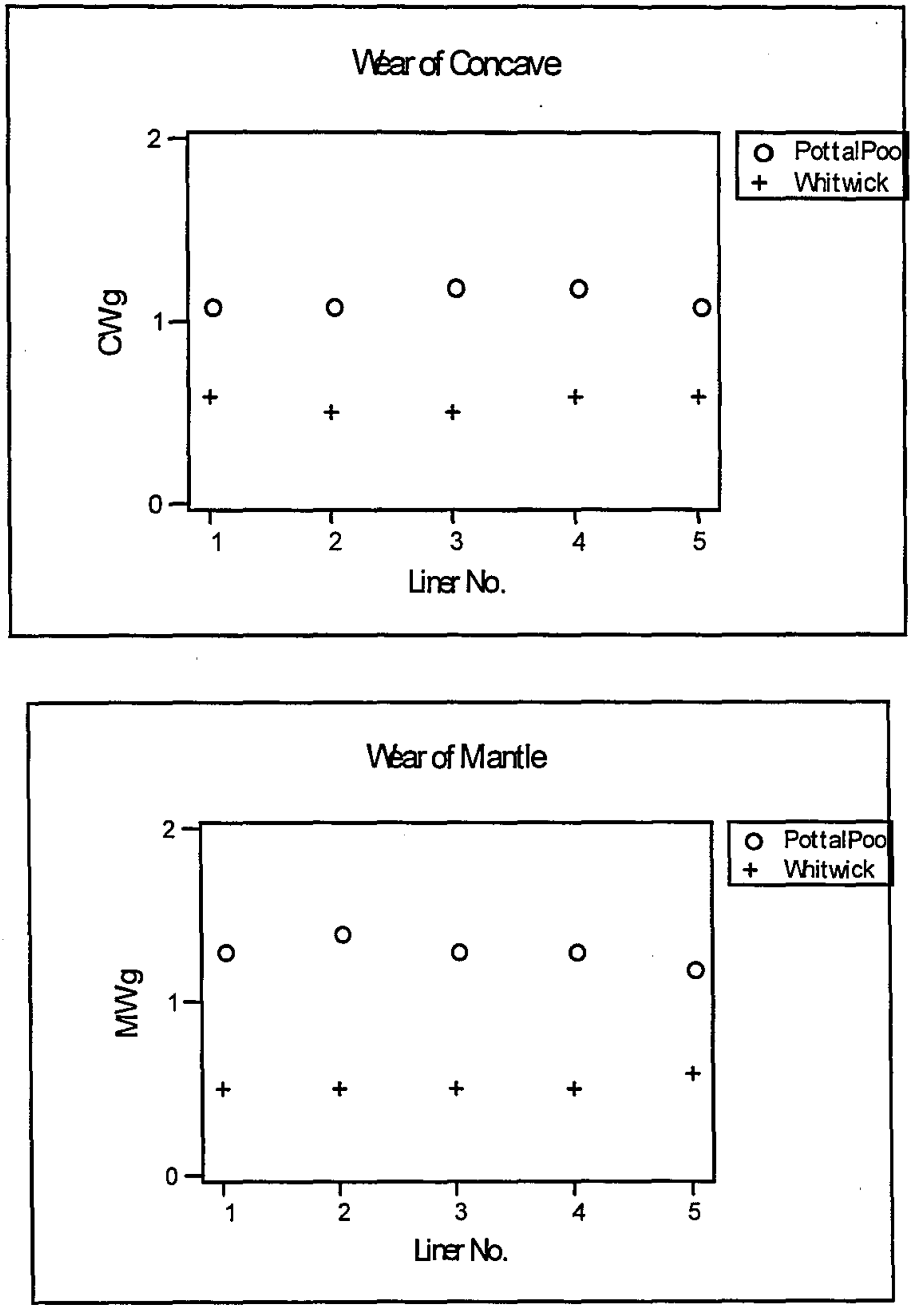

Figure 5.1 Comparison of the wear performance of different liners

5.2 Correlation Between Wear and Rock Weight

Table 5.2 shows the results of the experiments conducted to investigate the relationship between the weight of crushed rock and liner wear. The test was repeated using the two rock types, Pottal Pool and Whitwick, and at three different Closed-side settings, 4,6, and 8mm. The results show a strong linear relationship between wear and rock weight for both rock types and all the settings. Graphical presentation of the results are shown in Figures 5.2 and 5.3. Also shown are the total wear, **TW**, i.e. the wear combined of concave and mantle.

Table 5.2 Relationship Between Rock Weight and Wear

Whitwick Rock

CSS/mm	Wgt/Kg	CW/g	MW/g	TW/g
4.0	25	0.6	0.5	0.9
4.1	50	1.1	0.9	2.0
4.1	75	1.9	1.6	3.5
4.0	100	2.3	2.1	4.4
6.0	25	0.3	0.3	0.6
6.1	50	0.6	0.6	1.2
6.0	75	0.8	0.9	1.7
6.1	100	1.3	1.3	2.6
8.0	25	0.1	0.1	0.2
8.0	50	0.2	0.2	0.4
7.9	75	0.2	0.3	0.5
8.0	100	0.4	0.5	0.9

Table 5.3 Relationship Between Rock Weight and Wear

Pottal Pool Rock

CSS/mm	Wgt/Kg	CW/g	MW/g	TW/g
4.0	25	1.1	1.3	2.4
5.8	25	0.5	0.3	0.8
8.1	25	0.2	0.2	0.4
4.1	50	2.1	2.5	4.6
4.0	75	3.4	4.0	7.4
3.9	100	4.5	5.3	9.8
6.0	50	0.9	0.5	1.4
6.1	75	1.5	0.9	2.4
6.1	100	1.9	1.3	3.2
8.0	50	0.4	0.4	0.8
7.9	75	0.6	0.5	1.1
8.0	100	0.9	0.8	1.7

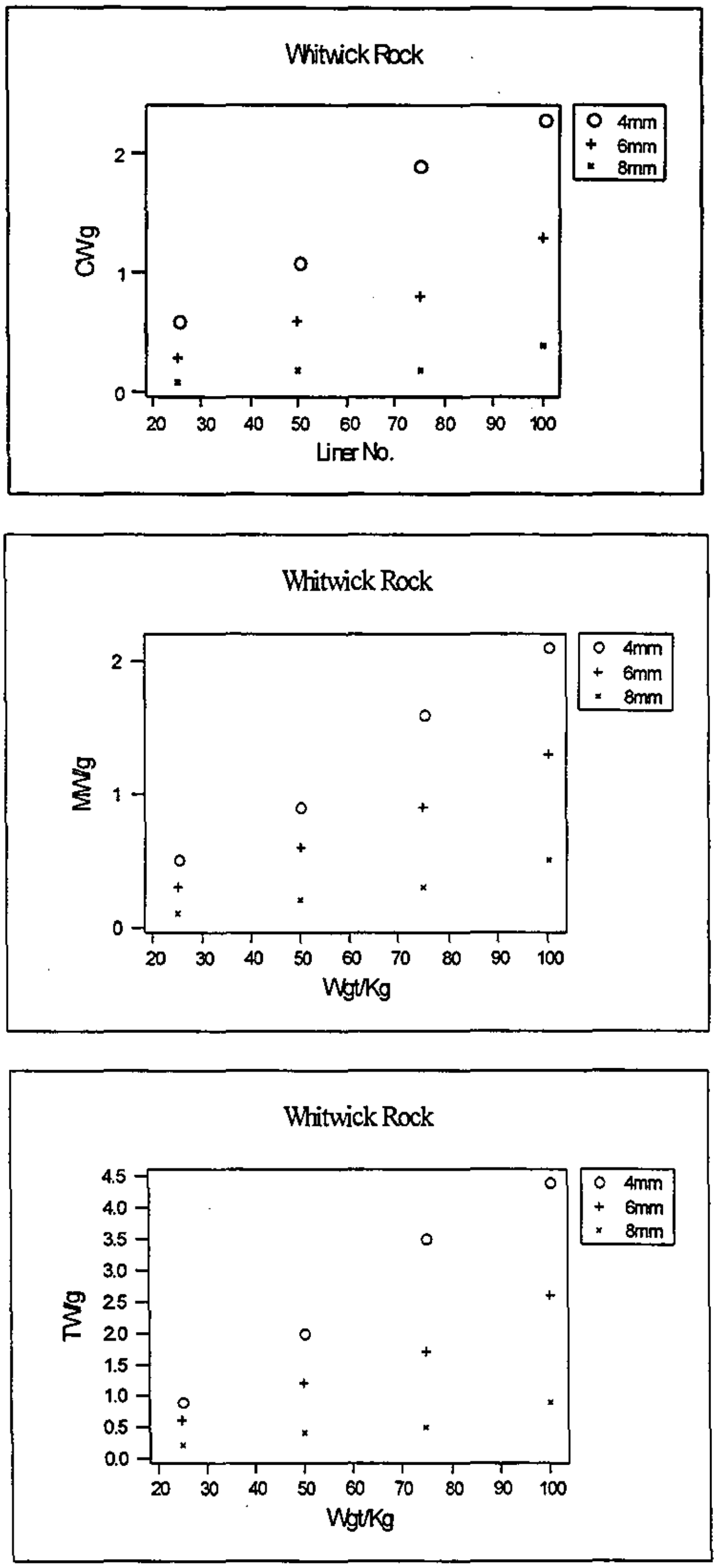

Figure 5.2 The wear of concave, CW(g), mantle, MW(g), and the total wear, TW(g), vs Whitwick rock weight at three crusher settings

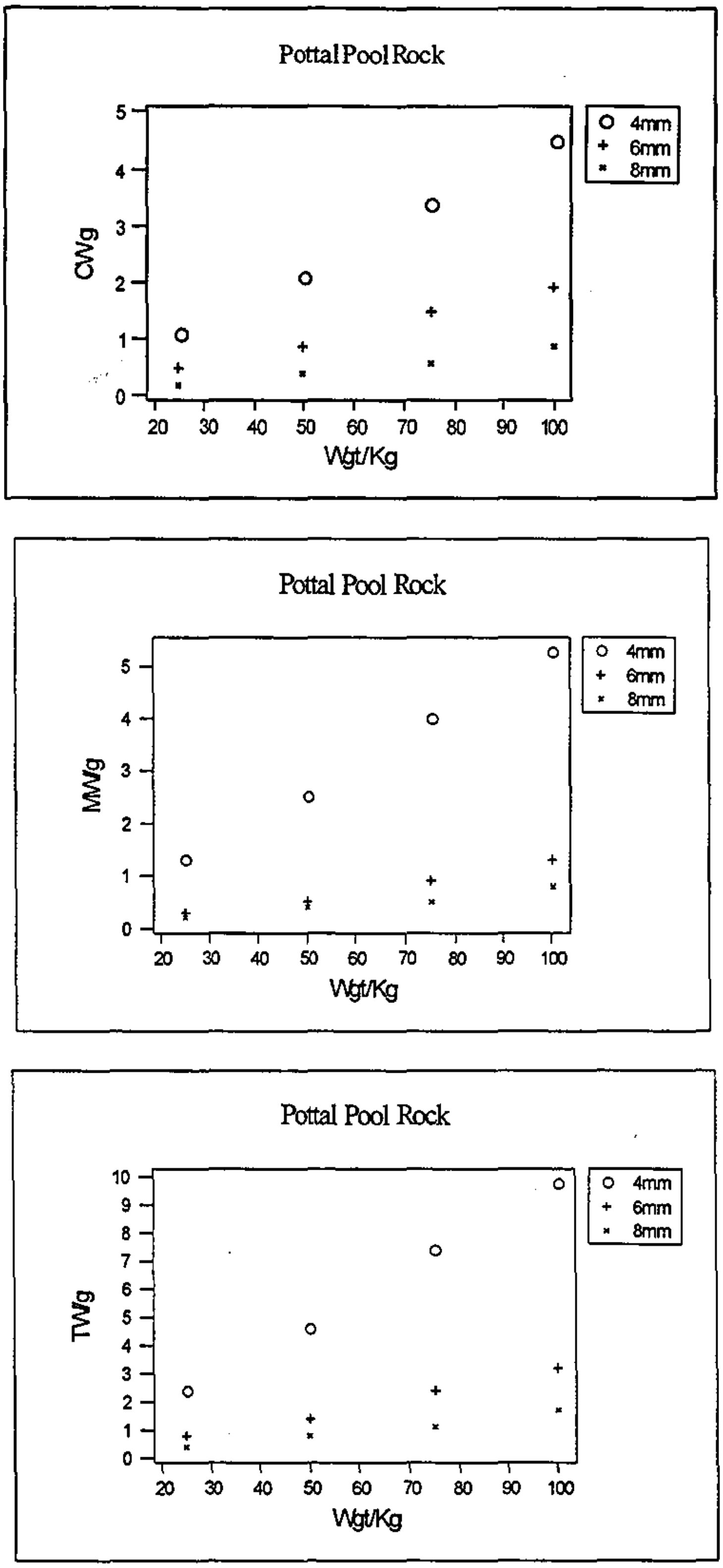

Figure 5.3 The wear of concave, CW(g),mantle, MW(g), and the total wear, TW(g), vs Pottal Pool rock weight at three crusher settings

5.3 The Physical Model

In general, physical models are used as broad guide line for the expected relationship between various tested variables and the output. They are based on the prior knowledge of the physical phenomenon behind the process under investigation, and the expected system behaviour. Such models, when available, provide valuable information on the appropriateness of any statistical model formulated. In the present investigations, the following equations summarize the main expected trends in system behaviour.

1. The amount of wear is proportional to the length of contact time between the rock particle and liners, i.e.

$$\mathbf{W \propto \text{Crushing Time}} \qquad 5.1$$

2. The amount of wear is inversely proportional to the closed-side setting, i.e. the smaller the discharge opening the higher the wear:

$$\mathbf{W \propto 1/CSS} \qquad 5.2$$

3. As the closed-side setting gets larger, less crushing occurs. In the case of the setting exceeding the size of the feed particles, the feed particles are discharged without any significant crushing. In this limiting case no wear will occur as the contact between the liners and the rock particles becomes negligible, therefore:

$$\text{if} \quad \mathbf{CSS \gg \text{Feed Size}} \ \text{ then } \mathbf{W \rightarrow} 0 \qquad 5.3$$

4. For wet rocks, the amount of wear is proportional to the moisture content:

$$\mathbf{W \propto \text{Moisture.}} \qquad 5.4$$

5.4 Correlation Between Wear and Closed-Side Setting For Dry Rock

One of the most important aspects of the present study was to establish the relationship between the crusher setting and liner wear. The ten rock types were all tested for the relationship. The two lime stone rocks from Breedon and Pant quarries were only tested at 4 and 5mm discharge settings, as at higher crusher settings no measurable wear was observed. The rest of the rocks were tested at five settings. The results of the experiments are shown in table A2.1

The amount of rock needed to produce measurable wear, i.e. 0.1 gram weight loss, was different according to the abrasivity of the rock and the closed-side setting. To enable easy comparison between the results of the various experiments, the rate of wear is presented in terms of wear per Tonne of rock according to

$$\mathbf{Wear(g/Tonne)} = \frac{\mathbf{1000 \times Measured\ Wear(g)}}{\mathbf{Weight\ of\ rock}} \qquad \mathbf{5.5}$$

In the following section the statistical models obtained for the eight rock types tested at the five crushing settings are presented.

5.4.1 The Statistical Models

The experimental data covers a limited range of crusher settings between 4mm to 8mm. This range was considered to be appropriate to the chosen size of the feed, i.e. +10-14mm. To obtain the best fit, the data should be modelled over this range and not over the entire possible values of crusher setting. Considering equation 5.2, the wear could be modelled using a polynomial of the following type:

$$\mathbf{W = a_0 + a_1\, 1/CSS + a_2\, 1/CSS^2 + .. + a_n\, 1/CSS^n} \qquad \mathbf{5.6}$$

However, the limiting case described by equation 5.3 of the physical model, requires the fitted models to predict very high wear values when crusher setting tends to zero (large reduction ratios) and zero wear for very large crusher settings (low reduction ratios). This means that the constant term $\mathbf{a_0}$ in the polynomial model of equation 5.7 must be set to zero. This condition in effect expands the application of the model beyond the data range and over all possible crushing settings. Consequently, the model prediction over the experimental range could suffer from higher errors. Furthermore, the appropriateness of models fitted without a constant term is not easily determinable by usual statistical tests. However, for completeness, these models, named "*no-constant*" models, were also included in the study.

For each rock type, four possible models were investigated as follows:

1. $\mathbf{W = a_0 + a_1\ (1/CSS)}$
2. $\mathbf{W = a_0 + a_1\ (1/CSS)^2}$
3. $\mathbf{W = a_0 + a_1\ (1/CSS) + a_2\ (1/CSS)^2}$
4. $\mathbf{W = a_1\ (1/CSS) + a_2\ (1/CSS)^2}$.

The wear for concave and mantle was modelled separately, as they were found to differ from each other. The total wear has also been modelled.

Tables 5.4, 5.5, and 5.6 show the formulated models for each rock type according to cases 1 and 2 above. The standard deviation of the fitted data is also included in the table for comparison. Table 5.7 presents the coefficient of determination $\mathbf{R^2}$, adjusted for the degrees of freedom, for the first three model types. The higher the value of $\mathbf{R^2}$, the more significant the model. It can be seen that no one model can be chosen as the most appropriate for both concave and mantle and all the rock types tested. However, the three-termed second order model, represented as case three above, gave the best fit, i.e. the highest $\mathbf{R^2(adj)}$ values, more frequently than the other two model types. Therefore it was decided to choose it as this model for regression analysis.

In the following sections, the calculated Pearson Cross-Correlation between wear, crusher setting and crushing time; and the fitted second order models for each rock type are presented. The values of the standard deviation, **S**, the coefficient of determination, $\mathbf{R^2}$, and the coefficient of determination adjusted for degrees of freedom, $\mathbf{R^2(adj)}$, are given for each model. A summary of ANOVA for the data and the fitted regression model is also included in each case which includes the F-Test, and more importantly the p-Test showing the confidence level of the regression model. A p-Test value of 0.01 corresponds to a confidence level of 99.99%.

Also included are the "*no-constant*" models, case 4 above, that are similarly second order polynomials but with no constant term.

Table 5.4 First and Second Order Regression Models for Dry Concave Wear

Rock Type	Model Equation	St. Deviation
Cliffe Hill	**CW/(g/T)** = - 10.5 + 89.7 **1/CSS**	0.869
	CW/(g/T) = - 2.59 + 239 **1/CSS^2**	0.787
Ingleton Grey	**CW/(g/T)** = - 10.5 + 89.7 **1/CSS**	0.719
	CW/(g/T) = - 2.38 + 171 **1/CSS^2**	0.473
Judkins	**CW/(g/T)** = - 2.11 + 24.8 **1/CSS**	0.204
	CW/(g/T) = - 0.005 + 69.1 **1/CSS^2**	0.300
Pottal Pool	**CW/(g/T)** = - 27.9 + 280 **1/CSS**	3.092
	CW/(g/T) = - 4.58 + 781 **1/CSS^2**	2.369
Shap Blue	**CW/(g/T)** = - 3.45 + 150 **1/CSS**	1.249
	CW/(g/T) = 9.04 + 412 **1/CSS^2**	1.571
Shardlow	**CW/(g/T)** = - 20.7 + 213 **1/CSS**	1.456
	CW/(g/T) = - 1.88 + 565 **1/CSS^2**	2.735
Whitwick	**CW/(g/T)** = - 12.4 + 142 **1/CSS**	0.852
	CW/(g/T) = 0.241 + 379 **1/CSS^2**	0.381
Waterswallows	**CW/(g/T)** = - 3.67 + 44.2 **1/CSS**	0.993
	CW/(g/T) = 0.110 + 123 **1/CSS^2**	0.777

Table 5.5 First and Second Order Regression Models for Dry Mantle Wear

Rock Type	Model Equation	St. Deviation
Cliffe Hill	$MW/(g/T) = -12.4 + 109\ 1/CSS$	1.515
	$MW/(g/T) = -2.91 + 293\ 1/CSS^2$	0.932
Ingleton Grey	$MW/(g/T) = -8.69 + 66.9\ 1/CSS$	0.610
	$MW/(g/T) = -2.82 + 181\ 1/CSS^2$	0.416
Judkins	$MW/(g/T) = -4.03 + 47.2\ 1/CSS$	0.785
	$MW/(g/T) = -0.047 + 132\ 1/CSS^2$	0.604
Pottal Pool	$MW/(g/T) = -26.0 + 319\ 1/CSS$	1.702
	$MW/(g/T) = 1.05 + 867\ 1/CSS^2$	3.638
Shap Blue	$MW/(g/T) = -19.1 + 229\ 1/CSS$	4.145
	$MW/(g/T) = 0.21 + 616\ 1/CSS^2$	2.767
Shardlow	$MW/(g/T) = -32.3 + 315\ 1/CSS$	1.994
	$MW/(g/T) = -4.00 + 817\ 1/CSS^2$	2.763
Whitwick	$MW/(g/T) = -7.51 + 108\ 1/CSS$	0.858
	$MW/(g/T) = 2.15 + 287\ 1/CSS^2$	0.921
Waterswallows	$MW/(g/T) = -3.60 + 44.11/CSS$	0. 970
	$MW/(g/T) = 0.166 + 1221/CSS^2$	0.756

Table 5.6 First and Second Order Regression Models for Total Wear

Rock Type	Model Equation	St. Deviation
Cliffe Hill	$TW/(g/T) = -22.9 + 198\ 1/CSS$	2.025
	$TW/(g/T) = -5.49 + 532\ 1/CSS^2$	1.103
Ingleton Grey	$TW/(g/T) = -16.6 + 130\ 1/CSS$	1.329
	$TW/(g/T) = -5.20 + 352\ 1/CSS^2$	0.842
Judkins	$TW/(g/T) = -4.85 + 65.8\ 1/CSS$	0.984
	$TW/(g/T) = 0.68 + 186\ 1/CSS^2$	0.941
Pottal Pool	$TW/(g/T) = -53.9 + 599\ 1/CSS$	2.357
	$TW/(g/T) = -3.53 + 16471/CSS^2$	4.088
Shap Blue	$TW/(g/T) = -22.6 + 379\ 1/CSS$	3.027
	$TW/(g/T) = 9.25 + 10291/CSS^2$	5.222
Shardlow	$TW/(g/T) = -53.0 + 528\ 1/CSS$	3.446
	$TW/(g/T) = -5.88 + 13811/CSS^2$	2.201
Whitwick	$TW/(g/T) = -19.9 + 251\ 1/CSS$	1.558
	$TW/(g/T) = 2.39 + 666\ 1/CSS^2$	1.288
Waterswallows	$TW/(g/T) = -7.27 + 88.3\ 1/CSS$	1.963
	$TW/(g/T) = 0.28 + 245\ 1/CSS^2$	1.533

Table 5.7Adjusted R^2(%) for Different Regression Models

Rock Type	Regression Model	Model Predictors		
		1/CSS	!/CSS^2	1/CSS & 1/CSS^2
	CW(g/T)	96.4	97.0	95.6
Cliffe Hill	MW(g/T)	97.2	92.6	99.1
	TW(g/T)	96.0	98.8	98.9
	CW(g/T)	93.7	97.4	98.0
Ingleton Grey	MW(g/T)	96.2	98.2	97.5
	TW(g/T)	95.2	98.2	97.9
	CW(g/T)	93.5	97.0	98.2
Judkins	MW(g/T)	88.2	93.0	96.1
	TW(g/T)	85.3	91.5	99.8
	CW(g/T)	97.4	95.6	96.6
Pottal Pool	MW(g/T)	95.2	98.9	99.5
	TW(g/T)	98.3	99.4	99.3
	CW(g/T)	97.8	96.6	97.2
Shap	MW(g/T)	95.5	89.9	95. 8
	TW(g/T)	98.0	94.0	97.8
	CW(g/T)	94.3	98.4	99.5
Shardlow	MW(g/T)	98.6	97.2	97.8
	TW(g/T)	98.5	99.4	99.1
	CW(g/T)	98.5	99.7	99.6
Whitwick	MW(g/T)	97.5	97.1	96.5
	TW(g/T)	98.4	98.9	98.6
	CW(g/T)	80.3	87.9	99.6
Waterswallows	MW(g/T)	81.0	88.5	99.4
	TW(g/T)	80.7	88.2	99.5

Cliffe Hill Rock

a. Three-Termed Second Order Model

1. **CW/(g/T)** = - 4.63 + 23.0 **1/CSS** + 178 **1/CSS^2**
s = 0.950 **R^2**= 97.8% **R^2(adj)** = 95.6%

Analysis of Variance

SOURCE	DF	SS	MS	F	p
Regression	2	80.901	40.450	44.80	0.022
Error	2	1.806	0.903		
Total	4	82.707			

2. **MW/(g/T)** = 10.0 - 145 **1/CSS** + 677 **1/CSS^2**
s = 0.528 **R^2**= 99.6% **R^2(adj)** = 99.1%

Analysis of Variance

SOURCE	DF	SS	MS	F	p
Regression	2	124.387	62.194	223.16	0.004
Error	2	0.557	0.279		
Total	4	124.944			

3. **TW/(g/T)** = 5.37 - 122 **1/CSS** + 854 **1/CSS^2**
s = 1.049 **R^2**= 99.5% **R^2(adj)** = 98.9%

Analysis of Variance

SOURCE	DF	SS	MS	F	p
Regression	2	403.54	201.77	183.39	0.005
Error	2	2.20	1.10		
Total	4	405.74			

b. No-Constant Second Order Model

1. **CW/(g/T)** = - 28.4 **1/CSS** + 312 **1/CSS^2**
s = 0.830.

2. **MW/(g/T)** = - 34.0 **1/CSS** + 386 **1/CSS^2**
s = 0.768

3. **TW/(g/T)** = - 62.5 **1/CSS** + 698 **1/CSS^2**
s = 0.9221

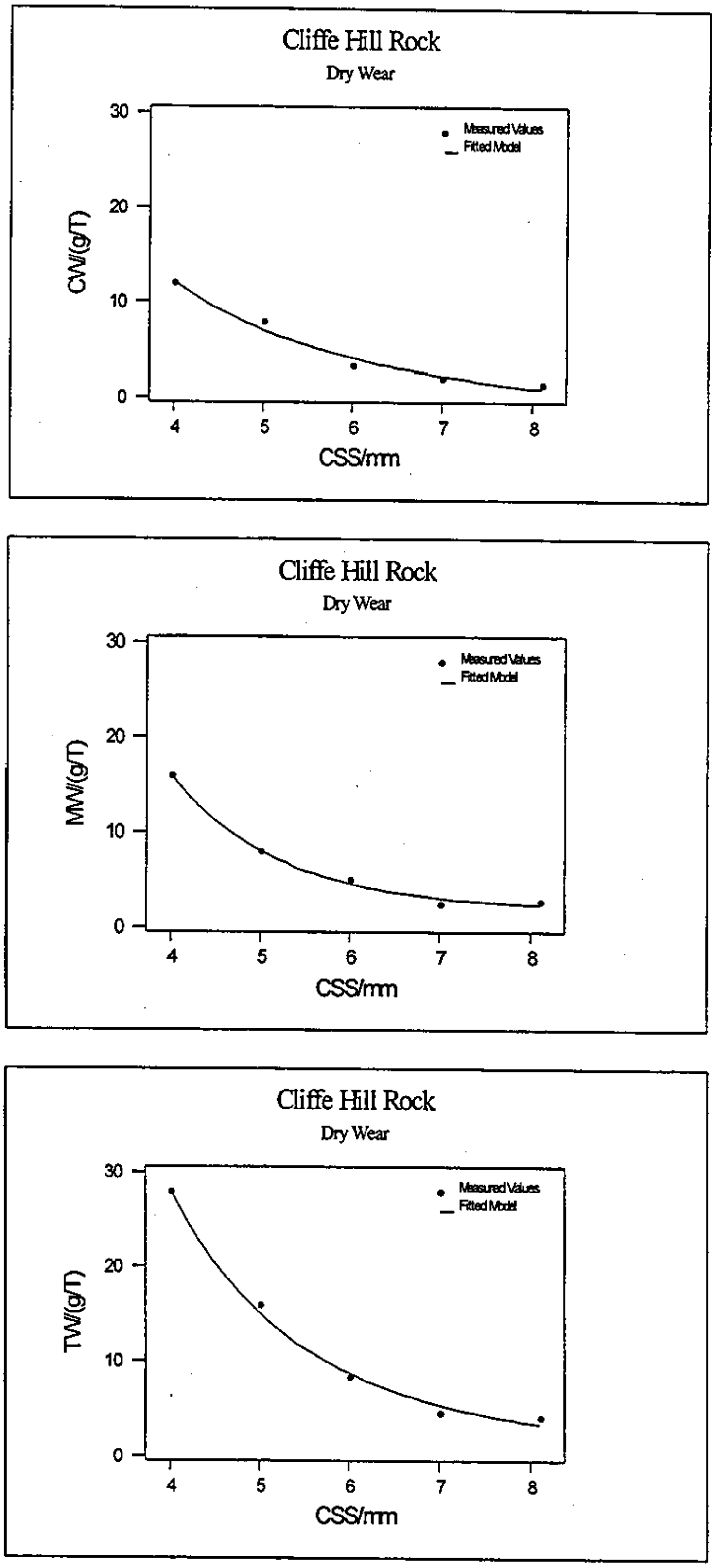

Figure 5.4 Comparison of measured and fitted values of wear vs Closed-side setting for Cliffe Hill Rock (Three term 2nd order model)

Ingleton Grey Rock

a. Three-Termed Second Order Model

1. **CW/(g/T)** = 3.32 - 64.2 **1/CSS** + 342 **1/CSS²**
   s = 0.414 **R²**= 99.0% **R²(adj)** = 98.0%

Analysis of Variance

SOURCE	DF	SS	MS	F	p
Regression	2	34.787	17.394	101.25	0.010
Error	2	0.344	0.172		
Total	4	35.131			

2. **MW/(g/T)** = - 0.86 - 22.0 **1/CSS** + 240 **1/CSS²**
   s = 0.490 **R²**= 98.8% **R²(adj)** = 97.5%

Analysis of Variance

SOURCE	DF	SS	MS	F	p
Regression	2	38.390	19.195	79.69	0.012
Error	2	0.482	0.241		
Total	4	38.872			

3. **TW/(g/T)** = 2.46 - 86.2 **1/CSS** + 582 **1/CSS²**
   s = 0.876 **R²**= 99.0% **R²(adj)** = 97.9%

Analysis of Variance

SOURCE	DF	SS	MS	F	p
Regression	2	146.109	73.055	95.04	0.010
Error	2	1.537	0.769		
Total	4	147.646			

b. No-Constant Second Order Model

1. **CW/(g/T)** = - 27.2 **1/CSS** + 245 **1/CSS²**
   s = 0.3890

2. **MW/(g/T)** = - 31.6 **1/CSS** + 265 **1/CSS²**
   s = 0.4038

3. **TW/(g/T)** = - 58.8 **1/CSS** + 510 **1/CSS²**
   s = 0.7298

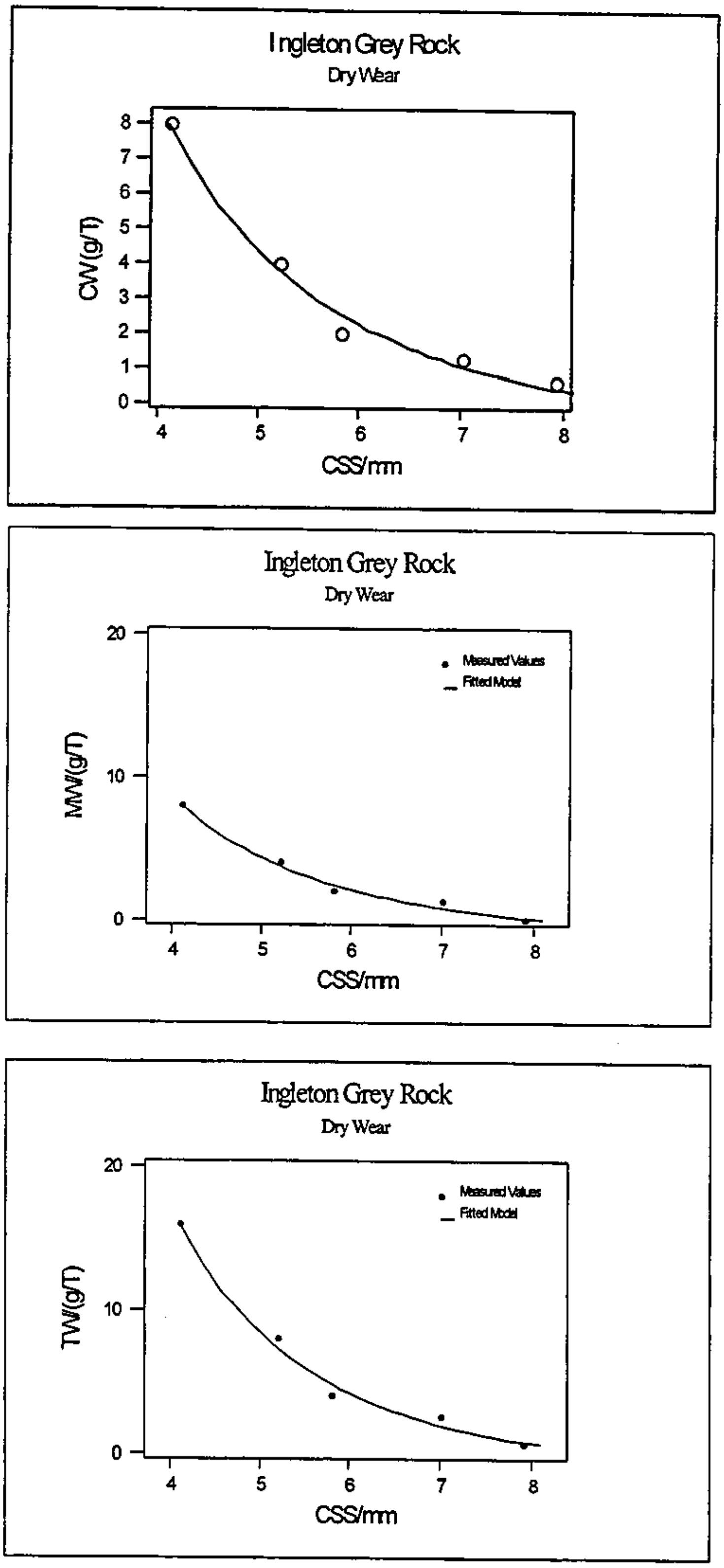

Figure 5.5 Comparison of measured and fitted values of wear vs Closed-side setting for Ingleton Grey Rock (Three term 2nd order model)

Table 5.8 Pearson Correlation Between Different Variables- Cliffe Hill

	1/CSS	1/CSS^2	CW/(g/T)	MW/(g/T)	TW/(g/T)
$1/CSS^2$	0.995				
CW/(g/T)	0.986	0.989			
MW/(g/T)	0.972	0.990	0.974		
TW/(g/T)	0.985	0.995	0.992	0.995	
TIME(H/T)	0.998	0.999	0.988	0.983	0.991

Table 5.9 Pearson Correlation Between Different Variables- Ingleton Grey

	1/CSS	$1/CSS^2$	CW/(g/T)	MW/(g/T)	TW/(g/T)
$1/CSS^2$	0.995				
CW/(g/T)	0.976	0.990			
MW/(g/T)	0.985	0.993	0.996		
TW/(g/T)	0.982	0.993	0.999	0.999	
TIME(H/T)	0.923	0.885	0.852	0.881	0.868

Table 5.10 Pearson Correlation Between Different Variables- Judkins

	1/CSS	$1/CSS^2$	CW/(g/T)	MW/(g/T)	TW/(g/T)
$1/CSS^2$	0.996				
CW/(g/T)	0.944	0.944			
MW/(g/T)	0.893	0.919	0.983		
TW/(g/T)	0.943	0.968	0.986	0.992	
TIME(H/T)	0.912	0.938	0.951	0.990	0.983

Table 5.11 Pearson Correlation Between Different Variables- Pottal Pool Rock

	1/CSS	$1/CSS^2$	CW/(g/T)	MW/(g/T)	TW/(g/T)
$1/CSS^2$	0.993				
CW/(g/T)	0.982	0.990			
MW/(g/T)	0.996	0.980	0.967		
TW/(g/T)	0.998	0.993	0.991	0.993	
TIME(H/T)	0.984	0.987	0.975	0.978	0.985

Judkins Rock

a. Three-Termed Second Order Model

1. **CW/(g/T)** = 3.04 - 35.1 **1/CSS** + 165 **1/CSS^2**
   s = 0.158 **R^2** = 99.1% **R^2(adj)** = 98.2%

Analysis of Variance

SOURCE	DF	SS	MS	F	p
Regression	2	5.5146	2.7573	109.94	0.009
Error	2	0.0502	0.0251		
Total	4	5.5647			

2. **MW/(g/T)** = 9.10 - 106 **1/CSS** + 421 **1/CSS^2**
   s = 0.454 **R^2** = 98.0% **R^2(adj)** = 96.1%

Analysis of Variance

SOURCE	DF	SS	MS	F	p
Regression	2	20.575	10.288	49.79	0.020
Error	2	0.413	0.207		
Total	4	20.989			

3. **TW/(g/T)** = 18.6 - 207 **1/CSS** + 752 **1/CSS^2**
   s = 0.142 **R^2** = 99.9% **R^2(adj)** = 99.8%

Analysis of Variance

SOURCE	DF	SS	MS	F	p
Regression	2	41.891	20.945	1028.55	0.001
Error	2	0.041	0.020		
Total	4	41.932			

b. No-Constant Second Order Model

1. **CW/(g/T)** = - 0.39 **1/CSS** + 70.8 **1/CSS^2**
   s = 0.204

2. **MW/(g/T)** = - 1.53 **1/CSS** + 138 **1/CSS^2**
   s = 0.600

3. **TW/(g/T)** = - 1.92 **1/CSS** + 209 **1/CSS^2**
   s = 0.740

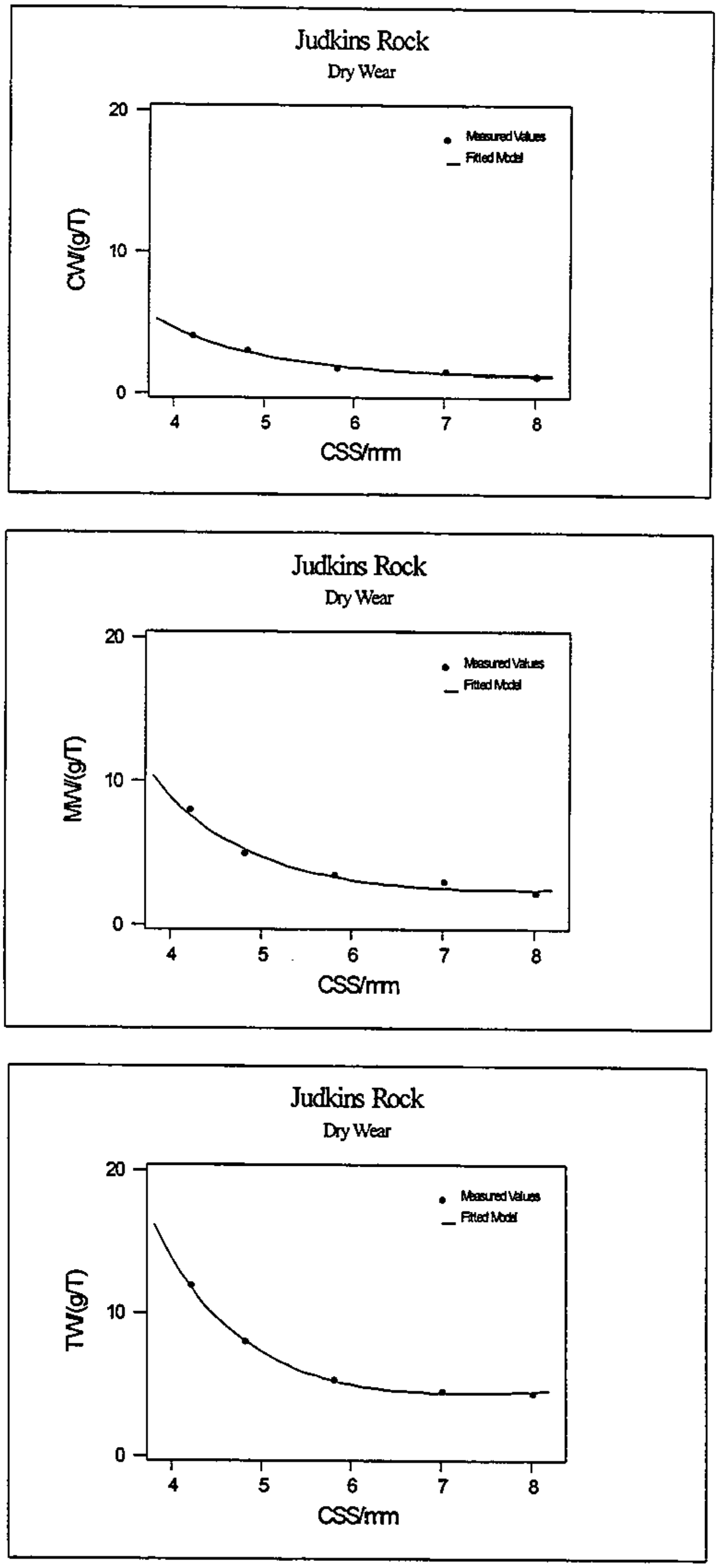

Figure 5.6 Comparison of measured and fitted values of wear vs Closed-side setting for Judkins Rock (Three term 2nd order model)

Pottal Pool Rock

a. Three-term Second Order Model

1. **CW/(g/T)** = - 3.3 - 15 **1/CSS** + 822 **1/CSS^2**
   s = 2.733 **R^2** = 97.9% **R^2(adj)** = 96.6%

Analysis of Variance

SOURCE	DF	SS	MS	F	p
Regression	2	1065.10	532.55	71.32	0.003
Error	3	22.40	7.47		
Total	5	1087.50			

2. **MW/(g/T)** = - 43.0 + 523 **1/CSS** - 568 **1/CSS^2**
   s = 1.159 **R^2** = 99.7% **R^2(adj)** = 99.5%

Analysis of Variance

SOURCE	DF	SS	MS	F	p
Regression	2	1361.31	680.65	507.05	0.000
Error	3	4.03	1.34		
Total	5	1365.33			

3. **TW/(g/T)** = - 46.3 + 508 **1/CSS** + 254 **1/CSS^2**
   s = 2.62 **R^2** = 99.6% **R^2**(adj) = 99.3%

Analysis of Variance

SOURCE	DF	SS	MS	F	p
Regression	2	4788.1	2394.1	346.76	0.000
Error	3	20.7	6.9		
Total	5	4808.8			

b. No-Constant Second-Order Model

1. **CW/(g/T)** = - 53.7 **1/CSS** + 927 **1/CSS^2**
   s = 2.381

2. **MW/(g/T)** = 20.9 **1/CSS** + 791 **1/CSS^2**
   s = 3.531

3. **TW/(g/T)** = - 32.8 **1/CSS** + 1718 **1/CSS^2**
   s = 4.298

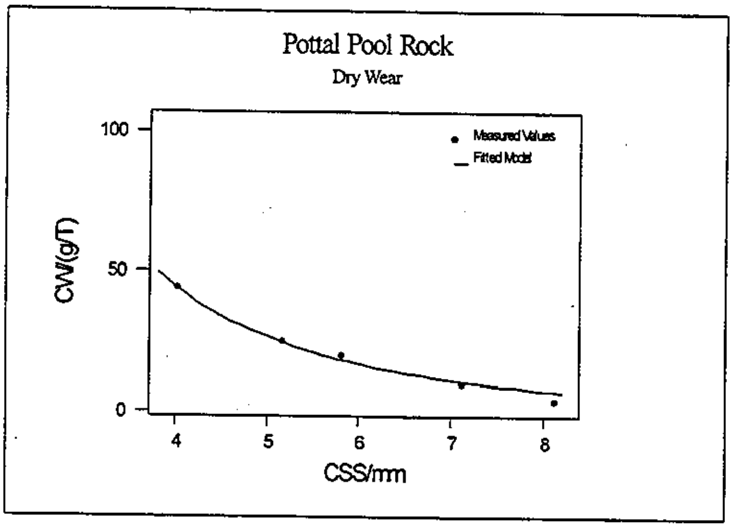

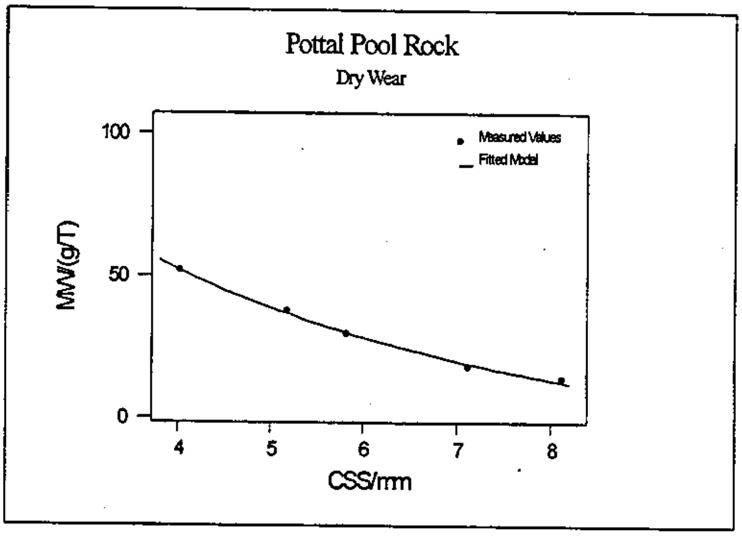

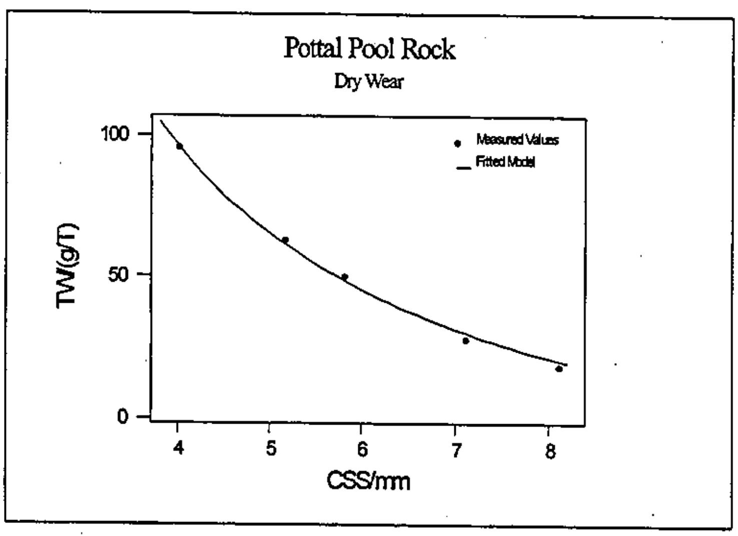

Figure 5.7 Comparison of measured and fitted values of wear vs Closed-side setting for Pottal Pool Rock (Three term 2nd order model)

Shap Blue Rock

a. Three Term Second Order Model

1. $CW/(g/T) = -0.80 + 118\ 1/CSS + 90\ 1/CSS^2$
   $s = 1.407 \quad R^2 = 98.3\% \quad R^2(adj) = 97.2\%$

Analysis of Variance

SOURCE	DF	SS	MS	F	p
Regression	2	353.56	176.78	89.26	0.002
Error	3	5.94	1.98		
Total	5	359.50			

2. $MW/(g/T) = -34.0 + 410\ 1/CSS - 504\ 1/CSS^2$
   $s = 2.657 \quad R^2 = 97.5\% \quad R^2(adj) = 95.8\%$

Analysis of Variance

SOURCE	DF	SS	MS	F	p
Regression	2	827.65	413.83	58.61	0.004
Error	3	21.18	7.06		
Total	5	848.83			

3. $TW/(g/T) = -34.8 + 527\ 1/CSS - 414\ 1/CSS^2$
   $s = 3.177 \quad R^2 = 98.7\% \quad R^2(adj) = 97.8\%$

Analysis of Variance

SOURCE	DF	SS	MS	F	p
Regression	2	2253.1	1126.5	111.63	0.002
Error	3	30.3	10.1		
Total	5	2283.3			

b. No-Constant Second Order Model

1. $CW/(g/T) = 108\ 1/CSS + 1151/CSS^2$
   $s = 1.221$

2. $MW/(g/T) = 12.4\ 1/CSS + 562\ 1/CSS^2$
   $s = 4.092$

3. $TW/(g/T) = 121\ 1/CSS + 678\ 1/CSS^2$
   $s = 4.423$

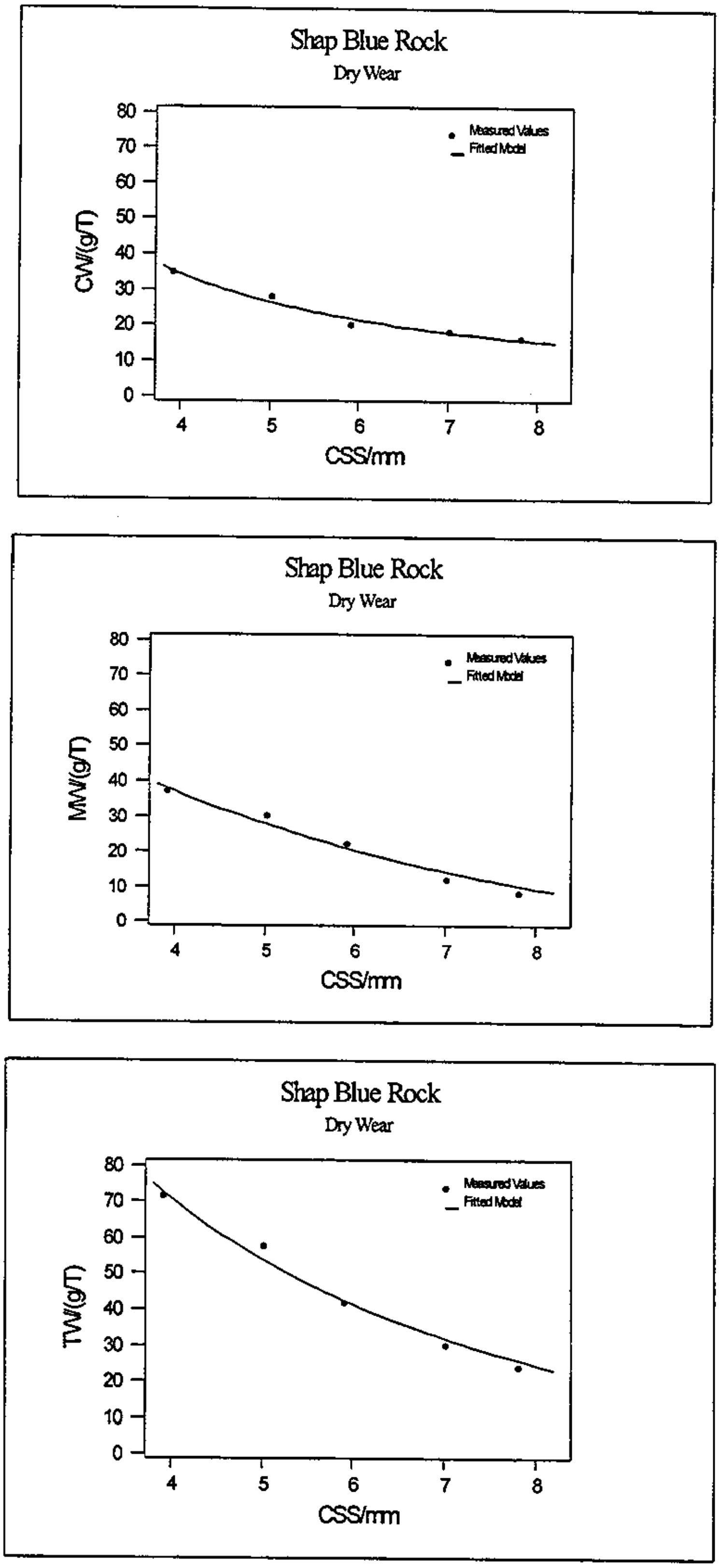

Figure 5.8 Comparison of measured and fitted values of wear vs Closed-side setting for Shap Blue Rock (Three term 2nd order model)

Shardlow Rock

a. Three Term Second Order Model

1. **CW/(g/T)** = 17.0 - 209 **1/CSS** + 1108 **1/CSS²**
   s = 0.7727 R^2 = 99.8% R^2(adj) = 99.5%

Analysis of Variance

SOURCE	DF	SS	MS	F	p
Regression	2	523.61	261.80	438.45	0.002
Error	2	1.19	0.60		
Total	4	524.80			

2. **MW/(g/T)** = - 31.5 + 306 **1/CSS** + 24 **1/CSS²**
   s = 2.441 R^2 = 98.9% R^2(adj) = 97.8%

Analysis of Variance

SOURCE	DF	SS	MS	F	p
Regression	2	1095.28	547.64	91.92	0.011
Error	2	11.92	5.96		
Total	4	1107.20			

3. **TW/(g/T)** = - 14.5 + 96 **1/CSS** + 1132 **1/CSS²**
   s = 2.593 R^2 = 99.6% R^2(adj) = 99.1%

Analysis of Variance

SOURCE	DF	SS	MS	F	p
Regression	2	3103.4	1551.7	230.83	0.004
Error	2	13.4	6.7		
Total	4	3116.8			

b. No-Constant Second Order Model

1. **CW/(g/T)** = - 23.4 **1/CSS** + 630 **1/CSS²**
   s = 1.332

2. **MW/(g/T)** = - 39.9 1/CSS + 911 **1/CSS²**
   s = 2.952

3. **TW/(g/T)** = - 63.2 1/CSS + 1541 **1/CSS²**
   s = 2.343

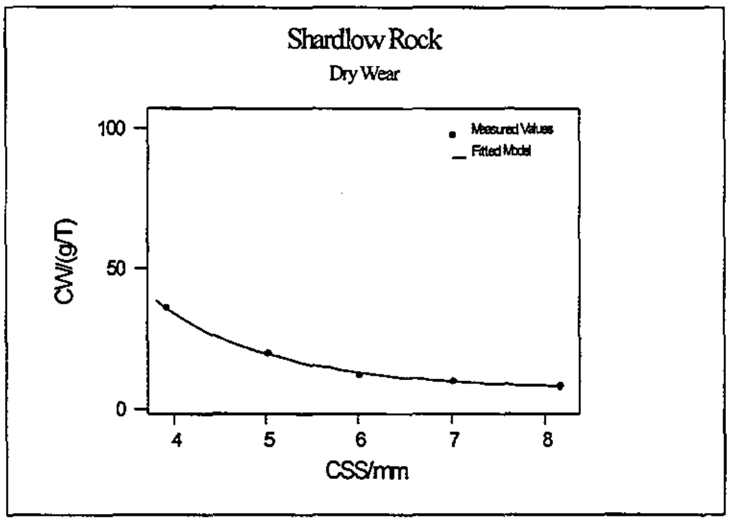

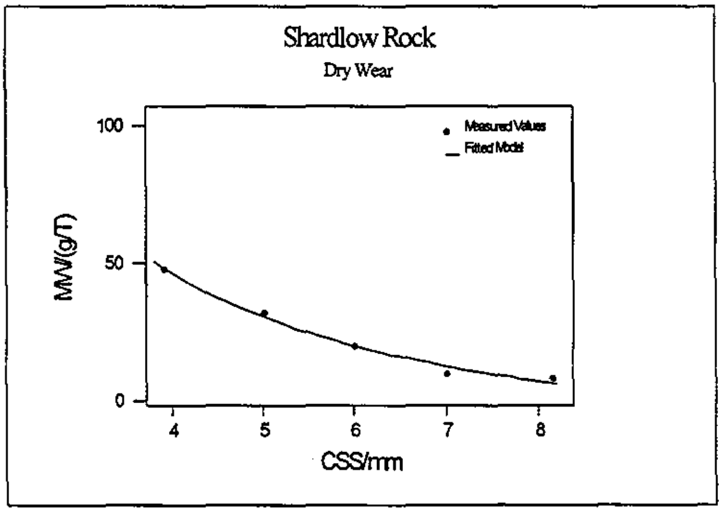

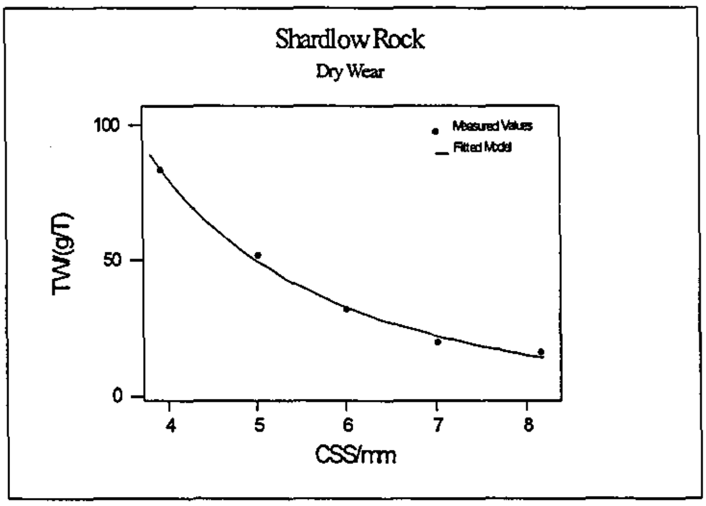

Figure 5.9 Comparison of measured and fitted values of wear vs Closed-side setting for Shardlow Rock (Three term 2nd order model)

Table 5.12 Pearson Correlation Between Different Variables- Shap Blue

	1/CSS	$1/CSS^2$	CW/(g/T)	MW/(g/T)	TW/(g/T)
$1/CSS^2$	0.991				
CW/(g/T)	0.991	0.986			
MW/(g/T)	0.982	0.959	0.973		
TW/(g/T)	0.992	0.976	0.990	0.996	
TIME(H/T)	0.983	0.988	0.989	0.974	0.986

Table 5.13 Pearson Correlation Between Different Variables- Shardlow

	1/CSS	$1/CSS^2$	CW/(g/T)	MW/(g/T)	TW/(g/T)
$1/CSS^2$	0.995				
CW/(g/T)	0.978	0.994			
MW/(g/T)	0.995	0.990	0.974		
TW/(g/T)	0.994	0.998	0.991	0.996	
TIME(H/T)	0.991	0.974	0.947	0.977	0.971

Table 5.14 Pearson Correlation Between Different Variables-Whitwick

	1/CSS	$1/CSS^2$	CW/(g/T)	MW/(g/T)	TW/(g/T)
$1/CSS^2$	0.995				
CW/(g/T)	0.995	0.999			
MW/(g/T)	0.990	0.989	0.995		
TW/(g/T)	0.994	0.996	0.999	0.998	
TIME(H/T)	0.993	0.991	0.988	0.978	0.985

Table 5.15 Pearson Correlation Between Different Variables-Waterswallows

	1/CSS	$1/CSS^2$	CW/(g/T)	MW/(g/T)	TW/(g/T)
$1/CSS^2$	0.996				
CW/(g/T)	0.923	0.954			
MW/(g/T)	0.926	0.956	1.000		
TW/(g/T)	0.925	0.955	1.000	1.000	
TIME(H/T)	0.992	0.986	0.908	0.914	0.911

Whitwick Rock

a. Three Term Second Order Model

1. $CW/(g/T) = -0.53 + 8.6\ 1/CSS + 357\ 1/CSS^2$
   $s = 0.4629 \quad R^2 = 99.8\% \quad R^2(adj) = 99.6\%$

Analysis of Variance

SOURCE	DF	SS	MS	F	p
Regression	2	199.572	99.786	465.78	0.002
Error	2	0.428	0.214		
Total	4	200.000			

2. $MW/(g/T) = -4.12 + 70\ 1/CSS + 102\ 1/CSS^2$
   $s = 1.017 \quad R^2 = 98.2\% \quad R^2(adj) = 96.5\%$

Analysis of Variance

SOURCE	DF	SS	MS	F	p
Regression	2	114.732	57.366	55.47	0.018
Error	2	2.068	1.034		
Total	4	116.800			

3. $TW/(g/T) = -4.6 + 79\ 1/CSS + 458\ 1/CSS^2$
   $s = 1.480 \quad R^2 = 99.3\% \quad R^2(adj) = 98.6\%$

Analysis of Variance

SOURCE	DF	SS	MS	F	p
Regression	2	616.42	308.21	140.77	0.007
Error	2	4.38	2.19		
Total	4	620.80			

b. No-Constant Second Order Model

1. $CW/(g/T) = 2.77\ 1/CSS + 372\ 1/CSS^2$
   $s = 0.379$

2. $MW/(g/T) = 24.6\ 1/CSS + 221\ 1/CSS^2$
   $s = 0.870$

3. $TW/(g/T) = 27.4\ 1/CSS + 593\ 1/CSS^2$
   $s = 1.243$

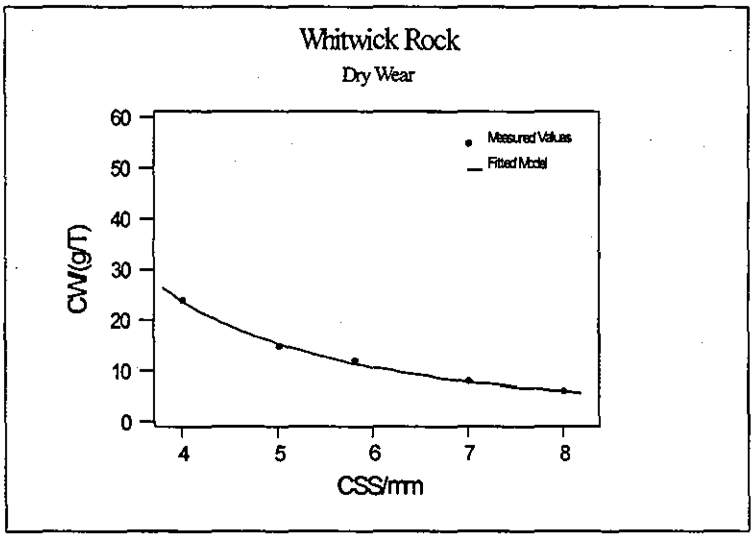

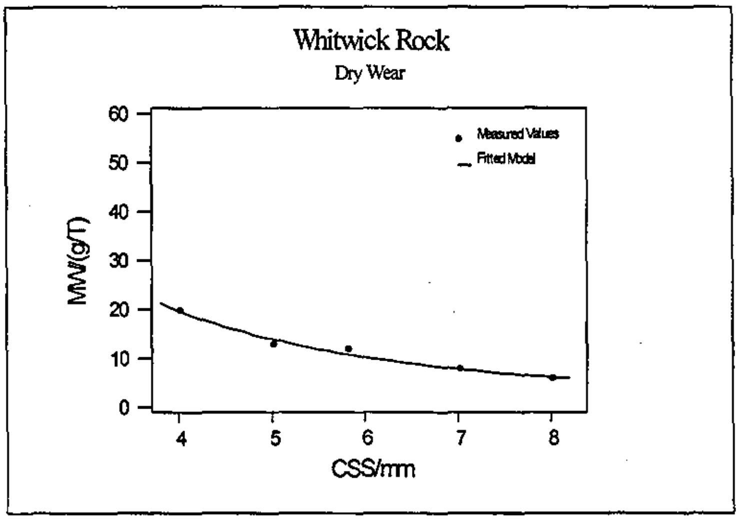

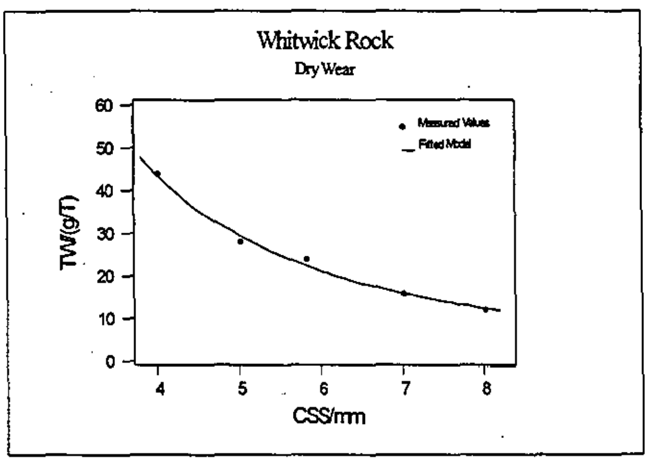

Figure 5.10 Comparison of measured and fitted values of wear vs Closed-side setting for Whitwick Rock (Three term 2nd order model)

Waterswallows Rock

a. Three Term Second Order Model

1. $CW/(g/T) = 14.2 - 159\ 1/CSS + 548\ 1/CSS^2$
$s = 0.1429 \quad R^2 = 99.8\% \quad R^2(adj) = 99.6\%$

Analysis of Variance

SOURCE	DF	SS	MS	F	p
Regression	2	20.031	10.016	490.58	0.002
Error	2	0.041	0.020		
Total	4	20.072			

2. $MW/(g/T) = 13.8 - 154\ 1/CSS + 533\ 1/CSS^2$
$s = 0.1745 \quad R^2 = 99.7\% \quad R^2(adj) = 99.4\%$

Analysis of Variance

SOURCE	DF	SS	MS	F	p
Regression	2	19.7671	9.8835	324.50	0.003
Error	2	0.0609	0.0305		
Total	4	19.8280			

3. $TW/(g/T) = 28.0 - 313\ 1/CSS + 1080\ 1/CSS^2$
$s = 0.311 \quad R^2 = 99.8\% \quad R^2(adj) = 99.5\%$

Analysis of Variance

SOURCE	DF	SS	MS	F	p
Regression	2	79.594	39.797	410.64	0.002
Error	2	0.194	0.097		
Total	4	79.788			

b. No-Constant Second Order Model

1. $CW/(g/T) = -0.31\ 1/CSS + 127\ 1/CSS^2$
$s = 0.780$

2. $MW/(g/T) = 0.37\ 1/CSS + 124\ 1/CSS^2$
$s = 0.761$

3. $TW/(g/T) = 0.1\ 1/CSS + 251\ 1/CSS^2$
$s = 1.541$

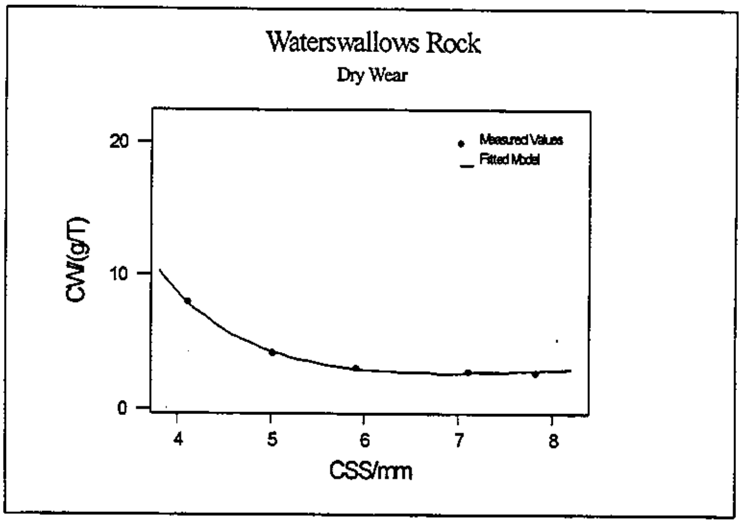

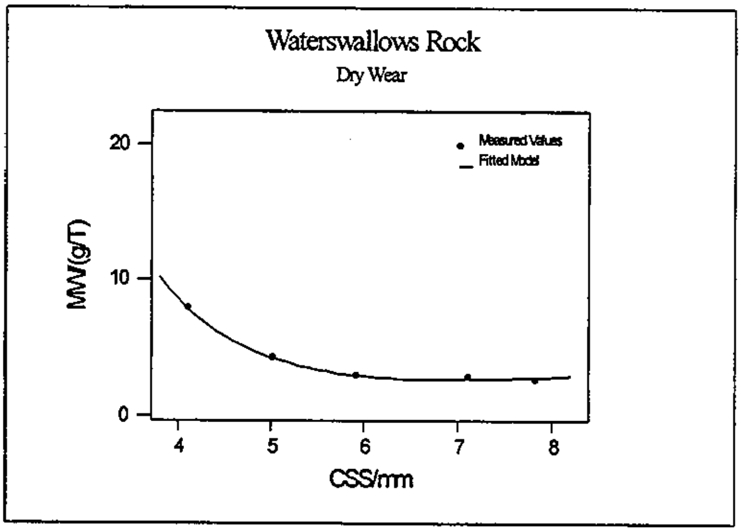

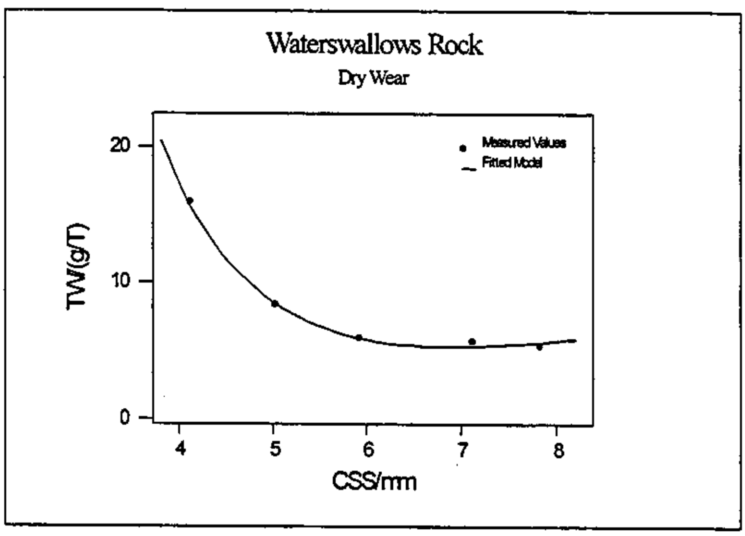

Figure 5.11 Comparison of measured and fitted values of wear vs Closed-side setting for Waterswallows Rock (Three term 2nd order model)

5.5 Correlation Between Dry Wear and Rock Properties

To find the best subset of rock property variables that could be used to describe dry liner wear, the effect of closed-side opening was first eliminated by grouping the wear data for all ten rock types, according to three crusher settings, 4, 6 and 8mm.

5.5.1 Correlation Between Wear and Silica Content and Rock Hardness

As discussed in Chapter 2, hardness and silica content are commonly taken as a measure for abrasivity of rock. Table 5.16 summarizes the Pearson correlation coefficients between measured dry wear, at a crusher setting of 4mm, and silica content, hardness and the two basic rock properties, density and water absorption.

Table 5.16 Pearson Correlation Coefficients Between Wear and Rock Hardness, Silica Content, Density and Water Absorption

	CW/(g/T)	MW/(g/T)	TW/(g/T)	Water Absorption (%)	silica (%)	Relative Density
MW/(g/T)	0.978					
TW/(g/T)	0.987	0.998				
Water Absorption (%)	-0.535	-0.517	-0.548			
Silica (%)	0.808	0.790	0.804	-0.580		
Relative Density	-0.481	-0.567	-0.527	-0.117	-0.234	
Hardness	0.679	0.714	0.710	-0.776	0.786	-0.396

It can be seen from Table 5.16 that the correlation between wear and silica content is the most significant one. As expected, hardness and silica content are related. A weaker relationship exists between silica content and the basic rock properties. Figures 5.12 and 5.13, show the observed variation of wear with rock hardness and silica content, for a crusher setting of 4mm. It can be seen that none of the two relationships could be considered as significantly linear. However, for both sets of graphs, it was possible to fit a line through groups of data points. This indicated that other rock properties also contribute towards the wear. Considering the correlation between the rock hardness and silica content, and the larger correlation between wear and silica content, it was chosen to be included in the wear models.

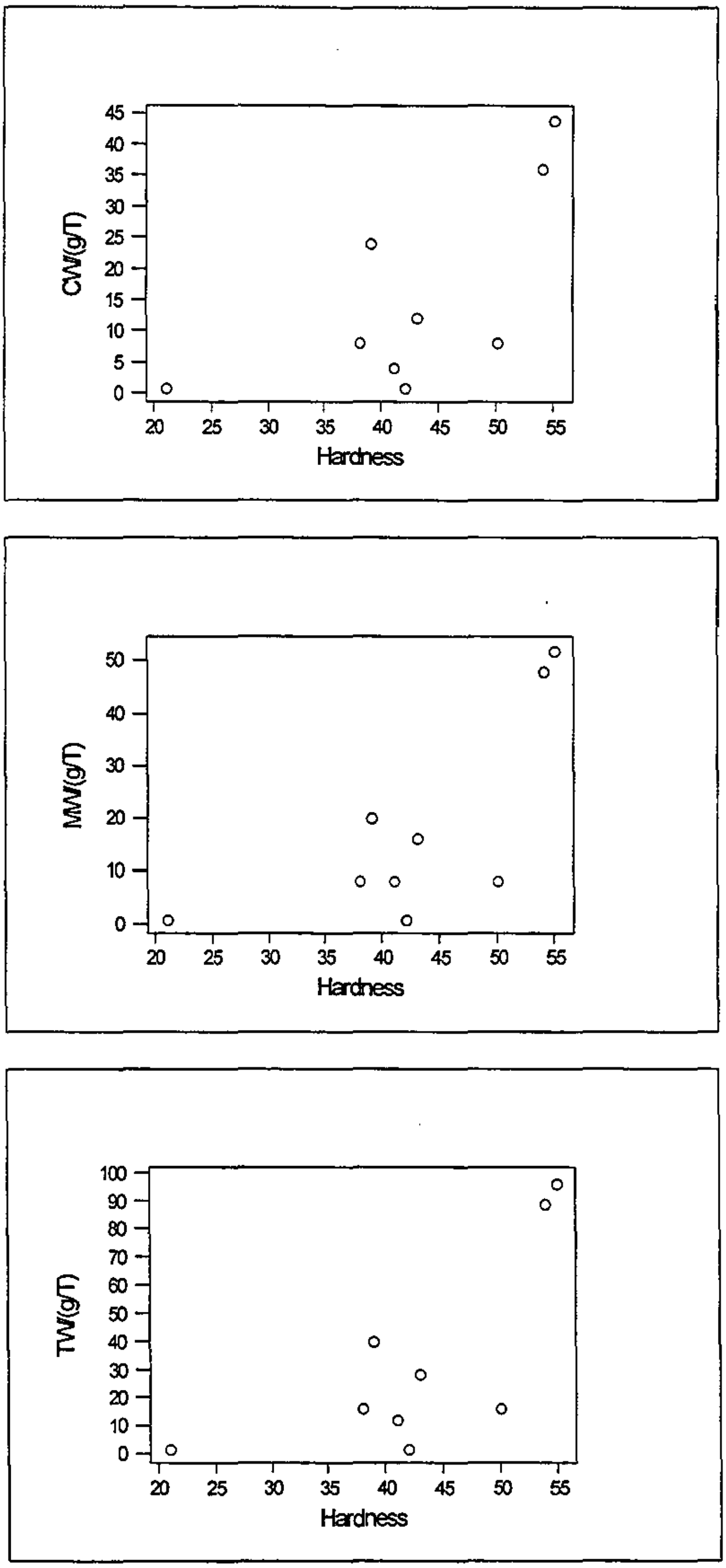

Figure 5.12 Variation of dry wear with rock hardness (crusher setting 4mm)

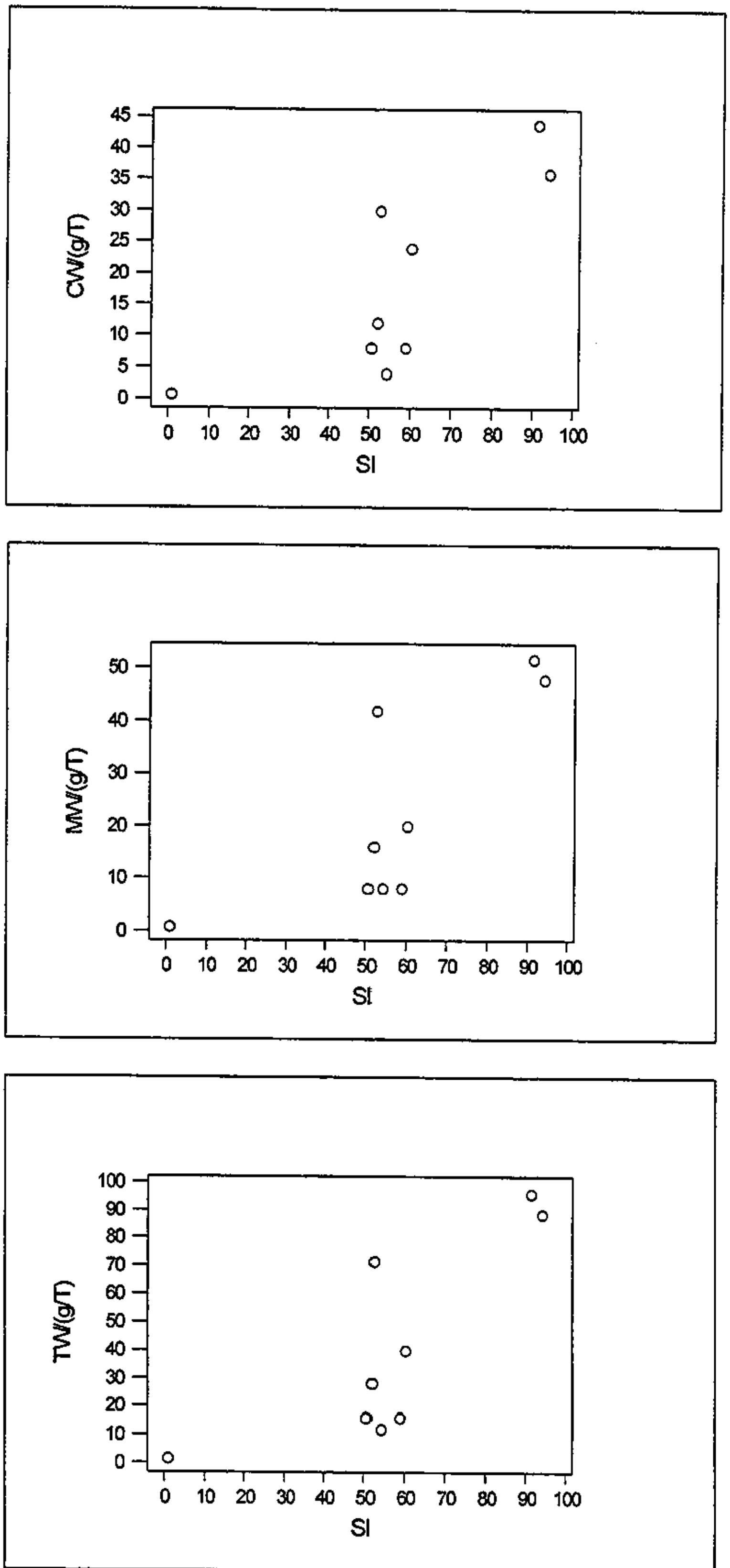

Figure 5.13 Variation of dry wear with silica content (crusher setting 4mm)

5.5.2 Correlation Between Wear and Other Rock Properties

Tables 5.17, 5.19 and 5.21 show the Pearson correlation coefficient between rock properties and liner wear data. It can be seen that for all settings, correlation exist between wear and all strength properties, with correlation between UCS and wear being the smallest observed and hence eliminated. Strong correlation also exists between wear and AAV. No significant correlation was found between the other crushing test values AIV and ACV and wear. It can also be seen that the highest correlation occur between wear and silica content with a correlation coefficient above 0.8, and wear and AAV with a slightly higher correlation coefficient..

Figure 5.14, 5.15 and 5.16 are the matrix plots of the data for the three crusher settings. Matrix plotting is a useful graphical technique to observe any obvious relationship which may exist between model variables. It can be seen that a strong linear relationship exists between different rock strength test variables, FT, UCS, BTS, and PL, as found by Bearman(1991). This suggests that only one of these variables could be used in the models.

Tables 5.18, 5.20 and 5.22 present the results of a sequential regression analysis carried out to obtain the best subset of variables to describe the wear at each setting. It can be seen that, in general, the best variable subset includes silica content, AAV and BTS.

From the three matrix plots it can be also seen that the relationship between none of the included rock properties and wear is completely linear. This indicated that a higher degree model would be more appropriate. It was found that including the interaction terms between the chosen variables, would considerably increase the significance of the model, indicated by higher $\mathbf{R}^2$ and lower error. The second order model based on linear and interaction terms was therefore chosen as the most appropriate for modelling the relationship between wear and rock properties.

Table 5.17 Pearson Correlation Coefficient for Various Rock Properties and Dry Wear at Closed-Side Setting of 4mm.

	CW/(g/T)	MW/(g/T)	TW/(g/T)	TIME(H/T)	Si	Al2O3	FT	UCS
MW/(g/T)	0.978							
TW/(g/T)	0.987	0.998						
TIME(H/T)	-0.766	-0.758	-0.769					
Si	0.808	0.790	0.804	-0.357				
Al2O3	-0.075	-0.079	-0.099	0.435	0.205			
FT	0.587	0.637	0.612	-0.256	0.592	0.550		
UCS	0.536	0.657	0.621	-0.367	0.512	0.379	0.886	
BTS	0.630	0.708	0.676	-0.476	0.492	0.451	0.878	0.908
PL	0.771	0.819	0.805	-0.432	0.798	0.407	0.926	0.883
AIV	-0.153	-0.135	-0.124	-0.102	-0.388	-0.812	-0.550	-0.392
ACV	0.158	0.125	0.149	-0.264	-0.106	-0.798	-0.462	-0.410
AAV	-0.853	-0.803	-0.815	0.897	-0.553	0.588	-0.380	-0.290
10%	0.497	0.502	0.505	-0.433	0.628	0.202	0.604	0.580

	BTS	PL	AIV	ACV	AAV
PL	0.884				
AIV	-0.566	-0.514			
ACV	-0.475	-0.395	0.938		
AAV	-0.489	-0.620	-0.011	-0.247	
10%	0.615	0.723	-0.637	-0.633	-0.871

Table 5.18 Adjusted R^2(%) and St. Deviation for Different Regression Models

Model Predictor	CW/(g/T)		MW/(g/T)		TW/(g/T)	
	R^2(adj)	S	R^2(adj)	S	R^2(adj)	S
Si	60.9	9.768	57.7	12.80	60.2	22.60
BTS	32.1	12.88	43.9	14.74	38.9	28.02
PL	54.4	10.55	63.0	11.98	60.3	22.57
AAV	67.2	8.637	57.5	12.43	59.7	22.15
Si, BTS	64.5	9.313	69.0	10.97	67.9	20.32
Si, Pl	61.0	9.760	64.3	11.77	63.9	21.52
Si, AAV	83.6	6.112	72.8	9.935	79.5	15.80
Si, BTS, AAV	85.0	5.845	94.2	4.591	94.7	8.056
Si, BTS, AAV. PL	81.8	6.435	95.0	4.281	95.4	7.468
Si, BTS (int.)	81.5	6.731	92.5	5.390	91.8	10.29

Table 5.19 Pearson Correlation Coefficient for Various Rock Properties and Dry Wear at Closed-Side Setting of 6mm

	CW/(g/T)	MW/(g/T)	TW/(g/T)	TIME(H/T)	Si	Al2O3	FT	UCS
MW/(g/T)	0.957							
TW/(g/T)	0.985	0.992						
TIME(H/T)	-0.879	-0.940	-0.924					
Si	0.520	0.720	0.642	-0.680				
Al2O3	-0.451	-0.622	-0.556	0.587	-0.923			
FT	0.486	0.475	0.485	-0.505	0.000	0.178		
UCS	0.403	0.435	0.425	-0.626	0.122	0.042	0.845	
BTS	0.639	0.549	0.594	-0.663	-0.009	0.116	0.816	0.868
PL	0.700	0.747	0.735	-0.821	0.412	-0.245	0.850	0.893
AIV	0.169	0.425	0.320	-0.415	0.813	-0.647	-0.074	0.019
ACV	0.358	0.557	0.478	-0.421	0.817	-0.692	-0.072	-0.151
AAV	-0.897	-0.869	-0.892	0.730	-0.553	0.588	-0.380	-0.290
10%	0.361	0.307	0.333	-0.347	0.192	-0.307	0.272	0.387

	BTS	PL	AIV	ACV	AAV
PL	0.867				
AIV	-0.248	0.190			
ACV	-0.230	0.185	0.896		
AAV	-0.489	-0.620	-0.011	-0.247	
10%	0.426	0.417	-0.354	-0.345	-0.871

Table 5.20 Adjusted R^2(%)and St. Deviation for Different Regression Models

Model Predictor	CW/(g/T)		MW/(g/T)		TW/(g/T)	
	R^2(adj)	S	R^2(adj)	S	R^2(adj)	S
Si	14.8	7.227	43.8	7.968	31.4	15.12
BTS	31.0	6.503	18.5	9.590	24.5	15.86
PL	40.6	6.038	48.4	7.634	46.3	13.37
AAV	76.6	3.797	70.6	5.736	75.4	9.011
Si, BTS	56.0	5.198	75.8	5.225	68.0	10.32
Si, PL	37.7	6.183	66.7	6.135	54.9	12.25
Si, AAV	70.8	4.240	77.2	5.049	74.6	9.168
Si, BTS, AAV	70.8	4.238	81.6	4.537	77.4	8.648
Si, BTS, AAV. PL	68.3	4.418	74.1	5.382	71.2	9.761
Si, BTS (int.)	52.1	5.422	70.3	5.795	62.4	11.19
Si, AAV (int.)	61.3	4.881	72.2	5.584	67.4	10.38

Table 5.21 Pearson Correlation Coefficient for Various Rock Properties and Dry Wear at Closed-Side Setting of 8mm.

	CW/(g/T)	MW/(g/T)	TW/(g/T)	TIME(H/T)	SI	Al2O3	FT	UCS
MW/(g/T)	0.496							
TW/(g/T)	0.852	0.815						
TIME(H/T)	-0.288	-0.249	-0.230					
SI	0.105	0.726	0.291	-0.452				
Al2O3	-0.141	-0.624	-0.263	0.375	-0.923			
FT	0.378	0.451	0.557	-0.257	0.000	0.178		
UCS	0.485	0.314	0.444	-0.579	0.122	0.042	0.845	
BTS	0.807	0.430	0.740	-0.389	-0.009	0.116	0.816	0.868
PL	0.603	0.674	0.687	-0.496	0.412	-0.245	0.850	0.893
AIV	-0.266	0.490	-0.031	-0.179	0.813	-0.647	-0.074	0.019
ACV	-0.129	0.674	0.176	0.078	0.817	-0.692	-0.072	-0.151
AAV	-0.633	-0.865	-0.842	0.554	-0.553	0.588	-0.380	-0.290
10%	0.425	0.177	0.320	-0.656	0.192	-0.307	0.272	0.387

	BTS	PL	AIV	ACV	AAV
PL	0.867				
AIV	-0.248	0.190			
ACV	-0.230	0.185	0.896		
AAV	-0.489	-0.620	-0.011	-0.247	
10%	0.426	0.417	-0.354	-0.345	-0.871

Table 5.22 Adjusted R^2(%) and St. Deviation for Different Regression Models

Model Predictor	CW/(g/T)		MW/(g/T)		TW/(g/T)	
	R^2(adj)	S	R^2(adj)	S	R^2(adj)	S
SI	0.0	5.508	44.9	3.344	0.0	8.189
BTS	59.3	3.272	4.9	4.394	47.2	5.756
PL	25.7	4.418	36.4	3.593	38.4	6.217
AAV	28.1	4.417	69.8	2.336	65.0	4.481
SI,BTS	52.9	3.519	60.6	2.829	49.1	5.654
SI,PL	14.4	4.744	57.6	2.934	26.1	6.810
SI,AAV	27.3	4.441	80.6	1.872	64.8	4.493
SI,BTS,AAV	43.3	3.921	75.5	2.102	68.8	4.230
Si,BTS,AAV.PL	96.0	1.038	64.2	2.541	69.2	4.205
SI,BTS (int.)	71.3	2.747	51.7	3.132	40.5	6.110
SI,AAV (int.)	51.1	3.643	87.3	1.512	53.1	5.188

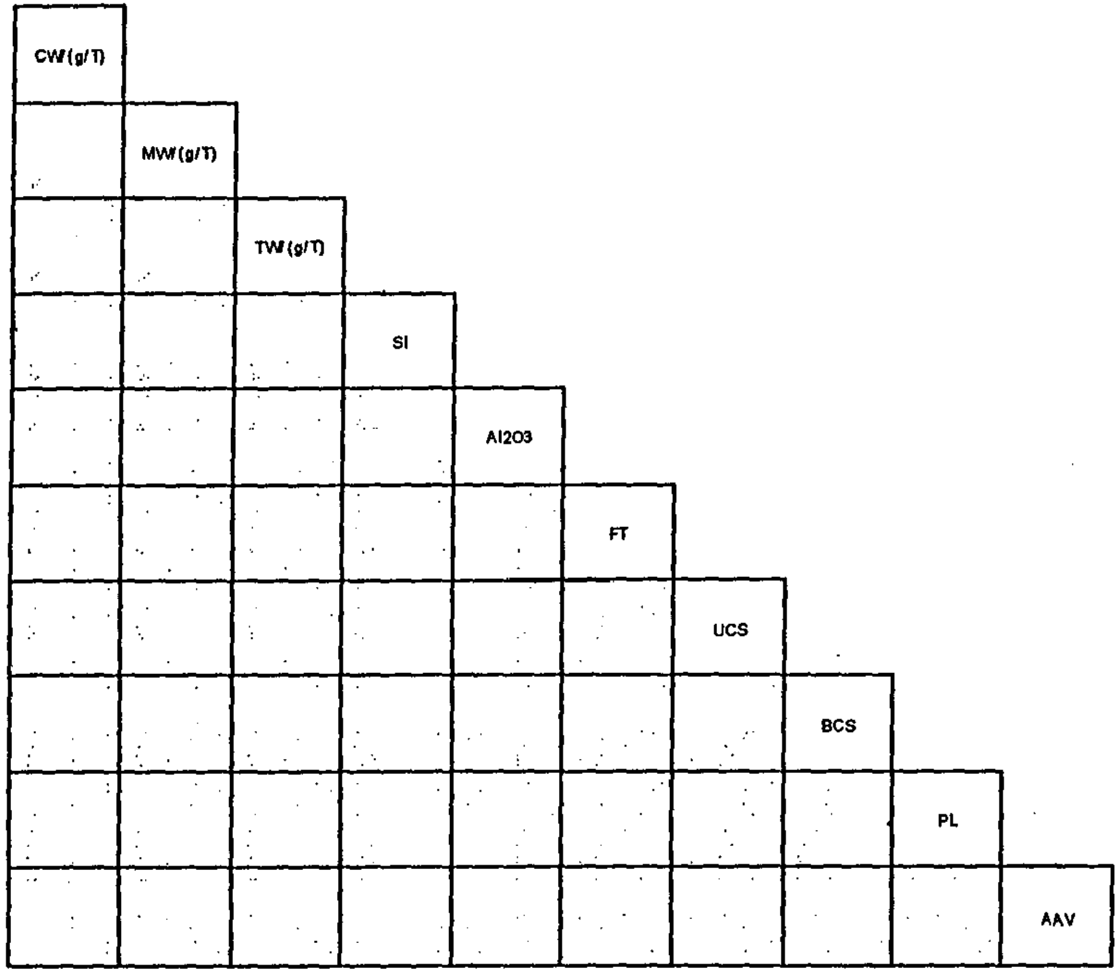

Figure 5.14 Matrix plot of different variables against wear and each other at crusher setting of 4mm

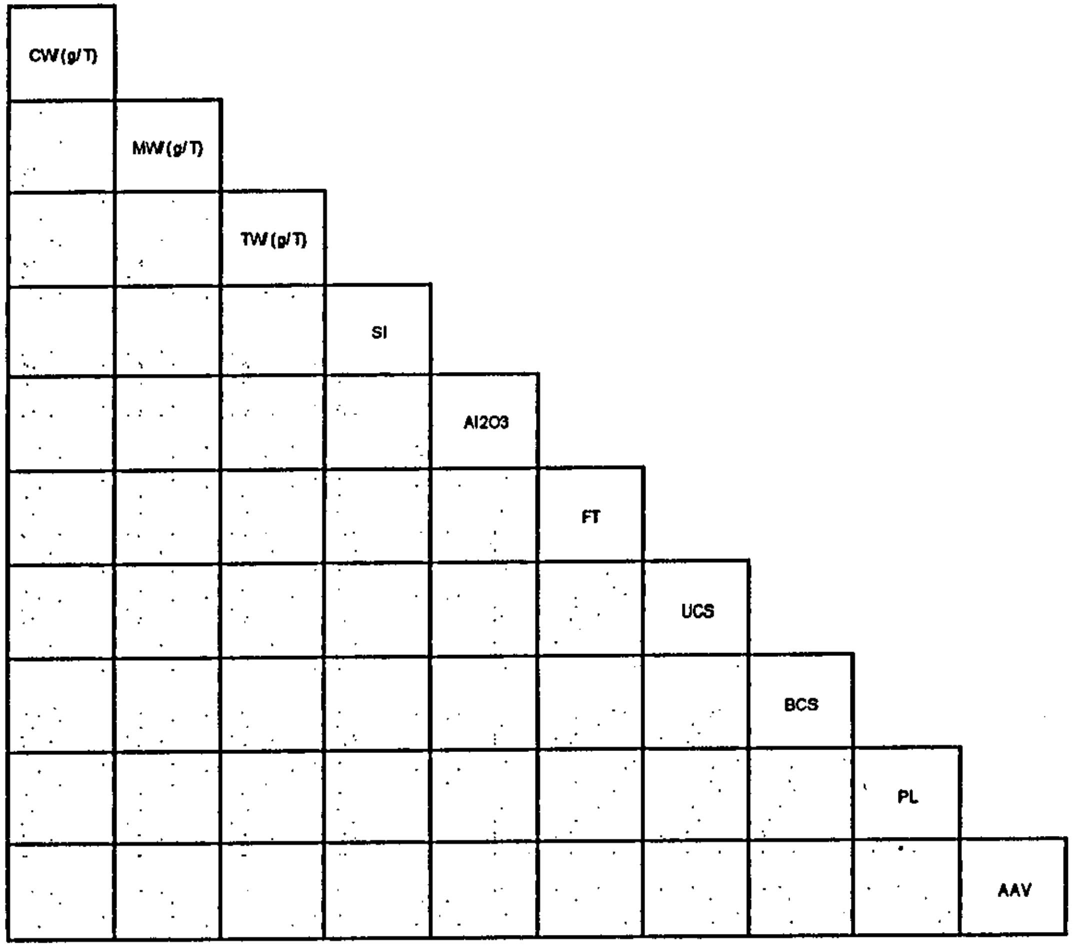

Figure 5.15 Matrix plot of different variables against wear and each other at crusher setting of 6mm

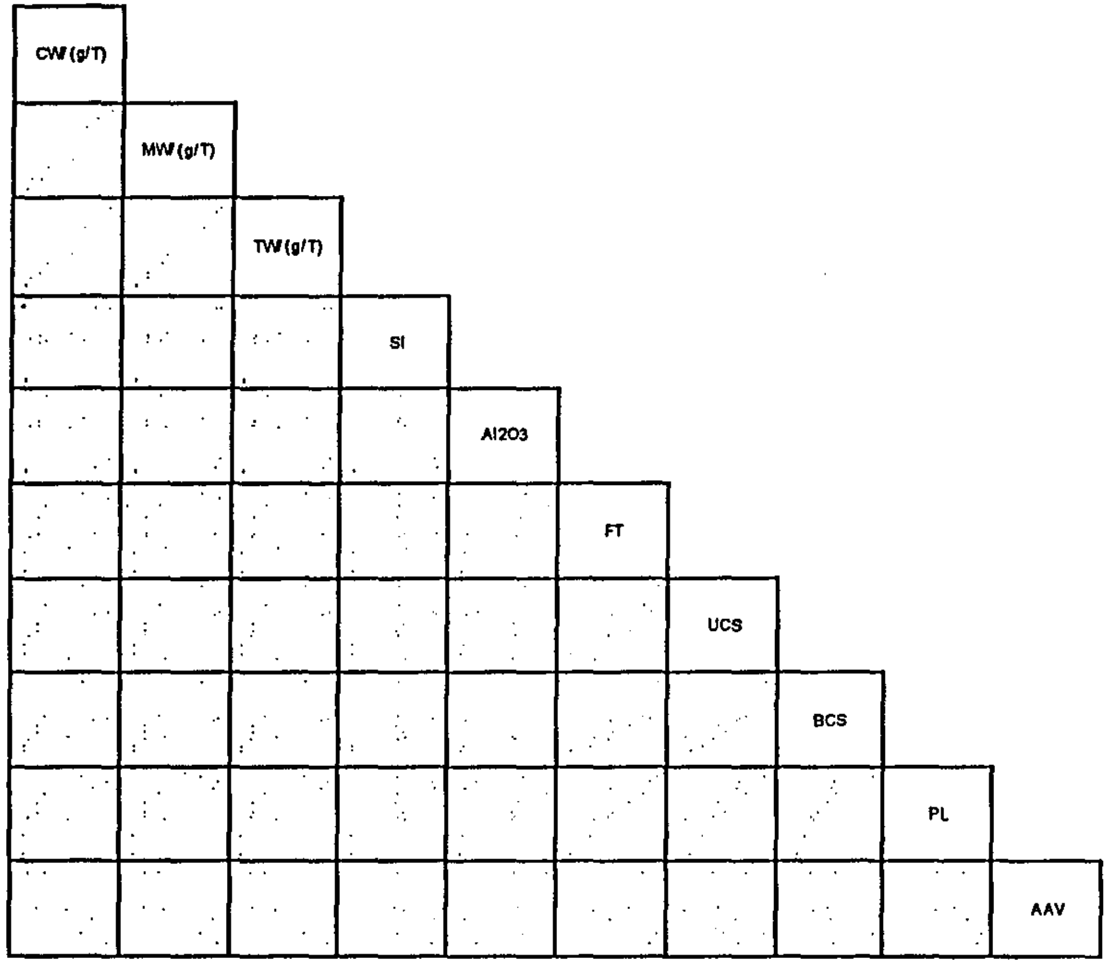

Figure 5.16 Matrix plot of different variables against wear and each other at crusher setting of 4mm

5.5.3 Correlation Between Dry Wear, Si, AAV and BTS

All the models formulated showed a perfect fit, i.e. a standard deviation of zero, and therefore are presented without further ANOVA analysis.

Crusher Setting 4mm

1. **CW/(g/T) = -633.4 +11.7Si +33.6BTS +8.1AAV -0.6 (Si×BTS) - 0.2(Si×AAV) +0.1(BTS×AAV)**
2. **MW/(g/T) = -530.3 +9.0Si +27.4BTS +11.9AAV -0.4 (Si×BTS) - 0.1(Si×AAV) -0.3(BTS×AAV)**
3. **TW/(g/T) = -963.0+16.8Si +50.0BTS +15.4AAV -0.8 (Si×BTS) - 0.2(Si×AAV) -0.2(BTS×AAV)**

Crusher Setting 6mm

1. **CW/(g/T) = -437.1 +7.8 Si + 23.7 BTS+10.4 AAV -0.4 (Si×BTS) -0.1 (Si×AAV) -0.2 (BTS×AAV)**
2. **MW/(g/T) = -422.8 +7.4 Si +22.0 BTS +13.8 AAV -0.4 (Si×BTS) - 0.2(Si×AAV) -0.3(BTS×AAV)**
3. **TW/(g/T) = -859.8 +15.2Si + 45.7BTS + 24.3AAV - 0.8 (Si×BTS) -0.3(Si×AAV) -0.5(BTS×AAV)**

Crusher Setting 8mm

1. **CW/(g/T) = -155.3+2.6 Si +9.5 BTS -0.4 AAV -0.2 (Si×BTS) -0.1 (Si×AAV) -0.2 (BTS×AAV)**
2. **MW/(g/T) = -122.8+2.4 Si +9.0 BTS -0.5 AAV -0.2 (Si×BTS) - 0.2(Si×AAV) -0.3(BTS×AAV)**
3. **TW/(g/T) = -277.9+6.0 Si +18.5BTS-0.9 AAV - 0.8 (Si×BTS) -0.3(Si×AAV) -0.5(BTS×AAV)**

5.5.4 Correlation Between Dry Wear, Si, AAV and PL

Crusher Setting 4mm

1. **CW/(g/T) = -1051 + 18Si +73 PL +23AAV - (Si×PL) - (PL×AAV)**
2. **MW/(g/T) = -1140 + 80Si +73 PL +34AAV - (Si×PL) -2(PL×AAV)**
3. **TW/(g/T) = -1952 + 31Si+137 PL+49AAV -2 (Si×PL) -2(PL×AAV)**

Crusher Setting 6mm

1. **CW/(g/T) = -736.2 + 12.1 Si +51.9 PL +24.2 AAV -0.8 (Si×PL) - 0.2 (Si× AAV) -1.1 (PL×AAV)**
2. **MW/(g/T) = -757.4 + 12.0 Si +52.7 PL +28.9 AAV -0.8 (Si×PL) -0.2 (Si× AAV) -1.3 (PL×AAV)**
3. **TW/(g/T) = -1493 + 24 Si +105 PL +53 AAV -2 (Si×PL) -2 (PL×AAV)**

Crusher Setting 8mm

1. **CW/(g/T) = - 352.2+ 5.2 Si +26.8 PL +8.1 AAV -0.4 (Si×PL) -0.8 (PL×AAV)**
2. **MW/(g/T) = -239.4 +4.0 Si +16.4 PL +10 AAV -0.3 (Si×PL) -0.3(PL×AAV)**
3. **TW/(g/T) = - 675. + 10.7 Si +48.8 PL +26.5 AAV -0.7 (Si×PL) -1.5 (PL×AAV)**

5.5.3 Correlation Between Wear, Si, AAV and FT

Crusher Setting 4mm

1. CW/(g/T) = 5909 -104 Si -1955FT -570 AAV +34 (Si×FT) +8 (Si×AAV) +53 (FT×AAV)
2. MW/(g/T) = 7830 -139 Si -2589 FT -753 AAV +46 (Si×FT) +11(Si×AAV) +67(FT×AAV)
3. TW/(g/T) = 13739 -243 Si -4546 FT -1323 AAV +80 (Si×FT) +19(Si×AAV)+120(FT×AAV)

Crusher Setting 6mm

1. CW/(g/T) = 5256 -93 Si -1741 FT -495 AAV +31 (Si×FT) +7 (Si×AAV) +44 (FT×AAV)
2. MW/(g/T) = 5373 -94 Si -1866 FT -5o4 AAV +31 (Si×FT) +7 (Si×AAV) +45 (FT×AAV)
3. TW/(g/T) = 10596 -187 Si -3507 FT -999 AAV +62 (Si×FT) 14 (Si×AAV) +89 (FT×AAV)

Crusher Setting 8mm

1. CW/(g/T) = 3161 -57 Si -1037 FT -300 AAV -31 (Si×FT) -7 (Si×AAV) -44 (FT×AAV)
2. MW/(g/T) = 1681-29 Si -558 FT -156 AAV +62 (Si×FT)+14 (Si×AAV) +89 (FT×AAV)
3. TW/(g/T) = 4842 -86 Si -1595 FT -455 AAV +28 (Si×FT) +7 (Si×AAV) +39 (FT×AAV)

5.6 Correlation Between Dry Wear, Crusher Setting and Rock Properties

Table 5.23 shows the Pearson correlation coefficients between dry wear and inverse of the crusher setting, **1/CSS**, and the rock properties for all ten rock types and all five crusher settings tested. Compared with the correlation values obtained for each separate setting, the coefficients are smaller in every case. The most striking decrease being that of silica content. However, the full matrix plot, Figure 5.17, shows similar relationship between wear and different variables. The following sections present three wear models based on the variable subset **1/CSS, Si, AAV** and one of the strength parameter **BTS, PL** and **FT**.

Table 5.23 Pearson Correlation Coefficient for Dry Wear and Various Rock Properties and Closed-Side Setting

	CW/(g/T)	MW/(g/T)	TW/(g/T)	1/CSS	TIME(H/T)	Si	Al2O3	FT
MW/(g/T)	0.952							
TW/(g/T)	0.977	0.991						
1/CSS	0.410	0.416	0.425					
TIME(H/T)	-0.106	-0.110	-0.104	0.759				
Si	0.451	0.547	0.515	-0.252	-0.457			
Al2O3	-0.245	-0.351	-0.316	-0.152	0.193	-0.411		
FT	0.399	0.399	0.396	-0.163	-0.316	0.271	0.315	
UCS	0.388	0.402	0.392	-0.111	-0.374	0.278	0.153	0.856
BTS	0.541	0.471	0.489	-0.115	-0.402	0.200	0.229	0.836
PL	0.570	0.588	0.579	-0.203	-0.489	0.605	0.024	0.881
AIV	0.020	0.176	0.124	0.193	-0.019	0.227	-0.710	-0.269
ACV	0.192	0.324	0.281	0.095	-0.110	0.474	-0.724	-0.200
AAV	-0.640	-0.614	-0.621	-0.006	0.467	-0.553	0.588	-0.380
10%	0.323	0.279	0.292	-0.111	-0.326	0.359	-0.144	0.385

	UCS	BTS	PL	AIV	ACV	AAV
BTS	0.880					
PL	0.877	0.865				
AIV	-0.131	-0.365	-0.129			
ACV	-0.227	-0.302	-0.026	0.909		
AAV	-0.290	-0.489	-0.619	-0.011	-0.247	
10%	0.445	0.483	0.531	-0.449	-0.442	-0.871

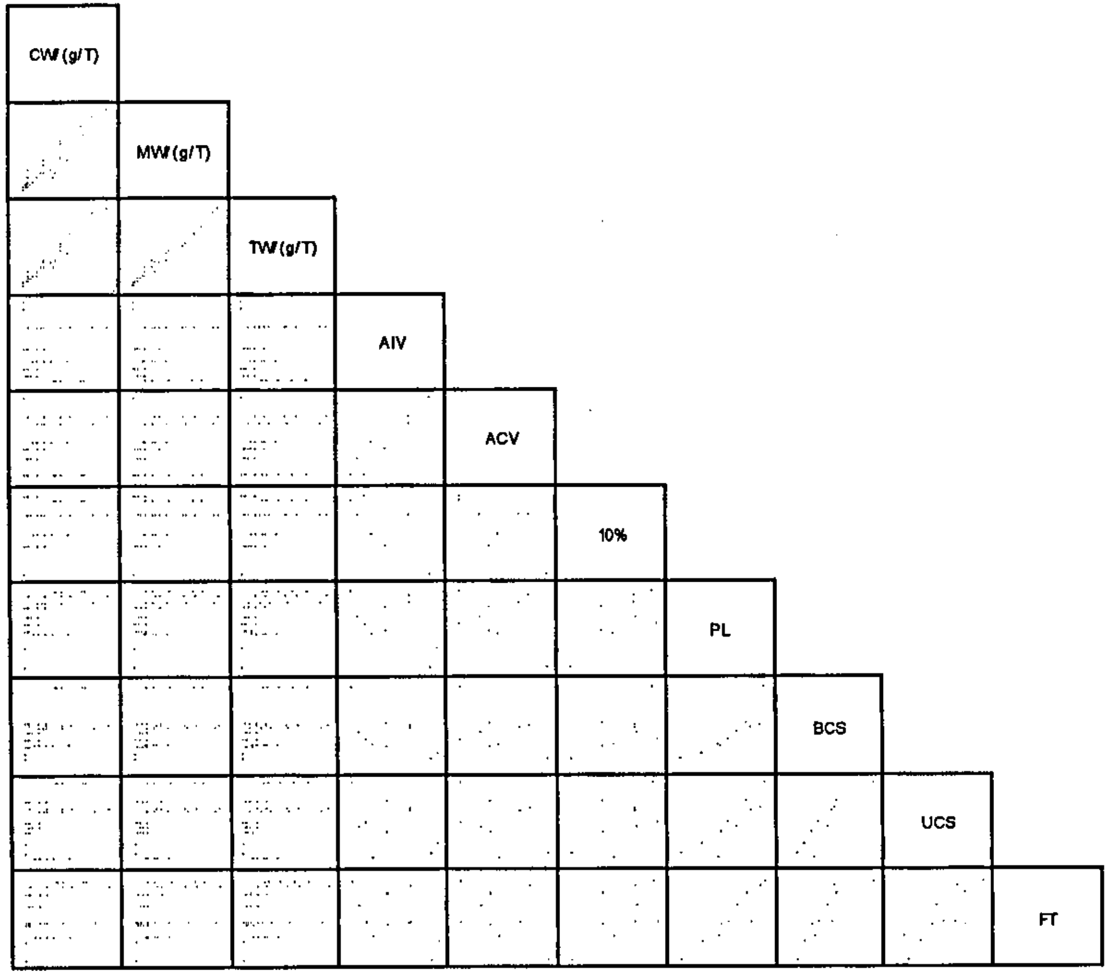
CW (g/T)
MW (g/T)
TW (g/T)
AIV
ACV
10%
PL
BCS
UCS
FT

5.6.1 Correlation Between Dry Wear, Closed-Side Setting, Si, AAV and BTS

1. $CW/(g/T) = a_0 + a_1 x_1 + a_2 x_2 + \ldots + a_4 x_4 + a_5 x_1 x_2 + \ldots + a_{10} x_3 x_4$

Term	Coef	Stdev	t-ratio	p
Constant	-391.0	74.318	-5.261	0.000
1/CSS	-82.2	118.078	-0.696	0.493
Si	6.6	1.294	5.104	0.000
BTS	21.8	3.829	5.682	0.000
AAV	9.3	2.708	3.445	0.002
1/CSS*Si	3.5	0.714	4.901	0.000
1/CSS*BTS	2.1	3.843	0.552	0.586
1/CSS*AAV	-13.0	6.786	-1.913	0.068
Si*BTS	-0.4	0.069	-5.523	0.000
Si*AAV	-0.1	0.029	-3.372	0.003
BTS*AAV	-0.2	0.085	-1.916	0.067

s = 2.554 R^2 = 96.2% R^2(adj) = 94.6%

Analysis of Variance for CW/(g/T)

Source	DF	Seq SS	Adj SS	Adj MS	F	p
Linear	4	3278.57	326.210	81.553	12.51	0.000
Interaction	6	698.95	698.949	116.492	17.86	0.000
Residual Error	24	156.52	156.517	6.522		
Total	34	134.04				

2. $MW/(g/T) = a_0 + a_1 x_1 + a_2 x_2 + \ldots + a_4 x_4 + a_5 x_1 x_2 + \ldots + a_{10} x_3 x_4$

Term	Coef	Stdev	t-ratio	p
Constant	-257.6	63.209	-4.075	0.000
1/CSS	-483.6	100.427	-4.815	0.000
Si	5.1	1.101	4.601	0.000
BTS	14.1	3.257	4.321	0.000
AAV	11.2	2.303	4.847	0.000
1/CSS*Si	4.7	0.607	7.679	0.000
1/CSS*BTS	21.0	3.269	6.418	0.000
1/CSS*AAV	-4.4	5.772	-0.765	0.452
Si*BTS	-0.3	0.059	-4.973	0.000
Si*AAV	-0.1	0.025	-5.099	0.000
BTS*AAV	-0.2	0.072	-3.342	0.003

s = 2.172 R^2 = 98.3% R^2(adj) = 97.6%

Analysis of Variance for MW/(g/T)

Source	DF	Seq SS	Adj SS	Adj MS	F	p
Linear	4	5538.26	352.13	88.032	18.66	0.000
Interaction	6	1033.02	1033.02	172.171	36.50	0.000
Residual Error	24	113.22	113.22	4.718		
Total	34	6684.51				

3. **TW/(g/T)** = $a_0 + a_1 x_1 + a_2 x_2 + \ldots + a_4 x_4 + a_5 x_1 x_2 + \ldots + a_{10} x_3 x_4$

Term	Coef	Stdev	t-ratio	p
Constant	-571.3	69.765	-8.189	0.000
1/CSS	-771.3	110.845	-6.959	0.000
Si	10.6	1.215	8.756	0.000
BTS	32.9	3.595	9.149	0.000
AAV	18.6	2.542	7.299	0.000
1/CSS*Si	9.9	0.670	14.828	0.000
1/CSS*BTS	26.4	3.608	7.313	0.000
1/CSS*AAV	-7.9	6.370	-1.243	0.226
Si*BTS	-0.6	0.065	-9.760	0.000
Si*AAV	-0.2	0.027	-8.194	0.000
BTS*AAV	-0.4	0.080	-4.817	0.000

s = 2.397 **R^2** = 99.3% **R^2(adj)** = 99.1%

Analysis of Variance for TW/(g/T)

Source	DF	Seq SS	Adj SS	Adj MS	F	P
Linear	4	16924.5	1248.56	312.141	54.31	0.000
Interaction	6	3573.9	3573.90	595.650	103.64	0.000
Residual Error	24	137.9	137.93	5.747		
Total	34	20636.3				

5.6.2 Correlation Between Dry Wear, Closed-Side Setting, Si, AAV and PL

1. **CW/(g/T)** = $a_0 + a_1 x_1 + a_2 x_2 + \ldots + a_4 x_4 + a_5 x_1 x_2 + \ldots + a_{10} x_3 x_4$

Term	Coef	Stdev	t-ratio	p
Constant	-656.8	99.311	-6.613	0.000
1/CSS	-122.4	147.417	-0.830	0.414
Si	10.5	1.618	6.490	0.000
AAV	20.8	3.970	5.246	0.000
PL	47.1	6.787	6.940	0.000
1/CSS*Si	3.4	0.566	6.063	0.000
1/CSS*AAV	-12.0	5.536	-2.165	0.041
1/CSS*PL	5.7	9.865	0.580	0.567
Si*AAV	-0.2	0.036	-4.535	0.000
Si*PL	-0.8	0.110	-6.909	0.000
AAV*PL	-0.8	0.224	-3.786	0.001

s = 2.263 **R^2** = 96.9% **R^2(adj)** = 95.5%

Analysis of Variance for CW/(g/T)

Source	DF	Seq SS	Adj SS	Adj MS	F	P
Linear	4	3016.01	343.418	85.855	16.77	0.000
Interaction	6	767.05	767.051	127.842	24.97	0.000
Residual Error	24	122.89	122.892	5.121		
Total	34	3905.95				

2. $MW/(g/T) = a_0 + a_1 x_1 + a_2 x_2 + ... + a_4 x_4 + a_5 x_1x_2 + ... + a_{10} x_3x_4$

Term	Coef	Stdev	t-ratio	p
Constant	-553.8	101.004	-5.482	0.000
1/CSS	-637.5	149.930	-4.252	0.000
Si	9.9	1.645	6.023	0.000
AAV	25.9	4.038	6.422	0.000
PL	37.5	6.903	5.439	0.000
1/CSS*Si	2.7	0.575	4.727	0.000
1/CSS*AAV	-11.8	5.631	-2.095	0.047
1/CSS*PL	51.0	10.033	5.080	0.000
Si*AAV	-0.2	0.037	-4.758	0.000
Si*PL	-0.7	0.112	-6.218	0.000
AAV*PL	-1.2	0.228	-5.080	0.000

$s = 2.301$ $R^2 = 98.1\%$ $R^2(adj) = 97.3\%$

Analysis of Variance for MW/(g/T)

Source	DF	Seq SS	Adj SS	Adj MS	F	P
Linear	4	5375.26	403.15	100.788	19.03	0.000
Interaction	6	1065.00	1065.00	177.500	33.51	0.000
Residual Error	24	127.12	127.12	5.297		
Total	34	6567.37				

3. $TW/(g/T) = a_0 + a_1 x_1 + a_2 x_2 + ... + a_4 x_4 + a_5 x_1x_2 + ... + a_{10} x_3x_4$

Term	Coef	Stdev	t-ratio	p
Constant	-1135	132.631	-8.555	0.000
1/CSS	-1017	196.878	-5.164	0.000
Si	20	2.160	9.058	0.000
AAV	46	5.303	8.633	0.000
PL	80	9.064	8.871	0.000
1/CSS*Si	7	0.755	9.679	0.000
1/CSS*AAV	-17	7.394	-2.293	0.031
1/CSS*PL	69	13.175	5.226	0.000
Si*AAV	-0	0.049	-6.813	0.000
Si*PL	-1	0.147	-9.613	0.000
AAV*PL	-2	0.300	-6.882	0.000

$s = 3.022$ $R^2 = 98.9\%$ $R^2(adj) = 98.5\%$

Analysis of Variance for TW/(g/T)

Source	DF	Seq SS	Adj SS	Adj MS	F	P
Linear	4	16525.0	1507.58	376.894	41.27	0.000
Interaction	6	3892.1	3892.08	648.680	71.03	0.000
Residual Error	24	219.2	219.19	9.133		
Total	34	20636.3				

5.6.3 Correlation Between Dry Wear, Closed-Side Setting, Si, AAV and FT

1. $CW/(g/T) = a_0 + a_1 x_1 + a_2 x_2 + \ldots + a_4 x_4 + a_5 x_1 x_2 + \ldots + a_{10} x_3 x_4$

Term	Coef	Stdev	t-ratio	p
Constant	4739	666.556	7.110	0.000
1/CSS	-208	123.261	-1.685	0.105
Si	-83	11.674	-7.140	0.000
AAV	-446	62.869	-7.100	0.000
FT	-1563	221.480	-7.056	0.000
1/CSS*Si	4	0.596	6.086	0.000
1/CSS*AAV	-10	5.338	-1.898	0.070
1/CSS*FT	54	35.160	1.546	0.135
Si*AAV	6	0.893	7.175	0.000
Si*FT	27	3.863	7.078	0.000
AAV*FT	41	5.983	6.777	0.000

$s = 2.246$ $\quad R^2 = 96.9\%$ $\quad R^2(adj) = 95.6\%$

Analysis of Variance for CW/(g/T)

Source	DF	Seq SS	Adj SS	Adj MS	F	P
Linear	4	2967.58	363.527	90.882	18.01	0.000
Interaction	6	817.29	817.289	136.215	27.00	0.000
Residual Error	24	121.08	121.084	5.045		
Total	34	3905.95				

2. $MW/(g/T) = a_0 + a_1 x_1 + a_2 x_2 + \ldots + a_4 x_4 + a_5 x_1 x_2 + \ldots + a_{10} x_3 x_4$

Term	Coef	Stdev	t-ratio	p
Constant	4509	819.844	5.499	0.000
1/CSS	-358	151.607	-2.363	0.027
Si	-79	14.359	-5.526	0.000
AAV	-420	77.327	-5.434	0.000
FT	-1495	272.414	-5.489	0.000
1/CSS*Si	4	0.733	4.904	0.000
1/CSS*AAV	-17	6.565	-2.593	0.016
1/CSS*FT	139	43.246	3.218	0.004
Si*AAV	6	1.098	5.569	0.000
Si*FT	26	4.752	5.491	0.000
AAV*FT	37	7.359	5.045	0.000

$s = 2.763$ $\quad R^2 = 97.2\%$ $\quad R^2(adj) = 96.0\%$

Analysis of Variance for MW/(g/T)

Source	DF	Seq SS	Adj SS	Adj MS	F	P
Linear	4	5318.80	360.04	90.009	11.79	0.000
Interaction	6	1065.39	1065.39	177.565	23.26	0.000
Residual Error	24	183.18	183.18	7.632		
Total	34	6567.37				

3. $TW/(g/T) = a_0 + a_1 x_1 + a_2 x_2 + \ldots + a_4 x_4 + a_5 x_1 x_2 + \ldots + a_{10} x_3 x_4$

Term	Coef	Stdev	t-ratio	p
Constant	8940	1093.01	8.179	0.000
1/CSS	-695	202.12	-3.437	0.002
Si	-157	19.14	-8.214	0.000
AAV	-836	103.09	-8.109	0.000
FT	-2951	363.18	-8.124	0.000
1/CSS*Si	9	0.98	8.717	0.000
1/CSS*AAV	-23	8.75	-2.617	0.015
1/CSS*FT	207	57.66	3.588	0.001
Si*AAV	12	1.46	8.259	0.000
Si*FT	52	6.34	8.139	0.000
AAV*FT	74	9.81	7.588	0.000

s = 3.683 **R^2** = 98.4% **R^2(adj)** = 97.8%

Analysis of Variance for TW/(g/T)

Source	DF	Seq SS	Adj SS	Adj MS	F	P
Linear	4	16286.3	1522.75	380.687	28.06	0.000
Interaction	6	4024.4	4024.44	670.740	49.44	0.000
Residual Error	24	325.6	325.59	13.566		
Total	34	20636.3				

5.7 Discussion of the Results and Comparison Between Measured and Predicted Liner Wear For Dry Rock

Appendix 3 shows the predicted results for the main models presented in this Chapter. As expected, the best fit is achieved by Rock specific models. The general fitted models for dry wear provide differing quality of fit for different rock types and closed-side settings. However, taking the diversity of the rock types used, and the range of experimental data, all the general models provide significant correlation with very high confidence range (above 99.999% represented by p-Test value of 0.000). In particular, the models for wear of all rocks at fixed closed-side setting (4mm,6mm,8mm) produce perfect fits with zero errors. This indicates that the origin of the error associated with the general models may be due to the closed-side setting.

The general wear model, with linear and interaction terms of **1/CSS**, **Si**, **BTS**, and **AAV** provide the best fit, represented by the highest $\mathbf{R^2(adj)}$ and lowest standard deviation, with a minimum number of variables and is therefore used in the following Chapter, as the basis for models of moist wear.

Chapter 6 WEAR RESULTS AND REGRESSION MODELS FOR MOIST ROCK

All rock types, except Breedon lime stone which showed no variation in wear for added moisture, were tested for the effect of moisture on wear. Pant lime stone was tested only at 4mm crusher setting and three moisture levels. Two other rock types, Shardlow and Shap Blue, were also tested at three moisture levels due to shortage of the available rock. The results of the experiments are shown in Table A2.2, Appendix 2.

6.1 The Statistical Models

The variation of wear with moisture and closed-side setting is shown graphically for eight rock types in Figures 6.1 to 6.8. It can be seen that the relationship between wear and moisture is not linear. Furthermore, the effect of moisture on wear depends on the closed-side setting and therefore, the interaction between moisture and closed-side setting must be included in the models. A sequential regression analysis was carried out to find the best variable subset to model the wear. It was found that an extended version of the three-term second order polynomial used in modelling dry wear, provided the best fit for all rock types. A further polynomial, with no constant term, was also considered which is presented in Table A1.1, Appendix 1.

In the following sections the regression models for each rock, the three dimensional response surface for variation of wear, and the corresponding statistical tests are presented. Due to its very low abrasivity, data obtained for Pant rock, which was tested only at 4mm setting, was not considered adequate for modelling. However, the test results were included in the general analysis and models.

6.1.1 Cliffe Hill Rock

Table 6.1 Correlation Between Wear and other Variables- Cliffe Hill Rock

	CW/(g/T)	MW/(g/T)	TW/(g/T)	1/CSS
MW/(g/T)	0.996			
TW/(g/T)	0.999	0.999		
1/CSS	0.754	0.746	0.750	
Moist	0.579	0.594	0.588	-0.022

1. **CW/(g/T)** = 0.2 -20.4 **1/CSS** + 265 **1/CSS^2** - 7.24 **Moist** + 3.57 **Moist^2**+ 36 **Moist/CCS**

   s = 0.789 **R^2**= 99.3% **R^2(adj)** = 98.9%

Analysis of Variance

SOURCE	DF	SS	MS	F	p
Regression	5	823.29	164.66	264.64	0.000
Error	9	5.60	0.62		
Total	14	828.89			

2. **MW/(g/T)** = - 6.49 + 62.4 **1/CSS** +96 **1/CSS^2** -7.28 **Moist** + 3.93 **Moist^2**+ 49.8 **Moist/CSS**

   s = 1.392 **R^2** = 98.7% **R^2(adj)** = 97.9%

Analysis of Variance

SOURCE	DF	SS	MS	F	p
Regression	5	1278.33	255.67	131.91	0.000
Error	9	17.44	1.94		
Total	14	1295.78			

3. **TW/(g/T)** = - 6.3 + 42 **1/CSS** + 362 **1/CSS^2**- 15.1 **Moist** + 7.49 **Moist^2**+ 80.9 **Moist/CSS**

   s = 2.045 **R^2** = 99.1% **R^2**(adj) = 98.6%

Analysis of Variance

SOURCE	DF	SS	MS	F	p
Regression	5	4150.87	830.17	197.81	0.000
Error	9	37.77	4.20		
Total	14	4188.64			

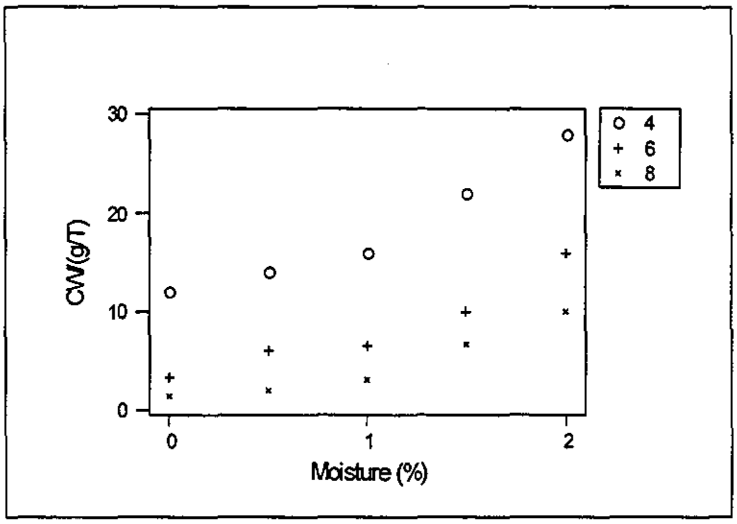

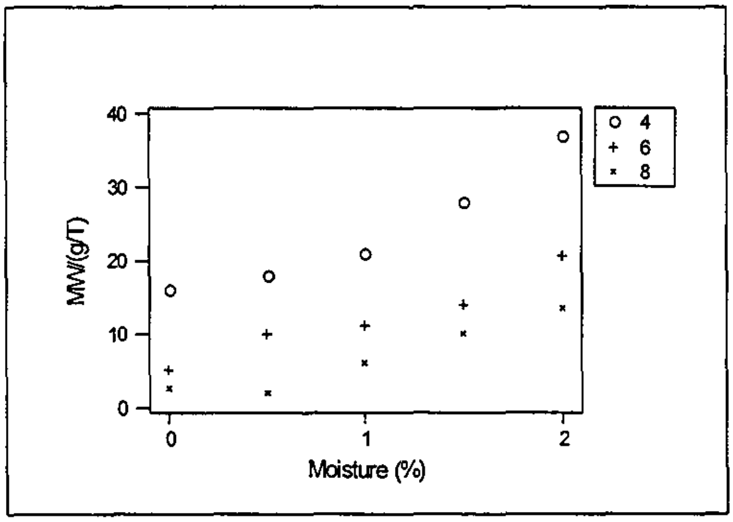

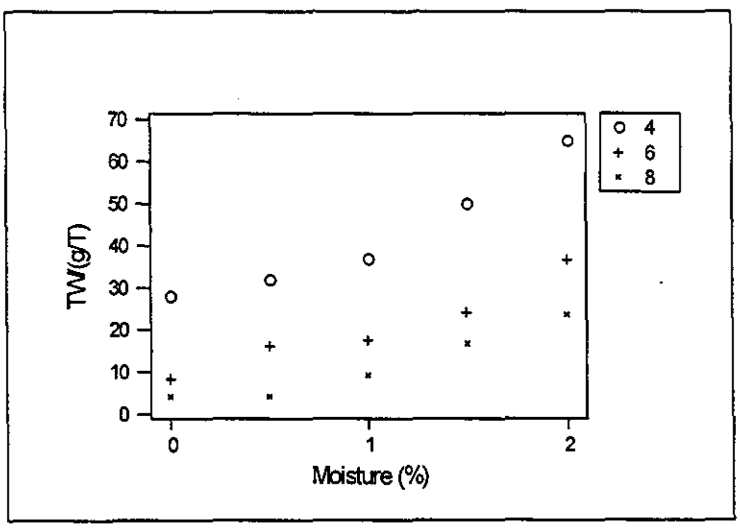

Figure 6.1 Measured wear against moisture content at three closed-side settings for Cliffe Hill rock

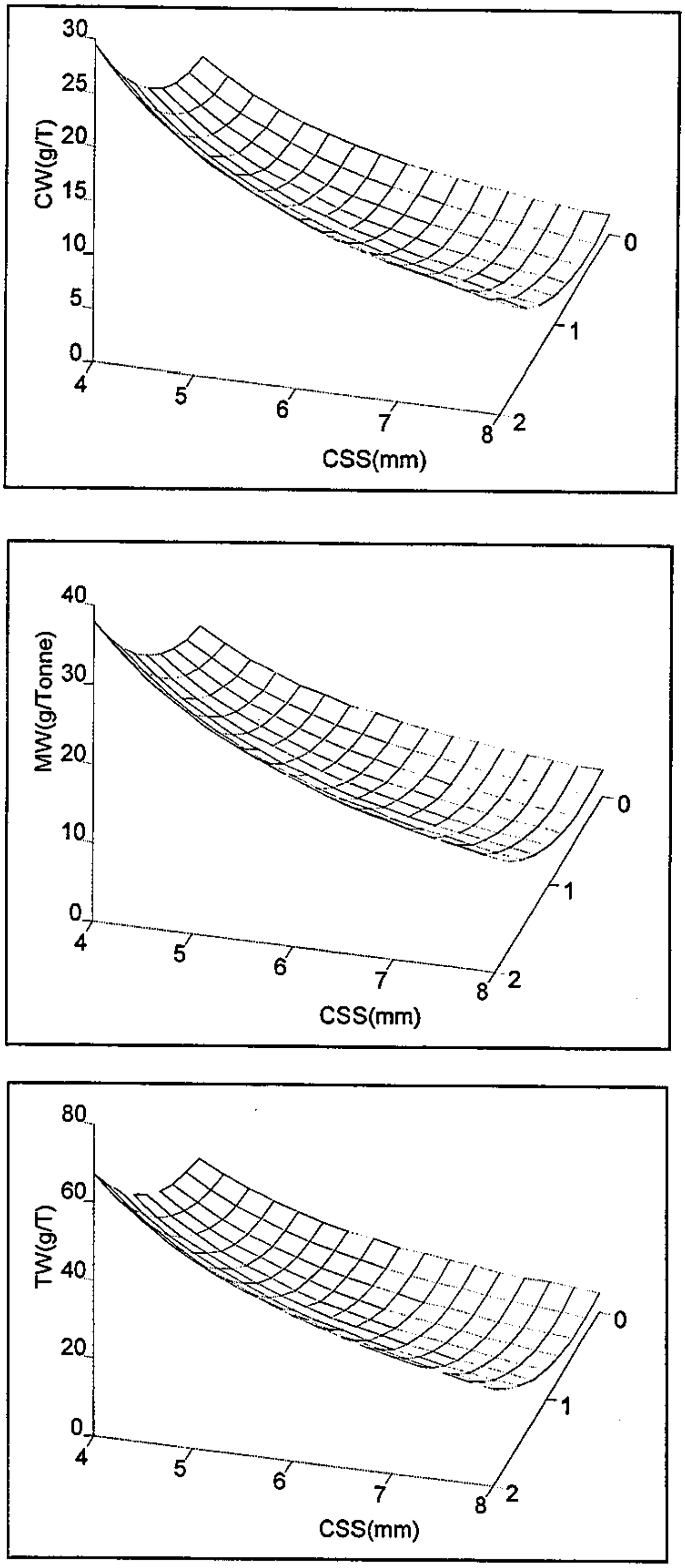

Figure 6.2 The predicted wear response surface for moist Cliffe Hill rock

6.1.2 Ingleton Grey Rock

Table 6.2 Correlation Between Wear and other Variables - Ingleton Grey

	CW/(g/T)	MW/(g/T)	TW/(g/T)	1/CSS
MW/(g/T)	0.978			
TW/(g/T)	0.994	0.995		
1/CSS	0.687	0.646	0.669	
Moist	0.633	0.709	0.677	-0.019

1. **CW/(g/T)** = -10.6 +103 **1/CSS** -127 **1/CSS²**- 7.25 Moist + 3.55 **Moist²** + 34.2 **Moist/CSS**

s = 1.334 R^2 = 97.5% R^2(adj) = 96.1%

Analysis of Variance

SOURCE	DF	SS	MS	F	p
Regression	5	628.94	125.79	70.71	0.000
Error	9	16.01	1.78		
Total	14	644.95			

2. **MW/(g/T)** = 2.66 -59 **1/CSS** + 333 **1/CSS²**- 3.54 **Moist** + 3.04 **Moist²** +28.52 **Moist/CSS**

s = 1.126 R^2 = 98.7% R^2(adj) = 97.9%

Analysis of Variance

SOURCE	DF	SS	MS	F	p
Regression	5	850.71	170.14	134.17	0.000
Error	9	11.41	1.27		
Total	14	862.12			

3. **TW/(g/T)** = -7.96 +44 **1/CSS** + 206 **1/CSS²**- 10.8 **Moist** + 6.6 **Moist²**+62.7 **Moist/CSS**

s = 2.121 R^2 = 98.6 R^2(adj) = 97.9%

Analysis of Variance

SOURCE	DF	SS	MS	F	p
Regression	5	2925.69	585.14	130.04	0.000
Error	9	40.50	4.50		
Total	14	2966.19			

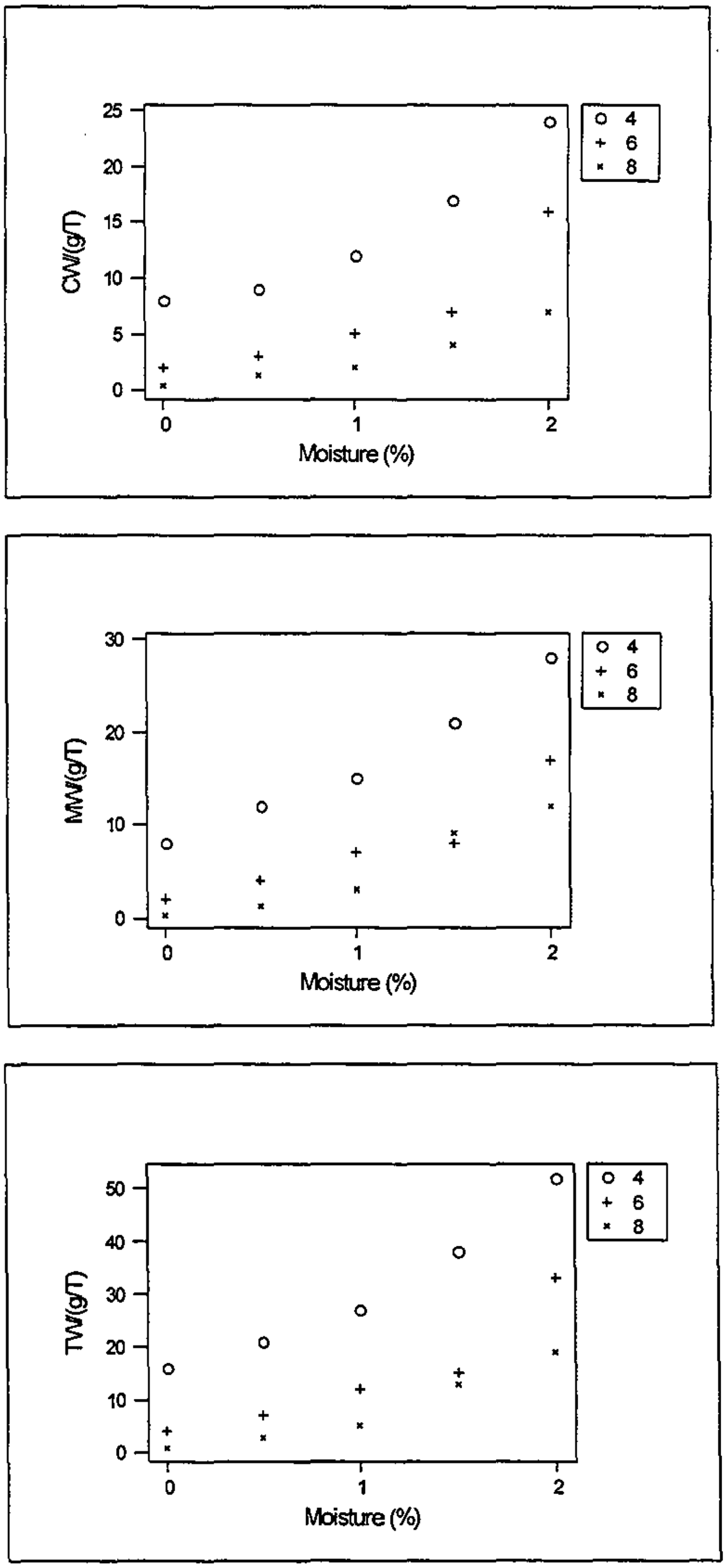

Figure 6.3 Measured wear against moisture content at three closed-side settings for Ingleton Grey rock

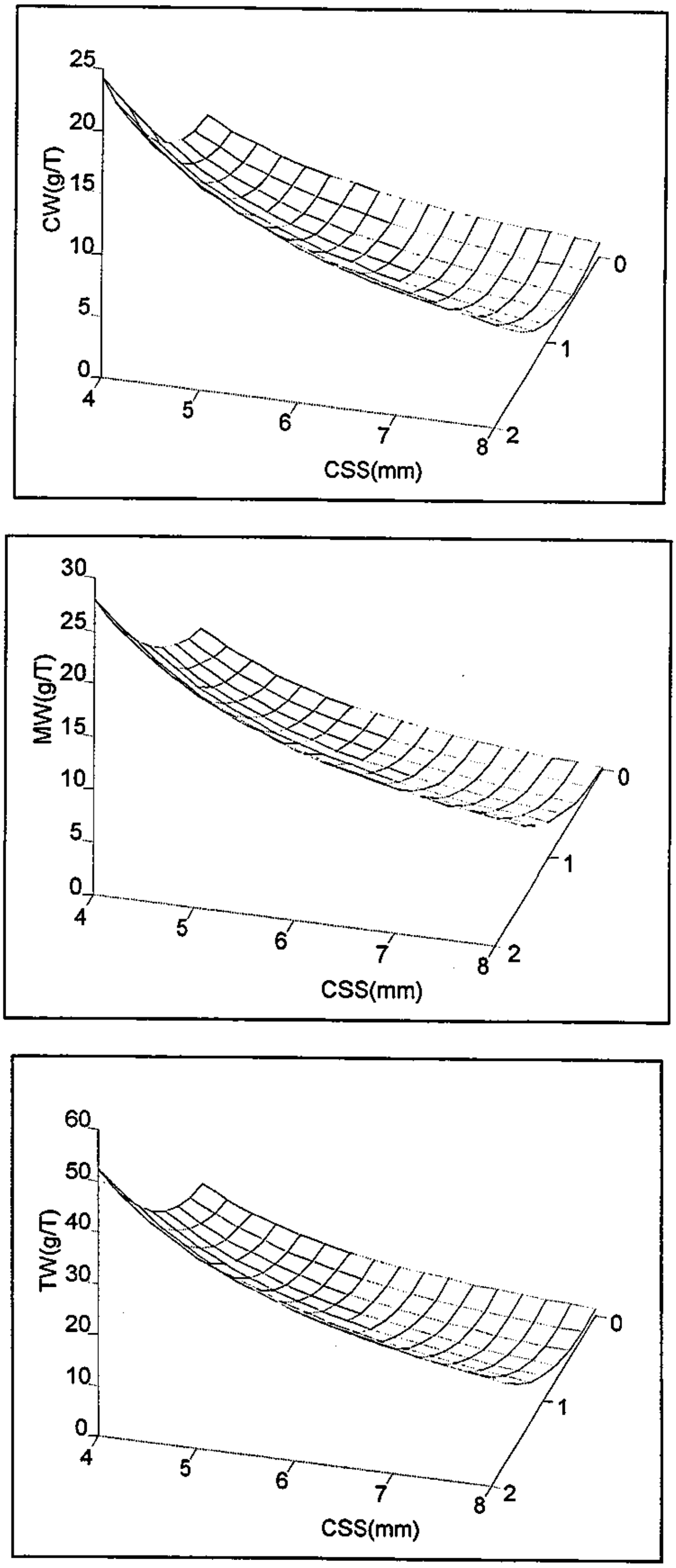

Figure 6.4 The predicted wear response surface for moist Cliffe Hill rock

6.1.3 Judkins Rock

Table 6.3 Correlation Between Wear and other Variables- Judkins Rock

	CW/(g/T)	MW/(g/T)	TW/(g/T)	1/CSS
MW/(g/T)	0.978			
TW/(g/T)	0.992	0.997		
1/CSS	0.556	0.642	0.610	
Moist	0.761	0.699	0.723	0.003

1. **CW/(g/T)** = 7.31 -73.8 **1/CSS** + 250 **1/CSS^2**- 4.62 **Moist** + 2.36 **Moist^2** +29.1 **Moist/CSS**

   s = 0.962 **R^2** = 97.8% **R^2(adj)** = 96.6%

Analysis of Variance

SOURCE	DF	SS	MS	F	p
Regression	5	371.705	74.341	80.34	0.000
Error	9	8.328	0.925		
Total	14	380.034			

2. **MW/(g/T)** = 3.27 -16.42 **1/CSS** +130 **1/CSS^2**- 7.58 **Moist** +2.27 **Moist^2** +60.26 **Moist/CSS**

   s = 0.979 **R^2** = 99.1% **R^2(adj)** = 98.6%

Analysis of Variance

SOURCE	DF	SS	MS	F	p
Regression	5	953.30	190.66	198.85	0.000
Error	9	8.63	0.96		
Total	14	961.93			

3. **TW/(g/T)** = 12.9 -109 **1/CSS** + 417 **1/CSS^2**- 13.3 **Moist** + 4.84 **Moist^2**+ 92.1 **Moist/CSS**

   s = 1.480 **R^2** = 99.2% **R^2(adj)** = 98.8%

Analysis of Variance

SOURCE	DF	SS	MS	F	p
Regression	5	2473.88	494.78	225.87	0.000
Error	9	19.71	2.19		
Total	14	2493.59			

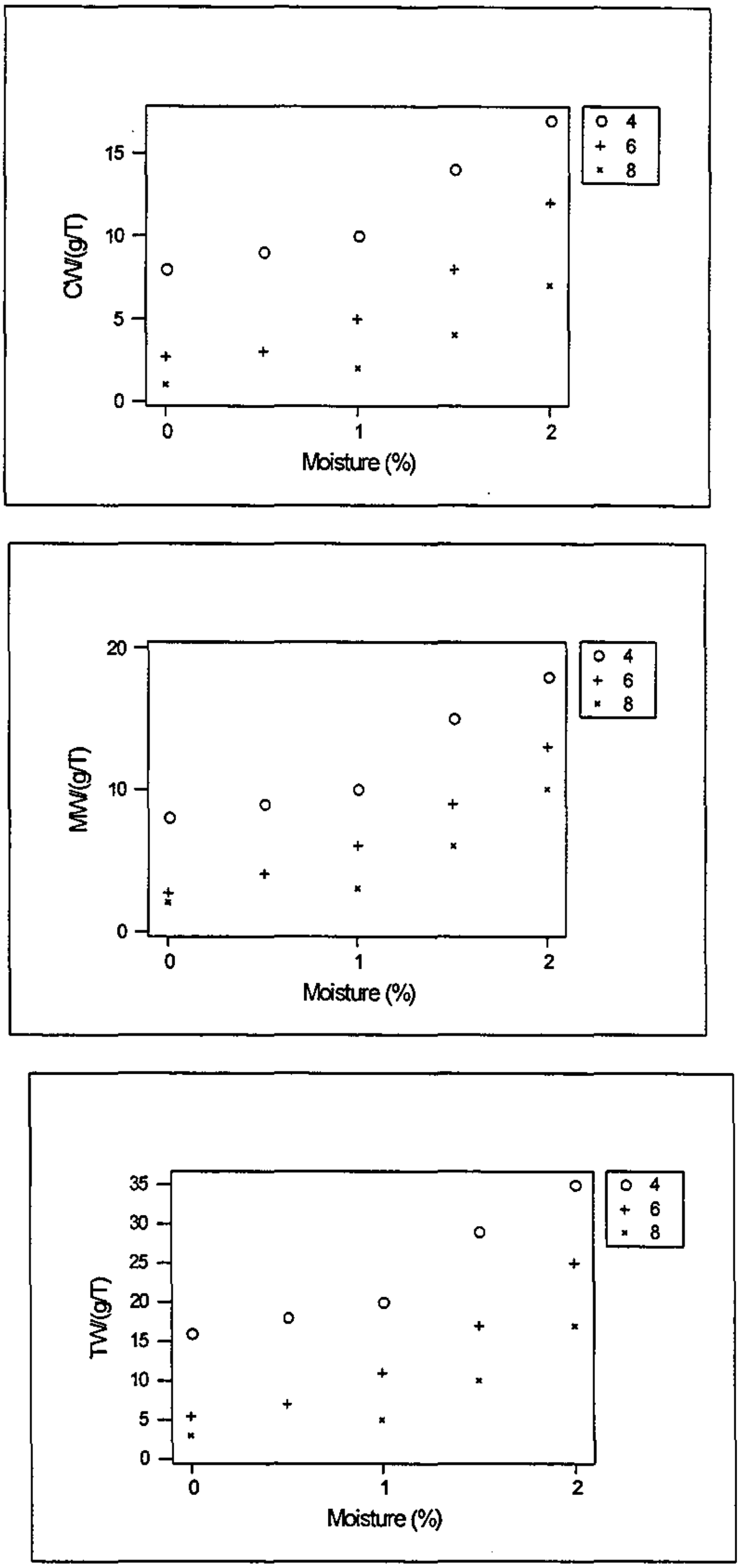

Figure 6.5 Measured wear against moisture content at three closed-side settings for Judkins rock

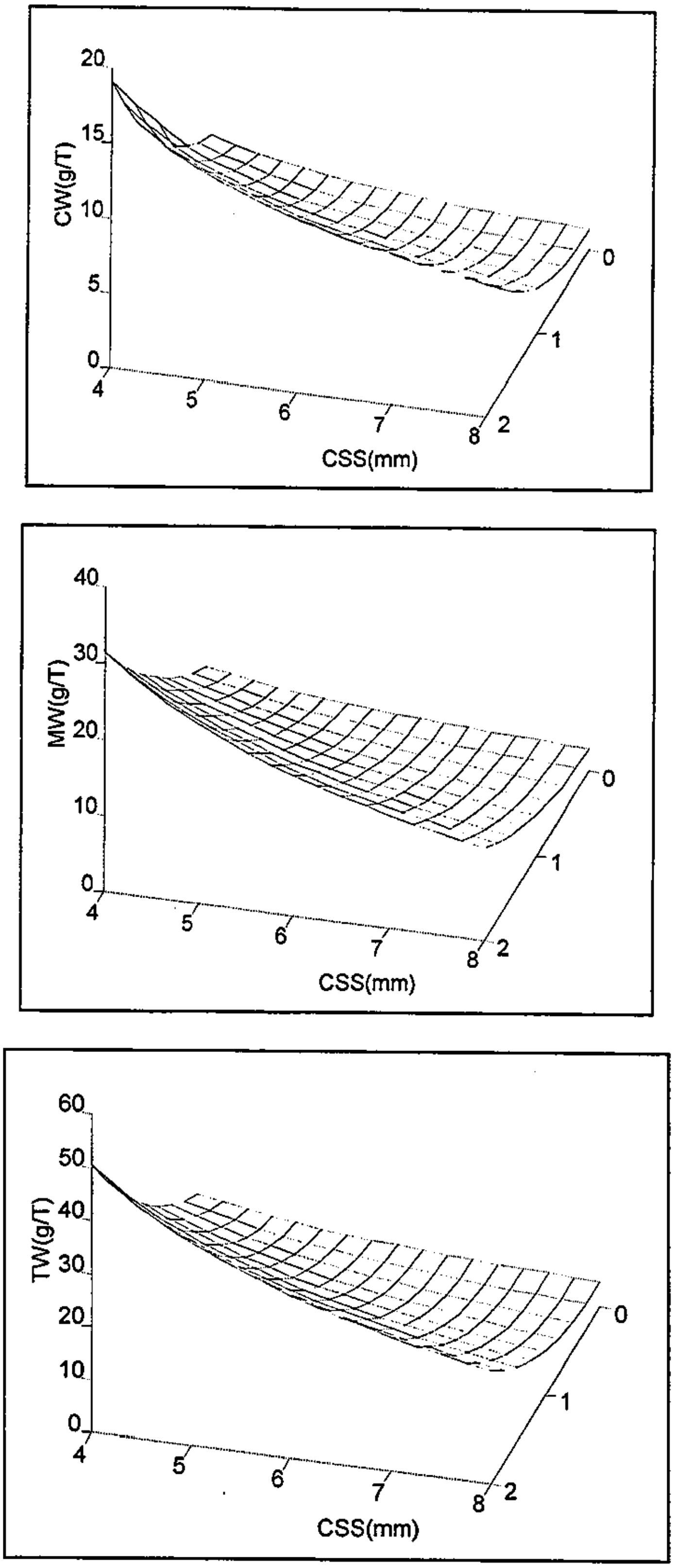

Figure 6.6 The predicted wear response surface for moist Judkins rock

6.1.4 Pottal Pool Rock

Table 6.4 Correlation Between Wear and other Variables- Pottal Pool Rock

	CW/(g/T)	MW/(g/T)	TW/(g/T)	1/CSS
MW/(g/T)	0.966			
TW/(g/T)	0.989	0.994		
1/CSS	0.940	0.967	0.964	
Moist	0.000	0.043	0.025	-0.006

1. **CW/(g/T)** = 7.8 - 104 **1/CSS** + 875 **1/CSS^2**+ 3.12 **Moist** - 1.70 **Moist^2**

   s = 4.990 **R^2** = 89.8% **R^2(adj)** = 85.8%

Analysis of Variance

SOURCE	DF	SS	MS	F	p
Regression	4	2197.98	549.49	22.07	0.000
Error	10	248.96	24.90		
Total	14	2446.93			

2. **MW/(g/T)** = - 11.7 + 74 **1/CSS** + 653 **1/CSS^2** + 9.09 **Moist** - 4.09 **Moist^2**

   s = 4.807 **R^2** = 95.0% **R^2(adj)** = 92.9%

Analysis of Variance

SOURCE	DF	SS	MS	F	p
Regression	4	4351.3	1087.8	47.07	0.000
Error	10	231.1	23.1		
Total	14	4582.4			

3. **TW/(g/T)** = - 3.9 - 29 **1/CSS** + 1528 **1/CSS^2** + 12.2 **Moist** - 5.79 **Moist^2**

   s = 8.881 **R^2** = 94.2% **R^2**(adj) = 91.8%

Analysis of Variance

SOURCE	DF	SS	MS	F	p
Regression	4	12711.0	3177.7	40.29	0.000
Error	10	788.7	78.9		
Total	14	13499.7			

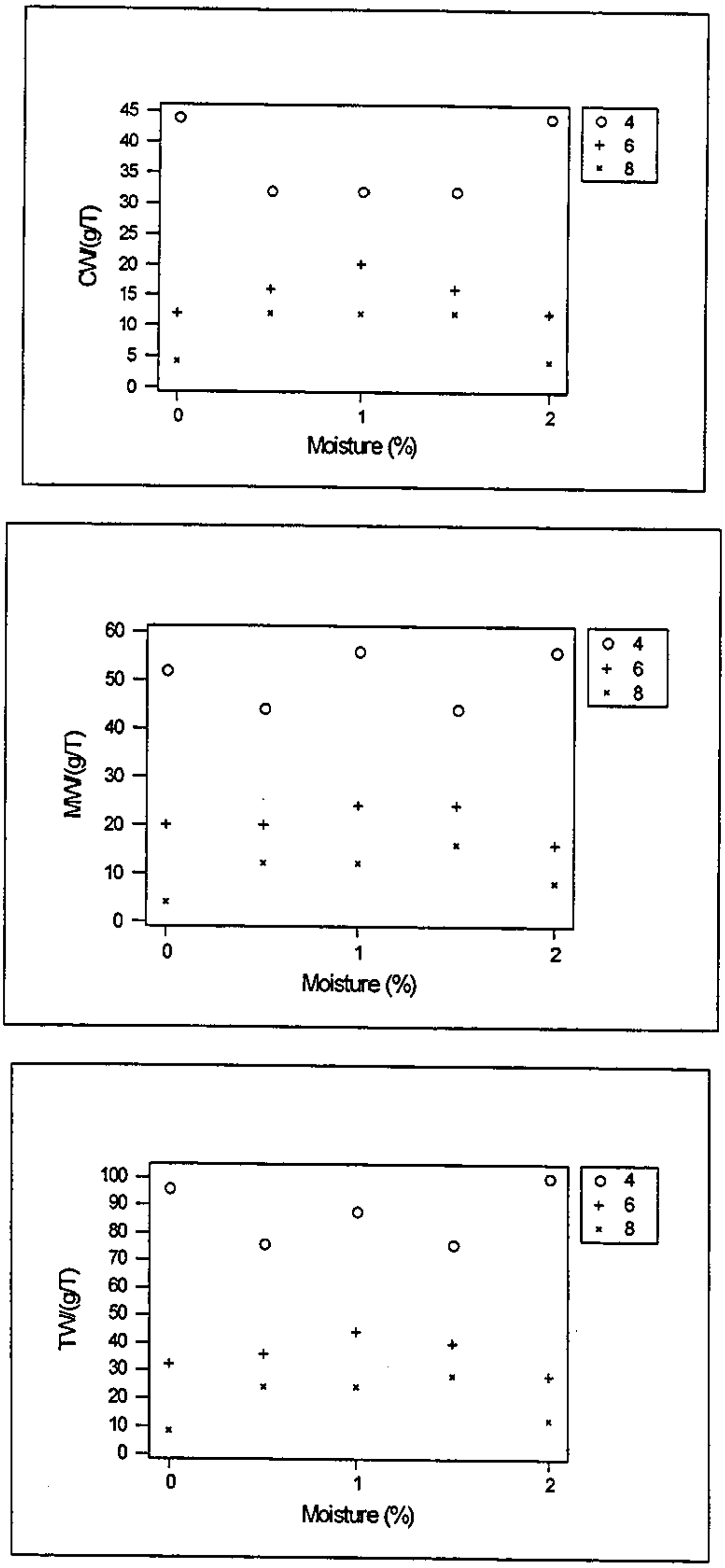

Figure 6.7 Measured wear against moisture content at three closed-side settings for Pottal Pool rock

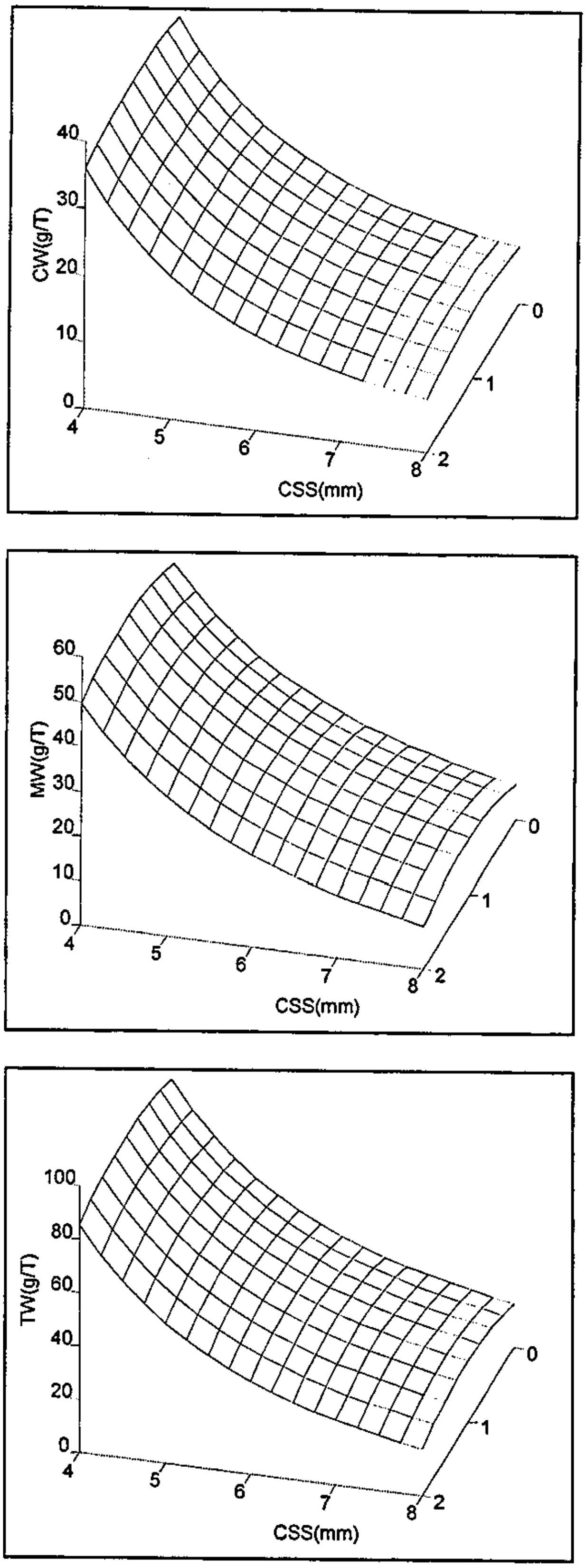

Figure 6.8 The predicted wear response surface for moist Pottal Pool rock

6.1.5 Shap Blue Rock

Table 6.5 Correlation Between Wear and other Variables - Shap Blue Rock

	CW/(g/T)	MW/(g/T)	TW/(g/T)	1/CSS
MW/(g/T)	0.994			
TW/(g/T)	0.999	0.999		
1/CSS	0.941	0.907	0.925	
Moisture	0.349	0.442	0.396	0.045

1. **CW/(g/T) = - 18.4 + 21 1/CSS -148 1/CSS^2 -2.5 Moist + 2.75 Moist^2 -20 Moist/CSS**

s = 3.088 **R^2 = 98.4%** **R^2(adj) = 95.6%**

Analysis of Variance

SOURCE	DF	SS	MS	F	p
Regression	5	1717.39	343.48	36.01	0.007
Error	3	28.61	9.54		
Total	8	1746.00			

2. **MW/(g/T) = -7.83+168 1/CSS + 45.3 1/CSS^2 +4.5 Moist + 2.25 Moist^2 -20 Moist/CSS**

s = 1.862 **R^2 = 99.4%** **R^2(adj) = 98.4%**

Analysis of Variance

SOURCE	DF	SS	MS	F	p
Regression	5	1693.15	338.63	97.66	0.002
Error	3	10.40	3.47		
Total	8	1703.56			

3. **TW/(g/T) = - 26.6+420 1/CSS -103 1/CSS^2 +7 Moist + 5 Moist^2 -40 Moist/CSS**

s = 4.063 **R^2 = 99.3** **R^2(adj) = 98.1%**

Analysis of Variance

SOURCE	DF	SS	MS	F	p
Regression	5	6881.4	1376.3	83.37	0.002
Error	3	49.5	16.5		
Total	8	6930.9			

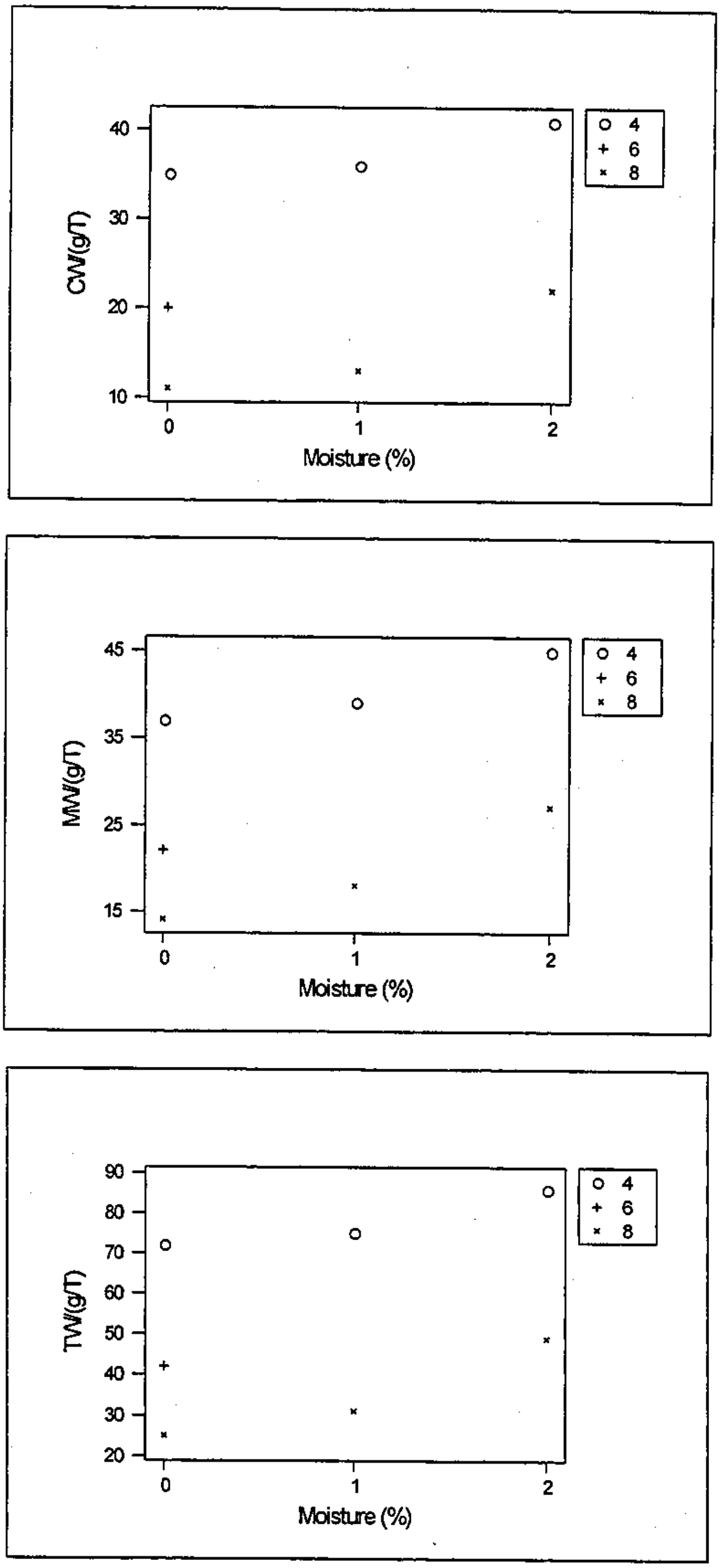

Figure 6.9 Measured wear against moisture content at three closed-side settings for Shap Blue rock

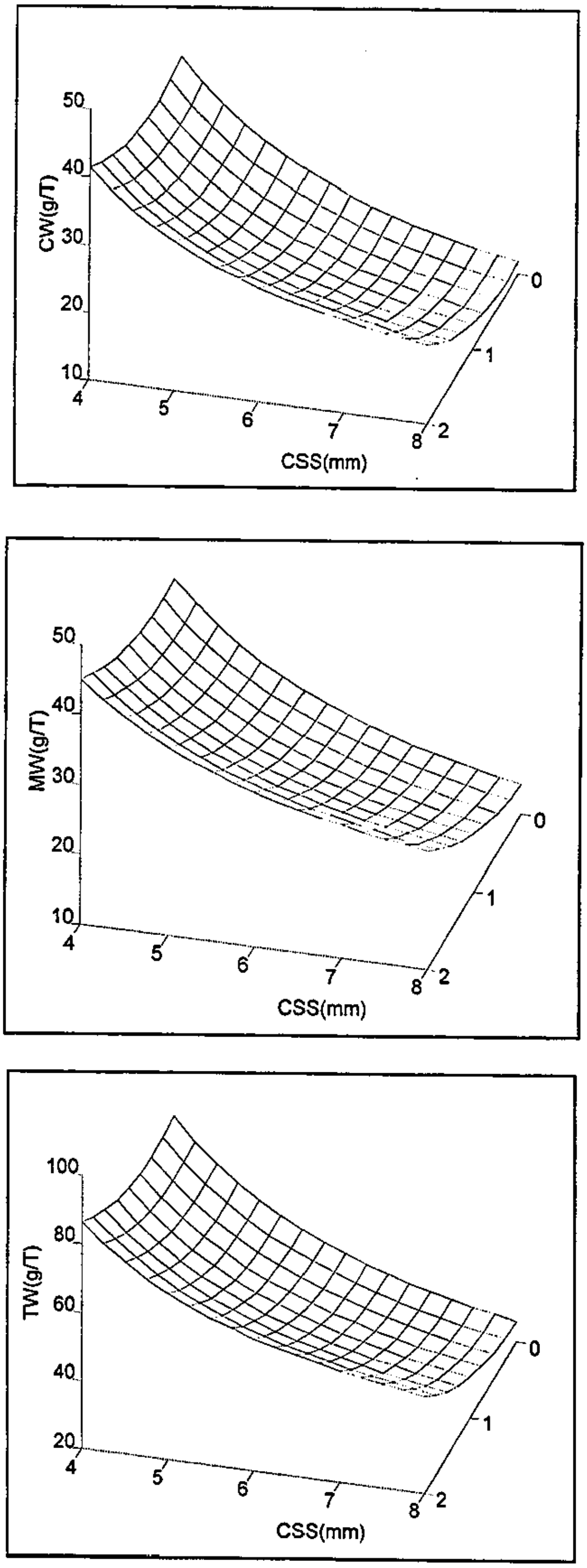

Figure 6.10 The predicted wear response surface for moist Shap Blue rock

6.1.6 Shardlow Rock

Table 6.6 Correlation Coefficients Between Wear and other Variables for Wet Shardlow Rock

	CW/(g/T)	MW/(g/T)	TW/(g/T)	1/CSS
MW/(g/T)	0.968			
TW/(g/T)	0.988	0.995		
1/CSS	0.930	0.974	0.964	
Moist	-0.252	-0.028	-0.117	0.006

1. **CW/(g/T)** = 28.6 - 307 **1/CSS** + 1307 **1/CSS^2** - 12.2 **Moist** + 4.57 **Moist^2**

   s = 3.096 **R^2** = 97.1% **R^2(adj)** = 94.1%

Analysis of Variance

SOURCE	DF	SS	MS	F	p
Regression	4	1266.54	316.63	33.03	0.003
Error	4	38.35	9.59		
Total	8	1304.89			

2. **MW/(g/T)** = 25.1 - 342 **1/CSS** + 1722 **1/CSS^2** - 15.0 **Moist** + 7.38 **Moist^2**

   s = 3.641 **R^2 = 98.3%** **R^2(adj)** = 96.6%

Analysis of Variance

SOURCE	DF	SS	MS	F	p
Regression	4	3099.85	774.96	58.45	0.001
Error	4	53.03	13.26		
Total	8	3152.89			

3. **TW/(g/T)** = 53.7 - 649 **1/CSS** + 3029 **1/CSS^2**- 27.2 **Moist** + 11.9 **Moist^2**

   s = 6.366 **R^2** = 98.1% **R^2(adj)** = 96.1%

Analysis of Variance

SOURCE	DF	SS	MS	F	p
Regression	4	8221.9	2055.5	50.73	0.001
Error	4	162.1	40.5		
Total	8	8384.0			

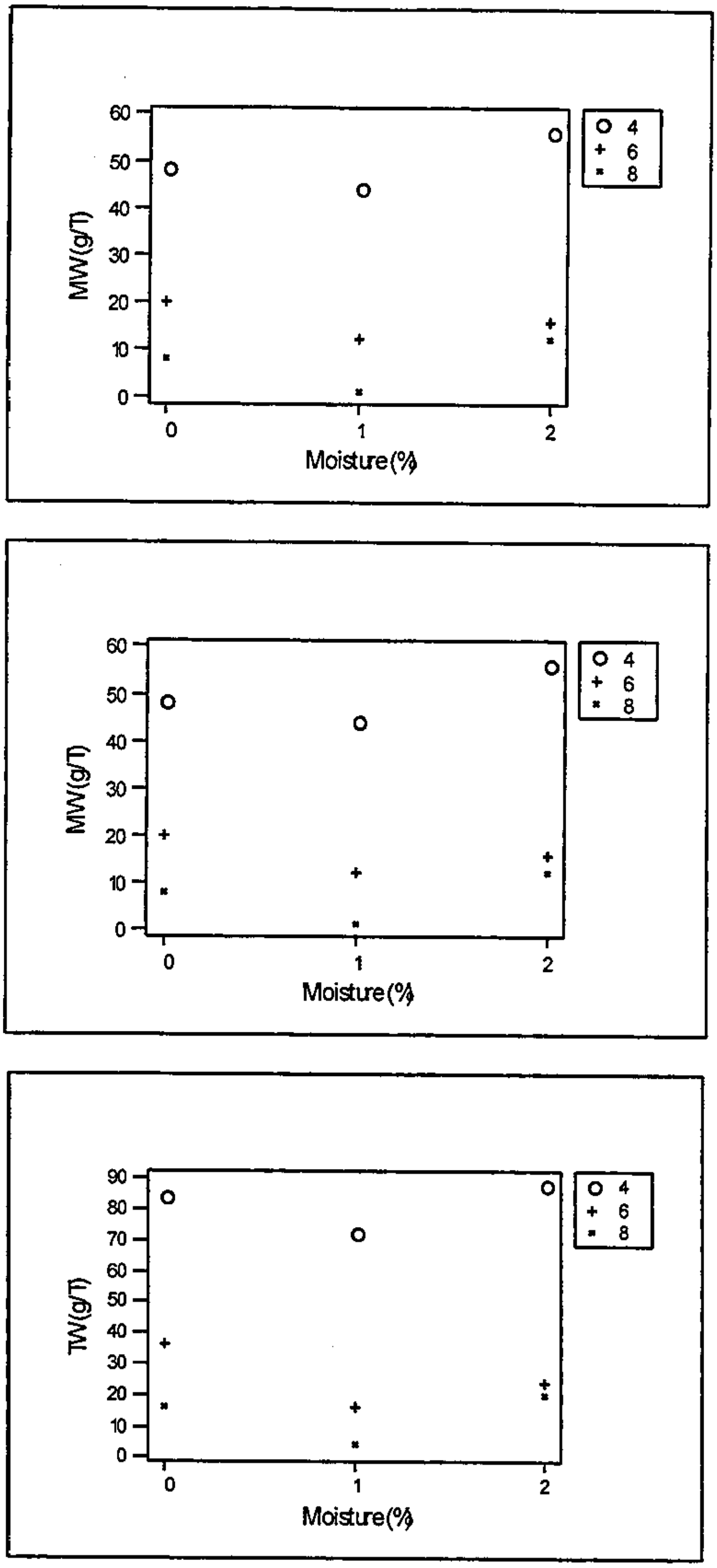

Figure 6.11 Measured wear against moisture content at three closed-side settings for Shardlow rock

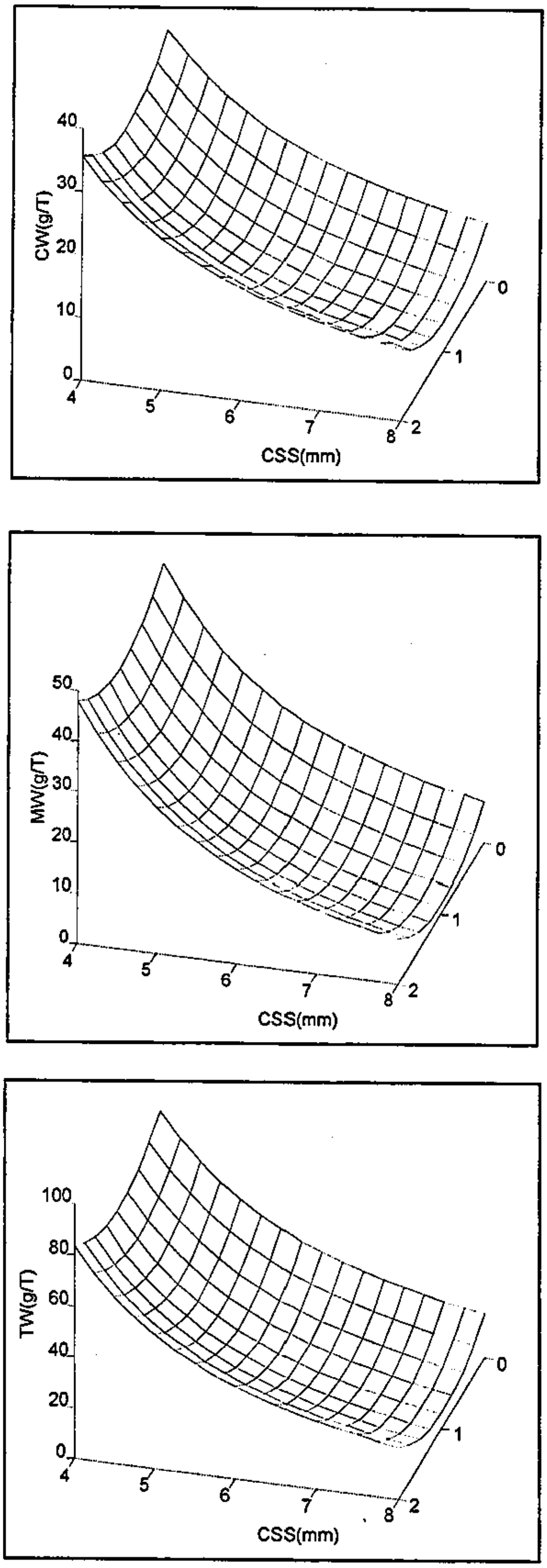

Figure 6.12 The predicted wear response surface for moist Shardlow rock

6.1.7 Whitwick Rock

Table 6.7 Correlation Between Wear and other Variables- Whitwick Rock

	CW/(g/T)	MW/(g/T)	TW/(g/T)	1/CSS
MW/(g/T)	0.930			
TW/(g/T)	0.974	0.989		
1/CSS	0.912	0.808	0.864	
Moist	0.358	0.446	0.419	-0.017

1. **CW/(g/T)** = 20.67 +262 **1/CSS** -400.4 **1/CSS²** -1.44 **Moist** + 1.4 **Moist²** + 12.48 **Moist/CSS**

   s = 0.874 R^2 = 99.0% R^2(adj) = 98.5%

Analysis of Variance

SOURCE	DF	SS	MS	F	p
Regression	5	694.45	138.89	181.66	0.000
Error	9	6.88	0.76		
Total	14	701.33			

2. **MW/(g/T)** = 2.37 +27.8 **1/CSS** + 163 **1/CSS²** - 15.7 **Moist** + 4.1 **Moist²** + 79.41**Moist/CSS**

   s = 2.448 R^2 = 96.7% R^2(adj) = 94.9%

Analysis of Variance

SOURCE	DF	SS	MS	F	p
Regression	5	694.45	138.89	181.66	0.000
Error	9	6.88	0.76		
Total	14	701.33			

3. **TW/(g/T)** = - 18.3 +290 **1/CSS** -236 **1/CSS²** - 17.0 **Moist** + 5.49 **Moist²** + 91.89 **Moist/CSS**

   s = 2.281 R^2 = 98.9% R^2(adj) = 98.3%

Analysis of Variance

SOURCE	DF	SS	MS	F	p
Regression	5	1602.28	320.46	53.46	0.000
Error	9	53.95	5.99		
Total	14	1656.23			

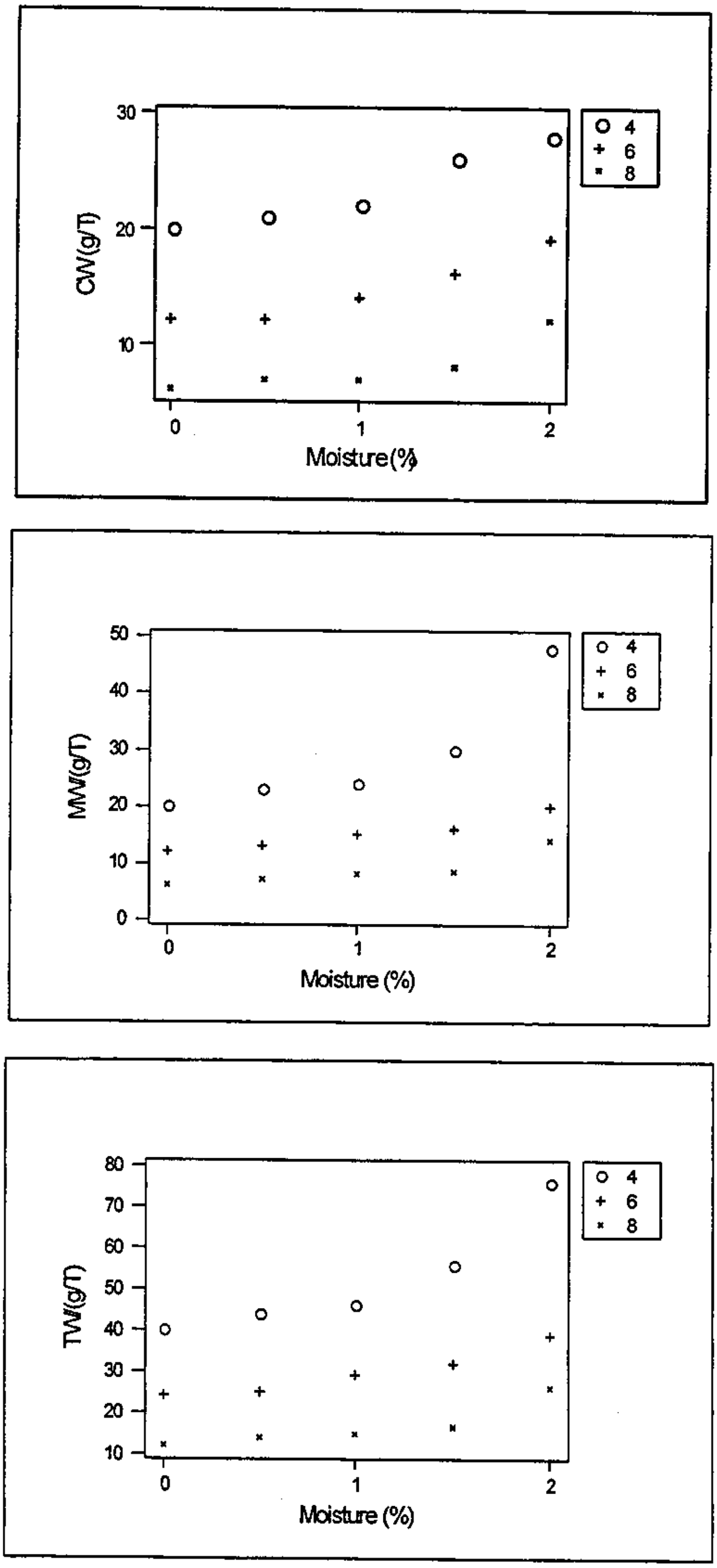

Figure 6.13 Measured wear against moisture content at three closed-side settings for Whitwick rock

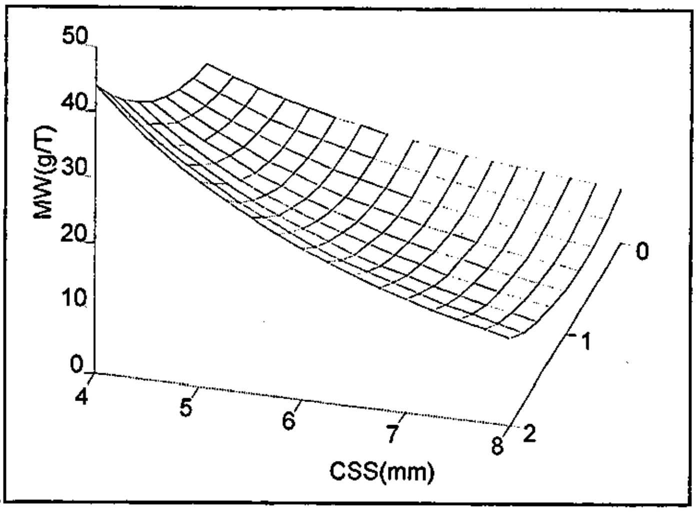

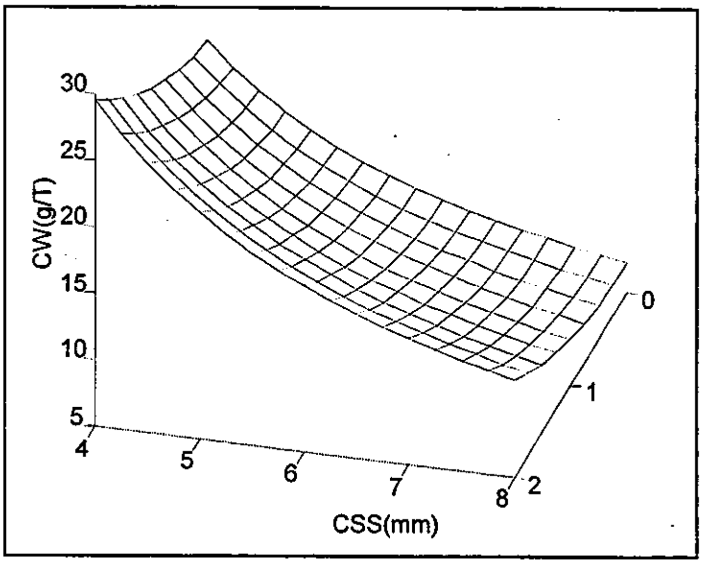

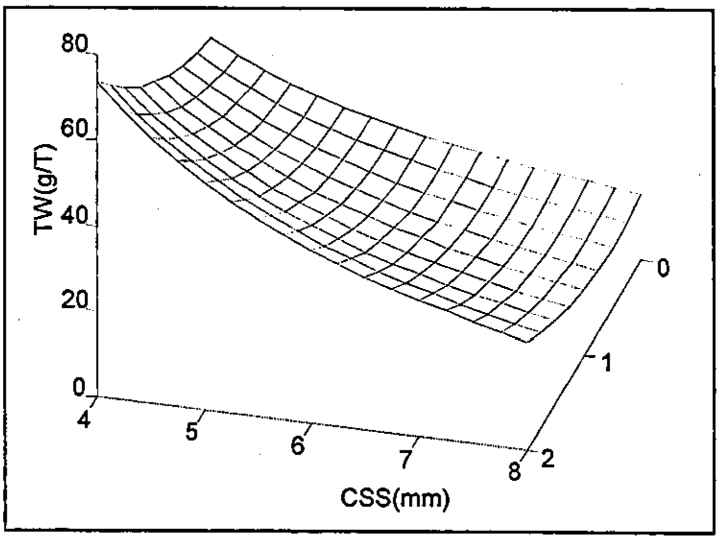

Figure 6.14 The predicted wear response surface for moist Whitwick rock

6.1.8 Waterswallows Rock

Table 6.8 Correlation Between Wear and other Variables - Waterswallows

	CW/(g/T)	MW/(g/T)	TW/(g/T)	1/CSS
MW/(g/T)	0.985			
TW/(g/T)	0.996	0.996		
1/CSS	0.758	0.655	0.709	
Moist	0.598	0.706	0.654	-0.015

1. **CW/(g/T) = -14 +134 1/CSS -180 $1/CSS^2$ + -0.72 Moist + 1.93 $Moist^2$ + 4.94 Moist/CSS**

   s = 0.933 R^2 = 96.9% R^2(adj) = 95.0%

Analysis of Variance

SOURCE	DF	SS	MS	F	p
Regression	5	220.658	44.132	50.70	0.000
Error	8	6.964	0.871		
Total	13	227.623			

2. **MW/(g/T) = - 7.79 + 75.8 1/CSS -44 $1/CSS^2$ - 0.1 Moist + 2.15 $Moist^2$ +2.5 Moist/CSS**

   s = 1.200 R^2 = 96.4% R^2(adj) = 94.1%

Analysis of Variance

SOURCE	DF	SS	MS	F	p
Regression	5	306.165	61.233	42.54	0.000
Error	8	11.516	1.439		
Total	13	317.681			

3. **TW/(g/T) = - 21.8 +210 1/CSS - 223 $1/CSS^2$ + 0.82 Moist + 4.08 $Moist^2$ +7.4 Moist/CSS**

   s = 2.343 R^2 = 95.6% R^2(adj) = 92.9%

Analysis of Variance

SOURCE	DF	SS	MS	F	p
Regression	5	1027.56	205.51	54.21	0.000
Error	8	30.33	3.79		
Total	13	1057.89			

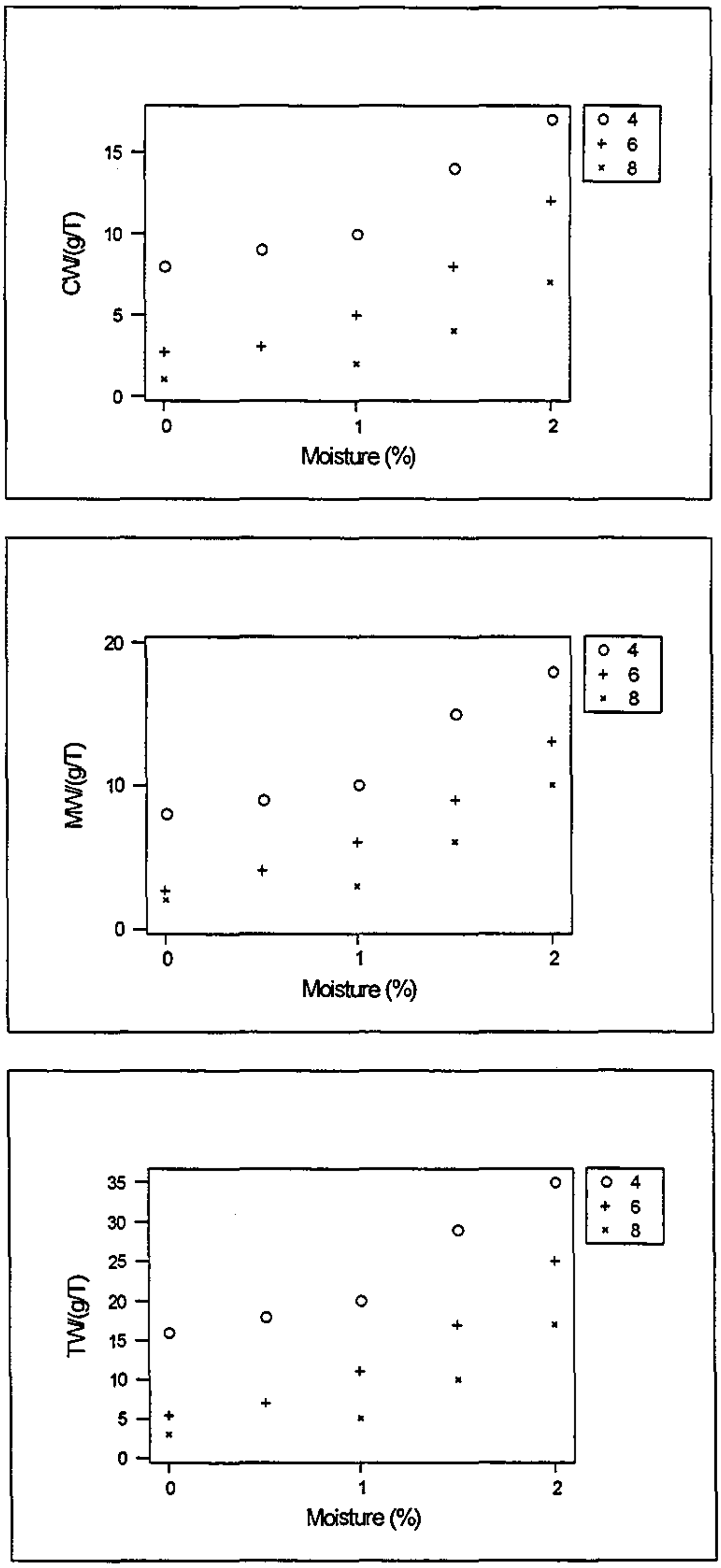

Figure 6.15 Measured wear against moisture content at three closed-side settings for Waterswallows rock

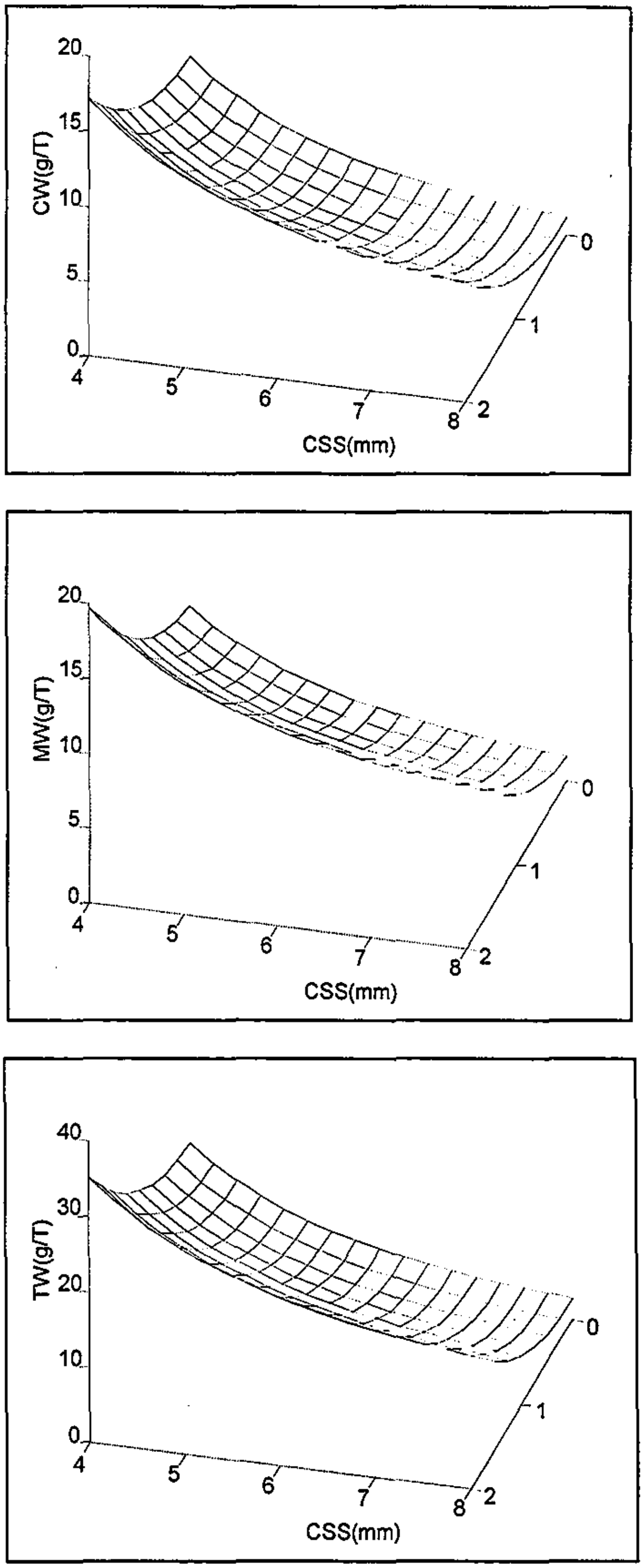

Figure 6.16 The predicted wear response surface for moist Waterswallows rock

6.1.9 Discussion of the Results

The measured wear for all rock types tested, except the two gravel type rocks:- Pottal Pool and Shardlow, increased with moisture. Pottal Pool and Shardlow rocks exhibited totally different characteristics. The wear of both rocks decreased originally with moisture. As the moisture was increased further at 4mm crusher setting, the wear for both rocks, increased reaching slightly higher values than the dry wear for a moisture level of 2%. The Pottal Pool rock exhibited a local wear maxima for 1% moisture level. This was not observed for Shardlow Rock. At crusher settings of 6mm and 8mm, the wear decreased as the moisture increased beyond 1% to 2%.

The marked difference between these two gravel type rocks and the others may be due to their low water absorption and near neutral pH values. It was observed that for these rocks the crushing time originally decreased as moisture levels increased which resulted in a higher crusher throughput. This finding indicates that for these rocks, small amounts of water may act as a lubricant aiding the crushing process, and therefore reducing the contact time between the rock and the liners which lowers the wear. This however, does not explain the local wear maxima observed for Pottal Pool rock, which remains unexplained.

6.2 Correlation Between Wear, Closed-Side Setting, Moisture and Rock properties

The data used for general regression models presented in this section excluded that measured for Whitwick rock. This moderately abrasive rock type was used to examine the performance of the general models by comparing the model predictions with the wear measured during the experiments.

The three rock variables, **Si**, **BTS**, and **AAV**, chosen in the last Chapter as the best variable subset for modelling dry wear have been also used for the general models.

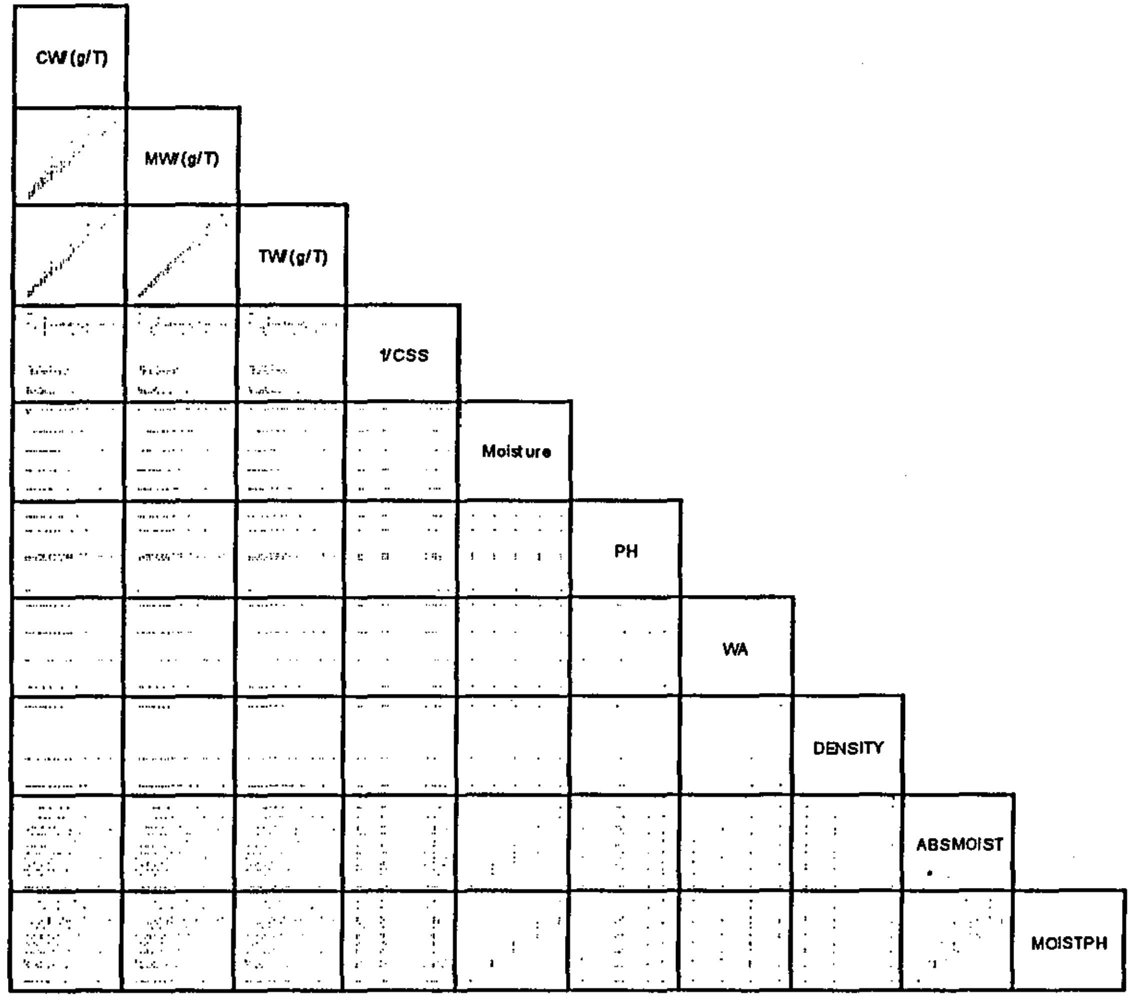

Figure 6.17 Matrix plot of variables affecting wear of moist rock

Table 6.9 Pearson Correlation Coefficient Between Wear, Rock Properties, Closed-Side Setting and Moisture

	CW/(g/T)	MW/(g/T)	TW/(g/T)	1/CSS	Moisture	Si	BTS	AAV
MW/(g/T)	0.962							
TW/(g/T)	0.989	0.992						
1/CSS	0.493	0.495	0.498					
Moisture	0.361	0.427	0.400	-0.004				
Si	0.231	0.234	0.235	-0.280	-0.002			
BTS	0.452	0.409	0.433	-0.056	0.001	0.111		
AAV	-0.276	-0.174	-0.222	-0.146	-0.002	0.480	-0.489	
pH	-0.023	-0.002	-0.012	-0.135	0.002	0.516	0.139	0.181
WA	-0.247	-0.188	-0.217	-0.212	0.081	0.058	-0.218	0.393
DENSITY	-0.159	-0.225	-0.198	0.019	0.018	-0.718	0.298	-0.353
MOIST*pH	0.362	0.430	0.402	-0.029	0.978	0.086	0.024	0.029
WA*MOIST	0.293	0.369	0.337	-0.051	0.973	0.014	-0.046	0.082

In addition two other variables, rock pH value and the water absorption, were found to be significant in modelling the wear of moist rocks. However, the wear caused by moist rock has been considered as a more generic form of dry wear. Therefore, the terms corresponding to rock's pH value and Water absorption had to be connected to the moisture levels above zero. This was achieved by including "pH ×moisture", and " water absorption ×moisture" as the added model variables. This ensures that in the case of dry rock, these two variables, as well as other moisture terms, would become zero, reducing the model to that for dry wear. Table 6.9 and Figure 6.17 shows the Pearson cross correlation moment, and the matrix plot of different variables.

In terms of the involved physical phenomena, the pH value describes any acceleration of wear due to the synergistic effects of corrosion on abrasive wear. Water absorption on the other hand contributes to the impact of the moisture level on the crushing process in terms of the increased crushing time due to clogging.

Considering the marked difference between the two gravel type rocks, Shardlow and Pottal Pool rocks, and the other rocks tested, two general models have been considered. First model excludes the two anomalous rocks, and the second includes them. As expected the first model provides a better fit for non-gravel rock types.

6.3.1 General Wear Model For Moist Rock Excluding The Gravel Type Rocks

1. $\mathbf{CW/(g/T)} = a_0 + a_1\,\mathbf{x_1} + a_2\,\mathbf{x_2} + \ldots + a_n\,\mathbf{x_n}\,\mathbf{x_{n-1}}$

Predictor	Coef	Stdev	t-ratio	p
Constant	14.89	50.88	0.29	0.771
1/CSS	-266.3	103.2	-2.58	0.012
1/CSS^2	-45.0	123.2	-0.36	0.716
Si	-0.5798	0.8807	-0.66	0.513
BTS	2.879	3.047	0.94	0.348
AAV	23.153	1.936	11.96	0.000
CSS*AAV	-10.943	3.654	-3.00	0.004
CSS*Si	5.252	1.073	4.89	0.000
BTS*CSS	7.399	2.044	3.62	0.001
BTS*AAV	-1.7111	0.1370	-12.49	0.000
BTS*Si	-0.02758	0.05459	-0.51	0.615
Moisture	-17.173	3.651	-4.70	0.000

moist2	2.2544	0.4389	5.14	0.000
MOIST*CSS	17.666	5.153	3.43	0.001
MOIST*pH	1.5095	0.3070	4.92	0.000
WA*MOIST	5.692	2.853	2.00	0.050

s = 1.697 **R^2 = 96.9%** **R^2(adj) = 96.2%**

Analysis of Variance

SOURCE	DF	SS	MS	F	p
Regression	15	6027.45	401.83	139.61	0.000
Error	67	192.84	2.88		
Total	82	6220.29			

2. $MW/(g/T) = a_0 + a_1 x_1 + a_2 x_2 + \ldots + a_n x_n x_{n-1}$

Predictor	Coef	Stdev	t-ratio	p
Constant	73.79	94.29	0.78	0.437
1/CSS	-401.9	191.3	-2.10	0.039
1/CSS^2	83.5	228.3	0.37	0.716
Si	-1.891	1.632	-1.16	0.251
BTS	0.666	5.647	0.12	0.907
AAV	26.356	3.588	7.35	0.000
CSS*AAV	-7.805	6.771	-1.15	0.253
CSS*Si	7.317	1.989	3.68	0.000
BTS*CSS	5.282	3.788	1.39	0.168
BTS*AAV	-1.9496	0.2540	-7.68	0.000
BTS*Si	0.0351	0.1012	0.35	0.730
Moisture	-28.854	6.766	-4.26	0.000
moist2	2.5290	0.8135	3.11	0.003
MOIST*CSS	35.975	9.551	3.77	0.000
MOIST*pH	2.1667	0.5690	3.81	0.000
WA*MOIST	13.682	5.287	2.59	0.012

s = 3.144 **R^2= 92.5%** **R^2(adj) = 90.8%**

Analysis of Variance

SOURCE	DF	SS	MS	F	p
Regression	15	8159.98	544.00	55.03	0.000
Error	67	662.38	9.89		
Total	82	8822.37			

3. $TW/(g/T) = a_0 + a_1 x_1 + a_2 x_2 + \ldots + a_n x_n x_{n-1}$

Predictor	Coef	Stdev	t-ratio	p
Constant	84.9	132.9	0.64	0.525
1/CSS	-668.9	269.6	-2.48	0.016
1/CSS^2	47.1	321.7	0.15	0.884
Si	-2.402	2.300	-1.04	0.300
BTS	3.848	7.958	0.48	0.630
AAV	49.772	5.055	9.85	0.000
CSS*AAV	-19.187	9.541	-2.01	0.048
CSS*Si	12.568	2.802	4.49	0.000
BTS*CSS	12.593	5.337	2.36	0.021

BTS*AAV	-3.6733	0.3579	-10.26	0.000
BTS*Si	0.0021	0.1426	0.02	0.988
Moisture	-46.222	9.534	-4.85	0.000
moist2	4.820	1.146	4.20	0.000
MOIST*CSS	54.07	13.46	4.02	0.000
MOIST*pH	3.6955	0.8018	4.61	0.000
WA*MOIST	19.176	7.450	2.57	0.012

s = 4.431 R^2= 95.5% R^2(adj) = 94.5%

Analysis of Variance

SOURCE	DF	SS	MS	F	p
Regression	15	27935.9	1862.4	94.87	0.000
Error	67	1315.2	19.6		
Total	82	29251.1			

6.3.2 General Wear Model for Moist Rock Including the Gravel Type Rocks

1. $CW/(g/T) = a_0 + a_1 x_1 + a_2 x_2 + ... + a_n x_n x_{n-1}$

Predictor	Coef	Stdev	t-ratio	p
Constant	-39.52	26.90	-1.47	0.145
1/CSS	-148.5	102.9	-1.44	0.153
1/CSS^2	184.2	173.4	1.06	0.291
Si	0.3595	0.3172	1.13	0.260
BTS	3.994	1.174	3.40	0.001
AAV	12.652	1.805	7.01	0.000
CSS*AAV	-11.195	5.221	-2.14	0.035
CSS*Si	2.2572	0.4295	5.26	0.000
BTS*CSS	5.512	2.915	1.89	0.062
BTS*AAV	-1.2287	0.1219	-10.08	0.000
BTS*Si	-0.04549	0.01510	-3.01	0.003
Si*AAV	0.08413	0.01662	5.06	0.000
Moist	-13.252	3.271	-4.05	0.000
moist2	2.2518	0.6349	3.55	0.001
MOIST*CSS	8.371	7.010	1.19	0.236
MOIST*pH	0.8730	0.3274	2.67	0.009
WA*MOIST	9.290	1.373	6.77	0.000

s = 2.816 R^2= 93.7% R^2(adj) = 92.6%

Analysis of Variance

SOURCE	DF	SS	MS	F	p
Regression	16	10588.65	661.79	83.45	0.000
Error	90	713.75	7.93		
Total	106	11302.40			

2. $MW/(g/T) = a_0 + a_1 x_1 + a_2 x_2 + ... + a_n x_n x_{n-1}$

Predictor	Coef	Stdev	t-ratio	p

Constant	33.82	35.49	0.95	0.343
1/CSS	-314.4	135.8	-2.31	0.023
1/CSS^2	202.2	228.7	0.88	0.379
Si	-1.1337	0.4185	-2.71	0.008
BTS	1.298	1.549	0.84	0.404
AAV	13.372	2.381	5.62	0.000
CSS*AAV	-5.191	6.889	-0.75	0.453
CSS*SI	4.9568	0.5667	8.75	0.000
BTS*CSS	5.127	3.847	1.33	0.186
BTS*AAV	-1.3658	0.1608	-8.49	0.000
BTS*SI	0.01701	0.01993	0.85	0.396
Si*AAV	0.09733	0.02192	4.44	0.000
Moisture	-15.263	4.316	-3.54	0.001
moist2	2.2819	0.8376	2.72	0.008
MOIST*CSS	21.866	9.249	2.36	0.020
MOIST*pH	1.0259	0.4319	2.38	0.020
WA*MOIST	9.818	1.811	5.42	0.000

s = 3.716 R^2= 93.7% **R^2(adj)** = 92.6%

Analysis of Variance

SOURCE	DF	SS	MS	F	p
Regression	16	18408.3	1150.5	83.34	0.000
Error	90	1242.5	13.8		
Total	106	19650.7			

3. **TW/(g/T)** $= a_0 + a_1 x_1 + a_2 x_2 + \ldots + a_n x_n x_{n-1}$

Predictor	Coef	Stdev	t-ratio	p
Constant	-6.15	57.46	-0.11	0.915
1/CSS	-462.9	219.9	-2.11	0.038
1/CSS^2	391.9	370.3	1.06	0.293
Si	-0.7692	0.6775	-1.14	0.259
BTS	5.312	2.507	2.12	0.037
AAV	26.156	3.855	6.78	0.000
CSS*AAV	-16.69	11.15	-1.50	0.138
CSS*SI	7.2032	0.9174	7.85	0.000
BTS*CSS	10.586	6.227	1.70	0.093
BTS*AAV	-2.5960	0.2603	-9.97	0.000
BTS*SI	-0.02860	0.03226	-0.89	0.378
Si*AAV	0.18084	0.03549	5.10	0.000
Moisture	-28.646	6.987	-4.10	0.000
moist2	4.561	1.356	3.36	0.001
MOIST*CSS	30.57	14.97	2.04	0.044
MOIST*pH	1.9017	0.6993	2.72	0.008
WA*MOIST	19.053	2.933	6.50	0.000

s = 6.015 R^2 = 94.5% **R^2(adj)** = 93.6%

Analysis of Variance

SOURCE	DF	SS	MS	F	p
Regression	16	56299.3	3518.7	97.25	0.000
Error	90	3256.3	36.2		
Total	106	59555.7			

6.3 Discussion and Comparison of Measured and Predicted Wear For Moist Rock

Table A3.2 shows the fitted wear values for models presented in this Chapter. Similar to the models for dry wear, the best fit was achieved by Rock specific models. The general models provided a differing quality of fit for different rocks, closed-side settings, and moisture levels.

As can be seen in Table A3.2, in some cases, the general models predict a negative wear value. Although due to the statistical errors, this phenomenon is not entirely irrelevant. During the experimental work, it was observed that with rocks of low abrasivity and moderate strength, the crushing of low amount of rock at larger crusher settings, would result in a weight gain rather than weight loss. Under these conditions, rock particles would become embedded in the liners, slightly increasing their weight. In such cases, higher amounts of rock were needed to cause measurable wear. The two general wear models tend to predict negative wear values under these conditions which could be taken as an indication that crushing one tonne of the rock at that setting, would not cause any measurable wear.

Chapter 7 EFFECT OF FEED SIZE ON WEAR

Eight rock types were tested to find the relationship between wear and feed size at two feed size and moisture levels, and a constant crusher setting of 4mm. No measurable wear could be recorded for any of the two lime stone rocks at the smaller feed size. Table A2.3 shows the experimental results.

7.1 The Statistical Models

Considering the limited number of experimental results, the statistical validity of the models obtained to describe the relationship between wear, feed size and moisture can not be certain. The value used for the feed size, was the numerical average of the upper and lower size fraction, and equal to 12mm and 8.35mm for the +10-14mm feed and +6.3-10mm feed sizes respectively. The models were found to be linear in the feed size, however, the examination of the effect of feed size on wear at the two moisture levels, reveals a strong interaction between the two variables. Therefore an interaction term was also included in the models presented in the following sections. Also shown are graphical plots of the variation of wear with feed size and moisture. No statistical test is included, as all models provided perfect fit for the limited data available. Due the same constraint, no attempt was made to generalize the models for rock properties.

7.1.1 Cliffe Hill Rock

CW/(g/T) = - 4.61 + 1.38 **FeedSize** + 3.84 **Moist** + 0.347 **FeedSize×Moist**
MW/(g/T) = - 2.70 + 1.56 **FeedSize** + 5.82 **Moist** + 0.390 **FeedSize×Moist**
TW/(g/T) = - 7.31 + 2.94 **FeedSize** + 9.66 **Moist** + 0.736 **FeedSize×Moist**

7.1.2 Ingleton Grey Rock

CW/(g/T) = - 12.7 + 1.73 **FeedSize** - 6.06 **Moist** + 1.17 **FeedSize×Moist**
MW/(g/T) = - 8.52 + 1.38**FeedSize** - 15.0 **Moist** + 2.08 **FeedSize×Moist**
TW/(g/T) = - 21.2 + 3.10 **FeedSize** - 21.0 **Moist** + 3.25 **FeedSize×Moist**

7.1.3 Judkins Rock

CW/(g/T) = 1.91 + 0.174 **FeedSize** - 2.41 **Moist** + 0.91 **FeedSize×Moist**
MW/(g/T) = 5.91 + 0.174 **FeedSize** + 3.66 **Moist** + 0.73**FeedSize×Moist**
TW/(g/T) = 7.82 + 0.348 **FeedSize** + 1.27 **Moist** + 1.64 **FeedSize×Moist**

7.1.4 Pottal Pool

CW/(g/T) = - 5.87 + 4.16 **FeedSize** + 37.4 **Moist** - 3.12 **FeedSize×Moist**
MW/(g/T) = 14.6 + 3.12 **FeedSize** + 64.3 **Moist** - 5.19 **FeedSize×Moist**
TW/(g/T) = 8.73 + 7.27 **FeedSize** + 102 **Moist** - 8.31 **FeedSize×Moist**

7.1.5 Shardlow Rock

CW/(g/T) = 36.0 + 29.0 **Moist** - 2.58 **FeedSize×Moist**
MW/(g/T) = 48.0+ 45.2 **Moist** - 3.43 **FeedSize×Moist**
TW/(g/T) = 84.0 + 72.6 **Moist** - 5.89 **FeedSize×Moist**

7.1.6 Shap Blue Rock

CW/(g/T) = - 11.8 + 3.90 **FeedSize** - 0.117 **Moist** + 0.260 **FeedSize×Moist**
MW/(g/T) = 8.95 + 2.34 **FeedSize** - 2.23 **Moist** + 0.519 **FeedSize×Moist**
TW/(g/T) = - 2.81 + 6.23 **FeedSize** - 2.35 **Moist** + 0.779 **FeedSize×Moist**

7.1.7 Whitwick Rock

CW/(g/T) = - 23.6 + 3.64 **FeedSize** + 0.88 **Moist** + 0.26 **FeedSize×Moist**
MW/(g/T) = - 4.94 + 2.08 **FeedSize** - 4.70 **Moist** + 1.56 **FeedSize×Moist**
TW/(g/T) = - 28.6 + 5.71 **FeedSize** - 3.82 **Moist** + 1.82 **FeedSize×Moist**

7.1.8 Waterswallows Rock

CW/(g/T) = - 12.7 + 1.73 **FeedSize** - 2.28 **Moist** + 0.56 **FeedSize×Moist**
MW/(g/T) = - 8.52 + 1.38 **FeedSize** - 4.38 **Moist** + 0.78 **FeedSize×Moist**
TW/(g/T) = - 21.2 + 3.10 **FeedSize** - 6.66 **Moist** + 1.35 **FeedSize×Moist**

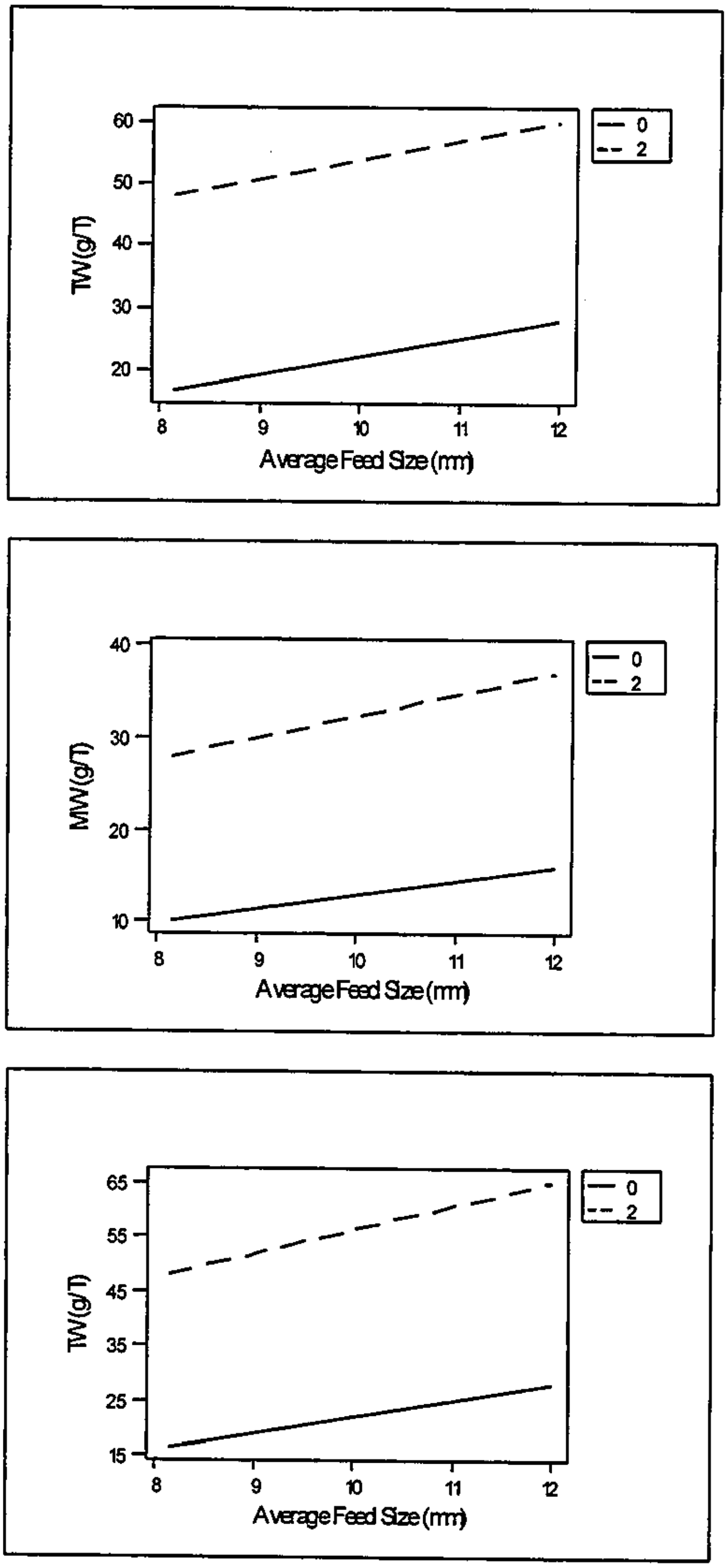

Figure 7.1 Measured wear vs moisture content and Feed average size at 4mm crusher setting for Cliffe Hill Rock

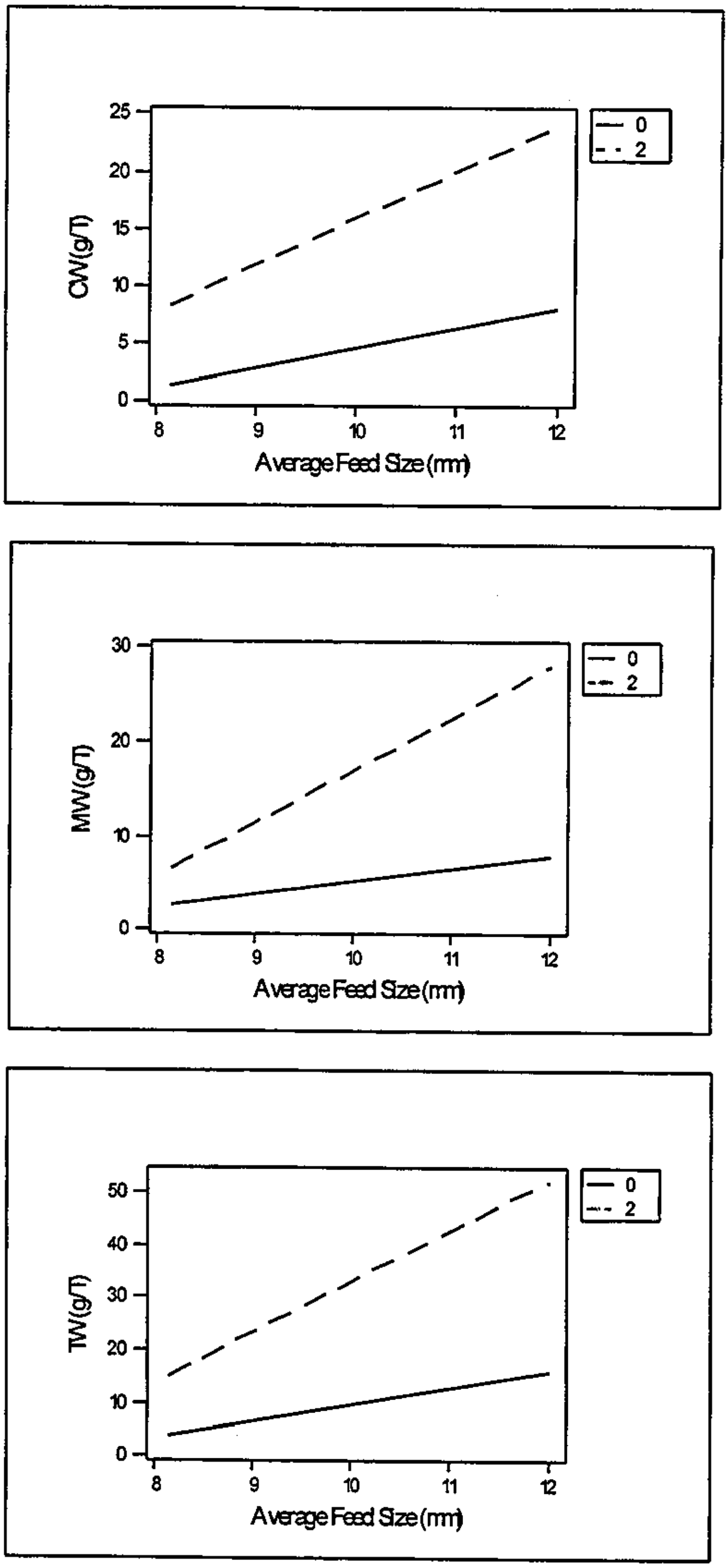

Figure 7.2 Measured wear Vs moisture content and Feed average size at 4mm crusher setting for Ingleton Grey Rock

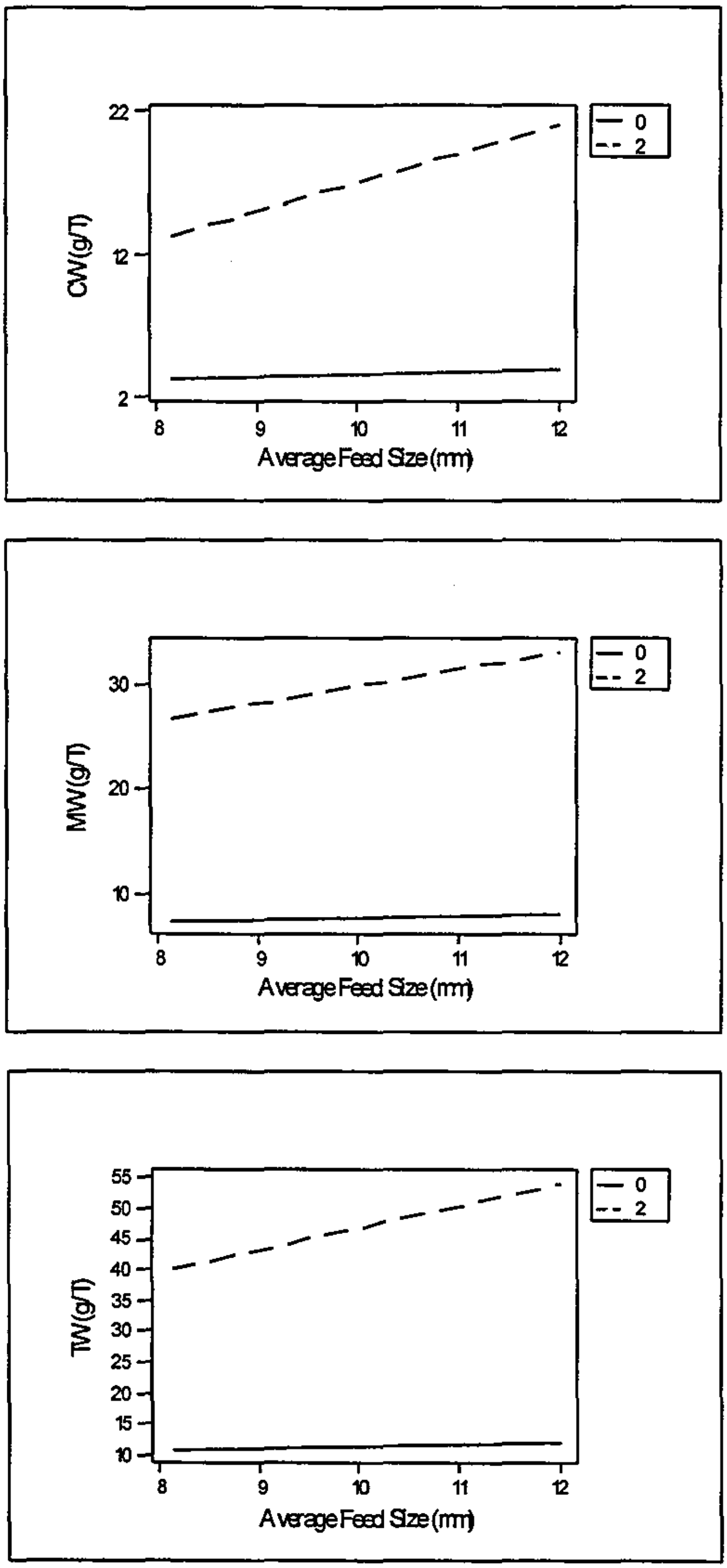

Figure 7.3 Measured wear vs moisture content and Feed average size at 4mm crusher setting for Judkins Rock

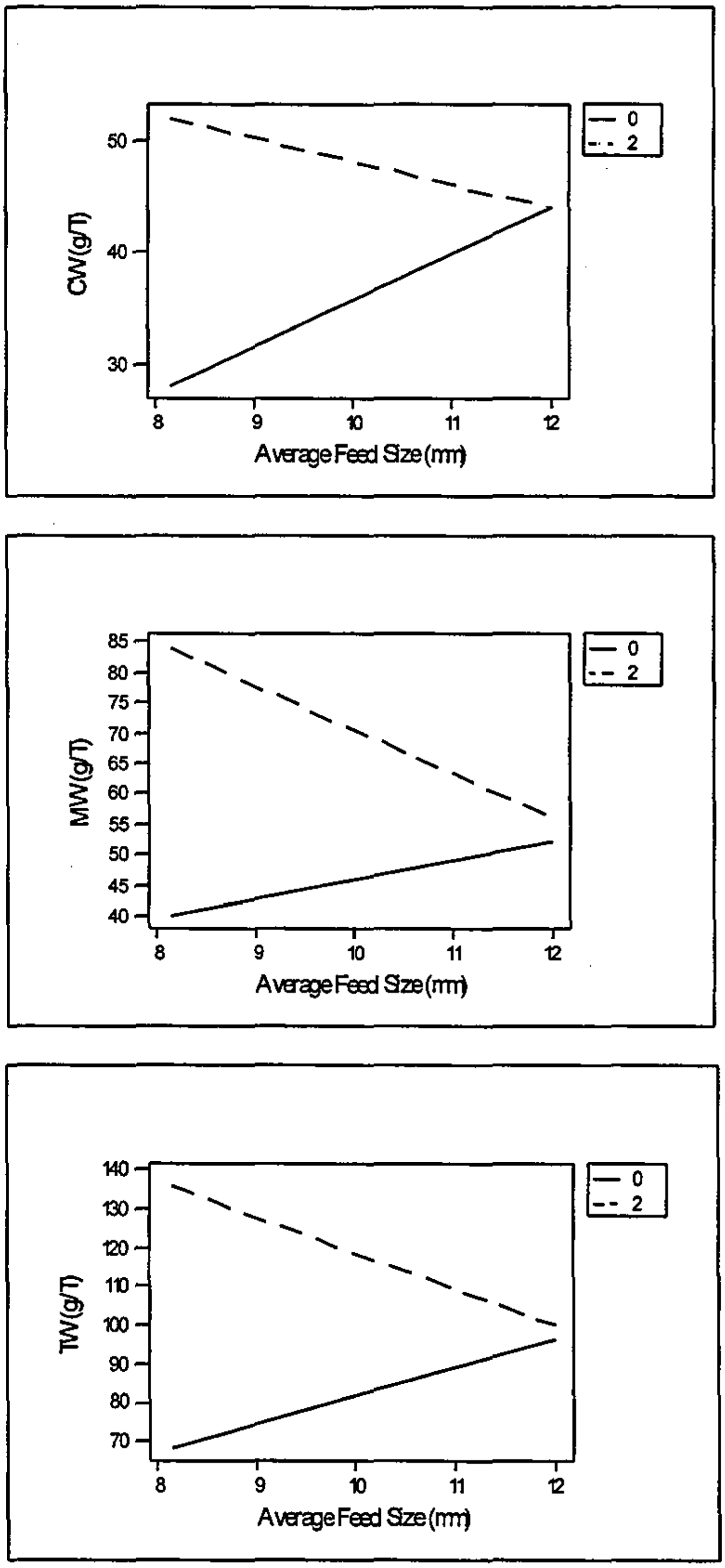

Figure 7.4 Measured wear vs moisture content and Feed average size at 4mm crusher setting for Pottal Pool Rock

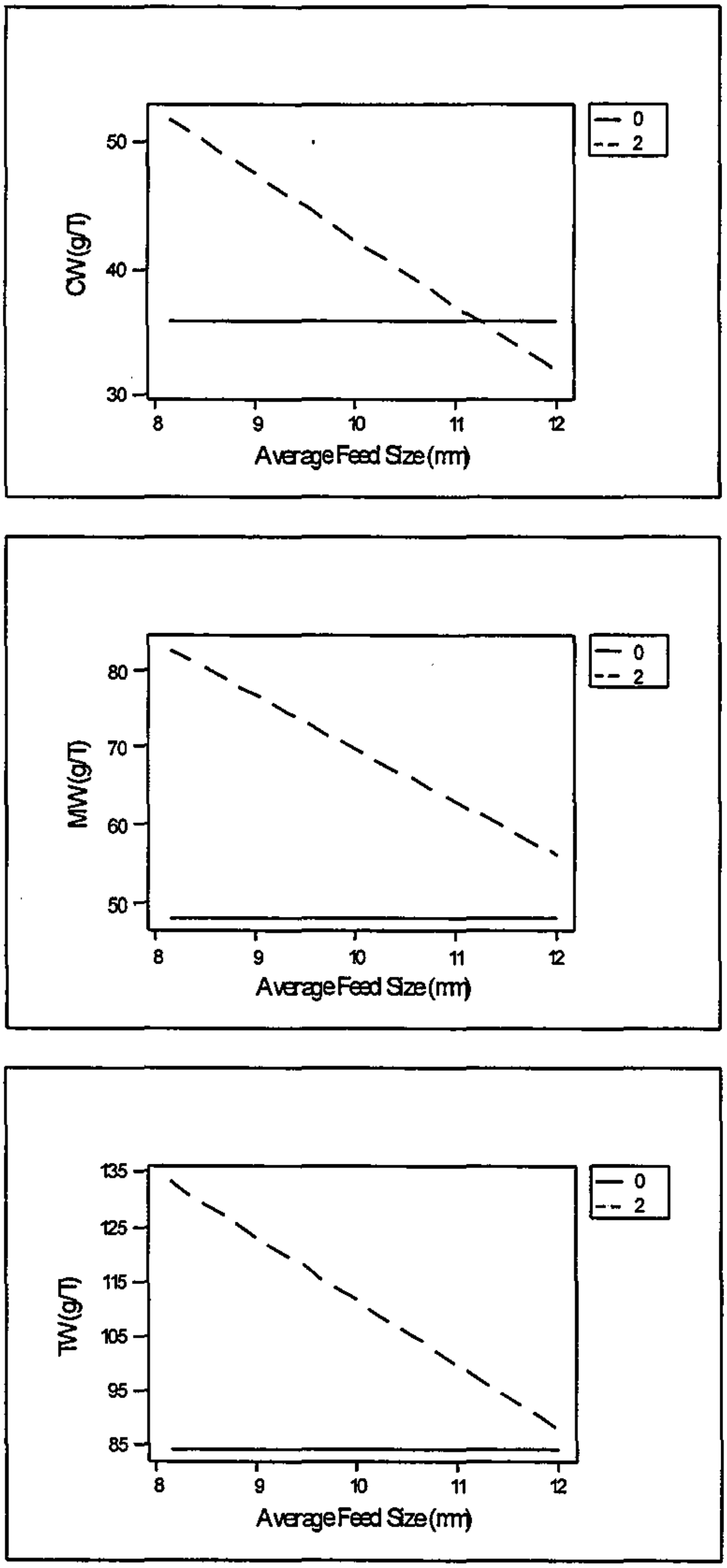

Figure 7.5 Measured wear vs moisture content and Feed average size at 4mm crusher setting for Shardlow Rock

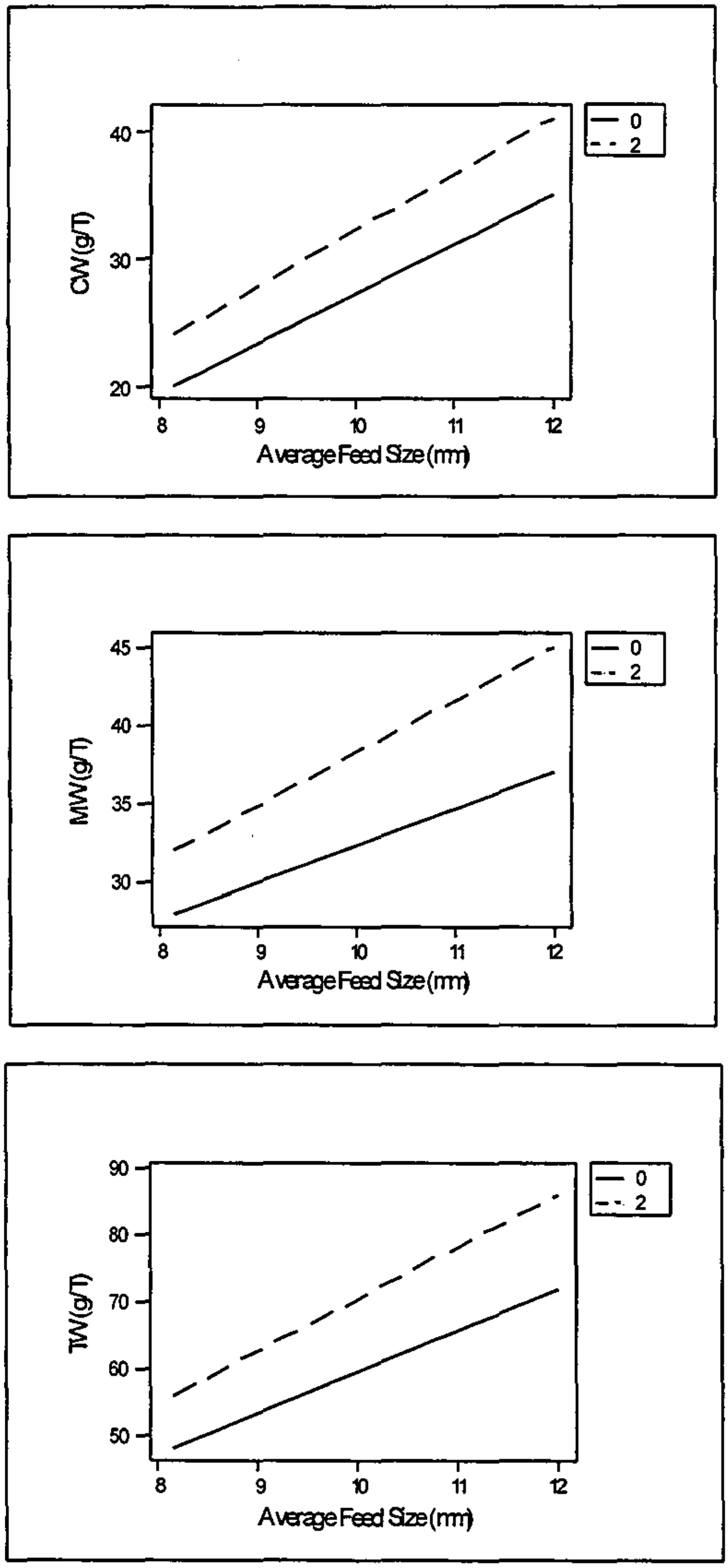

Figure 7.6 Measured wear vs moisture content and Feed average size at 4mm crusher setting for Shap Blue Rock

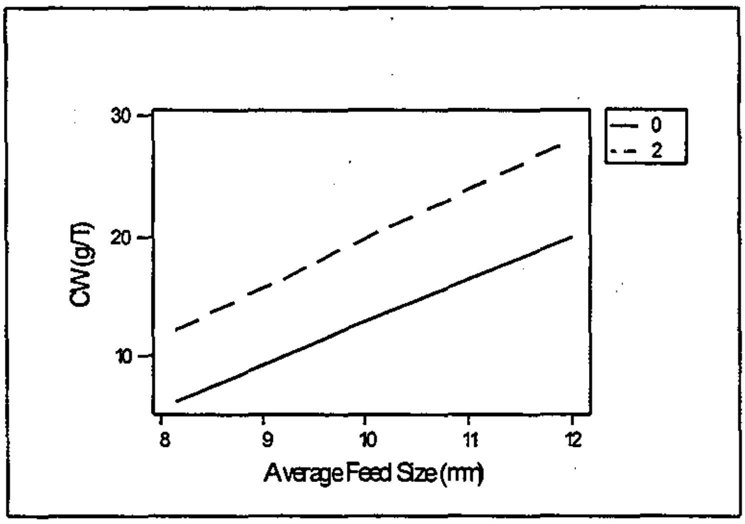

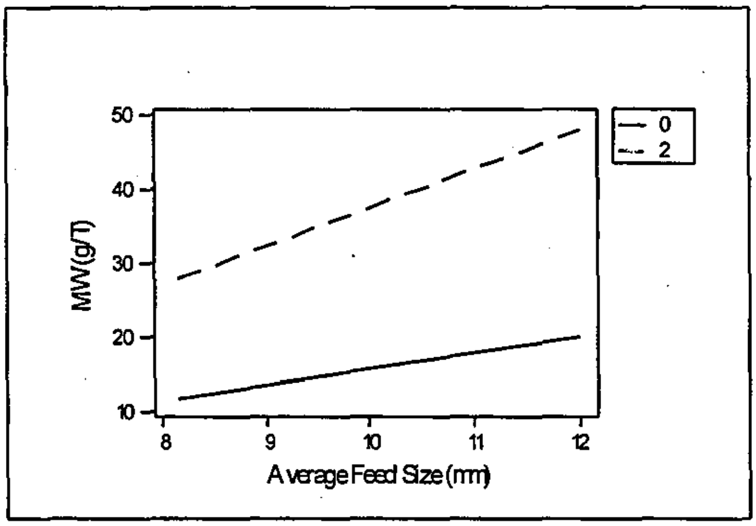

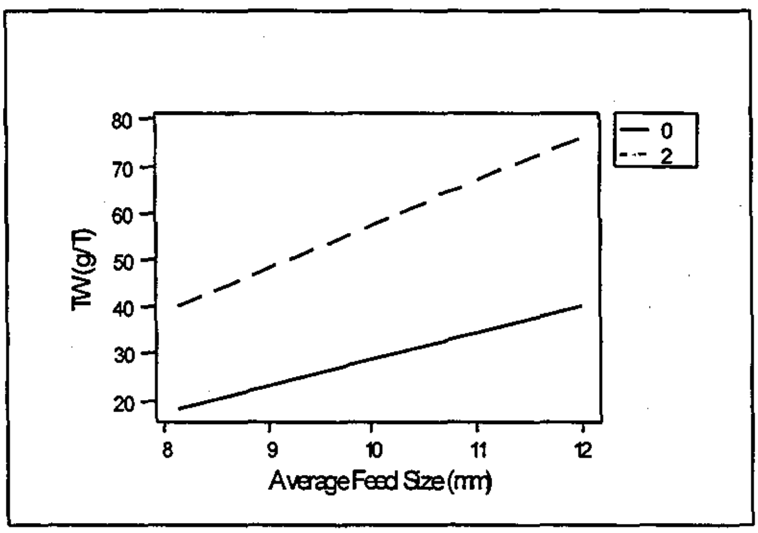

Figure 7.7 Measured wear vs moisture content and Feed average size at 4mm crusher setting for Whitwick Rock

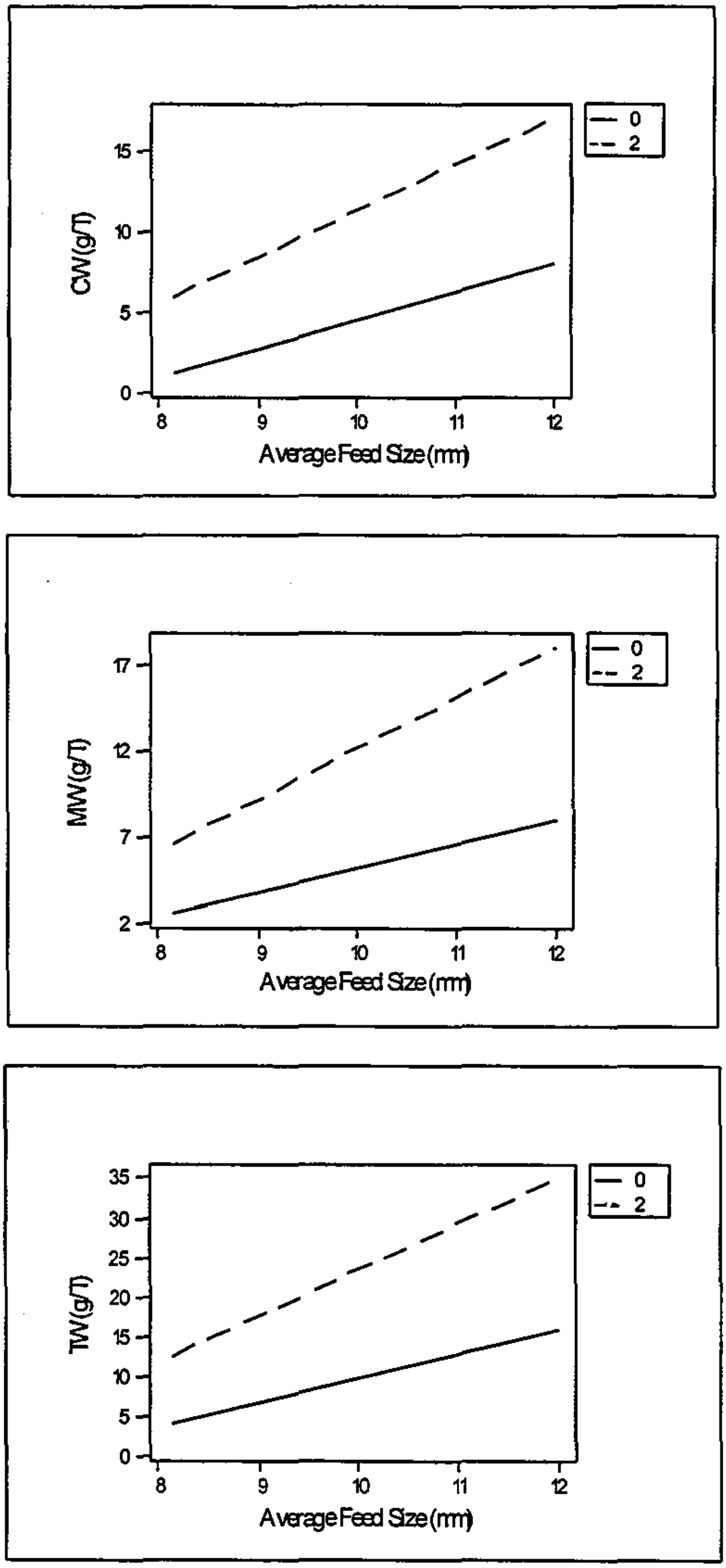

Figure 7.8 Measured wear vs moisture content and Feed average size at 4mm crusher setting for Waterswallows Rock

7.2 Discussion of the Result

The effect of feed size on wear, for the range of experimental data available, was found to be a reduction in wear for a lower nominal average of feed size fraction. Addition of moisture to the smaller nominal feed size, increased the wear for all rocks tested, including the gravel rock types, Shardlow and Pottal Pool. In the case of these two rocks, the lines describing wear versus feed size at 2% moisture level have negative slope. This is due to the anomalous effect of moisture on wear of these rocks at the higher feed size, which was described in the previous Chapter.

For all non-gravel rocks, the impact of moisture on wear depended on the feed size and was lower for the smaller feed size. The effect was modelled using the interaction term between the moisture and feed size.

Chapter 8 SURFACE AND METALLURGICAL INVESTIGATIONS

This chapter presents the results of the post-wear investigation of the surface characteristics of the liners used in the wear experiments. The investigation was carried out with two main objectives:- to compare the surface appearance and wear scars caused by different rock types; and to find the correlation between the rock hardness, mechanisms of wear, the micro-structure and hardness of Manganese steel.

8.1 Preparation of Specimens

After the completion of the wear experiments, two samples were taken from different areas of concave and mantle using a Plasma cutter. Each of the 2 samples was further cut in two, to provide two specimens for surface measurements, and another two for surface hardness and micro-structure tests. All specimens were thoroughly cleaned, using a hard plastic brush, to get rid of the rock fragments on the surface.

8.2 Surface Appearance and Wear Scars

Scanning Electron Microscopy (SEM) was used to investigate the surface appearance and the wear scars caused by each rock type. Plates 8.1 to 8.11 present a representative sample of the SEM observations. Micrographs under two different magnifications, 150 and 500 times, were used to capture different surface features. The low magnification plates provide a general view of the surface appearance, while the higher magnification plates reveal individual wear scars giving an insight into the dominant mechanisms of material removal.

8.2.1 Breedon Rock

Under low magnification, the surface exhibited a large number of ploughing grooves and pits. Under high magnification micro-cutting and larger grooves were also evident. The main feature of the surface was however, found to be an extensive plastic deformation and occasional larger pits and grooves.

8.2.2 Cliffe Hill Rock

Despite being subjected to the same cleaning procedure as other samples, a large amount of rock fragments were found embedded in the surface of the specimen. Under both low and high magnifications extensive plastic deformation and ploughing as well as some micro-cutting were observed.

8.2.3 Ingleton Grey Rock

Even under low magnification, the specimen showed large number of cutting grooves. Under high magnification this observation was further substantiated. At the bottom of the larger cutting grooves, finer scratches were also present. Under very low magnification (31 times) one of the specimens showed an unusual wear scar captured on Plate 8.4. The wear mechanism responsible for these deep parallel cuts is not known.

8.2.4 Judkins Rock

The wear scars created by this rock were found to be primarily caused by macro-cutting. Under low magnification, a high concentration of wide cutting grooves were observed. Under high magnification, smaller cutting grooves with material pile up were discovered at the bottom of larger grooves.

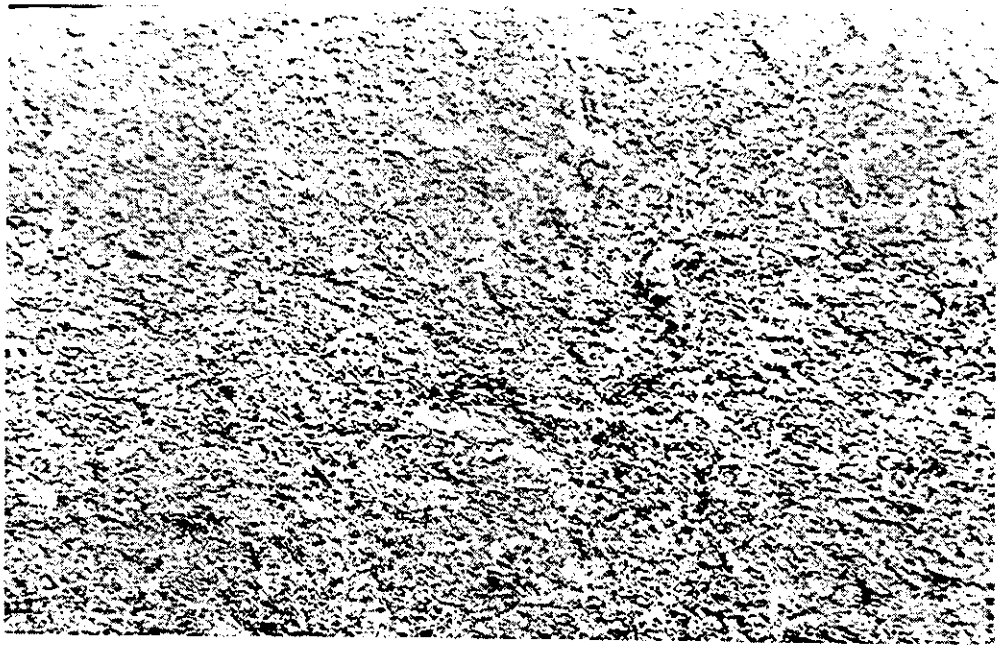

(a)

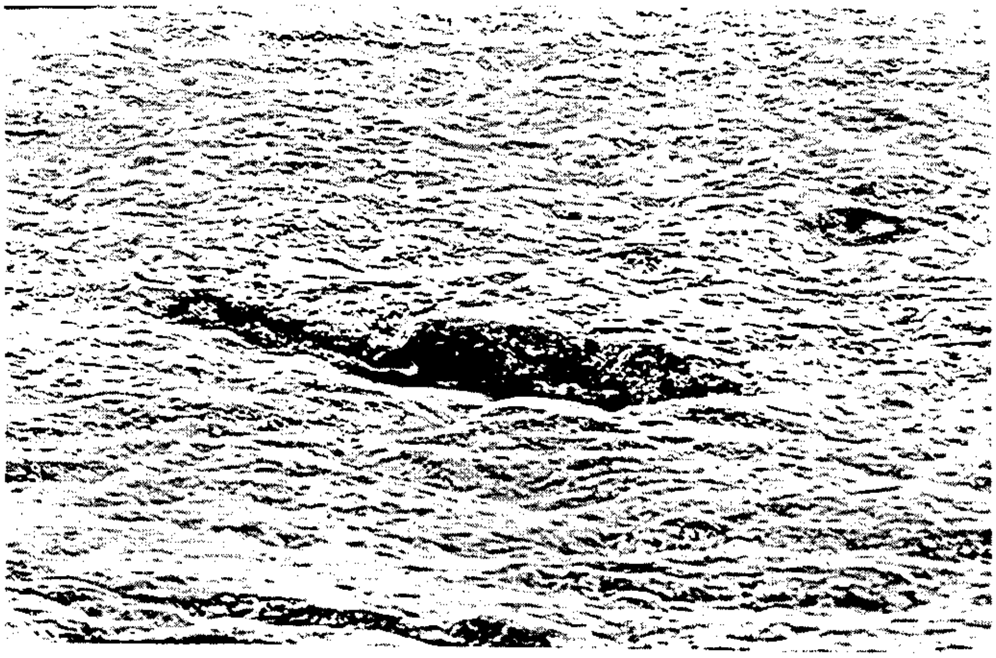

(b)

Plate 8.1 Wear scars caused by Breedon Rock a: ×150; b: ×500

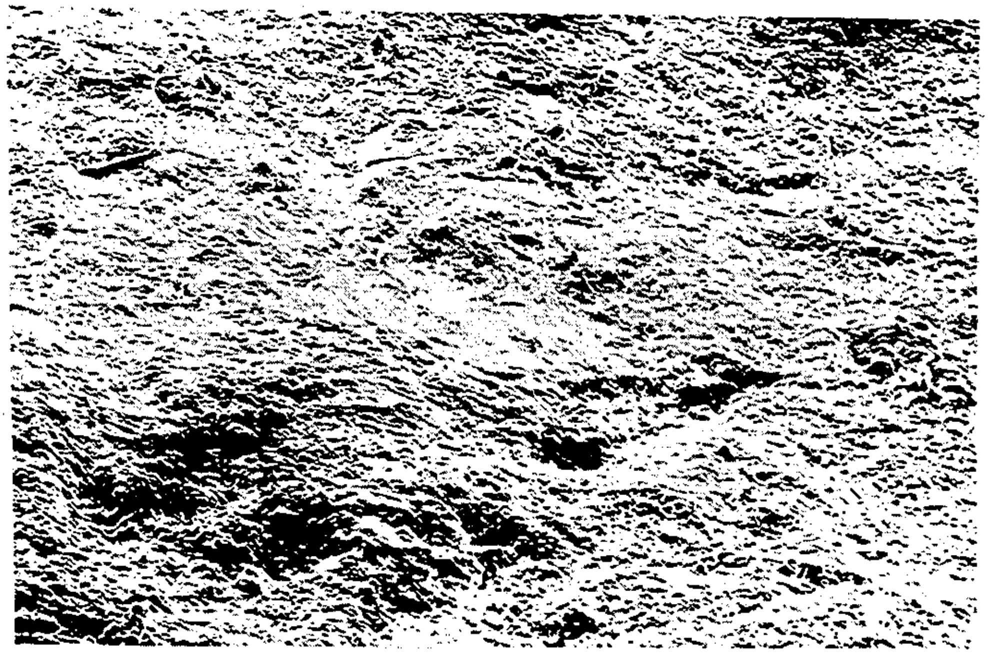

(a)

(b)

Plate 8.2 Wear scars caused by Cliffe Hill Rock a: ×150; b: ×500

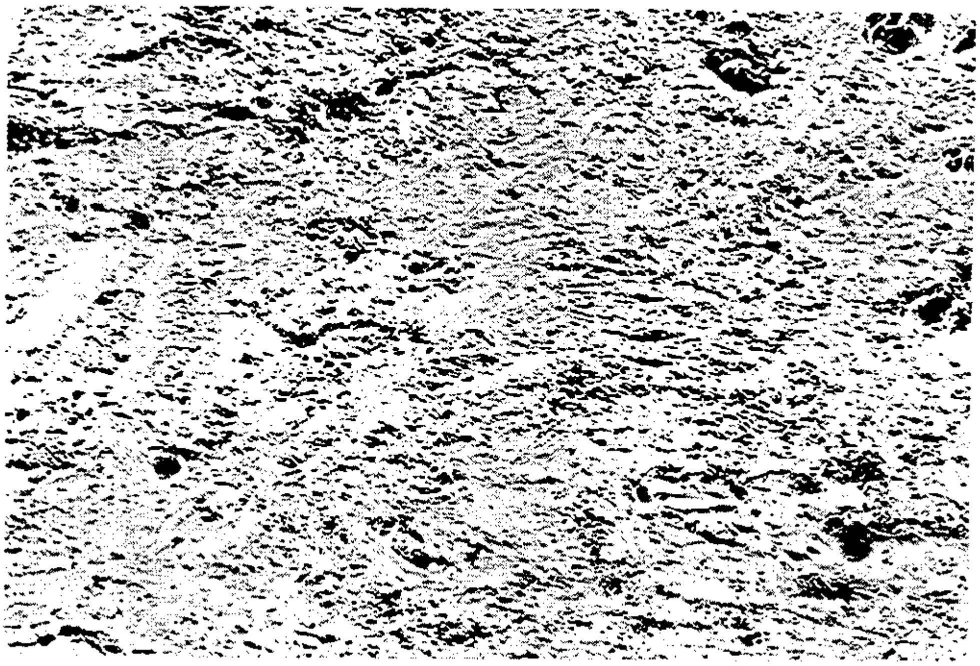

(a)

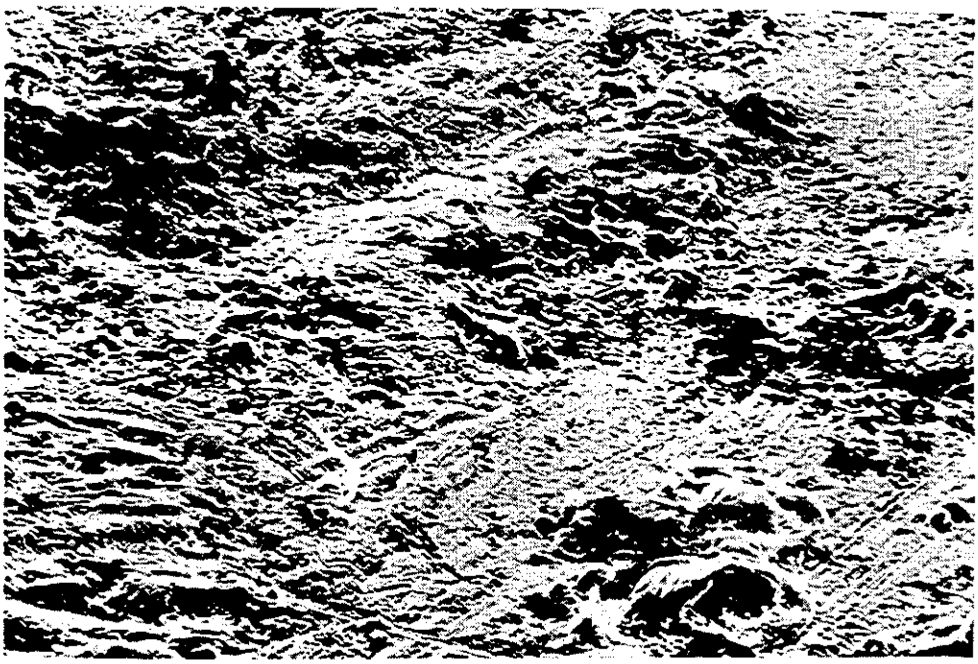

(b)

Plate 8.3 Wear scars caused by Ingleton Grey Rock a: ×150; b: ×500

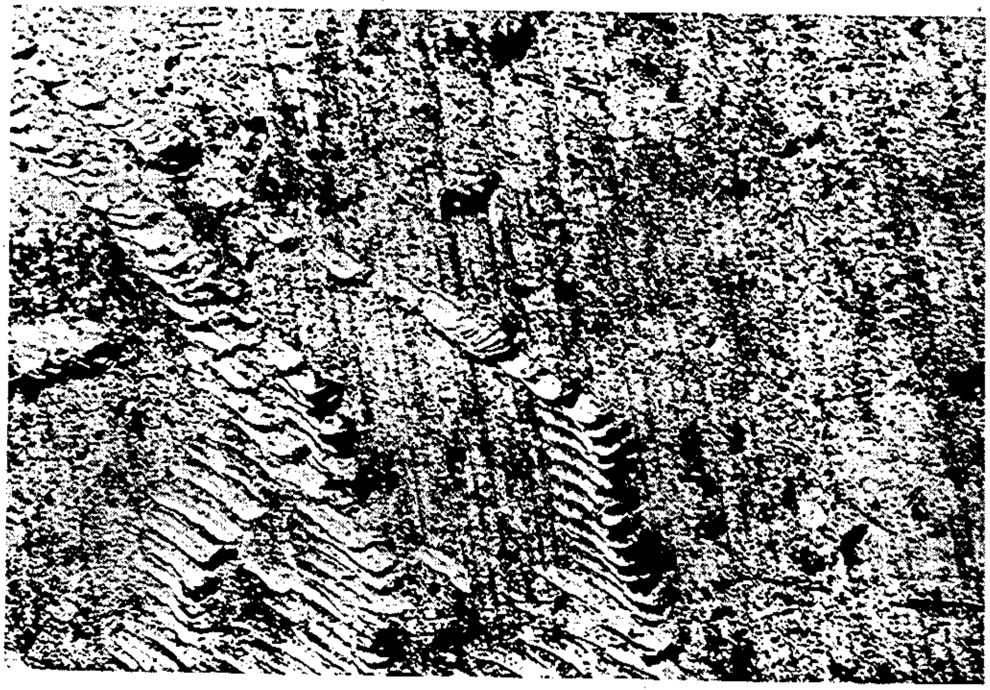

Plate 8.4 Anomalous Wear scars caused by Ingleton Grey Rock ×31

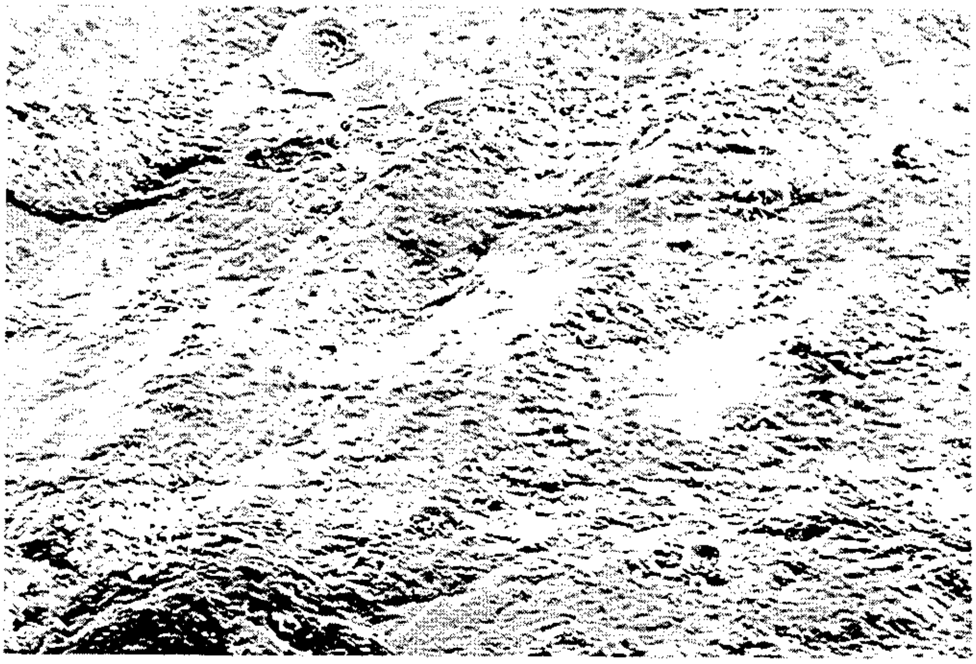

(a)

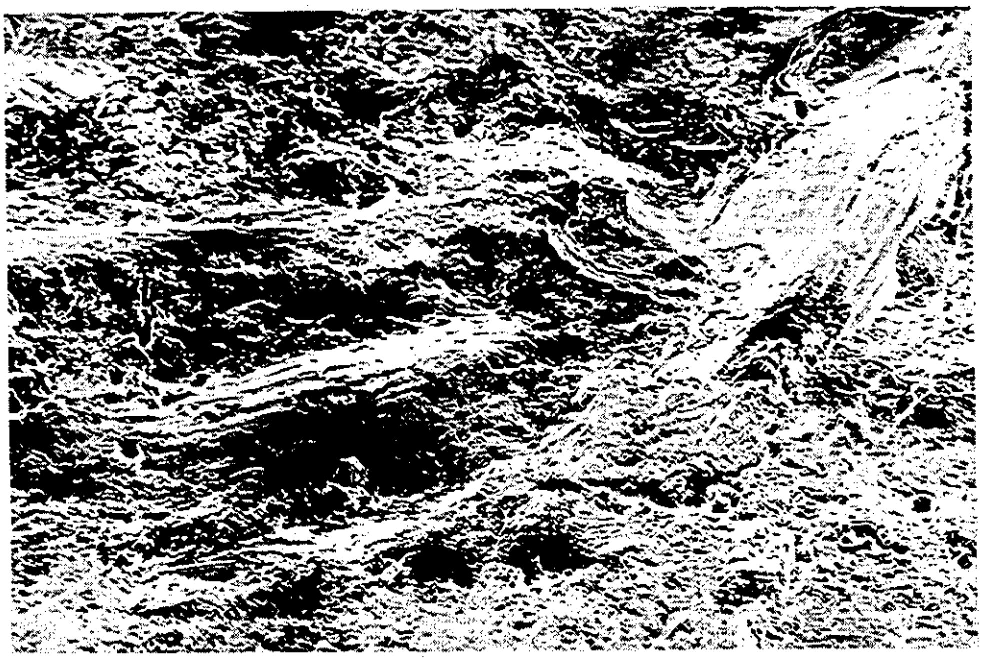

(b)

Plate 8.5 Wear scars caused by Judkins Rock a: ×150; b: ×500

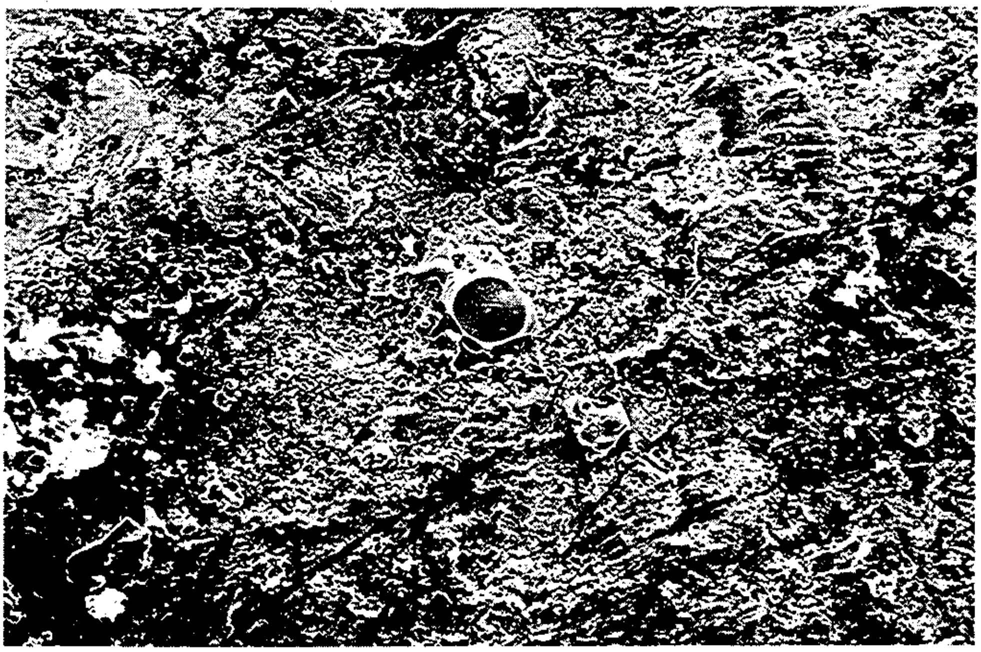

(a)

(b)

Plate 8.6 Wear scars caused by Shap Blue Rock a: ×150; b: ×500

8.2.5 Shap Blue Rock

Under low magnification, a significant number of surface fatigue scars could be observed. Under high magnification, cutting grooves and a number of micro-fractures were also present.

8.2.6 Shardlow Rock

Under low magnification, the scars were found to be predominantly caused by macro-cutting. Under higher magnification, very large cutting grooves at the bottom of which other substantial grooves were present, were observed. Extensive evidence of material pile up at front and edges of the grooves were also present.

8.2.7 Pant Rock

The surface under low magnification showed the evidence of plastic deformation and ploughing, as well as some holes. Under higher magnification, some cutting scratches were also found.

8.2.8 Pottal Pool Rock

A large number of deep and wide cutting grooves with material pile ups at all groove edges, extensive ploughing and deep pits were observed under low magnification. Under high magnification, a number of micro-fractures, and some evidence of surface fatigue and multi-grooved cuts were found.

8.2.9 Whitwick Rock

Under low magnification cutting scars and some ploughing grooves were found. Under high magnification finer scratches and shallow grooves and pits were also observed.

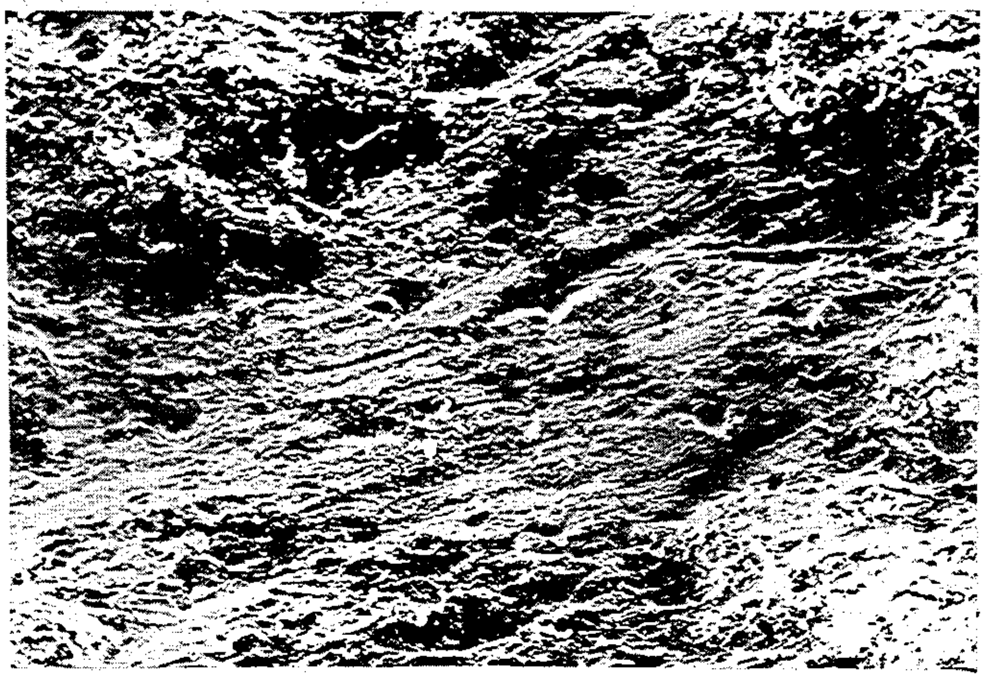

(a)

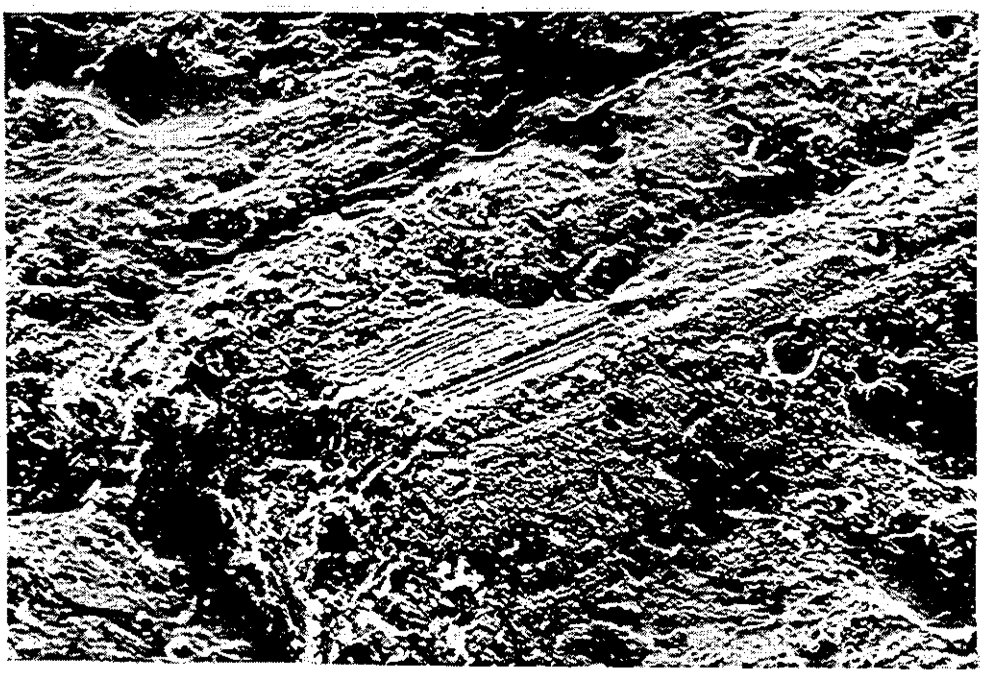

(b)

Plate 8.7 Wear scars caused by Shardlow Rock a: ×150; b: ×500

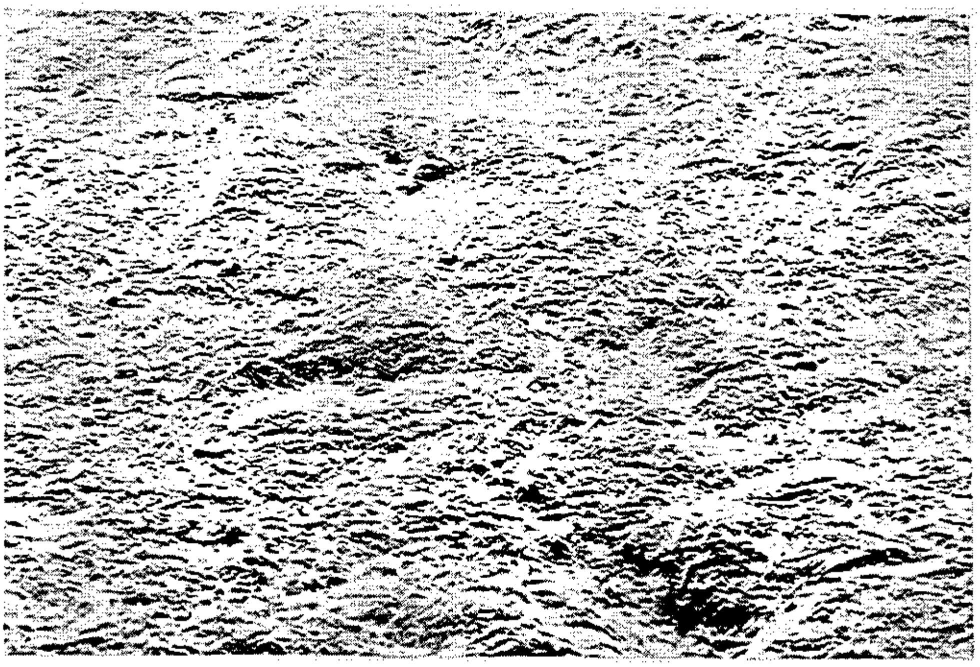

(a)

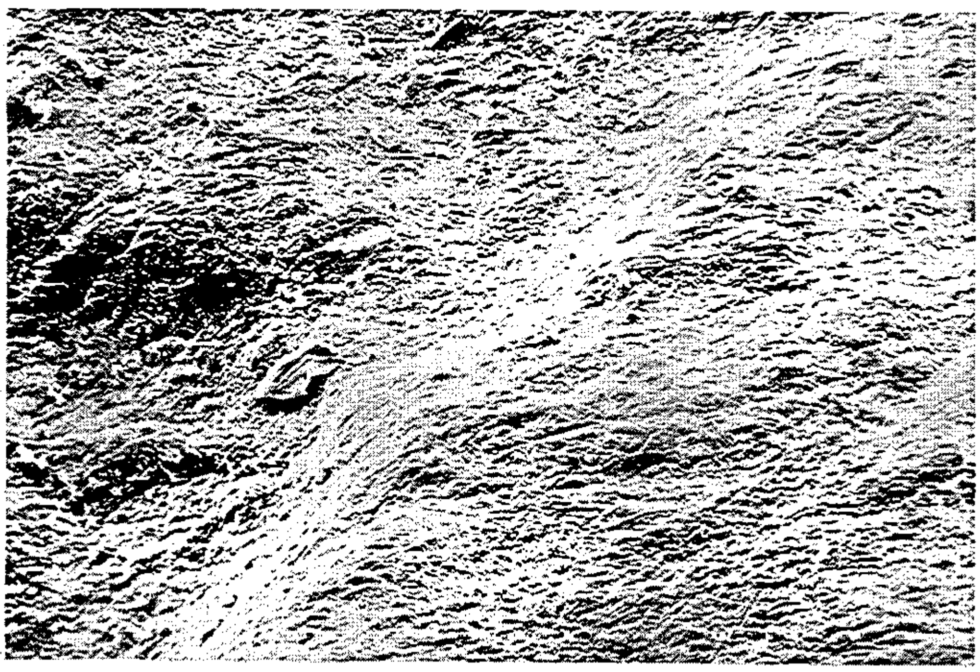

(b)

Plate 8.8 Wear scars caused by Pant Rock a: ×150; b: ×500

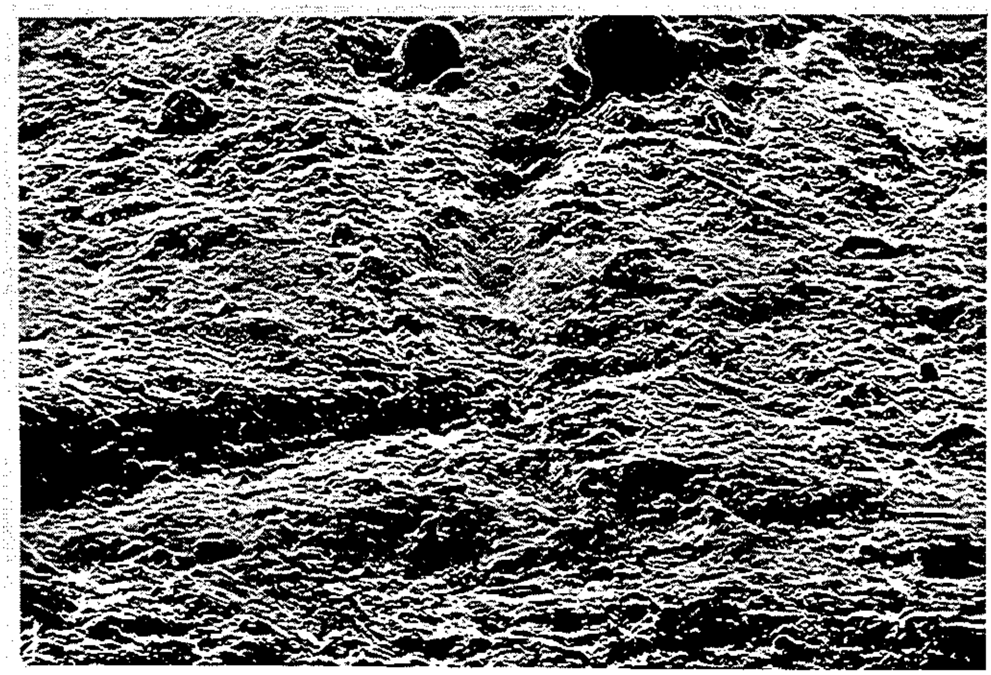

(a)

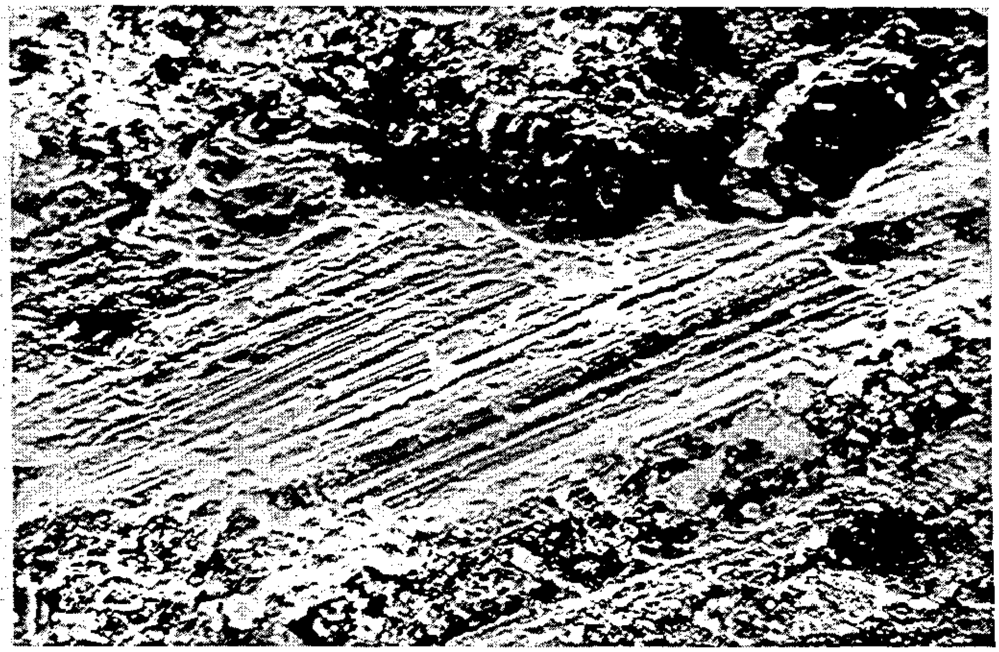

(b)

Plate 8.9 Wear scars caused by Pottal Pool Rock a: ×150; b: ×500

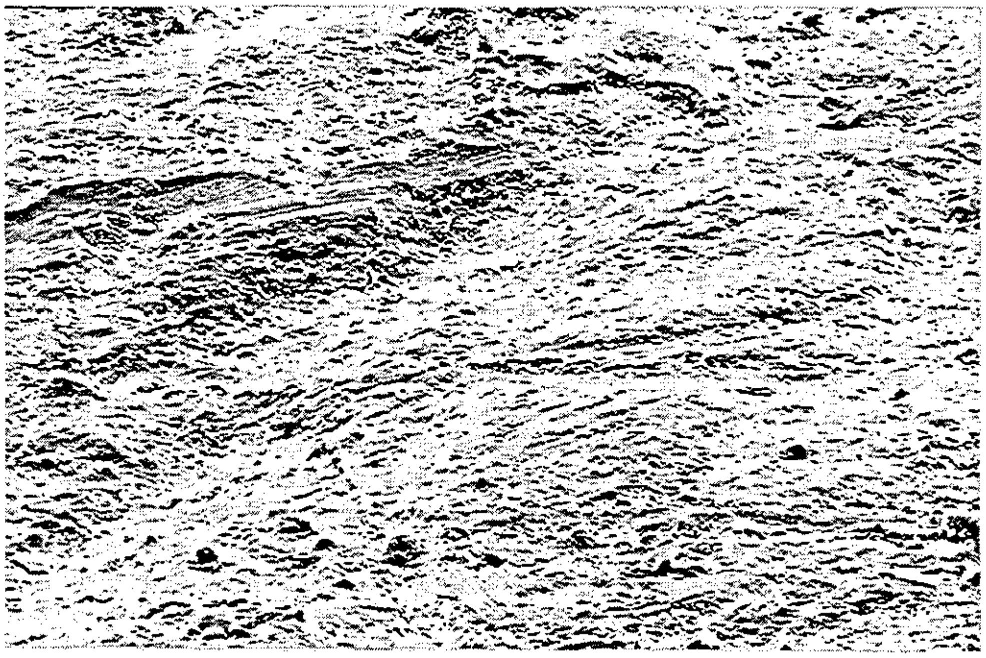

(a)

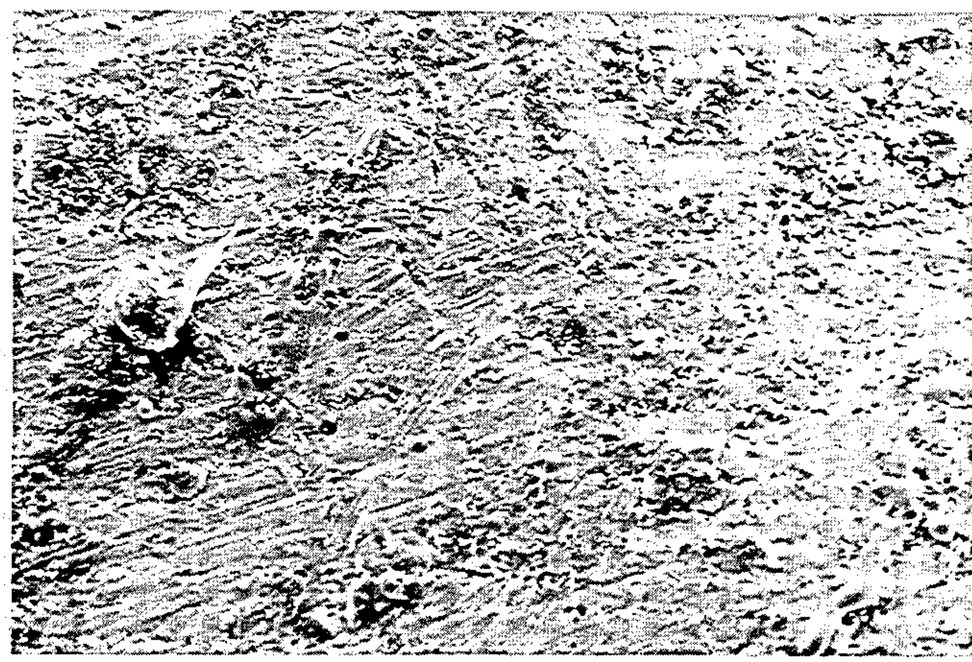

(b)

Plate 8.10 Wear scars caused by Whitwick Rock a: ×150; b: ×500

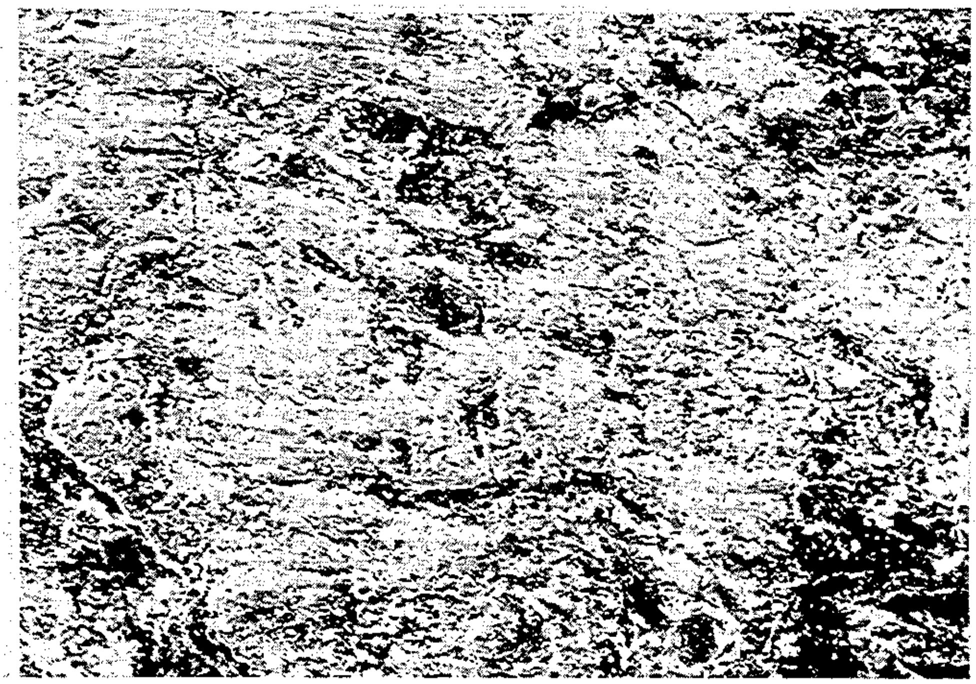

(a)

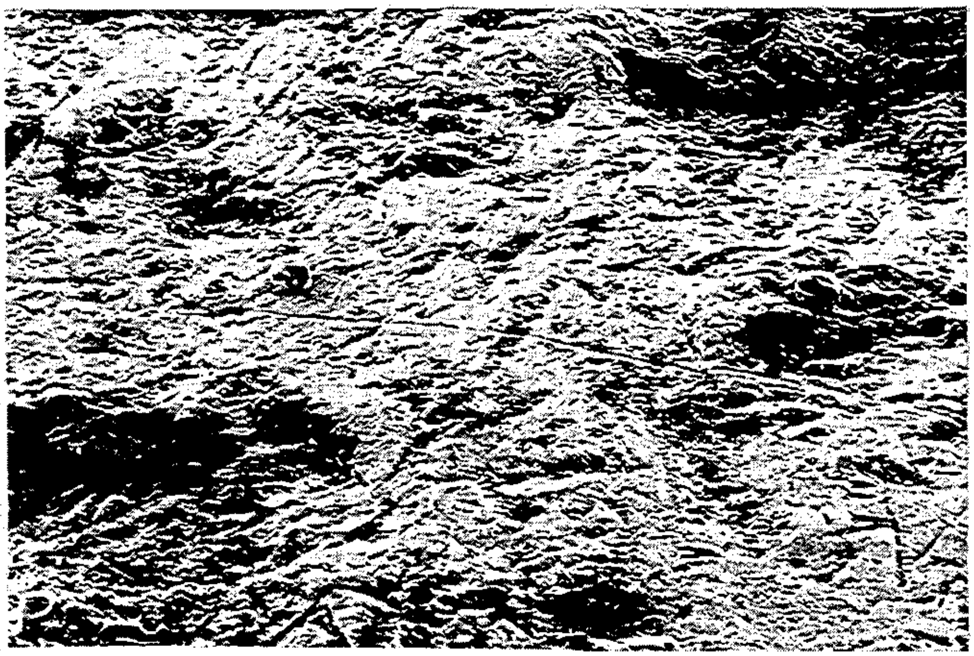

(b)

Plate 8.11 Wear scars caused by Waterswallows Rock a: ×150; b: ×500

8.2.10 Waterswallows Rock

The surface appearance of the specimen, under low and high magnification, was found to be different from that of the other samples. The dominant feature of the surface, under low magnification, was the presence of a large number of irregularly shaped pits. Some of the pits were elongated and resembled very wide cutting grooves. Under high magnification, apart from the pits, an extensive number of short cutting scars were also observed. No major evidence of ploughing or material pile up could be found.

8.3 Hardness Measurement

Table 8.1 shows the average of Vickers hardness measurements, carried out at 5 different points on the surface of each sample. It can be seen that the average hardness, for both mantle and concave are within the range expected for the work hardened Hadfield steel.

Table 8.1 Vickers Hardness of Different Liners

Liner Set No.	Vickers Hardness	
	Mantle	Concave
1	427	406
2	407	394
3	416	394
4	399	429
5	408	397

8.4 The Micro-Structure

Plate 8.12 shows the micro-structure of the specimen taken from concave No. 2. It is representative of the micro-structure observed for the samples taken from all the liner sets used. As can be seen, the micro-structure displayed relatively equiaxed grains of austenite with fine and well distributed carbides, some of of austenite with fine and well distributed carbides, some of which occurred at the grain boundaries. The observed micro-structure supports the results of the hardness measurement tests indicating the consistency of the liners' properties.

Plate 8.12 The typical Micro-structure of the liners used in the wear experiments

The agreement between the findings of the three independant tests undertaken, i.e. the hardness test, the micro-structure test, and the wear performance test which was discussed in Chapter 5, confirmed that a strong correlation exists between the wear performance of the liner and its material properties in terms of micro-structure and hardness.

Chapter 9 THE REAL-TIME CONE CRUSHER CONTROL STRATEGY

9.1 Traditional Control of Autocone Cone Crusher

The Autocone operating console, system 4 or the more sophisticated system 5, provides a centralised unit comprising a PLC and a supervisory computer to set the closed-side gap and maintain the position of the upper frame at the set point through the use of a feedback position sensor. The unit also provides automatic overload protection against the intrusion of foreign metal pieces (tramp iron) into the chamber. In such instances the increased load is sensed through pressure and temperature sensors which triggers the full opening of the chamber to discard the load.

To set the opening, after clearing the crushing chamber, the operator drives the hydraulic cylinders to move the upper frame until the concave and mantle come into contact. This provides a datum reference on the feedback position sensor. To achieve a desired close-side setting, the upper frame is then moved upwards until the position sensor output indicates the required opening. After an emergency discharge sequence, upon operator's request, the unit automatically returns the upper frame to its previous position. However, none of the presently available cone crusher control systems could be classed as fully automated as, in all cases, a great deal of operator intervention is still required. In the most advanced case, the controller provides two modes of control:- constant setting mode, and maximum power operation. In the constant setting mode the position of the upper frame is kept constant according to the last close-side setting. In the maximum power operation mode the setting is adjusted to ensure maximum crushing power. Yet, none of the two operation modes offers any in-process control over the actual size of the discharge opening, which as a result of wear is continuously enlarged, and hence on the consistency of the product characteristics.

To correct the discharge opening for the effect of liner wear, the crusher must be re-set off-line. This disruption in the production discourages the quarry operators from carrying out the necessary number of re-settings to keep the crusher opening constant. Furthermore, the accuracy of the re-setting procedure is dependant on the correctness of the required datum set which is based on the contact between the crushing members. If the liners' wear profile is not uniform, the datum set can become unreliable resulting in an erroneous discharge opening. The lack of any adequate in-process re-setting technique to account for liner wear, produces an undesirable drift in the size distribution of the product between successive re-settings.

9.2 A Product Driven Control Strategy for Cone Crushers

The current trends towards quality assurance and energy saving, emphasizes the benefits of a cone crusher control strategy based on the optimization of the product quality. The main requirement of such a product driven control strategy is the ability to control the size distribution of the product and hence minimize the re-circulating load, the produced fines, and the cost associated with re-processing or discarding the unsalable products. A controller based on this strategy must be able to perform the following tasks:

1. calculate the correct closed-side setting for the production of a particular grade of aggregate,

2. correct the crusher setting for the effects of liner wear to ensure consistent product characteristics in real-time and without any disruption,

3. maximize the crusher efficiency within the limits imposed by the operating conditions.

As discussed in Chapter Two, a number of workers (Whiten1972; Anderson & Nappier-Munn 1990; Bearman1991) have investigated the relationship between the feed properties, crusher's operating parameters and product size. Whiten's crusher model in particular is useful, as it decouples the effect of feed properties, in terms of the Breakage Function (**B** matrix) associated with a given rock type, from that of the operating parameters, in terms of the Classification Function (**C** matrix) associated with a given crusher design and closed-side setting, on product size. This model was therefore chosen as the basis for the design of the new control strategy.

According to this model, the calculation of the correct crusher setting for a given aggregate, would be based on a prior knowledge of the Breakage Function for that particular rock. The required information must be available to the system either in terms of the **B** matrix itself, or the parameter $\mathbf{t}_{10}$ (Bearman 1991) or the value of Fracture Toughness (Bearman 1991) from which the **B** matrix could be determined. With a knowledge of the **B** matrix and the required product vector, the crusher equation could be solved to obtain the optimum closed-side setting under a particular set of other operational conditions (e.g. rate and size of the feed). The calculated setting corresponds to the profile of a new set of liners and needs to be calculated only once at the beginning of a production batch.

The novel task of the control strategy is therefore to maintain the product size and crusher efficiency at an optimum level throughout the life of the liners. Except for the limited work by a number of workers on the effect of liner 'Age' on crushing performance (Anderson & Nappier-Munn 1990; White 1978), no published results on the effect of either liner wear or moisture content on product size and crushing performance could be found. However, the consideration of these issues are central to the design of a product based control system and, as described in the following sections, were investigated as part of the experimental work carried out.

9.3 Variation of Product Size and Power With Moisture and Crusher Setting

Bearman(1991) investigated the relationship between the size of cone crusher product, in terms of the 80% passing size, closed-side setting, energy consumption, feed size, and rock properties. His work represents the most comprehensive work in this field and is of considerable relevance to the present study. His findings can be summarized as follow:

1. energy consumption, in terms of kWh/t, is independent of feed size in both laboratory size and full-scale cone crushers,

2. energy consumption is inversely proportional to closed-side setting in both laboratory size and full-scale cone crushers,

3. product size, in terms of 80% passing size, is not affected by feed size in both laboratory size and full-scale cone crushers,

4. the 80% passing size of the product is directly proportional to the closed-side setting,

5. both the energy consumption and product size can be described in terms of fracture toughness (and other strength properties).

As part of the main wear experiments, both power drawn by the laboratory size cone crusher, and product size distribution were measured for the majority of the tests. The power drawn in each case is shown in tables A3.1, A3.2 and A3.3 together with other test results. The size distribution results are shown in tables A4.1 to A4.10. The size distribution results were used to determine the 80% passing size of the product for each test. From examination of the results a number of points have been concluded that are discussed below.

9.3.1 Correlation Between Power, Closed-side Setting and Moisture

The results obtained in this study confirm the findings of the Bearman(1991) with respect to energy consumption. The average power drawn by the laboratory size crusher was found to be independent of feed size, and inversely proportional to closed-side setting for all rock types tested (Tables A3.1 to A3.3). For dry rock, the energy consumption was found to be dependant on fracture toughness, according to the following equation:

Energy (kWh/t) = 4.41 **1/CSS** - 0.125 **FT** **9.1**
s = 0.1598

Analysis of Variance:

SOURCE	DF	SS	MS	F	p
Regression	2	11.6950	5.8475	228.91	0.000
Error	40	1.0218	0.0255		
Total	42	12.7167			

For moist rock the average power drawn, for all rocks, was found to decrease as the moisture content increased. Table 9.1 shows the correlation between the average power drawn, closed-side setting and moisture content for rocks tested.

Table 9.1 Correlation Between Average Power, Closed-Side Setting and Moisture Content

Waterswallows	Power (kW) = 0.227 + 0.056 1/CSS - 0.0238 Moist	s = 0.013
Whitwick	Power (kW) = 0.292 - 0.174 1/CSS - 0.0254 Moist	s = 0.014
Shardlow	Power (kW) = 0.220 + 0.068 1/CSS - 0.0149 Moist	s = 0.006
Pottal Pool	Power (kW) = 0.248 + 0.134 1/CSS - 0.0379 Moist	s = 0.018
Judkins	Power (kW) = 0.208 + 0.111 1/CSS - 0.0232 Moist	s = 0.008
Ingleton	Power (kW) = 0.244 + 0.196 1/CSS - 0.0363 Moist	s = 0.023
Cliffe Hill	Power (kW) = 0.211 + 0.264 1/CSS - 0.0321 Moist	s = 0.014

The relationship between average power and moisture content confirms that the presence of moisture, within the range tested, not only increases the wear but also reduces the crusher efficiency.

9.3.2 Correlation between Product Size, Closed-side Setting, and Moisture

The 80% passing size of the product for dry rock experiments, at the two tested feed sizes, were determined and are shown in Table A4.11. Also included are the passing size for one moist rock experiment at each closed-side setting tested. It was found that in accordance with the findings of Bearman(1991), the 80% passing size of product varies linearly with closed-side setting. Also, for dry rock the 80% passing size was found to depend on fracture toughness according to the following equation:

$$\mathbf{P80} = 1.25 + 1.53\ \mathbf{CSS} - 0.878\ \mathbf{FT} \qquad \mathbf{9.2}$$

$$s = 0.797 \qquad \mathbf{R}^2 = 90.2\% \qquad \mathbf{R}^2(\text{adj}) = 89.6\%$$

Analysis of Variance

SOURCE	DF	SS	MS	F	p
Regression	2	188.363	94.182	148.04	0.000
Error	32	20.358	0.636		
Total	34	208.722			

For moist rock, except in a few cases, it was found that the 80% passing size decreases with moisture. Furthermore, contrary to the finding of Bearman(1991), a weak dependence on feed size was also observed. However, the feed size was not tested at adequate number of levels for this result to be conclusive. Table 9.2 presents the correlation equations for each rock type tested. The Pant rock was only tested at one feed size.

Table 9.2 Correlation Between 80% Passing Size, Closed-Side Setting, Moisture Content and Feed Size

Waterswallows	P80(mm) = 1.37 CSS/mm - 0.315 Moist(%) - 0.0108 FeedSize	s = 0.666
Whitwick	P80(mm) = 1.56 CSS/mm - 0.089 Moist(%) - 0.0677 FeedSize	s = 0.562
Pottal Pool	P80(mm) = 1.23 CSS/mm - 0.366 Moist(%) + 0.0512 FeedSize	s = 0.642
Judkins	P80(mm) = 1.20 CSS/mm - 0.213 Moist(%) + 0.0457 FeedSize	s = 0.311
Ingleton	P80(mm) = 1.43 CSS/mm - 0.754 Moist(%) + 0.0418 FeedSize	s = 0.729
Cliffe Hill	P80(mm) = 1.42 CSS/mm - 0.208 Moist(%) - 0.0926 FeedSize	s = 0.688
Shardlow	P80(mm) = 1.33 CSS/mm - 0.577 Moist(%) + 0.0498 FeedSize	s = 0.825
Pant	P80(mm) = 1.48 CSS/mm - 0.777 Moist(%)	s = 0.757

In terms of Whiten's crusher model (Whiten 1972), the size distribution of the product could be related to the model classification parameters, $\mathbf{K_1}$, the minimum particle size below which no crushing occurs, and $\mathbf{K_2}$, the particle size above which all particles will be subjected to crushing. The investigations carried out by Whiten(1972) and other workers(Anderson & Napier-Munn 1990) have shown that ignoring the wear and under constant operating conditions K_1 and K_2 are given by:

$$K_1 = a_0 + a_1 D.O \qquad 9.3$$

$$K_2 = b_0 + b_1 D.O \qquad 9.4$$

where **a** and **b** are machine dependant model coefficients, and **D.O.** is the discharge opening.

Different grades of Judkins rock was crushed under choke feeding condition to investigate the correlation between K_1 and K_2, closed-side setting and moisture content. Tables 9.3 shows the K_1 and K_2 values, which were determined from a comparison between the size distribution of the product under single size and graded feeding conditions. For dry rock, the regression equations describing K_1 and K_2 in terms of closed-side setting were found to be in general agreement with equations 9.3 and 9.4 as follow:

$$K_1 = -0.16 + 0.54\ \mathbf{CSS} \qquad 9.5$$

$$s = 0.148 \quad R^2 = 97.8\% \qquad R^2(adj) = 97.0\%$$

$$K_2 = 3.25 + 1.30\ \mathbf{CSS} \qquad 9.6$$

$$s = 0.178 \qquad R^2 = 99.4\% \quad R^2(adj) = 99.2\%$$

Table 9.3 Model Parameters K1 and K2

Judkins Rock

CSS	K1	K2	Moist
4.2	2.0	8.5	0
4.8	2.5	9.7	0
6.0	3.3	11.1	0
7.0	3.7	12.3	0
8.0	4.1	13.6	0
4.0	1.9	6.8	1
3.9	0.9	5.8	2
6.1	1.8	10.1	2
8.0	3.5	13.5	1
8.0	3.0	13.2	2

For moist rock it can be seen from Table 9.3 that as moisture content increases, $\mathbf{K_1}$ and $\mathbf{K_2}$ decrease, indicating a finer product:

$$\mathbf{K_1} = 0.21 + 0.49\ \mathbf{CSS} - 0.6\ \mathbf{Moist} \qquad 9.7$$

$$s = 0.191 \qquad \mathbf{R^2} = 97.2\% \qquad \mathbf{R^2(adj)} = 96.4\%$$

$$\mathbf{K_2} = 1.54 + 1.58\ \mathbf{CSS} - 0.68\ \mathbf{Moist} \qquad 9.8$$

$$s = 0.467 \qquad \mathbf{R^2} = 97.8\% \qquad \mathbf{R^2(adj)} = 97.2\%$$

9.4 Effect of Wear on Product Size

9.4.1 Effect of Thickness Loss

Wear causes a continuous decrease in liners' thickness which consequently leads into an enlargement of the discharge opening. In the case of conventional cone crushers, the crusher is usually re-set at regular intervals (at the end of each shift for high rates of wear) to compensate the wear. The enlargement of the discharge opening during two successive re-settings is given by:

$$\mathbf{DO_T} = \mathbf{CSS_0} + \int_0^T (\mathbf{W_C} + \mathbf{W_M})\, \mathbf{dt} \qquad 9.9$$

where $\mathbf{T}$ is the time between two re-settings, $\mathbf{DO_T}$ is the discharge opening (closed side) at time $\mathbf{T}$, $\mathbf{CSS_0}$ is the closed-side setting at zero time, and $\mathbf{W_C}$ and $\mathbf{W_M}$ are the rate of wear, in mm/hour, of concave and mantle respectively.

As expected from Equation 9.2, the enlargement of the discharge opening causes a drift in the product size where the volume of oversize particles leaving the crushing chamber increases. To account for this observation in terms of the Whiten's model (1972), $\mathbf{K_1}$ and $\mathbf{K_2}$ must be considered as functions of time:

$$\mathbf{K_1(t)} = a_0 + a_1\mathbf{D.O(t)} - a_2\mathbf{L(t)} \qquad 9.10$$

$$\mathbf{K_2(t)} = b_0 + b_1\mathbf{D.O(t)} - b_2\mathbf{L(t)} \qquad 9.11$$

where $\mathbf{L(t)}$ is a machine dependent slow varying variable that represents the effect of the change in the profile of the liners, i.e. the increased length of the parallel part of the crushing chamber. As discussed in Chapter Two, the action of $\mathbf{L(t)}$ is similar to a reduction in the closed-side setting (Anderson and Napier-Munn 1990).

9.4.2 Effect of the Wear-Induced Change in Liner Profile on Product Size

To investigate the quantitative effect of wear-induced change in liner profile on product size, a set of tests using cast iron liners were carried out. Iron wears at a much higher rate than manganese steel which allows the effect of profile degradation to be observed under laboratory conditions. The test procedure for the experiment was as follow:

1 25 kg of Judkins rock was crushed at a setting of 4mm, a sample of product was taken to determine its size distribution, the wear in terms of the weight loss and crushing time were measured.

2 250 kg of wet Pottal Pool rock was then crushed at a setting of 4mm. The combination of low crusher setting, highly abrasive rock type and high moisture content created an accelerated wear situation causing a noticeable change in the liner profile. The wear in terms of weight loss was measured.

3 A further 25 kg of Judkins rock was crushed at 4mm setting using the worn liners. A sample of product was taken and used to determine its size distribution. The wear and crushing time was measured.

Table 9.4 Results of the Tests To Quantify L(t)

Rock Type	Discharge Setting mm	Crushed Weight kg	Concave Wear g/ tonne	Mantle Wear g/ tonne	Total Wear g/ tonne	Crushing Time h/tonne
Judkins (1)	4.00	25	18	30	48	4.50
Pottal Pool	4.00	250	186	204	390	10.45
Judkins (2)	4.10	25	20	31	51	4.56

Table 9.4 shows the results of the experiment. To calculate **L(t)** from this data, the equivalent crushing time required for Judkins rock to produce the same wear as Pottal Pool rock (in the second part of the experiment) had to be calculated. Assuming a linear wear regime, the rate of wear for Judkins rock is given by:

$$\textbf{Rate of Wear}_{(J)} = \frac{TW(g/T)_J}{T(h/T)} \qquad 9.12$$

where $\mathbf{TW(g/T)_J}$ is total wear per tonne of rock and $\mathbf{T(h/T)}$ is the crushing time per tonne of rock. The crushing time required by Judkins rock to produce the same wear as 250 kg of Pottal Pool rock is thus given by:

$$T_{(Eq.J)} = \frac{TW(g/T)_{(PP)}}{\text{Rate of Wear}_{(J)}} \qquad 9.13$$

Where $\mathbf{T_{(Eq.J)}}$ is the equivalent crushing time for Judkins rock, and $\mathbf{TW(g/T)_{PP}}$ is the total wear measured for Pottal Pool rock. Substituting for the values of each parameter from Table 9.4, the equivalent crushing time is given by:

$$T_{(Eq.J)}(\text{hour}) = \frac{390}{48/4.5} = 36.56 \qquad 9.14$$

Figure 9.1 shows the size distribution of the product with the new and worn liners. The 80% passing size and the measured $\mathbf{K_1}$ and $\mathbf{K_2}$ for each case are shown. $\mathbf{K_1}$ does not show a significant change over the tested range. Assuming the change in the profile of liners to be linear in time, $\mathbf{L(t)}$ is given by:

$$\frac{dL(t)}{dt} = \frac{dK_2}{dt} \qquad 9.15$$

$$\frac{dL(t)}{dt} \approx \frac{K_{2(Old)} - K_{2(New)}}{T} = \frac{7.2-8.1}{36.56} = -0.025(mm/h) \qquad 9.16$$

Thus substituting for different terms in Equations 9.10 and 9.11, the modified model parameters $\mathbf{K_1}$ and $\mathbf{K_2}$ incorporating the real-time effects of wear, for the laboratory size cone crusher used are given by:

$$K_1(t) = -0.16 + 0.54(CSS + W_T t) \qquad 9.17$$

$$K_2(t) = 3.25 + 1.30(CSS + W_T t) - 0.025t \qquad 9.18$$

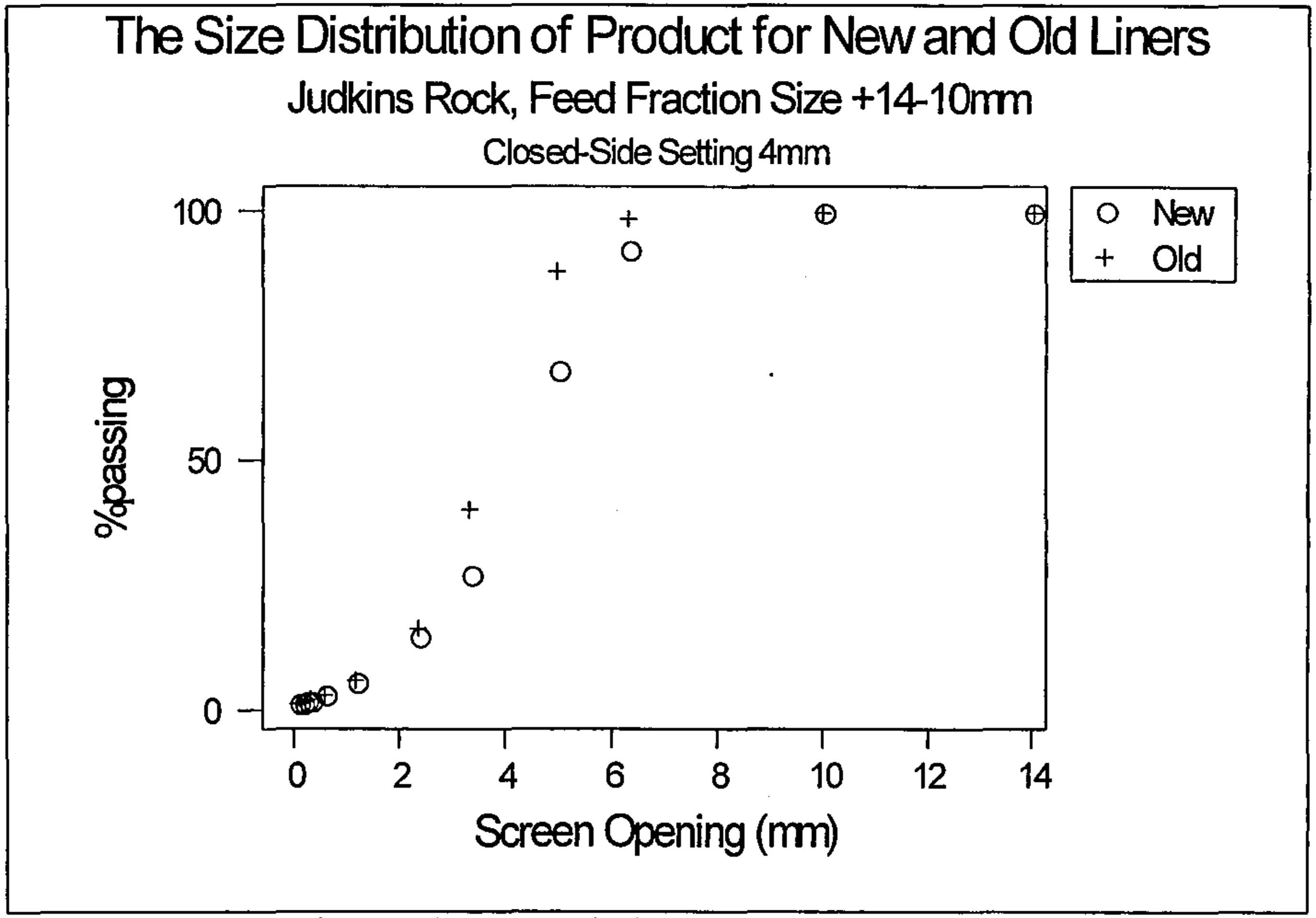

%80 Passing Size (mm): 'New' = 5.2 ; 'Old'= 4.8 - K_1 (mm) : 'New' = 2.1 ; 'Old'= 2.0 K_2 (mm) : 'New' = 8.1 ; 'Old'= 7.2 .

Figure 9.1 Effect of Liner 'Age' on product size

where $\mathbf{W_T}$ is the total rate of thickness loss in mm/hour, and $\mathbf{t}$ is the time since the last setting in hours. Including the effect of moisture, from Equations 9.5 and 9.6, $\mathbf{K_1}$ and $\mathbf{K_2}$ are given by:

$$\mathbf{K_1(t) = 0.21 + 0.49(CSS + W_T t) - 0.60Moist}$$

9.19

$$\mathbf{K_2(t) = 1.54 + 1.58(CSS + W_T t) - 0.025t - 0.68Moist} \qquad \mathbf{9.20}$$

9.4.3 A Time-Dependant Cone Crusher Model

Equations 9.19 and 9.20 in a general form are given by:

$$\mathbf{K_1(t) = a_1 + a_2(CSS + W_T t) - a_3 Moist}$$

9.21

$$\mathbf{K_2(t) = b_0 + b_1(CSS + W_T t) - b_2 t - b_3 Moist} \qquad \mathbf{9.22}$$

A time-dependant Classification Function incorporating the effect of moisture and liner wear can therefore be defined as:

$$\mathbf{C(x,t) = 0} \qquad \mathbf{x < K_1(t)}$$
$$\mathbf{C(x,t) = 1 - [\,(K_2(t) - x)\,/\,(K_2(t) - K_1(t))\,]^{K_3}} \qquad \mathbf{K_1(t) < x < K_2(t)}$$
$$\mathbf{C(x,t) = 1} \qquad \mathbf{x > K_2(t)}$$

where x is the particle size and $\mathbf{K_3}$ the third machine dependant model parameter defined by Whiten (1972) . A modified version of the Whiten's crusher equation can therefore be given as;

$$\mathbf{p(t) = [I - C(t)] \times [I - B \times C(t)]^{-1} \times f} \qquad \mathbf{9.23}$$

where $\mathbf{p(t)}$ is the time dependant product vector, $\mathbf{f}$ is the feed vector, $\mathbf{C(t)}$ is the time-dependant Classification Function, $\mathbf{B}$ is the Breakage Function and $\mathbf{I}$ is the unity matrix. Equation 9.23 provides a Time-Dependant Cone Crusher Model, incorporating the effects of liner wear and moisture. This model was used as the basis for a Model-Based Adaptive Control strategy for cone crushers as described in the following sections.

9.5 Model-Based Adaptive Control strategy for Cone Crushers

9.5.1 Real-Time Compensation of Closed-Side Setting for Wear

In order to keep the product vector **p(t)** in Equation 9.23 constant, the effect of wear on the model parameters, $\mathbf{K_1}$ and $\mathbf{K_2}$ must be compensated. Differentiating both sides of Equations 9.21 and 9.22, it follows that:

$$\frac{dK_1}{dt} = a_1\left[\frac{dCSS}{dt} + W_T\right] \qquad 9.24$$

$$\frac{dK_2}{dt} = b_1\left[\frac{dCSS}{dt} + W_T\right] - b_2 \qquad 9.25$$

Thus, to keep the size distribution of the product consistent, the closed-side setting needs to be changed as follow:

$$\frac{dCSS}{dt} = \frac{b_2}{b_1} - W_T \qquad 9.26$$

which leads to a constant $\mathbf{K_2}$ and a slightly increased $\mathbf{K_1}$ that helps to decrease the volume of produced fines.

9.5.2 The Adaptation Strategy

As discussed in Chapter Two, the adaptive control strategy is most useful in situations where the dynamics of the plant varies in time. Cone Crushing process falls within this category due to the effects of variation in ore properties and the wear induced change in liner profile. The Crusher Model, Equation 9.23, is used to define the optimum crusher setting for a given ore and product size distribution vector **P**. Recalling the general equation for Model-Based Adaptive Control, Equation 2.34 (Butler 1992), the adaptation strategy is given by:

$$dv_i / dt = [-k\, \partial e / \partial v_i]\, e \qquad i = 1,..\, n \qquad 2.34$$

where v_i are the adjustable control parameters available, and e is the model error given by:

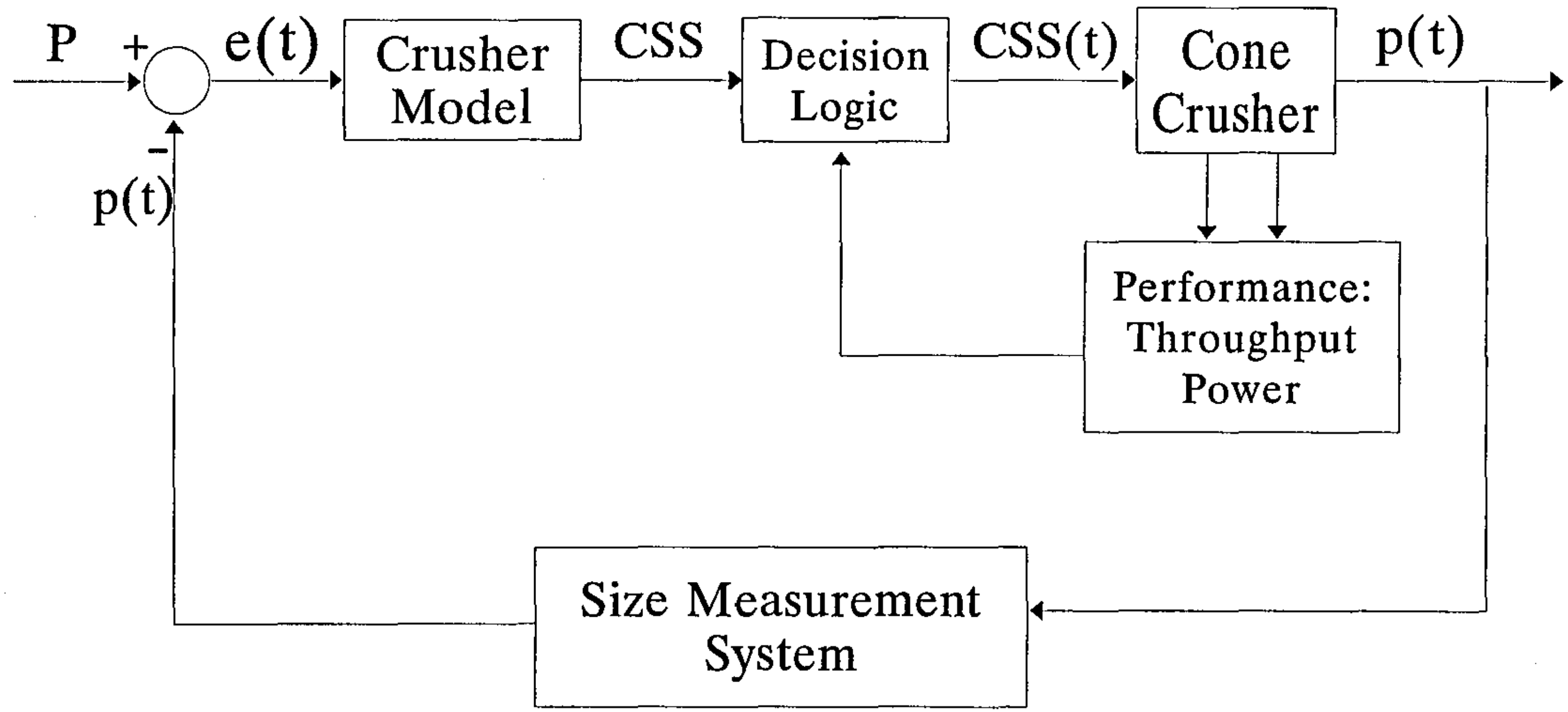

Figure 9.2 The Adaptation Strategy

$$e = \{y_k\}-\{y_{Mk}\} \qquad 2.35$$

where y_k is plant output, and y_{Mk} is the model output (required output). In cone crushing, the only control parameter available is the size of the closed-side gap. therefore the required adaptation is based on minimizing the error vector:

$$\mathbf{e(t)=p(t)-P} \qquad 9.27$$

The product size distribution vector **p(t),** must be determined by an on-line particle size measurement system. A new measurement system based on two-dimensional sensing technique was designed to cope with high volumes of partially overlapping rock particles which has obtained a grant for further research.

The optimization procedure relies on the minimization of the error vector, **e(t),** while keeping the throughput within a pre-defined range. The method of steepest ascent (Centner & Idelsohn 1963), represents one of the appropriate techniques for this purpose. The size of the incremental change in the closed-side setting is recursively calculated from solving the Time-Dependant Crusher Model for error vector **e(t)**. The adaptation strategy is shown in Figure 9.2.

9.5.3 The Closed-Loop Control System

The designed cone crusher control system consists of three loops shown in Figure 9.3. Two of the loops are cascaded. The outer loop calculates the optimum crusher setting, using adaptive control strategy discussed above, and the inner loop controls the positioning of the upper frame to actuate and maintain the crusher setting. A feedforward loop is used for wear compensation. The wear can be either be measured directly, or predicted using the developed wear models. The design is based on the well-proven architecture, where the main disturbance in the system, the liner wear in this case, is feedforwarded so that it is compensated for before the output is affected.

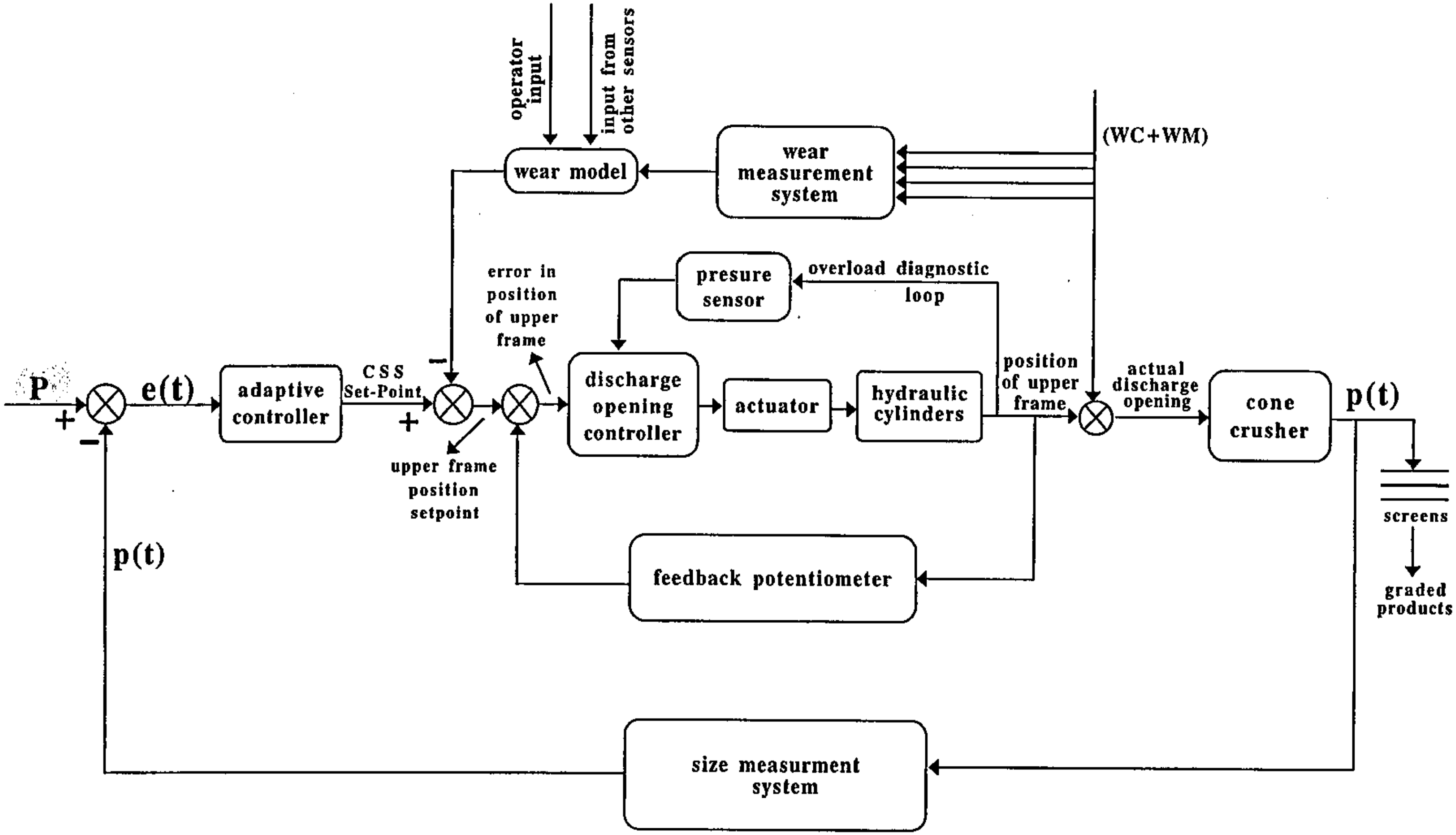

Figure 9.3 Block diagram of the closed-loop control system

The cascading feedback loops, on the other hand, represents an inherently robust design for providing a two-tier sampling rate and response time. The speed of the inner loop is commonly set to at least three times that of the outer loop. In the case of the cone crusher system, the outer loop sampling time must be long enough to allow the process to settle between the changes made. However, the inner loop response and sampling time must be fast enough to cope adequately with any overloading situation which may arise.

As discussed previously, the novel action of the designed control system is to maintain the optimum closed-side setting by compensating for liner wear. Calculation of optimum closed-side setting for a given product size, i.e. the task carried out in the outer cascading loop, has already been attempted in several simulation programs for the selection of crushing circuits (Bearman 1991). The action of the inner cascading loop, i.e. control of closed-side setting through the feedback loop for the positioning of the upper frame, the overload diagnostic loop and power monitoring and optimization loop are used in many existing cone crusher controller units. However, the combination of these elements would provides a comprehensive real-time strategy for optimization of cone crushers performance.

9.5.4 The Simulation Study of Wear Compensation Loop

To investigate the performance of the proposed feed-back control system, in comparison with existing cone crusher control methods, the MATLAB and Simulink mathematical modelling and simulation packages were used.

Figure 9.4 shows the system block diagram for the real-time controller, in the Laplace domain, produced using Simulink.. The general transfer functions of various system components are also shown. Figure 9.5 shows the block diagram of the existing System 4 cone crusher controller unit, comprising a feedback loop for control of crusher setting, but no facility for wear compensation, which were considered in an open-loop off-line mode.

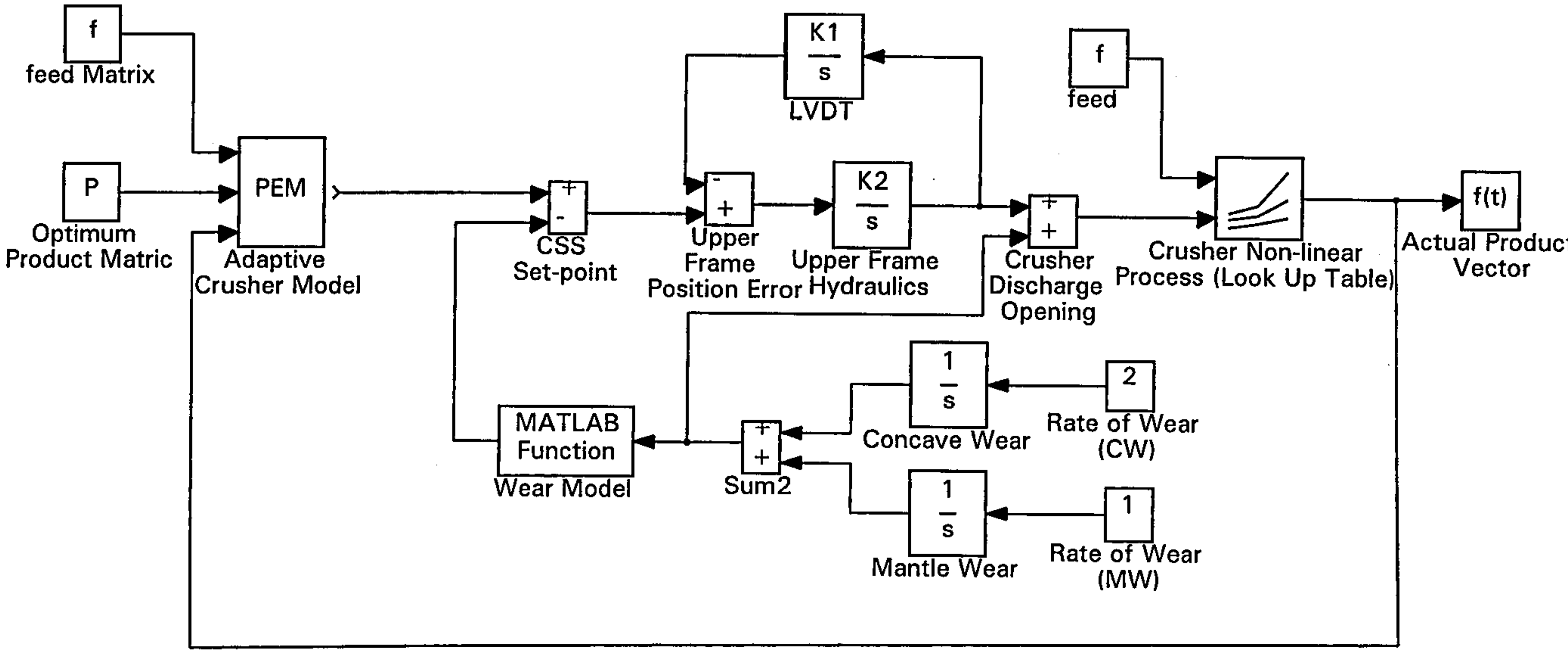

Figure 9.4 The general block diagram of the real-time control system

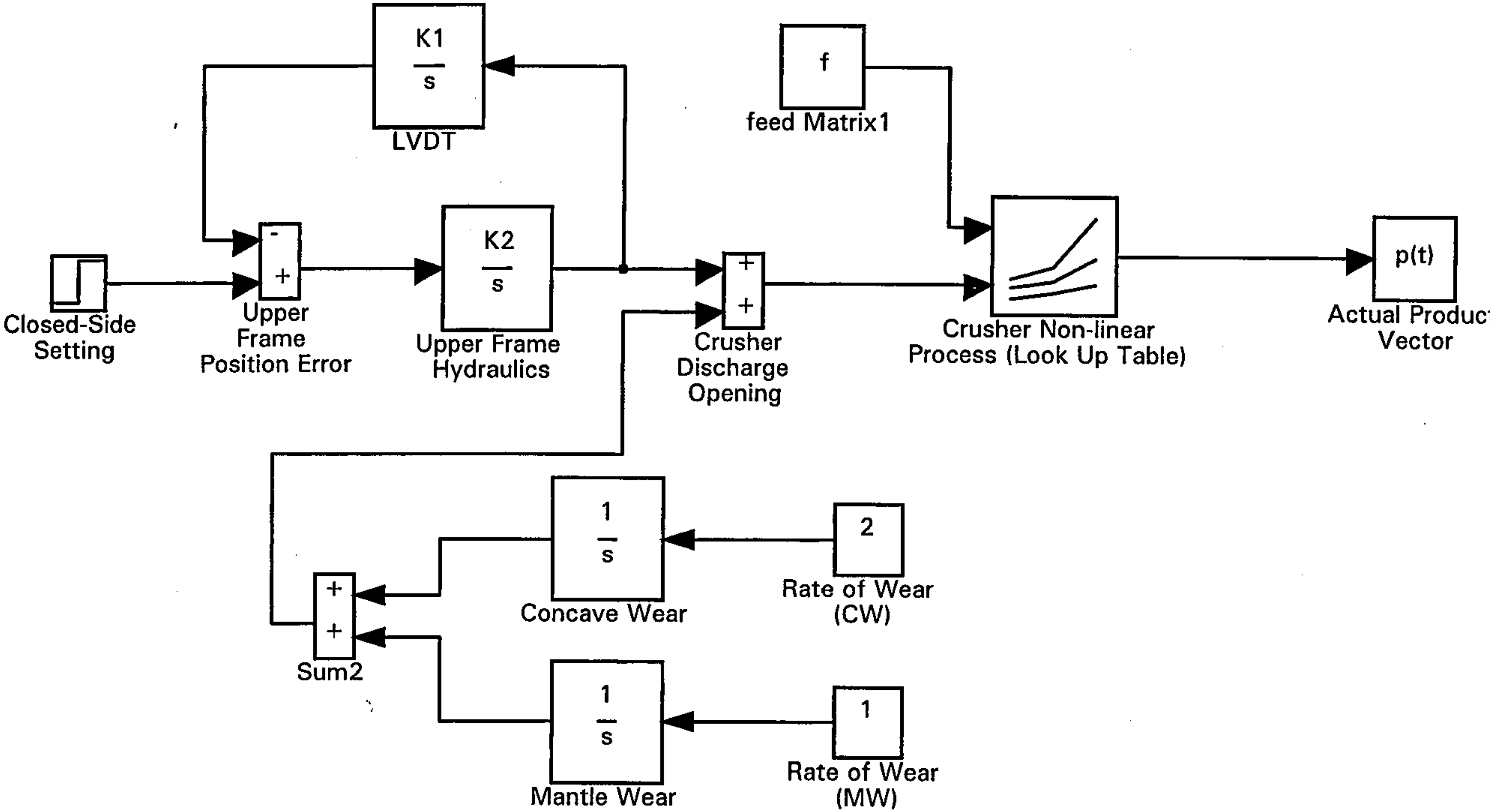

Figure 9.5 The block diagram of the existing cone crusher control systems

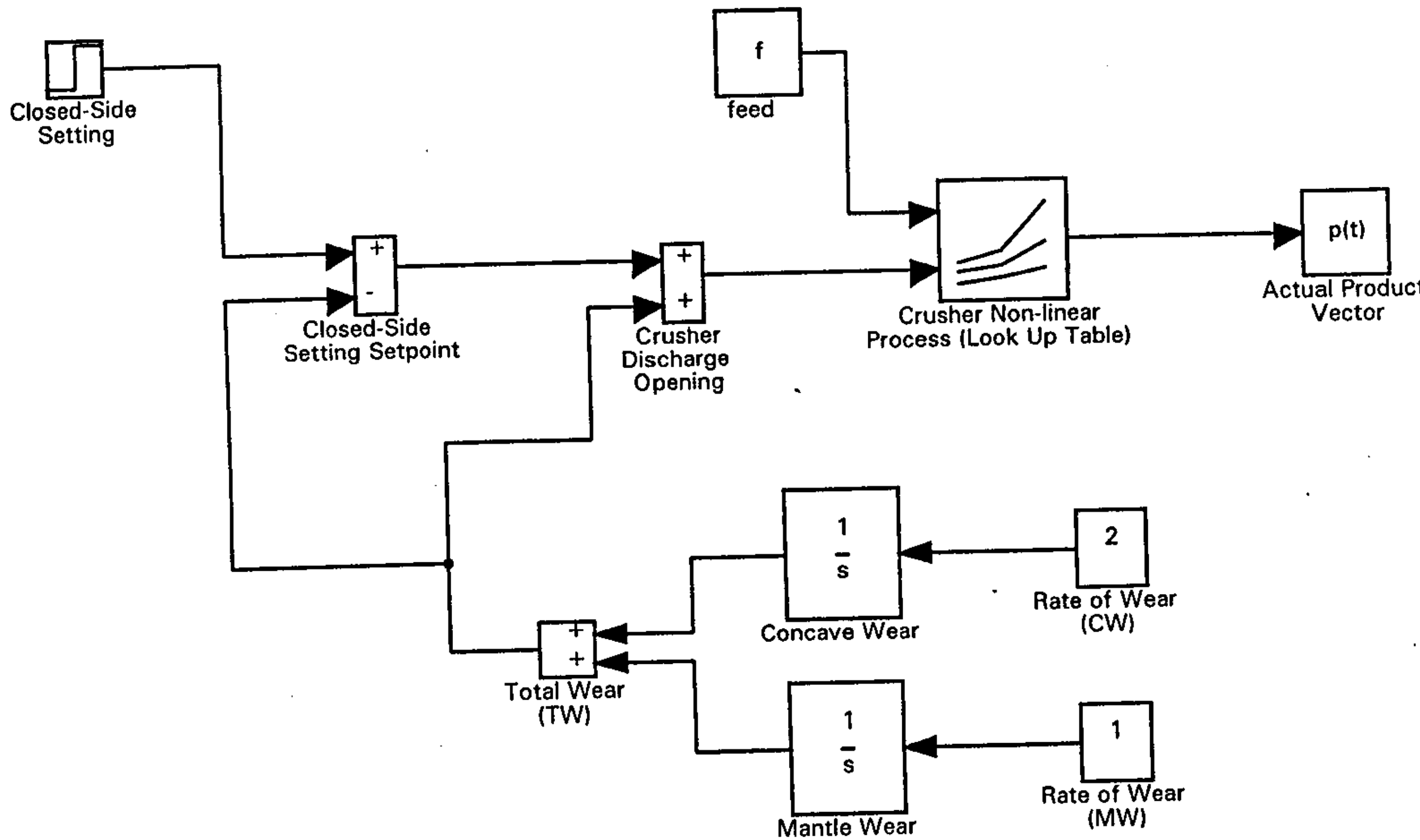

Figure 9.6 The reduced block diagram for MATLAB simulation of real-time compensation of wear

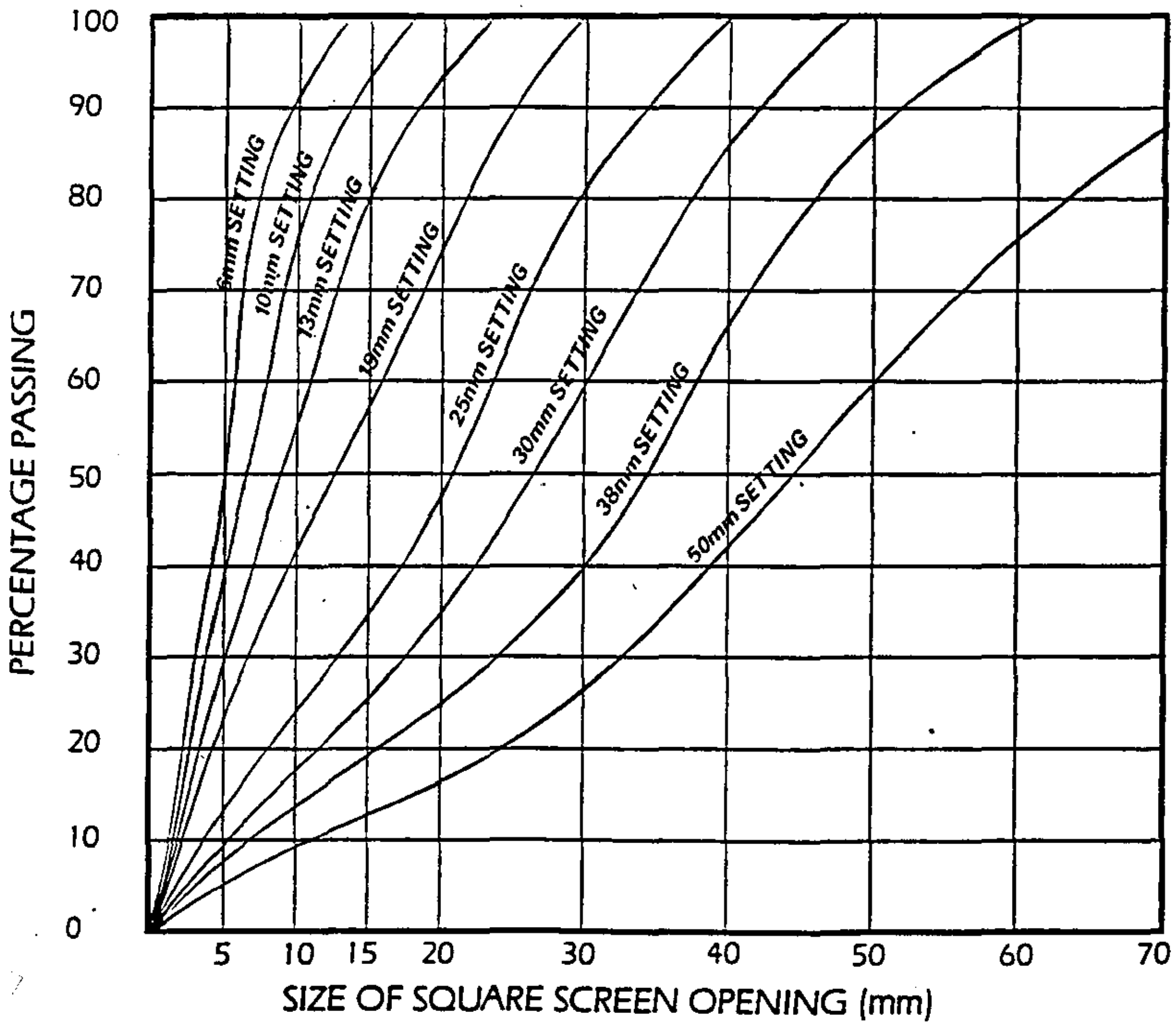

Figure 9.7 The expected product size dirstribution for Autocone 900 medium fine cone crusher

Figure 9.6 shows the reduced block diagram of the real-time control system, used for simulation. The simulation parameters used are shown in table 9.5.

Table 9.5 The Simulation Parameters

cone crusher type	Autocone 900 Medium Fine
feed fraction size	-20+14 mm, constant rate
concave wear rate	0.25 mm/h, parallel profile
mantle wear rate	0.25 mm/h, parallel profile
coefficient used for L(t)	0.025 mm/h
optimum product size	5mm - 15mm
original closed-side setting	10 mm
re-setting downtime	15 minutes

Figure 9.7 shows the expected size distribution of the product for Autocone 900 medium fine cone crusher . The size distribution curves were used to produce a look up table to represent the non-linear crushing process by a general and, in this case, rock independent transfer function.

9.5.5 Simulation Results and Discussion

Three simulation runs were carried out corresponding to three possible wear compensation methods: I) no wear compensation at all, II) off-line wear compensation at eight hourly intervals, and III) real-time wear compensation with a 1 hour sampling time. All other simulation parameters were kept constant for all three simulation runs. The simulated performance was compared in terms of the variation in the closed-side opening and product quality. To consider the product quality in objective terms, two size characteristics were defined as follow:

1. the percentage of product with the correct size specified as product vector **P**, %CS, in this case 5mm to 15mm;,

2. the percentage of product with a size above that specified by the product vector **P**, %OS, in this case with a size over 15mm.

Figure 9.8 shows the results of the three simulation runs. It can be seen that without compensation for wear, case I, the size of discharge opening drifts continuously causing a degradation in the product quality where the volume of correctly sized aggregate decreases and the volume of oversize aggregates increases. With off-line compensation, case II, the drift continuous between the re-setting exercises. The loss of production during re-setting downtime (15 minutes) is also shown. Although the product quality is better than the previous case, the average oversize volume remains high. The real-time compensation of wear, case III, exhibits major benefits over the off-line compensation case. No considerable variation in discharge opening and product quality is observed. The oversize re-circulated particles remains minimum as dictated by the Breakage Function. The elimination of the re-setting downtime, leads to a further increase in crusher efficiency. The benefits of a real-time wear compensation capability in the framework of an adaptive control strategy are therefore very significant.

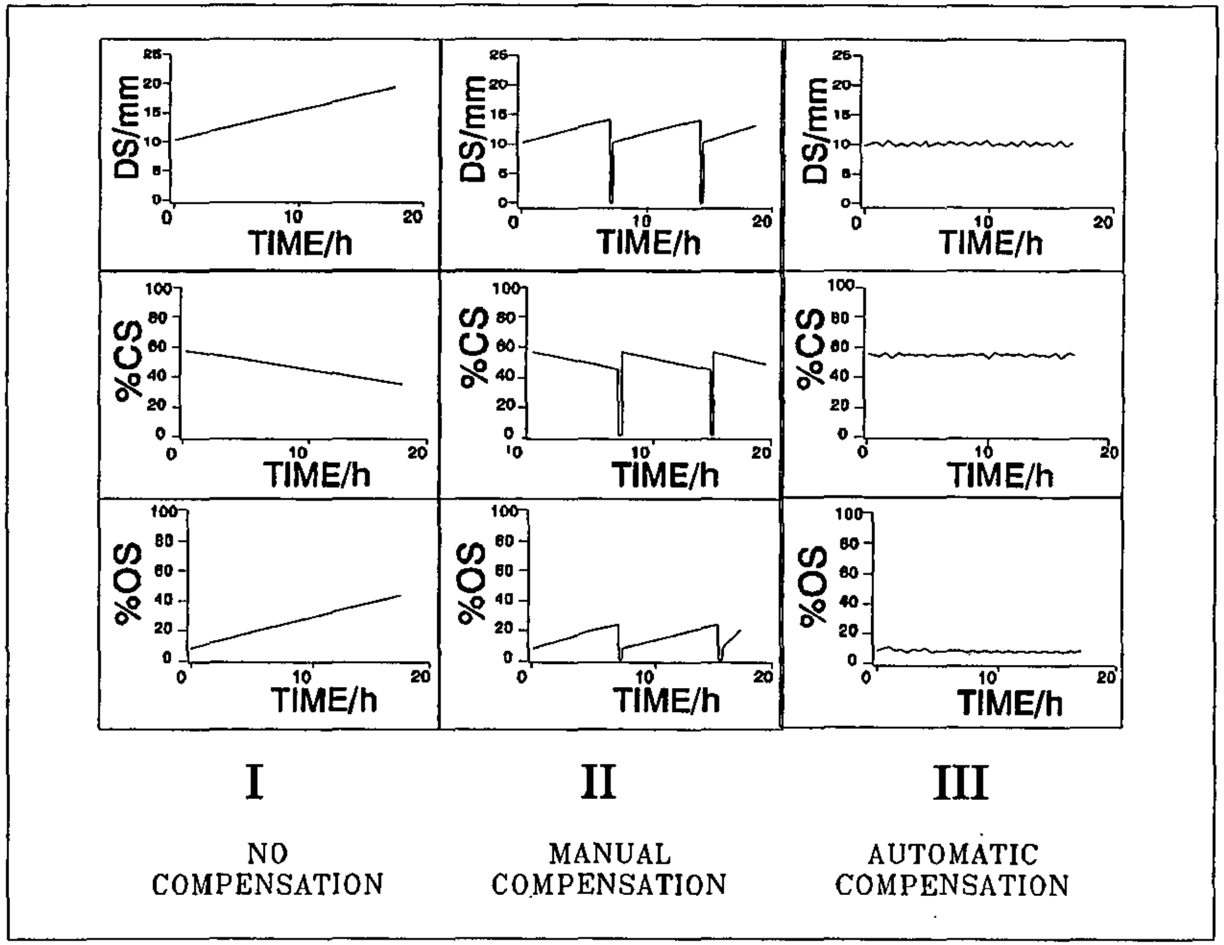

Figure 9.8 Comparison of three wear compensation strategies on product quality : I- no wear compensation; II- off-line wear compensation; III- real-time wear compensation

Chapter 10 THE APPLICATION OF FUZZY MODELLING TECHNIQUE TO THE PREDICTION OF LINER WEAR

The prediction of liner wear, using the models presented in the previous chapters, relies on an exact knowledge of rock properties, and added moisture. The rock properties can be measured, with reasonable accuracy, by the standard tests recommended by the international bodies. The amount of water added, on the other hand, is not always accurately controlled or measured. However, the addition of a relatively small amount of water to the cone crusher feed, can have a substantial impact on the observed wear.

As discussed in Chapter 2, Fuzzy mathematics is now widely accepted as a robust method for dealing with system uncertainties. It was therefore decided to apply the method to the prediction of liner wear, so that any uncertainty in the moisture level could be accommodated. The following section describes the Fuzzy wear model and a software application programme, in Turbo C++, that was written to carry out the necessary calculations for the Fuzzy model. The programme provides an interactive environment for selection of the rock properties and operating parameters from which, the expected rate of liner wear is calculated.

10.1 The Fuzzy Wear Model

10.1.1 The Linguistic Moisture Variable

A Fuzzy set with five linguistic variables, was defined to represent the moisture values considered in the experimental study. Figure 10.1 shows the membership function assigned to each linguistic variable. Each variable can be represented in mathematical notation by a two dimensional array. The elements of the array consist of the discrete moisture levels and their corresponding membership values. Using this notation the Fuzzy variables can be represented as follow:

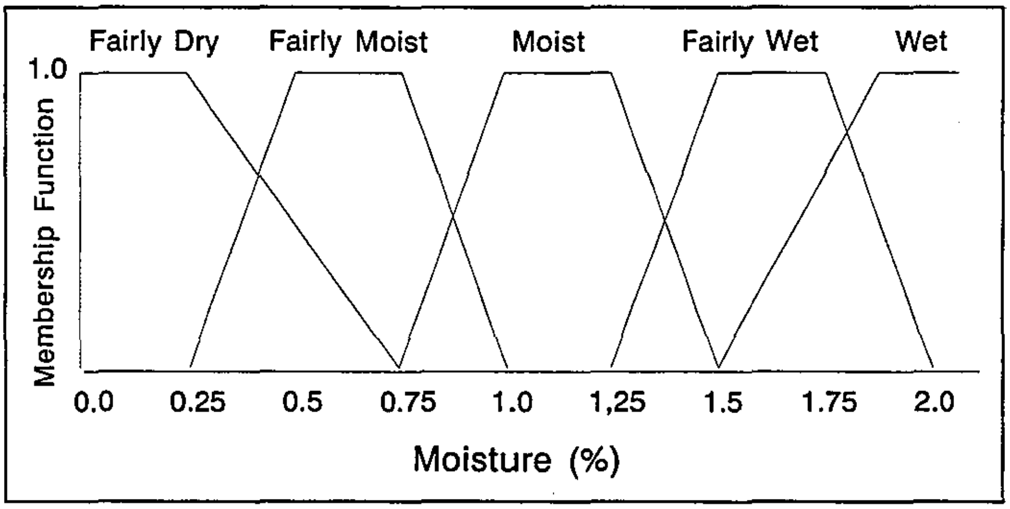

Figure 10.1 The membership function of the Fuzzy moisture variables

Fairly Dry :	[0,0 ; 0.25,1 ; 0.5,0.5 ; 0.75,0 ; 1.0,0 ; 1.25,0 ; 1.5,0 ; 1.75,0 ; 2.0,0]
Fairly Moist:	[0,0 ; 0.25,0 ; 0.5,1 ; 0.75,1 ; 1.0,0 ; 1.25,0 ; 1.5,0 ; 1.75,0 ; 2.0,0]
Moist:	[0,0 ; 0.25,0 ; 0.5,0 ; 0.75,0 ; 1.0,1 ; 1.25,1 ; 1.5,0 ; 1.75,0 ; 2.0,0]
Fairly Wet :	[0,0 ; 0.25,0 ; 0.5,0 ; 0.75,0 ; 1.0,0 ; 1.25,0 ; 1.5,1 ; 1.75,1 ; 2.0,0]
Wet :	[0,0 ; 0.25,0 ; 0.5,0 ; 0.75,0 ; 1.0,0 ; 1.25,0 ; 1.5,0 ; 1.75,0.75 ; 2.0,1]

10.1.2 The Fuzzy Inference Technique

To predict the rate of wear using the Fuzzy variable set the following Fuzzy statement should be evaluated:

IF **Moisture** IS **Moist$_i$** THEN **Wear** IS **f(Moist$_i$)**

where **Moist$_i$** is the linguistic moisture level, and **f(Moist$_i$)**, which reads 'function of Moist$_i$ ', is the relevant model equation.

To evaluate **f(Moist$_i$)**, the moisture term in the appropriate model equation is first replaced by the Fuzzy matrix for **Moist$_i$**. The equation is then evaluated using Fuzzy algebra. This gives another two dimensional matrix, which represents the Fuzzy set for the expected rate of wear. To calculate a crisp value for rate of wear, the Fuzzy wear is defuzzified using one of the methods discussed in Chapter 2.

The inference procedure is demonstrated in the following example which considers the wear due to Cliffe Hill rock at a crusher setting of 4mm, when feed has been described as being "Fairly Dry". The rock specific model for total wear due to moist Cliffe Hill rock, given in Chapter 6, has been used. The model equation is given by:

$$\mathbf{TW/(g/T)} = -6.3 + 42\ \mathbf{1/CSS} + 362\ \mathbf{1/CSS^2} - 15.1\ \mathbf{Moist} + 7.49\ \mathbf{Moist^2} + 80.9\ \mathbf{Moist/CSS} \qquad \mathbf{10.1}$$

Replacing the moisture terms with the matrix for "Fairly Dry" and substituting for CSS (4mm):

$$\mathbf{TW/(g/T)} = -6.3 + 42/4 + 362/16 - 15.1\ \mathbf{[F.D]} + 7.49\ \mathbf{[F.D]^2} + 80.9/4\ \mathbf{[F.D]} \qquad \mathbf{10.2}$$

where [F.D] is the matrix for the Fuzzy variable "Fairly Dry" given above. Eliminating the terms with a zero membership value the matrix reduces to:

$$\mathbf{[\,F.D]} = [0.25,1\ ;\ 0.5,0.5] \qquad \mathbf{10.3}$$

Calculating the first few terms in the equation:

$$\mathbf{TW/(g/T)} = 26.8 - 15.1\ \mathbf{[F.D]} + 7.49\ \mathbf{[F.D]^2} + 20.2\ \mathbf{[F.D]} \qquad \mathbf{10.4}$$

The first term in the above equation, i.e. 26.8, is the rate of wear for dry rock. The contribution to the rate of wear due to moisture is therefore equal to the sum of the Fuzzy terms. These terms are calculated by multiplying the coefficient with the first term in the matrix rows. As explained above, these are the discrete moisture levels. The second term in each row, i.e. the membership value assigned to the discrete moisture levels, are kept the same, i.e. :

$$15.1\ \mathbf{[F.D]} = [\,(15.1\times 0.25\,),1\ ;\ (15.1\times 0.5),0.5\,] = [\,3.7,1\ ;\ 7.5,\ 0.5\,]$$

$$7.49\ \mathbf{[F.D]^2} = [\,(7.49\times 0.25\times 0.25),1\ ;\ (7.49\times 0.5\times 0.5),0.5\,] = [\,0.93,1\ ;\ 1.87,0.5\,]$$

$$20.2\ \mathbf{[F.D]} = [\,(20.2\times 0.25),1\ ;\ (20.2\times 0.5),0.5] = [5.5,1\ ;\ 10.1,0.5]$$

Figure 10.2 shows the Fuzzy set representing the above three wear matrices, denoted 1,2, and 3 on the diagram.

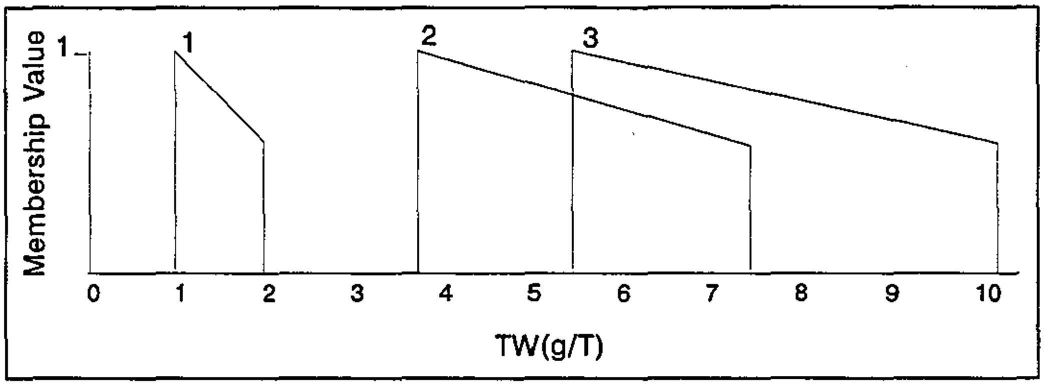

Figure 10.2 The Fuzzy wear sets

10.1.3 The Defuzzification Process

To calculate the crisp rate of wear, the Fuzzy set for wear must be defuzzified. Using the method of centre of gravity, it follows that:

$$\text{TW/(g/T)} = 26.8 - [(1\times 3.7)+(0.5\times 7.5)/2] + [(1\times 0.9)+(0.5\times 1.9)/2] + [(1\times 5.5)+(0.5\times 10.1)/2] \quad \textbf{10.5}$$

$$\text{TW/(g/T)} = 26.8 - 3.75 + 0.925 + 5.275 = 29.25 \quad \textbf{10.6}$$

Using the averaging method for defuzzification process would give:

$$\text{TW/(g/T)} = 26.8 - [(3.7+7.5)/2] + [(0.9+1.9)/2] + [(5.5+10.1)] \quad \textbf{10.7}$$

$$\text{TW/(g/T)} = 26.8 - 5.6 + 1.4 + 7.8 = 30.4 \quad \textbf{10.8}$$

In general, the choice about the defuzzification technique must be made on the basis of a validation exercise to ensure the best match between the predicted and measured values.

10.2 The Application Program for Prediction of Liner Wear In Cone Crushers

To automate the prediction of the rate of wear using the models developed in this and previous Chapters an application software, named the Wear Analyser System, was developed using Turbo C++ language. The software provides an interactive environment where the input of the relevant information about rock type and properties, crusher setting and added moisture fires an appropriate wear model. The execution of the wear model would provide an estimate of the total liner wear in gram per Tonne of rock.

Figure 10.3 shows the flowchart of the Wear Analyser System. The user interface consists of a number of menu screens. The opening screen is shown in Figure 10.4. The information about rock name and properties is either selected from a list containing eight of the more abrasive rock types tested, or inputted via the "other" option. The second screen summarizes the relevant properties of the rock type and request the input of the value for the closed-side setting , Figure 10.5. The third screen, Figure 10.6, initializes the system according to the information regarding the moisture content. If the user specifies that moisture is present but not quantified, the Fuzzy wear model would be invoked. For dry or moist rock of known moisture level the non-fuzzy models would be selected. The last screen summarizes the input data and the estimated rate of wear, Figure 10.7.

The appropriate model is chosen by the programme on the basis of the hierarchy shown in Figure 10.8. This structured approach ensures that the wear would be estimated using a model with the least number of variables and therefore highest accuracy. For example to estimate the wear due to a dry rock which was included in the experiments, the best model would be the corresponding rock-specific model for dry wear. Other more general models, the rock-specific model for moist rock or the general wear models for dry and moist rocks would provide a less accurate estimate and therefore would not be appropriate. Appendix 5 presents the listing of the software code

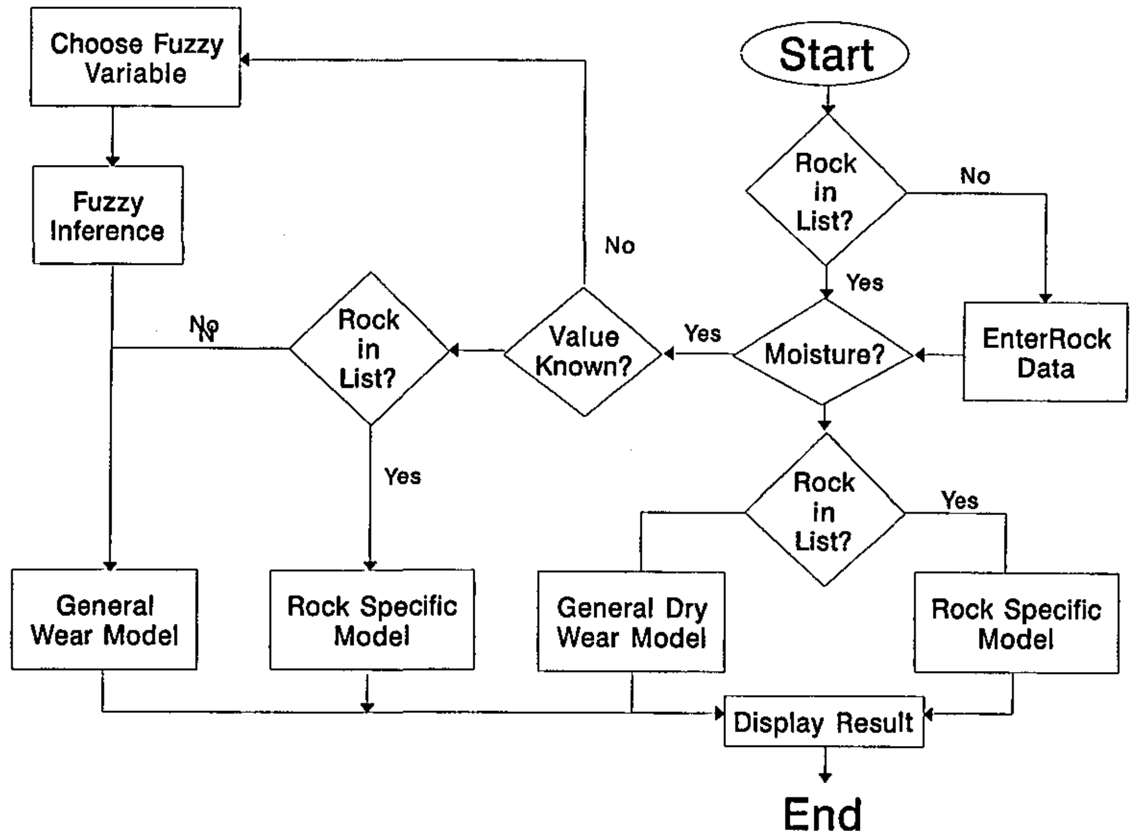

Figure 10.3 The flowchart of the Wear Analyser System

```
*************************************************************
              WEAR  ANALYSER  PROGRAMME
*************************************************************

                 1.      Cliffe Hill Rock
                 2.      Ingleton Grey Rock
                 3.      Judkins Rock
                 4.      Pottal Pool Rock
                 5.      Shap Blue Rock
                 6.      Shardlow Rock
                 7.      Whitwick Rock
                 8.      Waterswallows Rock

                 9.      Other..

          Enter a number:                          3
```

Figure 10.4 The opening screen of the Wear Analyser System

```
*************************************************************
              WEAR  ANALYSER  PROGRAMME
*************************************************************

                       Rock Properties

     Silica Content(%)                                53.8
     Brazilian Tensile Strength(MPa)                  14.16
     Aggregate Abrasion Value                         6.7
     Water Absorption (%)                             0.7
     PH                                               6.6

-------------------------------------------------------------------------------

     Enter Crusher Setting (mm):                      4

     Is Water Added To the Rock?(y/n)                 y
     Is the Amount of Added Water Known? (y/n)        n

Which one of the following phrases best describe the rock moisture level:

          1. Fairly Dry      2.  Fairly Mois      3.  Moist
                   4.  Fairly Wet       5.  Wet

          Please Enter a number (1-5):                       3
```

Figure 10.5 The second screen of the Wear Analuser System

```
**********************************************************
                 WEAR  ANALYSER  PROGRAMME
**********************************************************

                        Rock Properties

Silica Content (%)                                    53.8
Brazilian Tensile Strength(MPa)                       14.16
Aggregate Abrasion Value                              6.7
Water Absorption (%)                                  0.7
PH                                                    6.6

---------------------------------------------------------------

Is Water Added To the Rock?(y/n)                      y
Is the Amount of Added Water Known? (y/n)             y

Please enter the amount in (% of rock weight)         1.5
```

Figure 10.6 The third screen of Wear Analyser System corresponding to non-Fuzzy model

```
**********************************************************
              WEAR   ANALYSER   PROGRAMME
**********************************************************

                        SUMMARY

   Silica Content (%)                          53.8
   Brazilian Tensile Strength (MPa)            14.16
   Aggregate Abrasion Value                    6.7
   Water Absorption (%)                        0.7
   PH                                          6.6

------------------------------------------------------------------

   EXPEXTED RATE OF WEAR (g/T)                     38.00

------------------------------------------------------------------
```

Figure 10.7 The final screen of the Wear Analyser System showing the estimated rate of wear

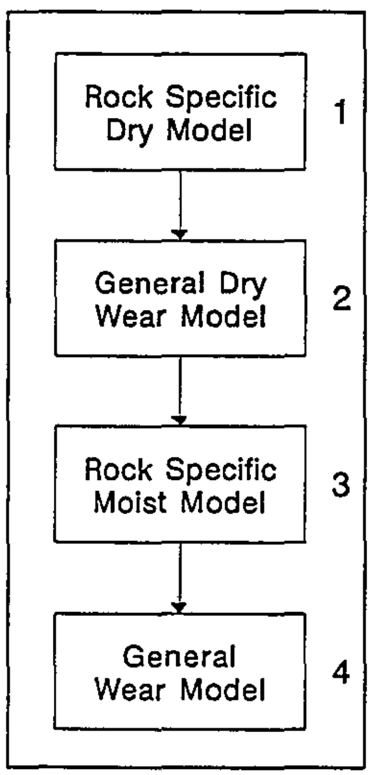

Figure 10.8 The hierarchy of the chosen wear models

Chapter 11 DISCUSSION

The aims of this project were to examine liner wear in cone crushers and its impact on crusher performance and product quality and hence design a control system capable of compensating its adverse effects. This involved a multi-disciplinary investigation comprising experimental study of liner wear, development of predictive and process models and control system design.

Although based on the tests utilizing a laboratory size cone crusher, the findings of the project are expected to be representative of those anticipated for an industrial cone crusher. This belief is based on the close similarity in kinematics of the two systems. The belief is further strengthened by the encouraging results of the comparison of the laboratory measured and industrially observed wear rates for two of the rocks.

11.1 Tribology of the Cone Crusher

The tribology of cone crushers in terms of system kinematics, mechanisms of contact and material removal, and classification of the involved wear process has been investigated for the first time. The following summarizes the main finding of the investigation, based on both industrial and laboratory tests and studies:

1. The majority of wear scars on liner surface, under a low magnification, were found to be spiral in shape. Also present were the less frequent but deeper straight scratches. This observation suggests that the rock particles rotate while sliding across the liners and hence the contact between rock and liners is not primarily a sliding one.

2. Considering the measured values of average roughness, $\mathbf{R_a}$, measured using a contact TALYSURF stylus system, the surface roughness decreases from top of the liner (feed opening) to the bottom. This can be explained by considering the size effect of rock particles. At the top of the crushing chamber the rock particles are larger with sharper edges causing deeper wear scars and hence a higher surface roughness. As the rock particles progress down the crushing chamber, their size reduces which leaves a generally finer wear scar. The effect is similar to the difference in the surface texture obtained when a coarse and fine abrasive grain is used to abrade a surface.

3. Detailed examination of the samples taken from different sections of worn liners, using a Scanning Electron Microscopy technique, has revealed that the wear process in all parts of the two liners is largely identical and primarily due to abrasion with a secondary contribution from surface fatigue and impact modes of wear.

4. Based on the study of system kinematics, the wear regime in cone crushers was found to fall within the category of open-three body abrasive wear, changing from low stress to high stress wear mode along the length of the liners. The observed differential wear along the liners is due to this change and is explained by the intensification in the crushing torque along the nip angle.

5. Comparison of the wear scars caused by ten different rock types has shown that the dominant mechanism of material removal varies according to the rock hardness and abrasivity. For harder more abrasive rocks, the dominant mechanism of wear is micro-cutting with large number of deeper cuts and micro-fractures. For the soft and less abrasive rock types, ploughing, wedge forming and plastic deformation are the dominant mechanisms

11.2 Quantitative Study of Wear and The Predictive Models

The classification of wear process and mechanisms of material removal in cone crushers has made it possible to identify, scientifically, the significant parameters affecting liner wear.

The survey of the observed liner wear across the industry, along with the experimental investigation have proven that wear is dependant on a range of variables, that include crusher design and operating parameters as well as rock properties. Added moisture was also found to be highly significant.

11.2.1 Operational Parameters

For a given rock, and under constant operating conditions, the rate of wear was found to depend on the closed-side setting. For all rock types, a second order polynomial, based on the inverse of the closed-side setting, was found to adequately model the wear. The dependence of the wear on the closed-side setting can be explained, in fundamental terms, from the strong correlation that was found to exist between the setting and the throughput of the crusher. The setting controls the size reduction ratio and hence the length of the comminution cycle before a rock particle leaves the crushing chamber.

The size of the feed was also found to be significant and a smaller feed fraction size led to smaller rates of wear at the crusher setting of 4mm. The origin of the observation is once more due to the variation of the crushing time for different feed sizes at a constant crusher setting. The effect of the feed size was only tested at two levels which is not sufficient for statistical generalization. Therefore, feed size was not included in the general wear models.

11.2.2 Added Moisture

The wear due to moist rock is considerably higher than dry rock. The relationship between wear and moisture has been found to be non-linear. A second order polynomial in both closed-side setting and moisture content, and including an interaction term, was found to adequately model the wear. The interaction between the closed-side setting and moisture has been found to be particularly significant.

The two gravel type rocks tested showed an unusual characteristics. The wear decreased initially as moisture was increased. This may be due to the low water absorption of these rocks. In the case of non-gravel rocks, the addition of water created a sticky mixture of mud and rock which hindered the crushing process due to clogging. In contrast, no major clogging was observed for the two gravel rocks. In deed, the addition of moisture, up to one percent of rock weight, was found to assist the crushing process by reducing the crushing time.

With smaller feed size, no difference between gravel and non-gravel rocks was observed; and both rock types caused more wear as moisture was increased.

11.2.3 Rock Properties

Contrary to the common belief that the differing wear caused by different rock types can be explained on the basis of their hardness or silica content, the study showed that other rock properties are also highly significant. The strength parameters, BTS, FT, PL and UCS were found to correlate well with wear. However, the cross-correlation between these parameters means that only one of them could be included in the regression models. The impact of the strength parameters on wear originates from the fact that they affect the "crushability" of the rock and hence the crushing time for a given feed quantity. Among the strength parameters, BTS was found to provide the best correlation results. This further confirms the findings of Bearman (1991) that the mechanism of breakage in cone crushing is tensile failure.

The rebound hardness test was considered to be a more appropriate parameter than the penetration hardness tests. Rock hardness correlated strongly with silica content and was eliminated from the regression models. AAV showed a stronger correlation with wear than silica content. This is due to the test procedure which effectively incorporates the effect of any softer material in the rock structure on wear.

In the case of moist rock two other rock variables, Rock pH and water absorption, played a significant role in the extent by which added moisture accelerated the wear. It was found that in the case of acidic rocks with high water absorption rates, the effect of added moisture was the highest. In the case of Judkins rock for example, two per cent added water, at a crusher setting of 6mm, more than quintupled the wear, Table 11.1. This observation can be explained by the following considerations:-

1. The synergy between abrasive wear and corrosion:- this phenomenon can increase the wear considerably. This effect is expected to be higher under acidic condition. Due to this phenomenon, adding moisture to acidic rocks is expected to more significant than other rock types,

2. The rocks with higher porosity absorb more water and exhibit lower resistance to breakage. Higher volumes of fines are expected to be produced as a result of lower strength properties. The combination of high water absorption and excessive fines creates a higher degree of clogging and as a consequence, lower crusher throughputs. Therefore, adding identical amount of water to rocks of different water absorption, but similar pH, is expected to have distinct results

Table 11.1 Comparison of the Crusher Throughput And Total Wear for Different Moisture Contents And Feed Sizes

Rock	Water Absorption (% Rock Weight)	pH	Moist(%)	TH(T/h) Small Feed	TH(T/h) Large Feed	TW/(g/T) Small Feed	TW/(g/T) Large Feed
Cliffe Hill	-	-	0	0.468	0.277	16.67	28.00
Cliffe Hill	0.60	7.9	2	0.011	0.079	48.00	65.00
Ingleton Grey	-	-	0	0.552	0.319	4.05	16.00
Ingleton Grey	0.75	8.6	2	0.039	0.081	15.00	52.00
Judkins	-	-	0	0.483	0.220	16.66	12.00
Judkins	0.70	6.6	2	0.043	0.034	40.00	54.00
Pottal Pool	-	-	0	0.700	0.510	68.00	96.00
Pottal Pool	0.01	7.1	2	0.057	0.068	136.00	100.00
Shap	-	-	0	0.450	0.505	48.00	72.00
Shap	0.50	6.7	2	0.038	0.049	76.00	86.00
Shardlow	-	-	0	0.528	0.552	84.00	84.00
Shardlow	0.01	7.2	2	0.015	0.052	133.33	88.00
Whitwick	-	-	0	0.468	0.353	18.00	44.00
Whitwick	0.60	7.8	2	0.035	0.040	40.00	76.00
Waterswallows	-	-	0	0.341	0.300	4.05	16.00
Waterswallows	0.70	6.5	2	0.021	0.044	16.68	35.00

and for rocks of higher water absorption rate, the acceleration of the wear due to moisture is likely to be higher.

11.2.4 Relationship Between Wear and Crushing Time

The crushing time (the inverse of throughput) is the most fundamental variable affecting liner wear. In effect, it describes the highest possible contact time between a given rock particle and liners. However, as the wear models developed were intended to be predictive, the crushing time was not considered to be an appropriate model parameter and hence not included in the models.

As expected, a strong correlation was found between crushing time and closed-side setting. For all tests, the crushing time was found to decrease linearly as the closed-side setting was increased. This was accompanied by a corresponding decrease in wear. In the case of moist rock, the crushing time increased with added moisture except for the two gravel type rocks. As can be seen from Table A2.2, Appendix 2, the crushing time for these rocks decreases initially lowering the observed rate of wear.

Table 11.1 summarizes the observed total wear and crusher throughput, at a crusher setting of 4mm, for the two feed sizes and moisture levels of zero and 2%. As can be seen, the crushing time for smaller feed size exhibits a more complicated relationship with moisture and wear.

For dry rock the crushing time, in all the cases, was lower for the smaller feed size. This is accompanied by an equivalent reduction in wear. For moist rock the reverse was true and the observed crushing time was higher for the smaller feed size, Table 11.1. Yet despite this higher crushing times, in the case of non-gravel rock types the wear was found to be lower. These two apparently contradicting observations can be explained on the basis of the following observations:-

a. Crushing of the smaller feed size generally resulted in a finer product, as discussed in Chapter 8. This higher proportion of fines would cause a relatively higher degree of clogging, resulting in longer crushing times. This would explain the observed reduction in crusher throughput, shown in Table 11.1.

b. The combination of smaller feed particles and an excessive amount of moist and sticky fines could partially shield the liners, reducing the probability of effective contact with rock particles, represented by the constant **k** in Equation 2.14 :

$$\mathbf{V \propto k F_n L} \qquad \mathbf{2.14}$$

Under such conditions the observed volume of wear, **V** would be expected to reduce, as observed in the case of the wear due to smaller feed size combined with 2% moisture.

11.2.5 Performance Of The General Wear Model

The performance of the general wear models describing the relationship between rock properties, close-side setting, moisture and wear was tested using a comparison between the measured and predicted wear for Whitwick rock. Whitwick rock represents a non-gravel rock type of average abrasive properties which was not included in the data set for the general models. As discussed in Chapter 6, one of the two models is based on the data obtained for non-gravel rock types only, where as the other included these as well. Table 11.2 presents the measured and predicted wear values. It can be seen that the first model, based on non-gravel type rocks, provides a better prediction.

Table 11.2 Comparison Between Measured And Predicted Wear Values- Whitwick Rock

CSS/mm	Moist(%)	CW/(g/T)	Model 1	Model 2	MW/(g/T)	Model1	Model 2	TW/(g/T)	Model 1	Model 2
4.00	0.0	20.00	19.18	18.79	20.00	21.14	20.05	40.00	40.36	38.86
4.00	0.5	21.00	20.21	19.53	23.00	23.32	22.16	44.00	43.53	41.68
4.28	1.0	22.00	20.47	19.33	24.00	24.06	22.79	46.00	44.52	42.09
4.05	1.5	26.00	25.26	23.97	30.00	30.89	29.25	56.00	56.15	53.21
4.00	2.0	28.00	30.05	28.50	48.00	37.42	35.32	76.00	67.51	63.82
5.80	0.0	12.00	11.39	10.50	12.00	11.57	10.30	24.00	22.99	20.83
6.10	0.5	12.00	10.77	10.11	13.00	11.21	10.55	25.00	21.97	20.65
6.00	1.0	14.00	12.49	11.88	15.00	13.51	13.20	29.00	25.97	25.06
6.00	1.5	16.00	15.04	14.52	16.00	16.72	16.68	32.00	31.71	31.16
6.20	2.0	19.00	17.96	17.72	20.00	20.18	20.49	39.00	38.09	38.17
8.00	0.0	6.00	6.35	6.53	6.00	6.21	5.54	12.00	12.65	12.14
8.20	0.5	7.00	5.92	6.50	7.00	5.75	5.97	14.00	11.70	12.50
8.00	1.0	7.00	7.32	8.08	8.00	7.33	8.16	15.00	14.64	16.23
7.90	1.5	8.00	9.71	10.69	8.50	10.04	11.37	16.50	19.73	22.04
8.00	2.0	12.00	12.80	14.14	14.00	13.50	15.34	26.00	26.28	29.46

11.2.6 The Comparison Between Laboratory Measured and Industrially Observed Wear

The suite of models developed in this study corresponds to the tests on a small laboratory size cone crusher. Due to the lack of any available industrial rig, no industrial trials or validation of the models for full size crusher could be carried out. Yet some kind of comparison between the industrially observed, laboratory measured, and model predicted wear rates would be useful .

Table 3.6 in Chapter 3 presented the result of a survey of industrially observed wear rates. Two of the quarries surveyed which were also chosen for the experimental studies, Whitwick and Pottal Pool, use the same crusher- Autocone 900 Medium Fine. The utilization of the same machine and similar feed size and crusher setting provides the ground for a valid comparison to be carried out.

Table 11.3 shows the three sets of wear values for each rock type. The industrial service life of the liners in Pottal Pool quarry is about half that in Whitwick quarry. In another word, the industrially observed wear due to Pottal Pool rock is slightly more than twice that due to Whitwick rock. It can be seen that, the liner wear measured in the laboratory for Pottal Pool rock was also slightly more than twice that measured for Whitwick rock. The same is also true for the predicted wear using the generic wear model (based on all rock types). This a very encouraging result indicating that the results of the present study are relevant and applicable to full size cone crushers.

Table 11.3 Comparison Between Industrially Observed, Laboratory Measured And Model Predicted Wear Rates

Rock	Si (%)	Industrial Wear Service Life (Hours)	Laboratory Wear TW(g/T)	Predicted Wear (G.M) TW(g/T)
Pottal Pool	91.30	95	96	88.34
Whitwick	60.13	210	40	41.68

11. 2.7 Effect of Liner Properties

The metallurgical investigations carried out on the liners worn during industrial process as well as those used for laboratory experiments have revealed that a strong relationship exists between liner micro-structure and its wear performance. Surface hardness, measured after work hardening, is also indicative of liner's wear resistance. However, hardness itself was found to be highly dependant on the micro-structure. In all cases where the austenitic structure of Hadfield Steel differed from that expected, both surface hardness and wear liner performance were found to be considerably affected.

At present, no standard for ensuring the micro-structure, and hence the wear performance, of Hadfield steel liners is available. From the results of the current investigation it is clear that the development of quality assurance procedures and tests in this field would have a considerable impact on the consistency of the liners performance.

11.3 The Fuzzy Wear Model

A computer programme, written in Turbo C++, has been developed to combine and apply the wear models within an interactive automated environment. The programme provides a two tier predictive tool. At the first tier, explicit mathematical equations have been used to calculate the expected rate of wear for a given rock type, moisture and closed-side setting. In the absence of a precise knowledge of the moisture content, a linguistic moisture variable entailing five Fuzzy sets has been used to characterize the expected moisture level. The application of Fuzzy mathematics provides an estimate of the expected wear at the second tier.

Application of the Fuzzy set theory to the prediction of liner wear is a novel approach to account for the uncertainties associated with the quantity of the water sometimes added to cone crusher feed. It provides an effective technique for limiting the impact of such an uncertainty on the estimated rates of wear, which could otherwise become unreliable.

11.4 The Time Dependant Crusher Model

In accordance with the general findings of other workers (Anderson & Napier-Munn 1990; and White 1978) liner wear was found to change the size distribution of the product due to a combination of thickness loss and the change of profile. In addition the moisture was found to affect the product by shifting the size distribution curves towards a finer product.

The developed Time Dependant Crusher Model presents a new framework for incorporating these variables for predicting product characteristics in real-time. The application of the model could enhance the crushing circuit design and simulation. The Model also satisfies the basic prerequisite for employing a real-time control strategy for compensation of wear.

11.5 The Adaptive Control Strategy

An adaptive control strategy was considered to be the most suitable control regime for wear compensation in cone crushers. The consideration is based on that it generally provides the most reliable technique for accommodating any change in system dynamics. In cone crushing process, the change in system dynamics originates from two main sources.

First, the size distribution of the product, i.e. system output, depends both on controlled machine variables and uncontrollable rock properties.

Second, the wear instigated variation in liner profile alters one of the main machine characteristics influencing the product size, i.e. the retention of feed. This is due to an extension of the parallel part of the crushing zone which consequently results in a finer product.

An adaptive control strategy is able to account for both these predicaments during the service life of liners. A control system comprising two cascading feedback loops and a feedforward wear compensation loop has been designed and tested using MATLAB simulation package. The results of the simulation have demonstrated that the proposed controller would provide a very significant improvement in product quality and crusher efficiency, compared with that attainable with the best of the presently available systems. The achievable reduction in the average re-circulating load would minimise the overall energy utilisation and the production costs.

Chapter 12 CONCLUSION

This work has considered different aspects of system tribology and liner wear in cone crushers. The parameters influencing the rate of wear were identified. A comprehensive experimental study, involving ten different rock types, two feed sizes, five crusher settings and five moisture levels, was carried out to quantify the effect of the significant parameters. Based on the results obtained from the experimental work a suite of predictive mathematical and Fuzzy wear models were developed. The impact of liner wear on the crusher performance and product size was considered and a new time-dependant cone crusher model incorporating the effects of liner wear and moisture developed. The possibility of a real-time control strategy for compensation of liner wear and hence maintaining the consistency of the product quality was investigated and a new feedback control system was designed to meet these requirements. The discernible benefits of the real-time wear compensation strategy in term of product quality and crusher's overall efficiency was determined using simulation techniques.

The main conclusions reached by the study are:

1. The wear process in all parts of the two liners is largely identical and primarily due to abrasion with a secondary contribution from surface fatigue and impact modes of wear.

2. The wear regime in cone crushers was found to fall within the category of open-three body abrasive wear, changing from low stress to high stress wear mode along the length of the liners. This results in a differential wear rate along the liners, with the highest loss of material occurring at the main crushing zone.

3. The dominant mechanism of material removal depends on rock hardness and abrasivity, varying from ploughing, wedge forming in the case of softer rocks to micro-cutting for harder and more abrasive ones.

4. The wear performance of Hadfield steel, commonly used to produce cone crusher liners, was found to depend strongly on its austentic micro-structure. Surface hardness, measured after work hardening, is indicative of both the micro-structure and expected relative wear resistance.

5. The industrially observed liner wear was found to depend on a range of variables, including machine design variables, operating parameters and rock properties.

6. The experimental investigations have revealed that closed-size setting has an important impact on the wear. The wear increases as the closed-side setting decreases and their relation was best described by a second order model.

7. Moisture was found to significantly influence wear. In all rock types, except for the two gravel type rocks, Shardlow and Pottal Pool rocks, added moisture increased the wear. For the two rocks, addition of moisture initially reduced the wear. The relationship between wear and moisture was found to be second order with a major contribution from the interaction between closed-side setting and moisture. In the case of the two gravel type rocks, no interaction between closed-side setting and moisture was observed and the corresponding models exclude the interactive term.

8. Feed size was found to affect wear considerably. The limited tests indicated that in all ten rock types tested the use of smaller feed resulted in a reduction in wear. Added moisture to the smaller feed size resulted in an increase in wear for all rock types.

9. It has been possible to describe the wear due to a given rock type on the basis of the closed-side setting and moisture content. The predictive models developed provide a very good comparison between predicted and measured values.

10.Rock properties influencing wear include the silica content, impact hardness, strength parameters, and in the presence of water, water absorption and pH. The rock classification tests correlating with wear include **BTS**, **UCS**, **PL**, **FT** and **AAV**. None of these parameters on their own can however be used to predict wear accurately and a multi-variable modelling approach was found to be essential for prediction of wear.

11.The subset of rock variables providing the best correlation with wear included **Si**, **BTS** and **AAV**.

12.The data for different rock types were used to develop general wear models for dry and moist rock. The models showed a high degree of statistical significance and provide good agreement with the measured wear. However, their performance is understandably lower than the rock-specific models.

13.The effect of moisture on crusher performance both in terms of throughput and product size was investigated. It was found that in all cases, except for the gravel type rocks, the crusher throughput decreased as the moisture content was increased. In the case of the gravel type rocks, this was only true for the smaller feed size. For the larger feed size, in agreement with the decrease in rate of wear, the crusher throughput increased initially with added moisture. The size distribution of the product was found to become finer for higher moisture content. The relationship between moisture and both the eighty percent passing size, and k_1 and k_2 parameters (Whiten 1972) has been modelled.

14.Fuzzy modelling techniques have been used successfully to account for imprecise information regarding the amount of added moisture. The developed fuzzy wear model provides an estimate of wear on the basis of a linguistic description of moisture level.

15.It has been possible to quantify and model the effect of liners' wear condition on the size distribution of product. Both the eighty percent passing size and the k_2 parameter decrease with wear-induced change in liner profile. This confirms the general results of other workers that liner wear causes a shift in the size distribution of product similar to that caused by a reduction in the closed-side setting.

16.The overall effect of liner wear, both in terms of profile degradation and thickness loss, on product size has been considered in real time and a new time dependent model for cone crushers has been formulated. The model is a modification of the Whiten's cone crusher model and incorporates the effect of liner wear and moisture.

17.The application of adaptive control strategy for real-time compensation of liner wear and optimization of crusher performance was considered. A new control system, based on cascading feedback and feedforward loops, has been designed. Model-based adaptive control strategy has been identified as the suitable technique for compensating the effects of liner wear on product size.

18.The real-time performance of Autocone 900 (Medium Fine) cone crusher with different methods of wear compensation has been simulated. A real-time wear compensation, using the developed time dependant model and control system, shows a highly significant improvement in crusher performance in terms of consistent product characteristics, reduced re-circulating load and crusher efficiency.

SUGGESTION FOR FURTHER RESEARCH

The results of the present study provides considerable encouragement to carry out further research in the following areas:

1. verification of wear models for industrial cone crushers
2. validation of the suggested time-dependent crusher model for industrial cone crushers
3. stability analysis and full implementation of the designed adaptive control system.

REFERENCES

Anderson J.S. and Napier-Munn T.J., 1990, The influence of liner condition on cone crusher performance, Mineral Engineering, Vol. 3, No.1/2, p105.

Archard J.F., 1957b, Elastic deformation and the laws of friction, Proc. Roy. Soc., London, A 243, p.190.

Archard J.F., 1958/59, The temperature of rubbing surfaces, Wear, No. 2, p.438.

Archard J.F.,1957a, Wear, Interdisciplinary Approach to Friction and Wear (Editor P.M. Ku), NASA SP-181, Washington, , p. 267.

Astrom K.J, Anton J.J & Arzen K.E, 1986, Expert Control, Automatica, Vol. 21, p. 539.

Astrom K.J, Borisson U., Ljung L., Wittenmark B., 1977, Theory and application of self-tunung regulators, Automatica, No. 13, p. 457.

Astrom K.J., 1980, in Applications of adaptive control, ed. Narendra K.S.& Monopoli R.V., Cloth Academic Prentice-Hall.

Astrom K.J., 1987, Adaptive feedback control, Proceedings IEEE, Vol. 75, No.2, p.185.

Astrom K.J., Wittenmark B., 1989, Adaptive control, Addison Wesely, New York.

Atkinson T., Cassapi V.B., 1989, Abrasive wear in the mineral industry, Mining Department Magazine, University of Nottingham, V. XLI.

Atlas Copco, 1981, Standard method of Cerchar test, Switzerland.

Batchelor A.W. and Stachowiak G.W., 1988, Predicting synergism between corrosion and abrasive wear, Wear, No. 123, p. 281.

Bayer R.G., Clinton W.C., Nelson C.W. and Schumachor R.A., 1962, Wear, no 5, p.378.

Bearman R.A. 1991a, The application of rock mechanics parameters to the prediction of crusher performance' PHD Thesis, Camborne School of Mines.

Bearman R.A., 1991b, Energy utilization in quarrying, Mine and Quarry, Vol. 20, No. 8, p.23.

Blick H., 1937, Theoretical study of temperature rise at surfaces of actual contact under oilness lubricating conditions, Proc. Gen. Disc. Lub., Inst. Mech. Engrs, London, , Vol. 2, p. 14.

Blickenderfer R., 1988, Design criteria and correlation factors for field wear testing, Wear, No. 122, p.165.

Blickensderfer A., Tylczak J.H, Madsen B.W., Hansen J.S, 1984, Evaluating and improving materials for mineral processing, IMech. Transactions, C 347, p. 15.

Bond F.C., 1964, Lab equipment and tests help predict metal consumption in crushing and grinding units, E & M Journal, June issue.

Boness R.J., McBride S.L., 1991, Adhesive and abrasive wear studies using acoustic emission techniques, Wear, No. 149, p. 41.

Boness R.J., McBride S.L., Sobczyk M., 1990, Wear studies using acoustic emission techniques, Tribology International, Vol. 5, No. 23, p. 291.

Borik, F., Sponseller D.L., 1971 a, Gouging abrasion test for material used in ore and rock crushing: part I- Description of the test, Journal of Materials, Vol 6., No. 3, p. 576.

Borik, F., Sponseller D.L., 1971 b, Gouging abrasion test for material used in ore and rock crushing: part II- Effect of metallurgical variables on gouging wear, Journal of Materials, Vol 6., No. 3, p. 590.

Bowden F.P. and Tabor D., 1964, The Friction and Lubrication of Solids, Clarendon press, Oxford.

Box G.E.P, Draper N., 1986, Impirical Model Building and Response surface, John Wiley New York.

Bristol E.H., 1986, The EXACT pattern recognition adaptive controller, a user-oriented commercial success, in Narendra K.S (1986) adaptive and learning systems, Plenum Press, New York, p. 149.

Bristow C.M., 1992, Long term trends affecting UK demand for minerals, Mine and Quarry, issue July/August, p. 7.

Bullens D.K., 1939, Steel and its heat treatment, Part II- Engineering and special purpose steels, New York, John Wiley & Sons Inc.

Burwell J.T., 1957, Survey of possible wear mechanisms, Wear, No. 1, p. 119.

Business Monitor 1991, Part PA1007: Minerals, Central Statistical Office, p. 56.

Butler H., 1992, Model reference adaptive control: closing the gap between theory and practice, Cloth Prentice-Hall.

Calkin D. W., Parkin R.M., 1994, 3D opto-Mechatronic Product Classifier for Sizing and Grading Roadstone Aggregates, IEEE Computer Society Press, Proceeding of Mechatronics & Machine Vision in Practice, 13-15 Sept. 1994, USQ Toowoomba, Australia, p. 133.

Carslaw H.S. and Jaeger J.C., 1947, Conduction of Heat in Solids, Clarendon Press, Oxford, P. 56.

Centner R.M., Idelsohn J.M, 1963, Adaptive controller for a metal cutting process, IEEE Proceedings of the Joint Automatic Control Conference, p. 262.

Chien I.L., Seborg D.E., Mellichamp D.A., 1985, A self-tuning controller for with systems with unknown or varying time delays, Int. Journal of Control, Vol. 42, No. 4, p. 949.

Clark D., Coutts J., 1932, The production and application of manganese steel in Australia, Trans. American Foundrymen's Association, V.40, p.29.

Clark D.W., Kanjilal P.P., Mohtadi C., 1985, A generalized LQG approach to self-tuning control, Int. J. Control, No. 41, p.1509.

Crook A.W., 1957, Simulated gear-tooth contacts: some experiments upon their lubrication and subsurface deformations, Proc. Conf. Lubr. Wear, I, Mech. Eng., p. 701.

Durning B., Earle D., 1992, Abrasive sandstone in the coal measures, Quarry Management, Sept. Issue, p. 29.

Dutta S., 1993, Fuzzy loggic applications: Technological and strategic issues, IEEE Transactions on Engineering Management, Vol. 40, No. 3, p. 237.

Eldredge K.R. and Tabor D., 1955, The mechanism of rolling friction, I, the plastic range, Proc. Roy. Soc., London, A 229, p. 181.

Engel P.A., 1976, Impact Wear of Materials, Elsevier, Amsterdam.

Eyre T.S., 1976, Wear characteristics of metals, Tribology International, p. 203.

Fang L., Zhou Q.D., Li Y.J., 1991, Explanation of the relationship between wear and material hardness, Wear, No. 151, p. 313.

Franklin J.A., Desseault M.B., 1989, Rock Engineering, p. 38, McGraw-Hill, New York.

Goodwin G.C., Sang Sin K., 1984, Adaptive filtering prediction and control, Prentice-Hall.

Greenwood J.A. and Tripp J.H., 1967, The elastic contact of rough spheres, Trans ASME: J. Appl. Mech., No.89, p. 153.

Greenwood J.A. and Williamson J.B.P., 1966, the contact of nominally flat surfaces, Proc. Roy. Soc., London, A 295,.p. 300.

Gribble C.D. 1991, Coastal quarries-an update, Quarry Management, , vol 18, no 11, p. 23.

Hamilton G.M., 1963, Plastic flow in rollers loaded above the yield point, Proc. Inst. Mech. Engrs, p.177.

Hatch C.C., Larsen C.R. and Mular A.L., 1982, Digital simulation of the Brenda Mines Limited secondary crushing plant - case study. Design and Installation of Comminution Circuits, ed. Mular A.L., Jergensen G.V. SME/AIME, p. 275.

Higgins R.A., 1983, Engineering metallurgy Part I- Applied Physical Metallurgy, London, English Universities Press Ltd.

Hokkirigawa K., Kato K., 1989, Theoretical estimate of abrasive resistance based on microscopic wear mechanisms, Wear of Materials, Vol. 1, p.1.

Holm R., 1948, Calculation of temperature development in a contact heated in the contact surface, and application to the problem of the temperature rise in a sliding contact, J. Appl. Phys., No. 19, p. 361.

Hornbogen E., 1975, The role of fracture toughness in the wear of metals, Wear, No. 33, p. 251.

Hurricks P.I, 1973, Some metallurgical factors controlling the adhesive and abrasive wear resistance of steels- a review, Wear, No. 25, p. 285.

International Society of Rock Mechanics (ISRM): Commission of Stand. Lab. & Field Tests: Suggested Methods for determining hardness of rocks, 1978, Int. J. Rock Mech. Sci. & Geomech. Abstr., No. 15, p. 89.

Jacobson S., Wallen P., Hogmark S., 1988, Fundamental aspects of abrasive wear studied by a new numerical simulation model,Wear, No. 123, p. 207.

Johnson M.A., 1989, Adaptive systems in control and signal processing, Ed., Paperboards Pergamon, Pub. 1990.

Khruschov M.M., 1957, Resistance of metals to wear by abrasion; related to hardness, Proc. Conf. Lubr. and Wear, Inst. Mech. Engrs, London, p. 655.

Khruschov M.M., 1974, Principles of abrasive wear, Wear, No. 28, p. 69.

Khruschov M.M., Babichev M.A., 1960, Research on wear of metals, Ch.2: NEL Translation No. 889, National Engineering Laboratory, East Kilbride.

Klein M., Marczinkowsky T., Pandit M., 1991, An elementary pattern recognition self-tuning PI controller, Proceedings of IFAC Intelligent and adaptive control, Singapore, p. 17.

Kounas P.S., Dimarogonas A.D. and Sandor G.N., 1972, The distribution of friction heat between a stationary pin and a rotating cylinder, Wear, no 19, p. 415.

Kovacevic R, Evizi M., 1990, Nozzle wear detection in abrasive waterjet cutting systems, Materials Evaluation, No. 48, p. 348.

Kovacevic R., 1991, A new sensing system to monitor abrasive waterject nozzle wear, in: Computer-Aided production Engineering, ed. V.C. Venkatesh and J.A. Mcgeough, Elsevier Publications.

Kragelski I.V., 1965, Friction and Wear, Butterworths, London.

Landheer D. and Zaat J.H., 1974, The mechanism of metal transfer in sliding friction, Wear, No. 27, p. 129.

Lelic M.A., Zarrop M.B., 1987, General pole-placement self-tuning controller, part I. basic algorithm, Int. J. Control, No. 46, p. 547.

Lingard S., Ng K.K., 1989, An investigation of acoustic emission in sliding friction and wear of materials, Wear, No. 130, p.367.

Liu S.T & Kelly G.E, 1989, Rule Based Diagnostic Method for HVAC fault detection, Proc. IBPSA Building Simulation, Vancouver P. 319-324.

Macmillan N.H., 1989, Wear of materials, Proceedings of the 10th RISO int. Symposium on Metallurgy and Materials Science, p. 153.

Mamdani E H, 1976, Advances in the linguistic synthesis of fuzzy controllers, Int. J. Man-Machine Studies, 8,P. 669-678.

Martin-Sanchez J.M., 1975, Anew solution to adaptive control, IEEE proceeding, Vol. 64, p.1209.

Mashloosh K.M., Akbasouglu F.C., Eyre T.S., 1984, Wear of digger teeth, IMech. Transactions, C 343, p. 29.

Misra A., Finnie I., 1980, A classification of three-body wear and design of a new tester, Wear, No. 60, p.111.

Mitchell L.A. and Osgood C., 1976, A theory of friction and wear based on a new characterization of asperity interactions, Wear, No. 40, p.203.

Moore M.A., 1971, A prelimanary investigation of frictional heating during abrasive wear, Wear, No. 17, p. 51.

Narayanann S.S. & Whiten W.J. , 1988, Determination of comminution characteristics from single-particle breakage tests and its application to ball-mill scale-up. Trans. Inst. Min. Met., No. 97, p.115.

Narendra K.S., Monopoli R.V., 1980, Applications of adaptive control, Cloth Academic Prentice-Hall.

Nathan G.K., Jones W.J., 1966, Influence of abrasive hardness on the abrasive wear of metals, Proc. Inst. Mech. Eng., No. 181(30), p. 215.

Prisecter samplying Plc, 1993, Technical information onVSI Autogranulometry system, Prisecter sampling Plc. Philips House, Station Rd., Hampshire, UK.

Rabinowicz E., 1965, Friction and wear of materials, Wiley, New York, p 167.

Rabinowicz E., Dunn L.A. and Russel P.G., 1961, A study of abrasive wear under three-body condition, Wear, No. 4, p. 245.

Rabinowicz E., Mutis A., 1965, Effect of abrasive particle size on wear, Wear, No. 8, p. 81.

Rock Products, February 1992, Vol. 95, No. 6, Macmilean Hunter Publication, p. 32.

Rock Products, May 1993, Vol. 96, No. 5, Macmilean Hunter Publication, p.27.

Rock Products, June 1992, Vol. 95, No. 6, Macmilean Hunter Publication, p.23.

Shah S.L., Dumont G., 1989,Adaptive control dtrategies for industrial use: workshop proceedings, Springer-Verlag.

Shen Q. & Leitch R.R, 1993, Fuzzy qualitative simulation, IEEE Transaction on Systems, Man and Cybernetics, Vol. 23, No.4.

Sorokin G.M., Gringorev S.P., Golova A.G., 1991Nature of impact-abrasive wear of steel, Strength of Materials, No. 23, p. 463.

Spero C., Hargreaves D.J., Kirkcaldie R.K., Flitt H.J., 1991, Review of test methods for abrasive wear in ore grinding, Wear, No. 146, p. 389.

Stolarski T.A, 1990, a probabilistic approach to wear prediction, J. Phys. D: Appl., No. 24, p.1143.

Suana M, Peters T, 1982, The Cerchar Abrasivity Index and its relation to rock mineralogy and petrology, Rock Mechanics, No. 15, p. 1.

Sugeno, 1985, Industrial applications of fuzzy control, Amsterdam, Elsevier.

Sugiyama Y., 1986, An algorithm for solving discrete-time Wiener-Hopf equations based on Euclidian algorithm, IEEE Trans. Inform. Theory, It 32, p. 394.

Suh, 1973, The delamination theory of wear, Wear, No. 25, p. 111.

Torrence A.A., 1980, The correlation of abrasive wear tests, Wear, No. 63, p. 359.

Wang S., Wang Z., 1988, An analysis of the influence of plastic indentation in three-body abrasive wear of materials, Wear, No. 122, p. 123.

Weisberg, 1985, Applied linear regression, Wiley & Sons, New York.

West G., 1986, A relationship between abrasiveness and quartz content for some coal measures sediments, Int. J. Mining & Geological Eng., No. 4, p. 73.

White M.E., 1978, An investigation of large-scale industrial crushing and screaning operation, PhD Thseis, University of Queensland.

Whiten W.J. 1972, The simulation of crushing plants with models developed using multiple spline regression, J. South Afr. Inst. Min. & Met., No. 72, p. 257.

Widrow, B., Stearns S.D., 1985, Adaptive signal processing, Prentice-Hall Englewood Cliff.

Yeo K.P., Cheung C.C., Ord A., Brown W.A., 1991, Proceedings of the Third International Conf. on Application of Transputers, p.142.

Yi Lin Ji., Cheng H.S., 1989, An analytical model for dynamic wear, Journal of Tribology No. 111, p.468.

Zadeh L.A., 1965, Fuzzy sets, Info. & Control, Vol. 8, p. 338.

Zadeh L.A., 1975, The concept of a linguist variable and its applications to approximate reasoning, part I, Information Sciences, Vol. 8, p. 120.

Zadeh L.A., 1988, Fuzzy logic, IEEE Computer, April issue, p. 83.

Zadeh L.A., 1992, The calculus of fuzzy if/then rules, AI Expert, March issue, p. 23.

Zimmerman H.J., 1991, Fuzzy set theory and applications, 2nd Edition, Boston, Kluwer.

Zum Gahr K.H., 1988, Modelling of Two-body Abrasive Wear, Wear, No. 124, p. 87.

Appendix 1 THE "NO-CONSTANT" MODELS

A1.1 Measured and Fitted Wear Values For The "No-Constant" Dry Wear Models

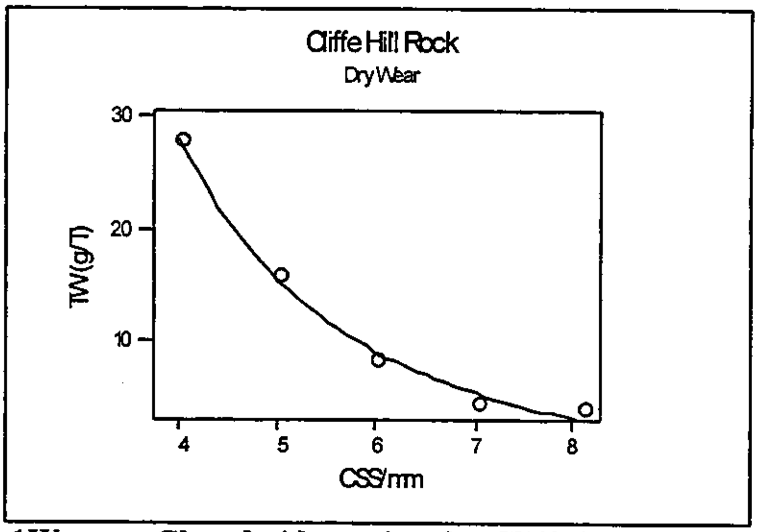

Figure A1. 1Wear vs Closed-side setting for Cliffe Hill Rock (no-constant model)

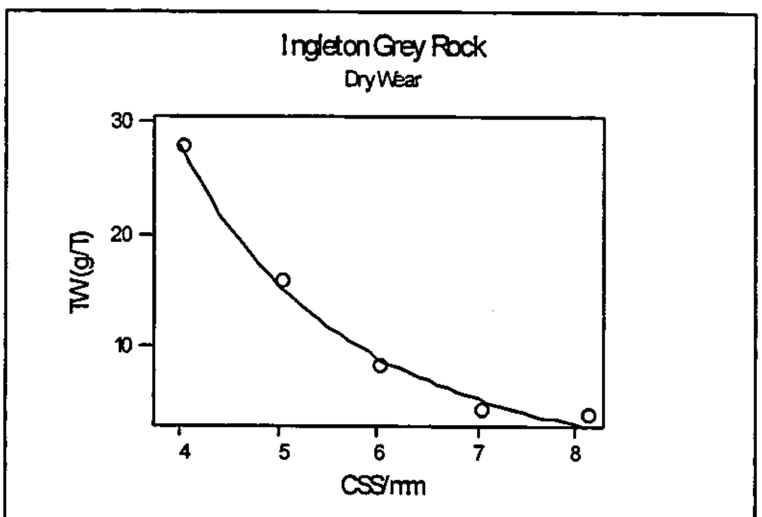

Figure A1. 2 Wear vs Closed-side setting for Ingleton Grey Rock(no-constant model)

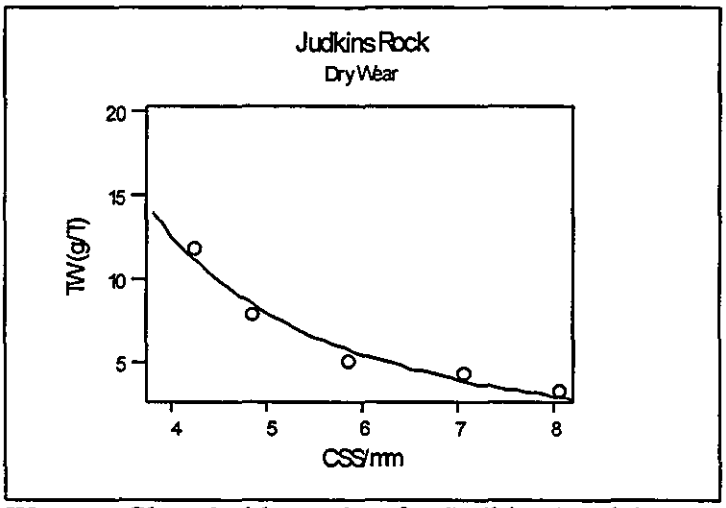

Figure A1. 3 Wear vs Closed-side setting for Judkins Rock(no-constant model)

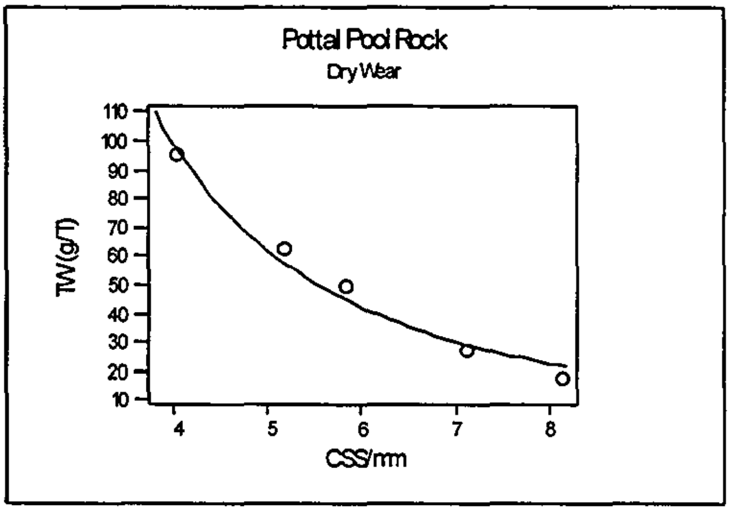

Figure A1. 4 Wear vs Closed-side setting for Pottal Pool Rock (no-constant model)

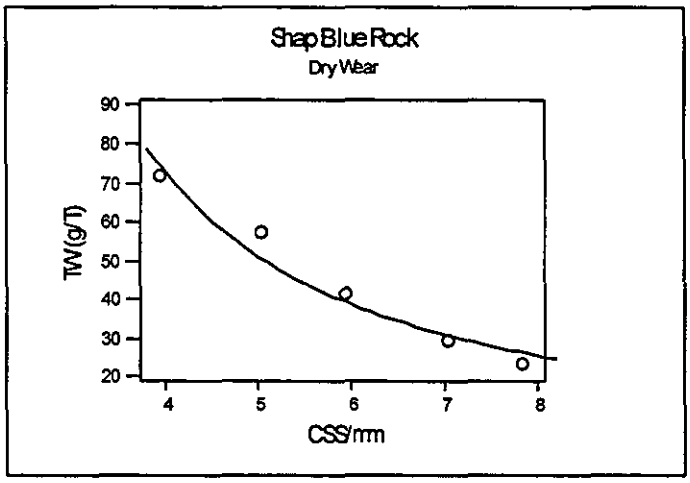

Figure A1. 5 Wear vs Closed-side setting for Shap Blue Rock (no-constant model)

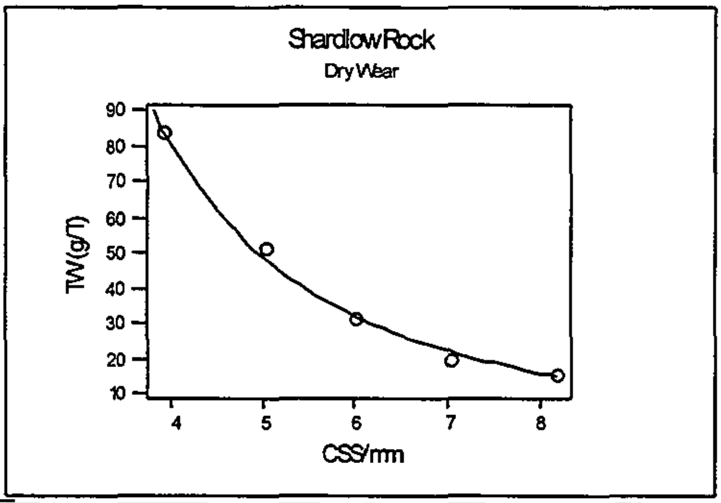

Figure A1. 6 Wear vs Closed-side setting for Shardlow Rock (no-constant model)

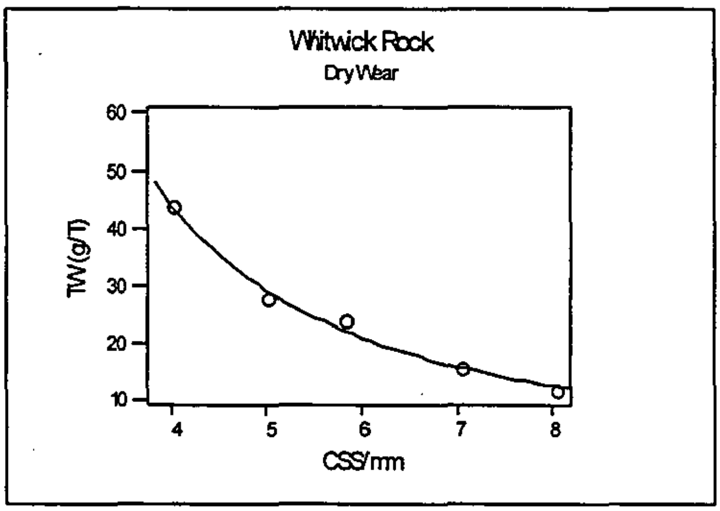

Figure A1. 7 Wear vs Closed-side setting for Whitwick Rock(no-constant model)

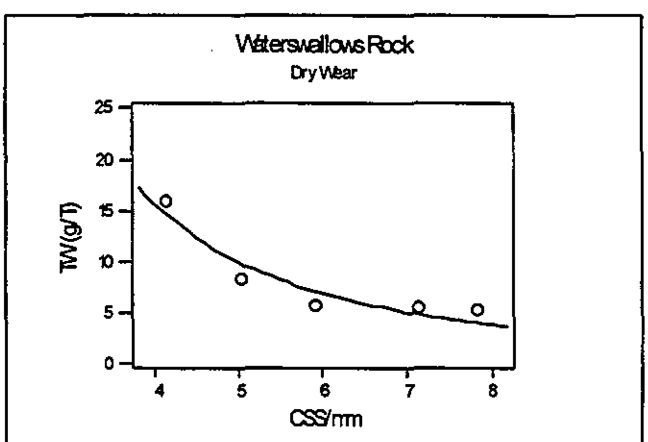

Figure A1. 8 Wear vs Closed-side setting for Waterswallows Rock (no-constant model)

A1.2 The Rock Specific "No-Constant" Models for Moist Rock

Table A 1.1 Model Equations and the Standard Deviation for Different Rock Types

Rock	Model	St.Deviation
Cliffe Hill	CW/(g/T) = - 18.2 1/CSS + 260 1/CSS^2 - 7.23 Moist + 3.56 Moist^2+ 36.0 Moist/CCS	0.748
	MW/(g/T) = - 8.0 1/CSS + 274 1/CSS^2 - 8.29 Moist + 3.97 Moist^2+ 47.0 Moist/CCS	1.369
	TW/(g/T) = - 26.2 1/CSS + 534 1/CSS^2 - 15.5 Moist + 7.53 Moist^2+ 83.0 Moist/CCS	1.975
Ingleton Grey	CW/(g/T) = -10.3 1/CSS + 159 1/CSS^2 - 7.98 Moist + 3.63 Moist^2+ 36.8 Moist/CCS	1.377
	MW/(g/T) = - 30.9 1/CSS + 261 1/CSS^2 - 3.36 Moist + 3.02 Moist^2+ 27.9 Moist/CCS	1.077
	TW/(g/T) = - 41.2 1/CSS + 420 1/CSS^2 - 11.3 Moist + 6.65 Moist^2+ 64.7 Moist/CCS	2.053
Judkins	CW/(g/T) = 4.3 1/CSS + 53.7 1/CSS^2 - 4.01 Moist + 2.24 Moist^2+27.4 Moist/CCS	1.010
	MW/(g/T) = 18.5 1/CSS + 42.6 1/CSS^2 - 7.31 Moist + 2.23 Moist^2 + 59.5 MOIST/CSS	0.948
	TW/(g/T) = 29.3 1/CSS + 71.0 1/CSS^2 - 12.2 Moist + 4.64 Moist^2+ 89.1 Moist/CCS	1.598
Pottal Pool	CW/(g/T) = - 16.7 1/CSS + 6491/CSS^2 + 3.15 Moist - 1.65 Moist^2	4.779
	MW/(g/T) = - 56.0 1/CSS + 991 1/CSS^2 + 9.05 Moist - 4.17 Moist^2	4.633
	TW/(g/T) = - 72.7 1/CSS + 1640 1/CSS^2 + 12.2 Moist - 5.81 Moist^2	8.471
Shap Blue	CW/(g/T) = 45.1 1/CSS + 389 1/CSS^2 + 0.96 Moist + 3.08 Moist^2- 17.0 Moist/CCS	1.271
	MW/(g/T) = 80.3 1/CSS + 274 1/CSS^2 + 3.84 Moist + 2.39 Moist^2 - 18.7 Moist/CCS	0.516
	TW/(g/T) = 125 1/CSS + 664 1/CSS^2 + 4.80 Moist + 5.47 Moist^2- 35.8 Moist/CCS	1.786
Shardlow	CW/(g/T) = 13.9 1/CSS + 481 1/CSS^2 - 10.9 Moist + 6.03 Moist^2- 0.252 Moist/CCS	2.000
	MW/(g/T) = - 57.7 1/CSS + 989 1/CSS^2 -14.0 Moist + 7.19 Moist^2+ 0.005 Moist/CCS	2.365
	TW/(g/T) = -43.8 1/CSS + 1470 1/CSS^2 - 24.9 Moist + 13.2 Moist^2- 0.248 Moist/CCS	3.742
Whitwick	CW/(g/T) = 35.8 1/CSS + 178 1/CSS^2 - 2.40 Moist + 1.35 Moist^2+ 17.8 Moist/CCS	1.441
	MW/(g/T) = 53.7 1/CSS + 97 1/CSS^2 - 15.6 Moist + 4.10 Moist^2+ 78.8 Moist/CCS	2.327
	TW/(g/T) = 89.5 1/CSS + 275 1/CSS^2 - 18.0 Moist + 5.45 Moist^2+ 96.6 Moist/CCS	2.402
Waterswallows	CW/(g/T) = - 16.2 1/CSS + 206 1/CSS^2 - 1.30 Moist + 1.97 Moist^2+ 6.18 Moist/CCS	1.067
	MW/(g/T) = - 8.0 1/CSS + 171 1/CSS^2 - 0.42 Moist + 2.17 Moist^2+ 3.19 Moist/CCS	0.865
	TW/(g/T) = - 24.3 1/CSS + 377 1/CSS^2 - 1.71 Moist + 4.13 Moist^2+ 9.4 Moist/CCS	1.866

Appendix 2 Experimental Results

Table A 2.1 Results from Wear Experiments Involving Dry Rock

Feed Fraction Size: +10-14mm

	CSS/mm	Wgt/Kg	CW/(g/T)	MW/(g/T)	TW/(g/T)	Time/S	TH/(T/H)	Power/kW
Breedon	3.70	150	0.67	0.67	1.34	1641.6	0.328	0.252
Cliffe Hill	4.00	25	12.00	16.00	28.00	324.0	0.277	0.301
Cliffe Hill	5.00	25	8.00	8.00	16.00	233.0	0.386	0.274
Cliffe Hill	6.00	60	3.33	5.00	8.33	402.0	0.537	0.257
Cliffe Hill	7.00	75	2.00	2.50	4.50	394.0	0.685	0.246
Cliffe Hill	8.10	75	1.33	2.66	3.99	302.4	0.892	0.230
Ingleton Grey	4.10	25	8.00	8.00	16.00	282.0	0.319	0.314
Ingleton Grey	5.20	50	4.00	4.00	8.00	543.0	0.331	0.296
Ingleton Grey	5.80	50	2.00	2.00	4.00	355.2	0.506	0.285
Ingleton Grey	7.00	75	1.30	1.30	2.60	344.0	0.784	0.263
Ingleton Grey	7.90	150	0.67	0.00	0.67	222.0	2.432	0.235
Judkins	4.20	25	4.00	8.00	12.00	408.0	0.220	0.285
Judkins	4.80	25	4.00	4.00	8.00	216.0	0.416	0.263
Judkins	5.80	57	1.74	3.48	5.28	383.0	0.535	0.246
Judkins	7.00	75	1.50	3.00	4.50	417.6	0.646	0.230
Judkins	8.00	94	1.19	2.19	4.38	432.0	0.783	0.219
PANT	3.90	300	0.60	0.60	1.20	3063.6	0.352	0.238
PANT	5.10	200	0.00	0.50	0.50	3391.2	0.212	0.213
Pottal Pool	4.00	25	44.00	52.00	96.00	176.4	0.510	0.307
Pottal Pool	5.15	25	25.00	38.00	63.00	134.4	0.669	0.274
Pottal Pool	5.80	25	20.00	30.00	50.00	93.6	0.961	0.263
Pottal Pool	7.10	25	12.00	16.00	28.00	78.0	1.153	0.246
Pottal Pool	8.10	25	4.00	14.00	18.00	67.2	1.339	0.235

Table A2.1 cont...

	CSS/mm	Wgt/Kg	CW/(g/T)	MW/(g/T)	TW/(g/T)	Time/S	TH/(T/H)	Power/kW
Shap	3.90	25	30.00	42.00	72.00	178.0	0.505	0.312
Shap	5.00	25	32.00	36.00	68.00	135.0	0.666	0.280
Shap	5.90	25	20.00	22.00	42.00	95.0	0.947	0.276
Shap	7.00	25	18.00	12.00	30.00	75.0	1.200	0.268
Shap	7.80	25	16.00	8.00	24.00	60.0	1.500	0.257
Shardlow	3.90	25	36.00	48.00	84.00	163.0	0.552	0.296
Shardlow	5.00	25	20.00	35.00	55.00	125.0	0.720	0.268
Shardlow	6.00	25	16.00	20.00	36.00	102.0	0.882	0.230
Shardlow	7.00	25	10.00	12.00	22.00	84.0	1.071	0.213
Shardlow	8.15	25	8.00	8.00	16.00	59.0	1.525	0.202
Whitwick	4.00	25	24.00	20.00	44.00	254.4	0.353	0.279
Whitwick	5.00	25	15.00	13.00	28.00	203.0	0.443	0.256
Whitwick	5.80	25	12.00	12.00	24.00	168.0	0.535	0.245
Whitwick	7.00	25	8.00	8.00	16.00	154.8	0.581	0.233
Whitwick	8.00	25	6.00	6.00	12.00	126.0	0.714	0.219
Waterswallows	4.10	25	8.00	8.00	16.00	300.0	0.300	0.252
Waterswallows	5.00	25	3.50	3.50	7.00	252.0	0.357	0.212
Waterswallows	5.90	25	3.00	3.00	6.00	192.0	0.468	0.202
Waterswallows	7.10	75	2.80	2.90	5.70	513.0	0.526	0.197
Waterswallows	7.80	75	2.70	2.70	5.40	422.4	0.639	0.191

Table A 2.2 Results of the Wear Experiments Involving Moist Rock

Feed Fraction Size: +10-14mm

Rock	CSS/mm	Wgt/Kg	CW/(g/T)	MW/(g/T)	TW/(g/T)	Time/S	Th/(T/H)	Power/kW	Moist(%)
Cliffe Hill	4.00	25	14.00	18.00	32.00	460.8	0.195	0.263	0.5
Cliffe Hill	4.00	25	16.00	21.00	37.00	720.0	0.125	0.224	1.0
Cliffe Hill	4.00	25	22.00	28.00	50.00	930.0	0.096	0.212	1.5
Cliffe Hill	4.20	25	28.00	37.00	65.00	1130.4	0.079	0.208	2.0
Cliffe Hill	5.80	50	6.00	10.00	16.00	432.0	0.416	0.246	0.5
Cliffe Hill	5.80	30	6.50	11.00	17.50	496.8	0.217	0.208	1.0
Cliffe Hill	6.00	30	10.00	14.00	24.00	950.4	0.113	0.202	1.5
Cliffe Hill	8.00	50	2.00	2.00	4.00	560.0	0.321	0.221	0.5
Cliffe Hill	8.00	50	3.00	6.00	9.00	749.0	0.240	0.214	1.0
Cliffe Hill	7.50	30	6.67	10.00	16.67	8892.0	0.012	0.202	1.5
Cliffe Hill	8.00	30	10.00	13.50	23.50	1036.0	0.104	0.197	2.0
Ingleton Grey	3.90	25	9.00	12.00	21.00	348.0	0.258	0.284	0.5
Ingleton Grey	4.00	25	12.00	15.00	27.00	588.0	0.153	0.235	1.0
Ingleton Grey	4.00	25	17.00	21.00	38.00	782.0	0.115	0.220	1.5
Ingleton Grey	4.00	25	24.00	28.00	52.00	1110.0	0.081	0.215	2.0
Ingleton Grey	6.20	50	3.00	4.00	7.00	480.0	0.375	0.256	0.5
Ingleton Grey	6.00	50	5.00	7.00	12.00	640.0	0.281	0.230	1.0
Ingleton Grey	6.10	25	7.00	8.00	15.00	514.8	0.174	0.207	1.5
Ingleton Grey	6.20	25	16.00	17.00	33.00	948.0	0.094	0.205	2.0
Ingleton Grey	7.60	75	1.33	1.33	2.66	475.2	0.568	0.235	0.5
Ingleton Grey	7.90	50	2.00	3.00	5.00	705.6	0.255	0.290	1.0
Ingleton Grey	7.80	50	4.00	9.00	13.00	907.2	0.198	0.208	1.5
Ingleton Grey	8.00	50	7.00	12.00	19.00	606.0	0.297	0.201	2.0
Shap	4.00	25	36.00	39.00	75.00	210.6	0.427	0.295	1.0
Shap	4.00	25	41.00	45.00	86.00	380.9	0.236	0.049	2.0
Shap	8.00	25	13.00	18.00	31.00	150.9	0.596	0.204	1.0
Shap	8.00	25	22.00	27.00	49.00	458.5	0.196	0.360	2.0

Table A2.2 Cont...

Rock	CSS/mm	Wgt/Kg	CW/(g/T)	MW/(g/T)	TW/(g/T)	Time/S	Th/(T/H)	Power/kW	Moist(%)
Judkins	3.80	25	8.00	12.00	20.00	531.4	0.169	0.219	0.5
Judkins	4.00	25	9.00	16.00	25.00	676.8	0.132	0.210	1.0
Judkins	4.00	25	12.00	24.00	36.00	1368.0	0.065	0.193	1.5
Judkins	3.90	25	21.00	33.00	54.00	2592.0	0.034	0.191	2.0
Judkins	6.00	50	3.00	7.00	10.00	525.6	0.342	0.219	0.5
Judkins	6.20	25	4.00	8.00	12.00	489.6	0.183	0.197	1.0
Judkins	6.20	25	8.00	12.00	20.00	792.0	0.113	0.197	1.5
Judkins	6.00	25	12.00	18.00	30.00	950.4	0.094	0.191	2.0
Judkins	8.00	50	3.00	5.00	8.00	345.6	0.520	0.202	0.5
Judkins	8.00	50	4.00	6.00	10.00	669.6	0.268	0.191	1.0
Judkins	8.00	50	5.10	8.00	13.10	1425.6	0.126	0.180	1.5
Judkins	8.10	30	9.00	12.00	21.00	892.8	0.120	0.178	2.0
Pant	3.70	200	1.00	1.50	2.50	5470.8	0.131	0.199	1.0
Pant	3.70	200	1.50	1.50	3.00	19536.0	0.036	0.189	2.0
Pottal Pool	4.20	25	32.00	44.00	76.00	192.0	0.468	0.285	0.5
Pottal Pool	4.10	25	32.00	56.00	88.00	424.8	0.211	0.237	1.0
Pottal Pool	3.90	25	32.00	44.00	76.00	1075.2	0.083	0.202	1.5
Pottal Pool	3.90	25	44.00	56.00	100.00	1307.8	0.068	0.200	2.0
Pottal Pool	6.10	25	16.00	20.00	36.00	138.0	0.652	0.246	0.5
Pottal Pool	6.10	25	20.00	24.00	44.00	189.0	0.476	0.213	1.0
Pottal Pool	6.09	25	16.00	24.00	40.00	372.0	0.241	0.208	1.5
Pottal Pool	6.30	25	12.00	16.00	28.00	422.4	0.213	0.197	2.0
Pottal Pool	8.00	25	12.00	12.00	24.00	86.4	1.041	0.246	0.5
Pottal Pool	8.00	25	12.00	12.00	24.00	188.4	0.477	0.257	1.0
Pottal Pool	8.20	25	12.00	16.00	28.00	288.7	0.311	0.208	1.5

Table A2.2 Cont...

Rock	CSS/mm	Wgt/Kg	CW/(g/T)	MW/(g/T)	TW/(g/T)	Time/S	Th(T/H)	Power/kW	Moist(%)
Shardlow	7.50	25	8.00	12.00	20.00	684.0	0.131	0.197	2.0
Shardlow	3.90	25	28.00	44.00	72.00	636.0	0.141	0.224	1.0
Shardlow	3.80	25	32.00	56.00	88.00	1706.4	0.052	0.202	2.0
Shardlow	5.90	25	4.00	12.00	16.00	324.0	0.277	0.219	1.0
Shardlow	6.00	25	8.00	16.00	24.00	588.0	0.153	0.208	2.0
Shardlow	8.00	25	3.00	1.00	4.00	216.0	0.416	0.208	1.0
Shardlow	8.40	25	4.00	8.00	12.00	300.0	0.300	0.202	2.0
Whitwick	4.00	25	28.00	48.00	76.00	2202.0	0.040	0.197	2.0
Whitwick	6.10	25	12.00	13.00	25.00	204.0	0.441	0.242	0.5
Whitwick	6.00	25	14.00	15.00	29.00	495.6	0.181	0.230	1.0
Whitwick	6.00	25	16.00	16.00	32.00	672.0	0.133	0.208	1.5
Whitwick	6.20	25	19.00	20.00	39.00	1044.0	0.086	0.202	2.0
Whitwick	8.20	25	7.00	7.00	14.00	144.0	0.625	0.252	0.5
Whitwick	8.00	25	7.00	8.00	15.00	396.0	0.227	0.252	1.0
Whitwick	7.90	25	8.00	8.50	16.50	801.6	0.112	0.235	1.5
Whitwick	8.00	25	12.00	14.00	26.00	984.0	0.091	0.246	2.0
Waterswallows	4.30	25	9.00	9.00	18.00	393.6	0.228	0.230	0.5
Waterswallows	4.00	25	10.00	10.00	20.00	820.8	0.109	0.207	1.0
Waterswallows	4.00	25	14.00	15.00	29.00	1784.4	0.050	0.191	1.5
Waterswallows	3.90	25	17.00	18.00	35.00	2032.8	0.044	0.197	2.0
Waterswallows	6.10	25	3.00	4.00	7.00	278.7	0.322	0.234	0.5
Waterswallows	6.20	25	5.00	6.00	11.00	447.6	0.201	0.208	1.0
Waterswallows	6.00	25	8.00	9.00	17.00	909.6	0.098	0.197	1.5
Waterswallows	6.10	25	12.00	13.00	25.00	1460.0	0.061	0.197	2.0
Waterswallows	8.10	50	2.00	3.00	5.00	924.0	0.194	0.186	1.0
Waterswallows	8.00	50	4.00	6.00	10.00	1257.6	0.143	0.196	1.5
Waterswallows	7.90	30	7.00	10.00	17.00	1062.0	0.101	0.205	2.0

Table A 2.3 Results of the Wear Experiments Involving a Feed Fraction Size of +6.8-8.0mm

Rock	CSS/mm	Feedsize	Wgt/Kg	CW/(g/T)	MW/(g/T)	TW/(g/T)	Time/S	TH(T/H)	Power/kW	Moist(%)
Cliffe Hill	4.0	8.15	30	6.67	10.00	16.67	230.4	0.468	0.285	0
Cliffe Hill	4.1	8.15	25	20.00	28.00	48.00	7884.0	0.011	0.186	2
Ingleton Grey	3.8	8.15	37	1.35	2.70	4.05	241.2	0.552	0.297	0
Ingleton Grey	3.7	8.15	30	8.33	6.67	15.00	2712.0	0.039	0.191	2
Judkins	4.0	8.15	30	3.33	13.33	16.66	223.2	0.483	0.285	0
Judkins	3.9	8.15	30	13.33	26.66	40.00	2484.0	0.043	0.191	2
Pottal Pool	4.1	8.15	25	28.00	40.00	68.00	128.4	0.700	0.285	0
Pottal Pool	4.2	8.15	32	52.00	84.00	136.00	1994.4	0.057	0.194	2
Shap	3.9	8.15	25	20.00	28.00	48.00	199.6	0.450	0.243	0
Shap	3.9	8.15	25	24.00	52.00	76.00	2347.0	0.038	0.199	2
Shardlow	4.0	8.15	25	36.00	48.00	84.00	170.4	0.528	0.307	0
Shardlow	4.0	8.15	18	51.89	82.44	133.33	4122.0	0.015	0.208	2
Whitwick	3.9	8.15	25	6.00	12.00	18.00	192.0	0.468	0.296	0
Whitwick	4.0	8.15	25	12.00	28.00	40.00	2294.4	0.035	0.191	2
Waterswallows	3.8	8.15	37	1.35	2.70	4.05	390.0	0.341	0.263	0
Waterswallows	3.7	8.15	30	10.00	6.68	16.68	4920.0	0.021	0.191	2

Appendix 3 Comparison of Measured and Fitted Wear Values

Table A 3.1Comparison of Measured and Fitted Wear Values for Rock Specific and General Dry Wear Models

FIT 1: Rock Specific Model FIT 2: The general wear model using BTS

Rock	CSS/mm	CW/(g/T)	FIT1	FIT2	MW/(g/T)	FIT1	FIT2
Cliffe Hill	4.00	12.00	12.23	9.07	16.00	16.014	14.62
Cliffe Hill	5.00	8.00	7.08	5.33	8.00	8.04	9.09
Cliffe Hill	6.00	3.33	4.14	3.92	5.00	4.61	5.40
Cliffe Hill	7.00	2.00	2.28	3.44	2.50	3.08	2.77
Cliffe Hill	8.10	1.33	0.91	3.38	2.66	2.40	0.63
Ingleton Grey	4.10	8.00	8.04	13.61	8.00	8.01	12.88
Ingleton Grey	5.20	4.00	3.64	7.73	4.00	3.75	8.53
Ingleton Grey	5.80	2.00	2.44	6.02	2.00	2.46	6.85
Ingleton Grey	7.00	1.30	1.14	4.04	1.30	0.87	4.37
Ingleton Grey	7.90	0.67	0.68	3.25	0.00	0.18	3.00
Judkins	4.20	4.00	4.03	4.42	8.00	7.82	5.09
Judkins	4.80	3.00	2.88	2.14	5.00	5.36	4.13
Judkins	5.80	1.74	1.89	0.31	3.48	3.40	2.96
Judkins	7.00	1.50	1.38	-0.43	3.00	2.60	2.01
Judkins	8.00	1.19	1.22	-0.55	2.19	2.47	1.44
Pant	3.90	0.60	*	-1.00	0.60	-	0.10
Pottal Pool	4.00	44.00	44.30	41.59	52.00	52.20	53.87
Pottal Pool	5.15	25.00	24.76	25.35	38.00	37.11	36.15
Pottal Pool	5.80	20.00	18.53	19.68	30.00	30.27	29.24
Pottal Pool	7.10	12.00	10.87	12.11	16.00	19.38	19.23
Pottal Pool	8.10	4.00	7.36	8.28	14.00	12.91	13.71
Shp	3.90	30.00	35.33	31.83	42.00	37.88	43.67
Shp	5.00	25.00	26.36	23.36	33.00	27.76	28.74
Shp	5.90	20.00	21.75	19.82	22.00	20.94	20.67
Shp	7.00	18.00	17.86	17.32	12.00	14.23	13.63
Shp	7.80	16.00	15.78	16.18	8.00	10.23	9.75
Shr	3.90	36.00	36.11	37.05	48.00	48.41	47.98
Shr	5.00	20.00	19.40	21.29	32.00	30.55	30.33
Shr	6.00	12.00	12.84	13.15	20.00	20.07	19.91
Shr	7.00	10.00	9.67	7.87	12.00	12.62	12.47
Shr	8.15	8.00	7.96	3.74	8.00	6.33	6.17
Whitwick	4.00	24.00	23.90	19.95	20.00	19.78	15.77
Whitwick	5.00	15.00	15.45	12.88	13.00	13.98	11.62
Whitwick	5.80	12.00	11.55	9.82	12.00	11.00	9.33
Whitwick	7.00	8.00	7.97	7.20	8.00	7.98	6.87
Whitwick	8.00	6.00	6.11	5.94	6.00	6.24	5.40
Waterswallows	4.10	8.00	7.97	9.51	8.00	7.97	9.17
Waterswallows	5.00	4.20	4.28	5.00	4.30	4.34	5.74
Waterswallows	5.90	3.00	2.96	2.76	3.00	3.03	3.37
Waterswallows	7.10	2.80	2.66	1.32	2.90	2.70	1.14
Waterswallows	7.80	2.70	2.81	0.89	2.70	2.83	0.16

Table A 3.2Comparison of Measured and Fitted Wear Values- Rock Specific Wear Models

Rock	CSS/mm	Moist(%)	CW/(g/T)	FIT	MW/(g/T)	FIT	TW/(g/T)	FIT
Cliffe Hill	4.00	0.0	12.00	12.54	16.00	16.65	28.00	29.06
Cliffe Hill	4.00	0.5	16.00	15.68	20.00	19.38	36.00	34.95
Cliffe Hill	4.00	1.0	20.00	19.46	24.00	23.26	44.00	42.88
Cliffe Hill	4.00	1.5	24.00	23.89	28.00	28.29	52.00	52.85
Cliffe Hill	4.20	2.0	26.00	26.55	32.00	32.62	60.00	60.43
Cliffe Hill	6.00	0.0	3.33	3.40	5.00	6.19	8.33	9.65
Cliffe Hill	5.80	0.5	6.00	5.77	10.00	9.09	16.00	14.65
Cliffe Hill	5.80	1.0	8.67	8.34	12.67	12.45	21.00	20.57
Cliffe Hill	6.00	1.5	10.00	10.84	16.67	16.16	26.67	26.99
Cliffe Hill	6.10	2.0	15.00	14.24	21.67	21.39	36.67	36.05
Cliffe Hill	8.10	0.0	1.33	0.99	2.66	1.10	3.99	2.40
Cliffe Hill	8.00	0.5	2.00	2.24	2.00	3.17	4.00	5.29
Cliffe Hill	8.00	1.0	4.00	4.07	6.00	6.21	10.00	9.99
Cliffe Hill	7.50	1.5	6.67	7.28	10.00	11.54	16.67	18.64
Cliffe Hill	8.00	2.0	10.00	9.65	16.67	15.77	26.67	25.52
Ingleton Grey	4.10	0.0	8.00	7.14	8.00	6.84	16.00	13.98
Ingleton Grey	3.90	0.5	9.00	11.80	12.00	13.94	21.00	25.74
Ingleton Grey	4.00	1.0	16.00	14.53	16.00	18.35	32.00	32.89
Ingleton Grey	4.00	1.5	20.00	18.69	28.00	23.92	48.00	42.61
Ingleton Grey	4.00	2.0	22.00	23.38	30.00	29.60	52.00	52.99
Ingleton Grey	5.80	0.0	2.00	1.73	2.00	1.21	4.00	2.95
Ingleton Grey	6.20	0.5	4.00	2.60	6.00	4.08	10.00	6.69
Ingleton Grey	6.00	1.0	5.00	4.81	8.00	7.77	13.00	12.59
Ingleton Grey	6.10	1.5	6.00	7.00	10.00	11.07	16.00	18.07
Ingleton Grey	6.20	2.0	8.00	9.64	12.00	14.38	20.00	24.02
Ingleton Grey	7.90	0.0	0.33	0.84	0.34	0.95	0.67	1.79
Ingleton Grey	7.60	0.5	1.33	1.50	1.33	3.31	2.66	4.82
Ingleton Grey	7.90	1.0	2.00	2.50	6.00	5.76	8.00	8.27
Ingleton Grey	7.80	1.5	4.00	4.23	10.00	8.44	14.00	12.68
Ingleton Grey	8.00	2.0	8.00	6.19	12.00	10.97	20.00	17.16
Judkins	4.10	0.0	4.00	3.73	8.00	6.56	12.00	10.36
Judkins	3.80	0.5	8.00	8.40	12.00	12.70	20.00	21.04
Judkins	4.00	1.0	12.00	10.89	16.00	17.24	28.00	28.02
Judkins	4.00	1.5	12.00	14.44	24.00	23.66	36.00	38.07
Judkins	3.90	2.0	20.00	18.53	32.00	31.37	52.00	50.07
Judkins	5.80	0.0	1.74	1.77	3.48	4.06	5.28	6.11
Judkins	6.00	0.5	4.00	3.21	6.00	5.60	10.00	8.85
Judkins	6.20	1.0	4.00	5.05	8.00	8.44	12.00	13.43
Judkins	6.20	1.5	8.00	6.86	12.00	11.90	20.00	18.64
Judkins	6.00	2.0	8.00	8.79	16.00	16.24	24.00	24.94
Judkins	8.00	0.0	1.19	1.80	2.19	3.23	4.38	5.65
Judkins	8.00	0.5	3.00	2.73	5.00	3.95	8.00	7.001
Judkins	8.00	1.0	4.00	3.66	6.00	5.28	10.00	9.041
Judkins	8.00	1.5	5.10	4.95	8.00	7.86	13.10	12.82
Judkins	8.10	2.0	6.00	6.14	10.33	10.83	16.33	17.00
Pant	3.95	0.0	0.60	*	0.60	*	1.20	*
Pant	3.70	1.0	1.00	*	1.50	*	2.50	*
Pant	3.70	2.0	1.50	*	1.50	*	3.00	*
Shap	4.00	0.0	35.00	34.84	37.00	36.11	72.00	71.40
Shap	4.00	1.0	37.00	38.93	40.00	42.06	79.00	82.11
Shap	4.00	2.0	57.00	55.20	63.00	61.81	90.00	117.46
Shap	6.10	0.0	20.00	18.05	22.00	21.95	42.00	39.78
Shap	6.00	1.0	22.00	20.76	25.00	24.19	47.00	45.40
Shap	6.00	2.0	32.00	35.11	39.00	39.84	71.00	74.73
Shap	8.00	0.0	8.00	10.10	16.00	16.93	37.00	26.81
Shap	8.00	1.0	12.00	11.30	18.00	16.73	44.00	28.48
Shap	8.00	2.0	26.00	24.68	30.00	30.33	56.00	54.80
Shardlow	3.90	0.0	36.00	35.74	48.00	50.78	84.00	86.52
Shardlow	3.90	1.0	28.00	28.07	44.00	43.21	72.00	71.28

Shardlow	3.80	2.0	32.00	32.03	56.00	54.13	88.00	86.17
Shardlow	6.00	0.0	16.00	13.68	20.00	16.05	36.00	29.74
Shardlow	5.90	1.0	4.00	7.84	12.00	16.34	16.00	24.19
Shardlow	6.00	2.0	8.00	7.47	16.00	15.67	24.00	23.14
Shardlow	8.15	0.0	8.00	10.56	8.00	9.16	16.00	19.72
Shardlow	8.00	1.0	3.00	2.92	1.00	1.78	4.00	4.71
Shardlow	7.50	2.0	8.00	4.64	12.00	9.84	20.00	14.48
Pottal Pool	4.00	0.0	44.00	36.61	52.00	47.62	96.00	84.24
Pottal Pool	4.20	0.5	32.00	33.89	44.00	46.47	76.00	80.37
Pottal Pool	4.10	1.0	32.00	36.03	56.00	50.21	88.00	86.24
Pottal Pool	3.90	1.5	32.00	39.64	44.00	54.66	76.00	94.31
Pottal Pool	3.90	2.0	44.00	38.23	56.00	52.06	100.00	90.29
Pottal Pool	5.80	0.0	12.00	15.96	20.00	20.49	32.00	36.45
Pottal Pool	6.10	0.5	16.00	15.48	20.00	21.52	36.00	37.00
Pottal Pool	6.10	1.0	20.00	15.76	24.00	23.00	44.00	38.77
Pottal Pool	6.09	1.5	16.00	15.25	24.00	22.52	40.00	37.77
Pottal Pool	6.30	2.0	12.00	12.85	16.00	18.36	28.00	31.21
Pottal Pool	8.15	0.0	4.00	8.27	4.00	7.23	8.00	15.50
Pottal Pool	8.00	0.5	12.00	9.66	12.00	11.29	24.00	20.96
Pottal Pool	8.00	1.0	12.00	9.95	12.00	12.78	24.00	22.73
Pottal Pool	8.20	1.5	12.00	9.04	16.00	11.50	28.00	20.54
Pottal Pool	8.40	2.0	4.00	7.31	8.00	8.22	12.00	15.54
Whitwick	4.00	0.0	20.00	20.75	20.00	20.65	40.00	41.41
Whitwick	4.00	0.5	22.00	22.34	26.00	24.69	48.00	47.04
Whitwick	4.28	1.0	24.00	21.98	28.00	26.71	52.00	48.69
Whitwick	4.05	1.5	26.00	25.79	30.00	35.72	56.00	61.51
Whitwick	4.00	2.0	28.00	28.50	48.00	44.19	76.00	72.69
Whitwick	5.80	0.0	12.00	11.31	12.00	11.98	24.00	23.30
Whitwick	6.10	0.5	12.00	11.51	14.00	12.04	26.00	23.55
Whitwick	6.00	1.0	12.00	13.27	16.00	14.57	28.00	27.85
Whitwick	6.00	1.5	14.00	14.94	16.00	17.99	30.00	32.93
Whitwick	6.20	2.0	16.00	16.10	20.00	21.35	36.00	37.45
Whitwick	8.00	0.0	6.00	5.85	6.00	7.93	12.00	13.78
Whitwick	8.20	0.5	6.00	6.49	8.00	7.00	14.00	13.50
Whitwick	8.00	1.0	8.00	8.09	8.00	7.99	16.00	16.08
Whitwick	7.90	1.5	10.00	9.76	10.00	10.16	20.00	19.92
Whitwick	8.00	2.0	12.00	11.25	14.00	12.97	26.00	24.22
Waterswallows	4.20	0.0	8.00	7.36	8.00	7.09	16.00	14.45
Waterswallows	4.30	0.5	8.00	7.83	10.00	8.74	18.00	16.58
Waterswallows	4.00	1.0	10.00	10.16	10.00	11.97	20.00	22.14
Waterswallows	4.00	1.5	12.00	11.88	16.00	15.47	28.00	27.36
Waterswallows	3.90	2.0	14.00	14.48	20.00	20.04	34.00	34.53
Waterswallows	5.90	0.0	2.00	3.62	2.00	4.17	4.00	7.79
Waterswallows	6.10	0.5	4.00	4.04	4.00	5.19	8.00	9.24
Waterswallows	6.20	1.0	4.00	5.04	8.00	7.14	12.00	12.19
Waterswallows	6.00	1.5	8.00	6.92	12.00	10.52	20.00	17.44
Waterswallows	6.10	2.0	10.00	8.81	14.00	14.04	24.00	22.85
Waterswallows	7.80	0.0	2.67	1.67	2.67	1.26	5.33	2.93
Waterswallows	8.10	1.0	4.00	3.18	4.00	3.87	8.00	7.05
Waterswallows	8.00	1.5	4.00	4.78	6.00	6.71	10.00	11.50
Waterswallows	7.90	2.0	6.00	6.84	10.00	10.38	16.00	17.22

Table A 3.3Comparison of Measured and Fitted Wear Values - General Wear Model Excluding Gravel Rocks

Rock	CSS/mm	Moist(%)	CW/(g/T)	FIT	MW/(g/T)	FIT	TW/(g/T)	FIT
Cliffe hill	4.00	0.0	12.00	10.90	16.00	10.80	28.00	21.71
Cliffe hill	4.00	0.5	14.00	12.76	18.00	14.17	32.00	26.91
Cliffe hill	4.00	1.0	16.00	15.74	21.00	18.80	37.00	34.52
Cliffe hill	4.00	1.5	22.00	19.85	28.00	24.69	50.00	44.55
Cliffe hill	4.20	2.0	28.00	23.64	37.00	29.91	65.00	53.58
Cliffe hill	6.00	0.0	3.33	3.45	5.00	3.77	8.33	7.24
Cliffe hill	5.80	0.5	6.00	5.16	10.00	6.19	16.00	11.32
Cliffe hill	5.80	1.0	6.50	7.46	11.00	9.42	17.50	16.84
Cliffe hill	6.00	1.5	10.00	10.19	14.00	13.16	24.00	23.32
Cliffe hill	6.10	2.0	16.00	14.34	20.67	18.42	36.67	32.74
Cliffe hill	8.10	0.0	1.33	-0.65	2.66	0.58	3.99	-0.00
Cliffe hill	8.00	0.5	2.00	0.25	2.00	1.81	4.00	2.07
Cliffe hill	8.00	1.0	3.00	2.12	6.00	4.19	9.00	6.31
Cliffe hill	7.50	1.5	6.67	6.16	10.00	8.88	16.67	15.01
Cliffe hill	8.00	2.0	10.00	9.26	13.50	12.75	23.50	22.00
Ingleton Grey	4.10	0.0	8.00	8.47	8.00	10.64	16.00	19.06
Ingleton Grey	3.90	0.5	9.00	11.32	12.00	14.90	21.00	26.18
Ingleton Grey	4.00	1.0	12.00	13.71	15.00	18.09	27.00	31.78
Ingleton Grey	4.00	1.5	17.00	17.77	21.00	23.38	38.00	41.18
Ingleton Grey	4.00	2.0	24.00	22.97	28.00	29.93	52.00	52.99
Ingleton Grey	5.80	0.0	2.00	2.59	2.00	3.22	4.00	5.81
Ingleton Grey	6.20	0.5	3.00	2.67	4.00	3.30	7.00	5.97
Ingleton Grey	6.00	1.0	5.00	5.39	7.00	6.44	12.00	11.83
Ingleton Grey	6.10	1.5	7.00	10.12	8.00	13.91	15.00	24.01
Ingleton Grey	6.20	2.0	16.00	14.81	17.00	19.84	33.00	34.64
Ingleton Grey	7.90	0.0	0.33	-1.40	0.34	-1.08	0.67	-2.42
Ingleton Grey	7.60	0.5	1.33	0.37	1.33	1.35	2.66	1.75
Ingleton Grey	7.90	1.0	2.00	2.30	3.00	3.98	5.00	6.30
Ingleton Grey	7.80	1.5	4.00	6.04	9.00	8.65	13.00	14.70
Ingleton Grey	8.00	2.0	7.00	10.33	12.00	13.85	19.00	24.22
Judkins	4.10	0.0	4.00	5.19	8.00	8.32	12.00	13.54
Judkins	3.80	0.5	8.00	6.94	12.00	12.28	20.00	19.21
Judkins	4.00	1.0	9.00	8.79	16.00	15.20	25.00	23.96
Judkins	4.00	1.5	12.00	12.20	24.00	20.37	36.00	32.54
Judkins	3.90	2.0	21.00	17.13	33.00	27.63	54.00	44.74
Judkins	5.80	0.0	1.74	3.12	3.48	4.81	5.28	8.06
Judkins	6.00	0.5	3.00	3.35	7.00	5.71	10.00	9.15
Judkins	6.20	1.0	4.00	4.63	8.00	7.69	12.00	12.39
Judkins	6.20	1.5	8.00	7.26	12.00	11.27	20.00	18.57
Judkins	6.00	2.0	12.00	11.39	18.00	16.72	30.00	28.13
Judkins	8.00	0.0	1.19	1.49	2.19	2.95	4.38	4.70
Judkins	8.00	0.5	3.00	1.54	5.00	3.35	8.00	5.08
Judkins	8.00	1.0	4.00	2.73	6.00	5.00	10.00	7.87
Judkins	8.00	1.5	5.10	5.04	8.00	7.92	13.10	13.07
Judkins	8.10	2.0	9.00	8.36	12.00	11.95	21.00	20.40
Pant	3.95	0.0	0.60	1.34	0.60	1.43	1.20	2.77
Pant	3.70	1.0	1.00	-1.65	1.50	-2.26	2.50	-3.92
Pant	3.70	2.0	1.50	3.25	1.50	4.08	3.00	7.36
Shap	4.00	0.0	35.00	33.66	37.00	35.52	72.00	69.20
Shap	4.00	1.0	36.00	36.12	39.00	39.55	75.00	75.66
Shap	4.00	2.0	41.00	43.09	45.00	48.63	86.00	91.76
Shap	5.90	0.0	20.00	*	22.00	*	42.00	*
Shap	8.00	0.0	11.00	14.05	14.00	19.32	25.00	33.43
Shap	8.00	1.0	13.00	14.30	18.00	18.85	31.00	33.13
Shap	8.00	2.0	22.00	19.06	27.00	23.44	49.00	42.48
WaterSwallows	4.20	0.0	8.00	8.49	8.00	8.39	16.00	16.94
WaterSwallows	4.30	0.5	9.00	9.09	9.00	10.26	18.00	19.36
WaterSwallows	4.00	1.0	10.00	12.47	10.00	15.50	20.00	27.97

WaterSwallows	4.00	1.5	14.00	15.81	15.00	20.56	29.00	36.36
WaterSwallows	3.90	2.0	17.00	20.87	18.00	27.77	35.00	48.66
WaterSwallows	5.90	0.0	2.67	4.25	2.67	4.38	5.33	8.71
WaterSwallows	6.10	0.5	3.00	4.21	4.00	5.08	7.00	9.31
WaterSwallows	6.20	1.0	5.00	5.44	6.00	7.09	11.00	12.52
WaterSwallows	6.00	1.5	8.00	8.49	9.00	11.13	17.00	19.58
WaterSwallows	6.10	2.0	12.00	11.94	13.00	15.62	25.00	27.52
WaterSwallows	7.80	0.0	1.00	1.49	2.00	2.35	3.00	3.97
WaterSwallows	8.10	1.0	2.00	2.23	3.00	3.91	5.00	6.16
WaterSwallows	8.00	1.5	4.00	4.59	6.00	6.85	10.00	11.43
WaterSwallows	7.90	2.0	7.00	8.12	10.00	11.11	17.00	19.20

Table A 3.4 Comparison Of Measured And Fitted Wear Values- General Wear Model

Rock	CSS/mm	Moist(%)	CW/(g/T)	FIT	MW/(g/T)	FIT	TW/(g/T)	FIT
Cliffe Hill	4.00	0.0	12.00	12.94	16.00	12.79	28.00	25.74
Cliffe Hill	4.00	0.5	14.00	14.16	18.00	15.46	32.00	29.61
Cliffe Hill	4.00	1.0	16.00	16.50	21.00	19.27	37.00	35.76
Cliffe Hill	4.00	1.5	22.00	19.97	28.00	24.22	50.00	44.18
Cliffe Hill	4.20	2.0	28.00	22.87	37.00	28.38	65.00	51.25
Cliffe Hill	6.00	0.0	3.33	3.55	5.00	4.08	8.33	7.66
Cliffe Hill	5.80	0.5	6.00	5.01	10.00	6.41	16.00	11.42
Cliffe Hill	5.80	1.0	6.50	7.03	11.00	9.38	17.50	16.38
Cliffe Hill	6.00	1.5	10.00	9.53	14.00	12.78	24.00	22.28
Cliffe Hill	6.10	2.0	16.00	13.47	20.67	17.60	36.67	31.05
Cliffe Hill	8.10	0.0	1.33	-0.30	2.66	0.67	3.99	0.43
Cliffe Hill	8.00	0.5	2.00	0.51	2.00	2.09	4.00	2.62
Cliffe Hill	8.00	1.0	3.00	2.33	6.00	4.53	9.00	6.86
Cliffe Hill	7.50	1.5	6.67	6.08	10.00	8.99	16.67	15.05
Cliffe Hill	8.00	2.0	10.00	9.35	13.50	12.84	23.50	22.17
Ingleton Grey	4.10	0.0	8.00	10.80	8.00	13.25	16.00	24.06
Ingleton Grey	3.90	0.5	9.00	12.74	12.00	16.99	21.00	29.73
Ingleton Grey	4.00	1.0	12.00	13.75	15.00	19.27	27.00	33.02
Ingleton Grey	4.00	1.5	17.00	16.60	21.00	23.60	38.00	40.20
Ingleton Grey	4.00	2.0	24.00	20.57	28.00	29.07	52.00	49.67
Ingleton Grey	5.80	0.0	2.00	4.34	2.00	5.19	4.00	9.59
Ingleton Grey	6.20	0.5	3.00	3.73	4.00	5.20	7.00	8.97
Ingleton Grey	6.00	1.0	5.00	5.53	7.00	8.04	12.00	13.59
Ingleton Grey	6.10	1.5	7.00	10.57	8.00	14.06	15.00	24.63
Ingleton Grey	6.20	2.0	16.00	14.87	17.00	19.20	33.00	34.09
Ingleton Grey	7.90	0.0	0.33	1.20	0.34	1.11	0.67	2.42
Ingleton Grey	7.60	0.5	1.33	2.53	1.33	3.25	2.66	5.84
Ingleton Grey	7.90	1.0	2.00	4.34	3.00	5.61	5.00	9.99
Ingleton Grey	7.80	1.5	4.00	7.71	9.00	9.75	13.00	17.50
Ingleton Grey	8.00	2.0	7.00	11.86	12.00	14.48	19.00	26.37
Judkins	4.10	0.0	4.00	5.35	8.00	8.86	12.00	14.25
Judkins	3.80	0.5	8.00	7.86	12.00	13.29	20.00	21.14
Judkins	4.00	1.0	9.00	9.11	16.00	15.54	25.00	24.65
Judkins	4.00	1.5	12.00	12.48	24.00	20.32	36.00	32.79
Judkins	3.90	2.0	21.00	17.53	33.00	27.11	54.00	44.64
Judkins	5.80	0.0	1.74	1.58	3.48	3.56	5.28	5.25
Judkins	6.00	0.5	3.00	2.13	7.00	4.80	10.00	7.01
Judkins	6.20	1.0	4.00	3.78	8.00	7.11	12.00	10.95
Judkins	6.20	1.5	8.00	6.78	12.00	10.91	20.00	17.73
Judkins	6.00	2.0	12.00	11.18	18.00	16.40	30.00	27.626
Judkins	8.00	0.0	1.19	0.12	2.19	1.18	4.38	1.50
Judkins	8.00	0.5	3.00	0.72	5.00	2.30	8.00	3.17
Judkins	8.00	1.0	4.00	2.43	6.00	4.57	10.00	7.12
Judkins	8.00	1.5	5.10	5.28	8.00	7.98	13.10	13.35
Judkins	8.10	2.0	9.00	9.19	12.00	12.40	21.00	21.68
Pant	3.95	0.0	0.60	-0.96	0.60	-1.77	1.20	-2.75
Pant	3.70	1.0	1.00	-0.35	1.50	-1.18	2.50	-1.54
Pant	3.70	2.0	1.50	4.50	1.50	6.45	3.00	10.98
Pottal Pool	4.00	0.0	44.00	38.43	52.00	49.89	96.00	88.34
Pottal Pool	4.20	0.5	32.00	33.60	44.00	45.19	76.00	78.79
Pottal Pool	4.10	1.0	32.00	34.20	56.00	47.53	88.00	81.74
Pottal Pool	3.90	1.5	32.00	37.70	44.00	53.58	76.00	91.32
Pottal Pool	3.90	2.0	44.00	39.19	56.00	56.38	100.00	95.65
Pottal Pool	5.80	0.0	12.00	20.72	20.00	25.60	32.00	46.33
Pottal Pool	6.10	0.5	16.00	16.65	20.00	21.47	36.00	38.10
Pottal Pool	6.10	1.0	20.00	15.49	24.00	20.98	44.00	36.45
Pottal Pool	6.09	1.5	16.00	15.53	24.00	21.72	40.00	37.24
Pottal Pool	6.30	2.0	12.00	15.39	16.00	21.68	28.00	37.07
Pottal Pool	8.15	0.0	4.00	10.54	4.00	11.32	8.00	21.89

Pottal Pool	8.00	0.5	12.00	8.55	12.00	9.91	24.00	18.46
Pottal Pool	8.00	1.0	12.00	7.24	12.00	8.99	24.00	16.22
Pottal Pool	8.20	1.5	12.00	6.41	16.00	8.28	28.00	14.68
Shap	4.00	0.0	35.00	33.98	37.00	35.08	72.00	69.09
Shap	4.00	1.0	36.00	35.57	39.00	39.35	75.00	74.91
Shap	4.00	2.0	41.00	41.66	45.00	48.18	86.00	89.86
Shap	5.90	0.0	20.00	*	22.00	*	42.00	*
Shap	8.00	0.0	11.00	14.25	14.00	17.78	25.00	32.08
Shap	8.00	1.0	13.00	14.79	18.00	19.31	31.00	34.09
Shap	8.00	2.0	22.00	19.84	27.00	25.41	49.00	45.22
Shardlow	3.90	0.0	36.00	31.83	48.00	45.78	84.00	77.57
Shardlow	3.90	1.0	28.00	29.27	44.00	45.79	72.00	75.02
Shardlow	3.80	2.0	32.00	32.84	56.00	52.91	88.00	85.77
Shardlow	6.00	0.0	16.00	13.12	20.00	17.68	36.00	30.80
Shardlow	5.90	1.0	4.00	10.37	12.00	16.63	16.00	26.97
Shardlow	6.00	2.0	8.00	10.99	16.00	18.35	24.00	29.33
Shardlow	8.15	0.0	8.00	5.04	8.00	5.11	16.00	10.19
Shardlow	8.00	1.0	3.00	2.88	1.00	1.77	4.00	4.66
Shardlow	8.40	2.0	4.00	6.72	8.00	8.68	12.00	15.41
Shardlow	7.50	2.0	8.00	4.23	12.00	7.28	20.00	11.53
Waterswallows	4.20	0.0	8.00	8.55	8.00	8.43	16.00	17.00
Waterswallows	4.30	0.5	9.00	8.98	9.00	10.15	18.00	19.13
Waterswallows	4.00	1.0	10.00	13.07	10.00	15.64	20.00	28.70
Waterswallows	4.00	1.5	14.00	16.40	15.00	20.36	29.00	36.74
Waterswallows	3.90	2.0	17.00	21.65	18.00	27.16	35.00	48.82
Waterswallows	5.90	0.0	2.67	2.32	2.67	2.76	5.33	5.12
Waterswallows	6.10	0.5	3.00	2.61	4.00	3.88	7.00	6.50
Waterswallows	6.20	1.0	5.00	4.22	6.00	6.29	11.00	10.50
Waterswallows	6.00	1.5	8.00	7.65	9.00	10.58	17.00	18.20
Waterswallows	6.10	2.0	12.00	11.50	13.00	15.23	25.00	26.70
Waterswallows	7.80	0.0	1.00	-0.58	2.00	0.26	3.00	-0.24
Waterswallows	8.10	1.0	2.00	1.33	3.00	3.27	5.00	4.61
Waterswallows	8.00	1.5	4.00	4.24	6.00	6.74	10.00	10.97
Waterswallows	7.90	2.0	7.00	8.29	10.00	11.39	17.00	19.66

Appendix 4 SIZE DISTRIBUTION OF PRODUCT OF WEAR EXPERIMENT

Table A 4.1 Product Grading - Cliffe Hill Rock

Cliffe Hill Discharge setting/ mm	% passing through sieve openings													
	Moisture %	20.00 mm	14.00 mm	10.00 mm	6.30 mm	5.00 mm	3.35 mm	2.36 mm	1.18 mm	0.60 mm	0.30 mm	0.212 mm	0150 mm	0.075 mm
4.00	0.0	100	100	100	98.5	90.5	54.4	35.0	17.6	10.4	6.4	4.8	3.6	2.0
3.50	1.0	100	100	100	99.0	93.6	58.8	37.7	19.4	11.8	7.3	5.7	4.5	2.6
4.00	1.5	100	100	100	99.3	95.8	64.7	27.0	18.4	11.0	6.9	5.5	4.5	2.9
5.00	0.0	100	100	99.2	78.3	50.2	27.4	17.7	8.8	4.5	2.5	2.0	1.8	1.2
6.00	0.0	100	100	94.4	42.6	25.3	13.9	10.2	6.1	4.4	3.3	2.9	2.5	1.7
.6.00	0.5	100	100	95.4	62.7	38.1	23.7	18.5	10.6	6.9	4.6	3.7	3.0	2.0
6.00	1.0	100	100	97.8	62.2	33.6	17.4	9.2	6.2	3.9	2.7	2.3	1.9	1.2
6.00	1.5	100	100	98.4	67.6	41.7	22.7	12.9	9.1	5.8	3.7	3.0	2.4	1.5
8.00	0.0	100	99.6	72.3	20.4	15.1	9.6	7.2	4.0	2.5	1.8	1.5	1.2	0.7
8.00	0.5	100	100	81.7	22.4	15.7	10.7	7.2	5.6	4.1	3.0	2.4	1.9	1.0
4.00 (6.3-10)	0.0	100	100	99.9	96.9	79.4	39.9	26.6	14.1	8.4	5.2	4.1	3.2	1.8
4.10 (6.3-10)	2.0	100	100	100	96.6	80.1	35.9	21.4	11.4	7.5	5.2	4.4	3.6	1.4

Table A 4.2 Product Grading - Judkins Rock

Judkins Discharge setting/ mm	% passing through sieve openings													
	Moisture %	20.00 mm	14.00 mm	10.00 mm	6.30 mm	5.00 mm	3.35 mm	2.36 mm	1.18 mm	0.60 mm	0.30 mm	0.212 mm	0150 mm	0.075 mm
4.20	0.0	100	100	100	92.4	67.9	26.9	14.6	5.3	2.6	1.6	1.3	1.0	0.9
3.80	0.5	100	100	100	98.4	88.1	49.1	29.3	13.0	6.4	3.2	2.6	2.1	1.3
4.00	1.0	100	100	100	99.2	92.8	58.2	36.1	17.8	10.8	6.5	4.9	3.9	2.2
4.00	1.5	100	100	100	98.8	91.4	54.2	36.1	17.5	10.8	6.8	5.4	4.3	2.4
3.90	2.0	100	100	99.7	98.2	91.2	53.3	34.4	17.4	11.6	7.9	6.3	5.0	1.7
4.80	0.0	100	100	99.9	86.1	61.8	29.6	17.7	7.5	3.3	1.4	1.1	0.9	0.5
6.00	0.5	100	100	97.8	66.2	39.6	22.7	11.6	7.6	4.2	2.6	2.2	1.9	1.2
6.20	1.0	100	100	97.9	65.0	36.5	20.6	11.1	7.3	4.4	2.8	2.7	2.3	1.3
6.20	1.5	100	100	95.1	54.5	31.4	17.5	10.0	7.2	4.9	3.2	2.6	2.0	1.2
6.10	2.0	100	100	97.2	66.6	42.5	28.0	17.5	13.1	8.8	6.0	4.8	3.9	2.4
7.00	0.0	100	100	92.4	37.6	23.8	14.4	8.4	5.9	3.4	2.0	1.7	1.4	1.0
8.00	0.0	100	100	83.3	19.8	14.0	8.2	5.5	2.5	1.2	0.6	0.5	0.4	0.2
8.00	0.5	100	100	79.1	20.6	12.2	7.0	3.5	2.3	1.4	0.9	0.8	0.7	0.4
8.00	1.0	100	99.2	76.0	18.6	11.8	8.1	4.8	3.4	2.3	1.6	1.3	1.0	0.7
8.00	1.5	100	99.8	86.8	27.2	18.9	12.7	7.9	5.8	3.8	2.6	2.1	1.7	1.1
8.00	2.0	100	99.7	87.5	31.4	20.4	13.7	8.8	7.3	5.5	4.1	3.5	3.0	2.1
4.00 (6.3-10)	0.0	100	100	100	98.1	87.7	45.8	28.4	12.7	6.6	3.7	2.9	2.3	1.3
4.00 (6.3-10)	2.0	100	100	100	99.2	91.0	51.4	32.9	17.2	11.0	7.5	6.0	4.8	1.5

Table A 4.3Product Grading - Ingleton Grey Rock

Ingleton Discharge setting/ mm	% passing through sieve openings													
	moisture %	20.00 mm	14.00 mm	10.00 mm	6.30 mm	5.00 mm	3.35 mm	2.36 mm	1.18 mm	0.60 mm	0.30 mm	0.212 mm	0150 mm	0.075 mm
4.10	0.0	100	100	99.7	90.7	68.6	32.8	21.6	9.3	4.7	2.9	2.2	1.8	1.0
3.90	0.5	100	100	99.6	93.3	76.2	37.2	16.5	9.8	5.5	3.6	3.1	2.6	1.7
4.00	1.0	100	100	99.7	94.3	75.8	35.3	21.8	10.7	6.2	3.9	3.2	2.6	1.6
4.00	1.5	100	100	100	95.4	78.3	40.1	27.4	16.6	11.5	8.4	7.2	6.0	3.9
4.00	2.0	100	100	100	87.6	61.0	31.0	17.2	12.1	8.4	5.7	4.7	3.9	2.4
5.20	0.0	100	100	97.8	65.5	35.7	20.3	11.2	7.0	4.0	3.0	2.8	2.6	2.0
6.00	0.0	100	100	94.4	45.6	26.9	16.0	7.6	5.3	3.6	2.8	2.6	2.5	2.2
6.20	0.5	100	100	94.1	46.5	22.8	12.8	6.7	4.6	3.1	2.2	1.9	1.6	1.0
6.00	1.0	100	100	96.0	46.9	26.9	16.9	9.7	7.2	5.0	3.5	2.8	2.2	1.2
6.10	1.5	100	100	96.2	49.2	25.5	16.0	9.6	7.3	5.3	4.0	3.4	2.8	1.5
6.20	2.0	100	100	96.6	56.7	31.1	20.3	13.3	10.5	8.0	6.0	5.1	4.2	2.2
7.00	0.0	100	99.0	79.1	23.4	15.0	9.8	6.2	4.6	3.4	2.6	2.2	1.9	1.3
7.75	0.0	100	98.1	51.3	6.2	3.8	2.0	1.4	0.7	0.5	0.4	0.3	0.1	0.0
7.60	0.5	100	100	81.2	18.8	13.5	9.2	5.3	3.7	2.3	1.6	1.4	1.2	0.8
7.90	1.0	100	99.7	82.4	21.1	16.5	11.5	7.7	6.1	4.7	3.7	3.1	2.7	1.4
8.00	1.5	100	100	86.8	28.6	18.5	11.4	7.1	5.4	3.9	2.9	2.4	2.1	0.9
8.00	2.0	100	100	91.1	32.9	21.6	13.0	8.6	6.9	5.2	3.9	3.3	2.8	2.0
4.0 (6.3-10)	0.0	100	100	100	93.6	61.5	25.0	15.1	6.2	2.9	1.5	1.1	0.9	0.7
4.0(6.3-10)	2.0	100	100	100	96.0	72.3	32.7	23.1	14.0	10.4	8.1	6.9	5.7	2.0

Table A 4.4Product Grading - Shardlow Rock

Shardlow Discharge setting/ mm	% passing through sieve openings													
	Moisture %	20.00 mm	14.00 mm	10.00 mm	6.30 mm	5.00 mm	3.35 mm	2.36 mm	1.18 mm	0.60 mm	0.30 mm	0.212 mm	0150 mm	0.075 mm
4.00	0.0	100	100	100	95.3	85.1	39.6	26.8	15.1	11.5	9.5	8.6	7.7	6.1
4.00	2.0	100	100	100	99.9	98.8	84.2	52.3	22.6	13.8	9.0	7.1	5.8	3.1
6.00	0.0	100	100	97.4	69.2	30.2	10.0	4.0	0.9	0.8	0.7	0.6	0.5	0.4
6.00	1.0	100	99.7	97.9	66.1	35.5	17.7	11.8	6.5	4.3	3.1	2.7	2.2	1.4
6.00	2.0	100	100	98.8	62.2	37.5	21.0	12.9	10.0	7.5	5.7	4.9	4.1	2.5
8.00	0.0	100	98.5	71.9	12.5	5.3	1.9	1.3	0.5	0.4	0.3	0.2	0.1	0.0
8.00	1.0	100	100	88.3	26.5	14.2	7.3	4.2	3.2	2.4	1.8	1.5	1.2	0.7
8.00	2.0	100	100	91.2	36.6	19.8	11.6	7.2	5.6	4.3	3.5	3.1	2.7	2.0
10.00	0.0	100	100	49.5	7.4	6.4	3.7	2.6	2.4	2.3	2.2	2.2	2.2	2.2
4.00 (6.3-10)	5.0	100	100	100	98.6	93.9	67.2	44.7	26.7	19.8	15.2	12.9	10.7	4.3

Table A 4.5 Product Grading - Shap Rock

Shap Discharge setting/ mm	% passing through sieve openings													
	Moisture %	20.00 mm	14.00 mm	10.00 mm	6.30 mm	5.00 mm	3.35 mm	2.36 mm	1.18 mm	0.60 mm	0.30 mm	0.212 mm	0150 mm	0.075 mm
3.90	0.0	100	100	100	98.6	90.1	55.9	35.1	15.0	7.8	5.3	4.6	3.9	2.5
4.20	2.5	100	99.4	99.4	95.9	80.0	39.6	25.3	12.9	8.0	5.1	4.0	2.8	0.3
4.00	5.0	100	100	100	99.7	96.1	69.5	48.1	28.9	20.6	15.0	12.4	10.1	5.0
6.10	0.0	100	100	98.5	58.6	36.0	20.0	13.5	5.6	2.9	1.9	1.7	1.0	0.5
8.00	0.0	100	99.7	84.7	24.3	15.2	9.2	4.6	3.1	2.0	1.6	1.5	1.4	1.2
8.00	2.5	100	100	82.7	27.9	20.5	13.5	7.9	5.8	4.2	3.1	2.7	2.3	1.1
8.00	5.0	100	99.8	83.7	24.7	18.4	12.1	8.1	6.6	4.9	3.6	3.1	2.6	1.6
10.00	0.0	100	99.0	38.4	4.3	2.5	1.5	0.8	0.7	0.6	0.5	0.5	0.4	0.3
4 .00(6.3-10)	0.0	100	100	100	96.4	86.5	38.4	18.2	3.5	1.4	1.0	0.8	0.6	0.4
4.00 (6.3-10)	5.0	100	100	100	99.6	95.2	62.3	38.7	20.9	13.2	8.5	6.8	5.1	1.0

Table A 4.6 Product Grading - Whitwick Rock

Whitwick	% passing through sieve openings													
Discharge setting/ mm	Moisture %	20.00 mm	14.00 mm	10.00 mm	6.30 mm	5.00 mm	3.35 mm	2.36 mm	1.18 mm	0.60 mm	0.30 mm	0.212 mm	0150 mm	0.075 mm
4.00	0.0	100	100	100	97.0	79.8	40.2	27.1	13.2	6.8	3.7	3.0	2.4	1.4
4.00	0.5	100	100	99.9	94.9	80.2	40.3	25.2	12.5	6.9	4.5	3.9	3.3	1.6
4.28	1.0	100	100	99.6	88.0	64.3	31.4	20.6	11.2	7.1	4.9	4.1	3.4	1.9
4.05	1.5	100	100	99.7	94.5	80.5	43.6	19.1	12.9	7.7	5.2	4.4	3.7	2.5
4.00	2.0	100	100	99.9	96.9	85.0	47.3	30.8	17.3	11.7	8.1	6.5	5.2	1.3
5.80	0.0	100	100	91.8	34.4	18.6	9.8	6.7	3.1	1.9	1.4	1.2	0.8	0.1
6.00	0.0	100	100	99.7	87.2	65.0	37.7	26.1	13.4	7.8	4.7	3.7	2.9	1.5
6.20	0.0	100	100	92.1	38.7	24.3	14.5	12.0	5.5	3.2	2.1	1.7	1.0	0.3
6.10	0.5	100	100	96.8	54.7	33.1	20.0	11.3	7.9	5.0	3.3	2.9	2.5	1.7
6.00	1.0	100	100	96.1	56.4	35.0	19.8	11.5	8.6	6.1	4.6	4.1	3.7	2.9
6.00	1.5	100	100	96.2	54.5	30.0	17.5	10.2	7.6	5.2	3.9	3.4	2.9	2.1
6.20	2.0	100	100	97.7	53.1	29.3	15.6	9.0	7.0	5.0	3.2	2.6	1.9	0.8
7.00	0.0	100	99.8	79.2	16.5	10.4	4.9	2.1	1.3	0.9	0.7	0.6	0.5	0.2
8.00	0.0	100	99.9	60.7	11.2	6.5	3.4	2.0	0.9	0.7	0.6	0.5	0.3	0.1
8.20	0.5	100	99.1	49.7	6.2	3.8	2.0	1.2	1.0	0.9	0.9	0.9	0.9	0.7
7.90	1.5	100	100	77.2	19.2	14.1	10.5	8.2	7.2	6.2	5.6	5.3	5.0	4.6
8.00	2.0	100	100	73.6	15.9	10.1	6.5	4.5	3.8	3.0	2.4	2.1	1.8	1.3
9.11	0.0	100	99.8	66.7	9.9	5.1	2.2	0.9	0.6	0.5	0.4	0.4	0.3	0.2
3.90 (6.3-10)	0.0	100	100	100	93.7	65.2	28.3	19.1	8.1	4.6	3.0	2.5	1.9	0.6
4.00 (6.3-10)	2.0	100	100	99.8	84.1	58.0	30.0	16.0	10.7	6.8	4.8	4.0	3.2	1.4

Table A 4.7 Product Grading - Waterswallows Rock

Waterswallows	% passing through sieve openings													
Discharge setting/ mm	Moisture %	20.00 mm	14.00 mm	10.00 mm	6.30 mm	5.00 mm	3.35 mm	2.36 mm	1.18 mm	0.60 mm	0.30 mm	0.212 mm	0150 mm	0.075 mm
4.20	0.0	100	100	100	91.5	68.1	24.7	14.9	6.0	4.1	3.3	3.1	2.9	2.5
4.20	0.5	100	100	100	95.2	75.9	35.2	23.5	12.3	8.3	6.2	5.4	4.7	3.1
3.90	1.0	100	100	99.6	98.3	88.0	44.1	24.3	16.0	11.8	9.9	9.3	8.7	6.2
4.00	1.5	100	100	100	99.1	91.5	52.2	34.5	19.6	13.0	9.0	7.4	5.0	0.6
3.90	2.0	100	100	100	98.0	83.2	39.8	25.3	13.7	8.9	6.2	5.2	4.3	2.6
5.00	0.0	100	100	99.8	86.2	57.6	25.9	12.1	7.9	5.0	3.8	3.5	3.2	2.5
5.90	0.0	100	100	97.7	44.9	26.3	13.6	9.3	4.6	3.0	2.3	2.1	1.9	1.3
6.10	0.5	100	100	96.4	52.0	27.7	15.0	7.9	6.0	4.3	3.4	3.1	2.9	2.2
6.20	1.0	100	100	96.2	51.0	27.3	15.5	10.5	6.4	4.6	3.6	3.2	2.8	2.0
6.00	1.5	100	100	98.6	67.1	36.3	22.2	13.6	10.5	7.8	5.9	5.0	4.1	2.4
6.10	2.0	100	100	98.7	67.2	34.8	19.9	12.4	9.5	7.1	5.5	4.8	4.0	2.5
7.80	0.0	100	100	80.5	17.1	10.8	5.7	4.9	1.4	1.0	0.9	0.8	0.3	0.0
8.00	0.5	100	100	71.3	14.0	8.6	5.3	3.3	2.4	1.8	1.4	1.3	1.2	0.8
8.00	1.5	100	96.4	77.5	19.3	6.8	3.7	2.9	2.6	2.2	2.0	1.9	1.8	1.5
7.90	2.0	100	99.7	90.3	23.9	15.7	10.3	7.2	5.9	4.7	3.8	3.4	2.9	2.0
3.80 (6.3-10)	0.0	100	100	100	99.4	94.0	52.4	29.7	13.4	7.9	5.6	4.9	3.7	1.0
3.70 (6.3-10)	2.0	100	100	100	99.7	97.5	67.3	39.4	19.6	13.6	10.0	8.6	7.2	4.4

Table A 4.8 Product Grading - Pottal Pool Rock

Pottal pool	% passing through sieve openings												
Discharge setting/ mm	Moisture %	20.0 mm	14.00 mm	10.00 mm	6.30 mm	5.00 mm	3.35 mm	2.36 mm	1.18 mm	0.60 mm	0.30 mm	0.212 mm	0150 mm	0.075 mm
4.00	0.0	100	100	100	94.1	77.1	34.1	21.1	8.4	4.4	2.7	2.3	2.0	1.3
4.20	0.5	100	100	99.9	93.8	72.9	34.1	21.3	9.0	5.0	3.1	2.6	2.3	1.6
4.10	1.0	100	100	100	97.5	87.3	50.1	21.8	13.8	8.5	5.8	4.9	4.1	2.4
3.90	1.5	100	100	99.9	97.7	87.7	50.0	31.2	14.9	9.7	6.9	5.9	5.0	2.3
3.90	2.0	100	100	99.9	97.8	88.4	52.8	33.2	16.3	11.0	8.1	6.9	5.9	3.5
5.15	0.0	100	100	99.6	74.8	45.6	22.0	10.7	7.1	4.1	2.7	2.2	1.8	1.2
5.80	0.0	100	100	98.4	43.5	26.3	12.9	8.2	3.5	2.0	1.4	1.2	1.0	0.5
6.10	0.5	100	100	97.4	44.1	23.1	12.3	8.6	4.0	2.6	2.1	1.9	1.7	1.2
6.10	1.0	100	100	97.3	49.6	25.3	12.9	8.6	4.1	2.6	1.9	1.7	1.5	1.0
6.09	1.5	100	100	98.6	50.4	28.1	16.4	9.8	7.6	5.7	4.4	3.7	3.1	2.0
6.30	2.0	100	100	97.7	46.9	27.8	16.0	9.1	6.9	5.2	4.0	3.6	3.1	2.1
7.10	0.0	100	100	91.0	27.8	15.4	8.6	4.3	3.0	2.0	1.5	1.4	1.3	1.0
8.15	0.0	100	99.8	72.2	10.4	6.2	3.3	2.0	0.9	0.6	0.5	0.4	0.1	0.0
8.00	0.5	100	100	88.1	23.7	13.4	7.5	4.0	2.7	1.8	1.3	1.1	1.0	0.7
8.00	1.0	100	100	90.0	27.8	15.4	8.7	4.9	3.7	2.8	2.2	2.0	1.8	1.6
8.20	1.5	100	100	88.8	24.7	14.5	8.3	5.2	4.1	3.2	2.6	2.3	2.1	1.6
8.40	2.0	100	100	87.4	24.1	14.4	8.8	6.1	5.0	3.9	3.1	2.7	2.3	1.7
9.00	0.0	100	98.9	62.1	10.7	6.3	3.7	2.0	1.4	1.0	0.8	0.7	0.6	0.5
4.10 (6.3-10)	0.0	100	100	99.7	96.5	85.2	48.5	37.3	13.1	6.3	3.1	2.3	1.8	0.8
4.20 (6.3-10)	2.0	100	100	99.7	98.2	90.0	48.8	29.7	14.6	10.6	8.0	6.9	5.8	3.5

Table A 4.9Product Grading - Breedon Rock

Breedon Discharge setting/ mm	% passing through sieve openings													
	Moistur e %	20.00 mm	14.00 mm	10.00 mm	6.30 mm	5.00 mm	3.35 mm	2.36 mm	1.18 mm	0.60 mm	0.30 mm	0.212 mm	0.150 mm	0.075 mm
3.70	0.0	100	100	100	99.9	98.8	82.3	45.9	17.7	9.4	5.4	4.3	3.2	1.0
3.40	1.0	100	100	100	99.6	95.5	68.9	43.5	22.4	13.6	7.9	5.9	4.2	0.9
4.00	1.5	100	100	99.7	98.1	85.9	47.2	30.6	16.5	11.0	7.5	5.9	4.5	1.7

Pant Discharge setting/ mm	% passing through sieve openings													
	Moisture %	20.00 mm	14.00 mm	10.00 mm	6.30 mm	5.00 mm	3.35 mm	2.36 mm	1.18 mm	0.60 mm	0.30 mm	0.212 mm	0150 mm	0.075 mm
3.80	0.0	100	100	99.7	94.0	83.8	48.5	28.7	13.2	8.2	5.6	4.6	3.8	1.2
3.70	1.0	100	100	100	98.0	90.5	57.5	35.5	16.1	9.3	5.7	4.5	3.7	1.8
3.70	2.0	100	100	100	99.1	95.2	69.5	43.2	22.8	14.2	9.5	8.2	6.9	3.6
5.10	0.0	100	100	99.4	71.0	39.5	15.7	10.3	3.4	1.9	1.5	1.3	1.1	0.9

Table A 4.10 Product Grading - Pant Rock

Table A 4.11The 80% Passing Size for Different Test Products

Rock	CSS/Mm	Moist(%)	80%(mm)
Breedon	3.7	0.0	3.2
Breedon	3.4	1.0	4.0
Breedon	4.0	1.5	4.8
Cliffe Hill	4.0	0.0	4.5
Cliffe Hill	3.5	1.0	4.3
Cliffe Hill	4.0	1.5	4.1
Cliffe Hill	5.0	0.0	6.4
Cliffe Hill	6.0	0.0	6.7
Cliffe Hill	6.0	1.0	6.0
Cliffe Hill	8.0	0.0	11.0
Cliffe Hill	8.0	1.5	10.0
Cliffe Hill	4.0	0.0	5.1
Cliffe Hill	4.0	2.0	4.9
Ingleton Grey	4.1	0.0	5.8
Ingleton Grey	4.0	1.5	5.0
Ingleton Grey	5.0	0.0	8.0
Ingleton Grey	6.0	0.0	9.0
Ingleton Grey	6.2	2.0	8.6
Ingleton Grey	7.0	0.0	10.5
Ingleton Grey	7.8	0.0	12.5
Ingleton Grey	8.0	2.0	9.2
Ingleton Grey	4.0	0.0	5.8
Ingleton Grey	4.0	2.0	5.2
Judkins	4.2	0.0	5.8
Judkins	3.9	2.0	4.5
Judkins	6.0	0.5	7.8
Judkins	6.0	2.0	7.7
Judkins	7.0	0.0	9.0
Judkins	8.1	0.0	10.0
Judkins	8.0	2.0	9.8
Judkins	4.0	0.0	4.8
Judkins	4.0	2.0	4.5
Pant	3.8	0.0	4.8
Pant	3.7	1.0	4.5
Pant	3.7	2.0	4.0
Pant	5.1	0.0	8.2

Rock	CSS/Mm	Moist(%)	80%(mm)
Pottal Pool	4.0	0.0	5.0
Pottal Pool	3.9	2.0	4.5
Pottal Pool	5.1	0.0	7.0
Pottal Pool	5.8	0.0	8.8
Pottal Pool	6.3	2.0	8.5
Pottal Pool	7.1	0.0	9.2
Pottal Pool	8.1	0.0	10.5
Pottal Pool	8.4	2.0	9.8
Pottal Pool	4.1	0.0	4.8
Pottal Pool	4.2	2.0	4.6
Shardlow	4.0	0.0	4.8
Shardlow	4.0	2.0	3.2
Shardlow	6.0	0.0	8.2
Shardlow	6.0	2.0	8.0
Shardlow	8.0	0.0	10.5
Shardlow	8.0	2.0	9.2
Whitwick	4.0	9.0	5.0
Whitwick	4.0	2.0	4.6
Whitwick	5.8	0.0	9.1
Whitwick	6.1	2.0	8.3
Whitwick	7.0	0.0	10.0
Whitwick	8.0	0.0	12.0
Whitwick	4.0	0.0	5.8
Whitwick	8.0	2.0	11.0
Whitwick	4.0	2.0	5.1
Waterswallows	4.2	0.0	5.6
Waterswallows	3.9	2.0	5.0
Waterswallows	5.0	0.0	6.0
Waterswallows	5.9	0.0	8.8
Waterswallows	6.1	2.0	8.0
Waterswallows	8.0	0.5	11.0
Waterswallows	7.8	2.0	9.5
Waterswallows	3.9	0.0	4.5
Waterswallows	3.8	2.0	4.0

Appendix 6 LISTING OF WEAR ANALYSER PROGRAMME

```
#include <stdio.h>
#include <stdlib.h>
#include <time.h>
#include <conio.h>
#include <graphics.h>
#include <string.h>
#include <math.h>


/* declaration of constants*/


#define TRUE    1

/* decleration of globals */

char     MOIST_PRESENT;
char   FUZZY_MOIST;
char     DISPLAY_RESULT;
char   CH;

float  DISCHARGE_SETTING;
float    CSS;
float    MOISTURE;
float    MOISTURE2;
float    FT;
float    UCS;
float    BTS;
float    PL;
float    PH;
float    SI;
float    AAV;
float  FM [2][2];
float    A[9];
float    WA;
float    OTHER;
float    WEAR;

/* declaration of functions */

void main();
void logo();
void rock_selection_option();
void material_property();
void shap();
void cliffe_hill();
void waterswallows();
void pottal_pool();
```

```
void whitwick();
void pant();
void judkins();
void shardlow();
void ingleton();
void show_material_property();
void moisture();
void drywear();
void moistwear();
void fuzzy_wear();
void general_drywear();
void display_results();


void main()

{

OTHER=0;

rock_selection_option();

}

void rock_selection_option()  /* allows the rock to be selected from a list*/

{

logo();

        printf("\n\n\n\n            THE MATERIAL SELECTION DATA BASE\n\n\n\n");
        printf("                        1.      Shap Blue\n");
        printf("                        2.   Cliffe Hill\n");
        printf("                        3.      Waterswallows\n");
        printf("                        4.      Pottal Pool\n");
        printf("                        5.      Whitwick\n");
        printf("                        6.   Judkins\n");
        printf("                        7.      Shardlow\n");
        printf("                        8.      Ingleton Grey\n\n\n");
        printf("                     9.  Other\n\n\n");

        printf("     Please Select A Number (1-9) :");


        do
        {
        CH=getch();
  CH=tolower( CH );
```

```
   } while ( CH != '1'&& CH != '2' && CH != '3' && CH != '4' && CH != '5' && CH != '6' && CH != '7'
&& CH != '8' && CH != '9');

{

switch ( CH )
 {
  case '1':
  shap();
   show_material_property();
    break;

  case '2':
   cliffe_hill();
    show_material_property();
         break;

  case '3':
   waterswallows();
    show_material_property();
    break;
  case '4':
   pottal_pool();
         show_material_property();
          break;

  case '5':
   whitwick();
         show_material_property();
          break;

  case '6':
   judkins();
         show_material_property();
          break;

  case '7':
   shardlow();
         show_material_property();
          break;

  case '8':
```

```
    ingleton();
     show_material_property();
          break;

  case '9':

  OTHER=1.0;
    material_property();
     show_material_property();
          break;


    }/*switch*/

    }/*while*/

    }

void logo()

{
clrscr();
printf("      ***********************************************************************\n");
printf("                              WEAR ANALYSER PROGRAMME\n");
printf("  ***********************************************************************\n");

}

void  shap() /* material properties of Shap Blue */

{


   BTS = 11.90;
   AAV = 1.43;
   WA  = 0.5;
   PH=6.7;
   SI = 52.12;
   A[1]= -34.8; A[2]=527.0; A[3]=-414.0; A[4]=-26.6; A[5]=420.0; A[6]=-103.0; A[7]=7.0; A[8]=5.0;
A[9]=-40.0;


        }
```

```
void  ingleton()  /* material properties of Ingleton Grey */

{

   BTS = 15.19;
   AAV = 4.80;
   PH=8.6;
   WA=0.7;
   SI=58.52;
   A[1]= 2.46; A[2]=-86.2; A[3]=-582.0; A[4]=-7.96; A[5]=44.0; A[6]=206.0; A[7]=-10.8; A[8]=6.6;
A[9]=62.7;

         }

 void cliffe_hill()  /* material properties of Cliffe Hill */

{

   BTS = 18.42;
   AAV = 3.0;
    PH=7.9;
    WA=0.6;
     SI=51.60;
     A[1]= 5.37; A[2]=-122.0; A[3]=854.0; A[4]=-6.3; A[5]=42.0; A[6]=366.0; A[7]=-15.6; A[8]=7.49;
A[9]=80.9;


         }

  void judkins()  /* material properties of Judkins */

{

   BTS = 14.16;
   AAV = 6.7;
    PH=6.6;
    WA=0.7;
     SI=53.80;
     A[1]= 18.6; A[2]=-207; A[3]=752.0; A[4]=12.9; A[5]=-109.0; A[6]=417.0; A[7]=-13.3; A[8]=4.87;
A[9]=92.1;

         }

 void pant()  /* material properties of Pant */

{

   BTS = 11.90;
   AAV = 0.0;
    PH=5.1;
     SI=0.52;

         }
```

```
void pottal_pool() /* material properties of Pottal Pool*/

{

  BTS = 18.06;

  AAV = 0.6;

  PH=7.1;
  WA= 0.01;
  SI=91.30;
  A[1]= -46.3; A[2]=508.0; A[3]=254.0; A[4]=-3.9; A[5]=-29.0; A[6]=-1528.0; A[7]=12.2; A[8]=5.79;
A[9]=0.0;


    }

void shardlow() /* material properties of Shardlow */

{


  BTS = 17.66;

  AAV = 2.7;

  PH=7.2;
  WA=0.01;
  SI=93.90;
  A[1]= -14.5; A[2]=96.0; A[3]=1132.0; A[4]=53.7; A[5]=-649.0; A[6]=3029.0; A[7]=-27.2;
A[8]=11.9; A[9]=0.0;

}

void whitwick() /* material properties of whitwick */

{

  BTS = 14.49;

  AAV = 3.4;

  PH=6.8;
  WA=0.6;
  SI=60.13;
  A[1]= -4.6; A[2]=79.0; A[3]=458.0; A[4]=-18.3; A[5]=290.0; A[6]=-236.0; A[7]=-17.0; A[8]=5.49;
A[9]=91.89;

    }
```

```
 void waterswallows()  /* material properties of Waterswallows */

{

   BTS = 16.55;

   AAV = 3.6;

    PH=6.5;
    WA=0.7;
    SI= 50.15;
    A[1]= 28.0; A[2]=-313.0; A[3]=1081.0; A[4]=-21.8; A[5]=210.0; A[6]=-223.0; A[7]=0.82;
A[8]=4.08; A[9]=7.4;


         }

void  show_material_property()

{
 char ch;


 logo();

 printf("            The Relevant Material Properties of the Chosen Rock\n\n\n");
 printf("               Brazilian Tensile Strength (MPa)     = %6.2f\n", BTS);
  printf("                        PH Value                              = %6.2f\n", PH);
 printf("               Aggregate Abrasive Index                 = %6.2f\n", AAV);
 printf("               Silica (percentage of weight)        =%8.2f\n", SI);

  printf("            Water Absorption (percentage of weight)=%6.2\n",WA);
  printf(" \n\n      Enter Crusher Setting (mm):             ");
  scanf("%f",&DISCHARGE_SETTING);
  CSS=1/DISCHARGE_SETTING;

  printf(" \n\n      Is water added to the Rock? (Y/N):");
   do
        {
         ch=getch();
       ch=tolower( ch );
     } while ( ch != 'y'&& ch != 'n');

{
```

```
switch ( ch )
  {
   case 'y':
    moisture();
      break;

  case 'n':
   drywear();
         break;
 }
 }}


void moisture()

 {
  char  ch;


  printf(" \n\n        Is the amount of added water known? (Y/N):");

    do
         {
          ch=getch();
  ch=tolower( ch );
      } while ( ch != 'y'&& ch != 'n');

{

switch ( ch )
 {
  case 'y':

 printf(" \n\Please enter the moisture content in percentage of rock weight:");
            scanf("%f",&MOISTURE);


   moistwear();
         break;

  case 'n':
   fuzzy_wear();
         break;
 }

 }}
```

```
void fuzzy_wear()

 {

 char ch;


 printf(" \n\nWhich one of the following phrases best describe the rock moisture level:");
 printf(" \n 1. Fairly Dry   2. Fairly Moist  3. Moist  4. Fairly Wet  5. Wet");
  printf("\n Please enter a number (1-5):");

  do
       {
       ch=getch();
 ch=tolower( ch );
       } while ( ch != '1' && ch != '2'&& ch != '3'&& ch != '4'&& ch != '5');

{

switch ( ch )
 {
  case '1':
  FM[1][1]= 0.25;FM[1][2]=1.0;FM[2][1]=0.5;FM[2][2]=0.5;
  break;

  case '2':
  FM[1][1]= 0.5;FM[1][2]=1.0;FM[2][1]=0.75;FM[2][2]=1.0;
  break;


  case '3':
  FM[1][1]= 1.0;FM[1][2]=1.0;FM[2][1]=1.25;FM[2][2]=1.0;
  break;


  case '4':
  FM[1][1]= 1.5;FM[1][2]=1.0;FM[2][1]=1.75;FM[2][2]=1.0;
  break;


  case '5':
  FM[1][1]= 1.75;FM[1][2]=0.75;FM[2][1]=2.0;FM[2][2]=1.0;
  break;

  }} /*case & while*/

  MOISTURE=(1/2)*((FM[1][1]*FM[1][2])+(FM[2][1]*FM[2][2]));
  MOISTURE2=(1/2)*((FM[1][1]*FM[1][1]*FM[1][2])+(FM[2][1]*FM[2][1]*FM[2][2]));

  if (OTHER>0)

       WEAR=-6.15-(462.9*CSS)+(391.9*CSS*CSS)-(0.76*SI)+(5.13*BTS)+(26.1*AAV)-
(16.69*AAV*CSS)+(7.2*SI*CSS)+(10.59*BTS*CSS)-(2.6*BTS*AAV)-
(0.02*BTS*SI)+(0.18*SI*AAV)-
```

```
(28.6*MOISTURE)+(4.56*MOISTURE2)+(30.57*MOISTURE*CSS)+(1.9*MOISTURE*PH)+(19.0*MO
ISTURE*WA);

        else

WEAR=A[4]+(A[5]*CSS)+(A[6]*(CSS*CSS))+(A[7]*MOISTURE)+(A[8]*(MOISTURE2))+(A[9]*MOI
STURE*CSS);
        display_results();
   }

   void moistwear()
   {

   if (OTHER>0)

   WEAR=-6.15-(462.9*CSS)+(391.9*CSS*CSS)-(0.76*SI)+(5.13*BTS)+(26.1*AAV)-
(16.69*AAV*CSS)+(7.2*SI*CSS)+(10.59*BTS*CSS)-(2.6*BTS*AAV)-
(0.02*BTS*SI)+(0.18*SI*AAV)-
(28.6*MOISTURE)+(4.56*MOISTURE*MOISTURE)+(30.57*MOISTURE*CSS)+(1.9*MOISTURE*PH
)+(19.0*MOISTURE*WA);

   else

WEAR=A[4]+(A[5]*CSS)+(A[6]*(CSS*CSS))+(A[7]*MOISTURE)+(A[8]*(MOISTURE*MOISTURE))
+(A[9]*MOISTURE*CSS);
        display_results();
        }

    void drywear()

    {
    if (OTHER>0)
        WEAR=-571.3-(771.3*CSS)+(10.6*SI)+(32.9*BTS)+(18.6*AAV)-
(7.9*AAV*CSS)+(9.9*SI*CSS)+(26.4*BTS*CSS)-(0.4*BTS*AAV)-(0.6*BTS*SI)-(0.2*SI*AAV);
        else
        WEAR=A[1]+(A[2]*CSS)+(A[3]*(CSS*CSS));
        display_results();

    }

void display_results()

{
        logo();

          printf("           The Relevant Material Properties of the Chosen Rock\n\n\n");

  printf("              Brazilian Tensile Strength (MPa)     = %6.2f\n", BTS);
  printf("              PH Value                                      = %6.2f\n", PH);
  printf("              Aggregate Abrasive Index                = %6.2f\n", AAV);
  printf("              Silica (percentage of weight)       =%8.2f\n", SI);
```

```
printf("             Water Absorption (percentage of weight)=%6.2\n",WA);

        printf("\__________________________________________________________________");

        printf("\n\n\n\n\n   The Predicted Total Wear (g/T) =%6.2f\n", WEAR);


        }

void material_property()

{
  logo();

  printf("\n\n       Enter Material Properties");

  printf("\n\n             Brazilian Tensile Strength (MPa):");
   scanf("%f",&BTS);

   printf("\n                   PH Value:");
   scanf("%f",&PH);

 printf("\n\n            Aggregate Abrasive Value:");
 scanf("%f",&AAV);

 printf("            Silica (percentage of weight)       =");
 scanf("%f",&SI);
  printf("           Water Absorption(percentage of weight)       =");
 scanf("%f",&WA);

 }
```

Appendix 7 LIST OF PUBLISHED PAPERS

Published Papers

1. The Application of KBS for Real Time Control of Cone Crushers
M Moshgbar, R Parkin, R Bearman.
Proceedings IEE: "Systems Engineering for Real Time Applications", , 13-14 September 1993, Royal College of Agriculture, Cirencester, ISBN 085296 593 1, ISSN 0537-9989, P172-177.

2. The Application of Fuzzy Logic for Real-time Evaluation of Wear in Cone Type Rock Crushers
M Moshgbar, R Parkin.
Proceedings: "International Conference of Condition Monitoring 94", 21-25 March 1994, University Colledge Swansea Ed M H Jones, ISBN 0 906674 83 2, P716-725.

3. A Mechatronic Solution for Automatic Control of Cone Crushers
M Moshgbar, R Parkin.
International Journal of Intelligent Mechatronics Design and Production, No.1, 1994, P1-13.

4. An Intelligent Distributed System for Real Time Control of Cone crushers
M Moshgbar, R Parkin.
Journal of Microprocessors and Microsystems, Vol.18, No.7, 1994, ISSN 0141-9331, P377-383.

5. The Compensation of Liner Wear for Optimum Control of Cone Crushers
M Moshgbar, R Parkin, R Bearman.
Progress in Mineral Processing Technology, Proceedings of 5th International Mineral Processing Symposium, September 6-8 1994, Cappadocia, Turkey, P549-555, ISBN 90 5410 5135.

6. The Application of Fuzzy Logic and Neural Networks in Comminution
M Moshgbar, R Parkin, R Bearman.
Journal of Minerals Engineering, Vol. 8, No. 1/2, 1995, P41-50, ISSN 0892 6875/95.

7. Optimum Control of Cone Crushers Utilizing an Adaptive Strategy for Wear Compensation
M Moshgbar, R Parkin, R Bearman
Journal of Minerals Engineering, Vol. 8, No. 4/5, 1995, P367-376, ISSN 0892 6875/95.

8. Adaptive and Intelligent Control of Cone crushers
M Moshgbar, R Parkin, R Bearman
Proceedings of APCOM XXV, "Application of Computers and Operations Research in the Minerals Industries", Brisbane, Australia, 10-14 July 1995.

9. The Impact of System Tribology on Automatic Control of Cone Crushers
M Moshgbar, R Parkin, R Bearman
Transactions of Institute of Measurement and Control, Vol. 17, No. 1, 1995, P2-9.